FACULTY OF MATHEMATICS AND PHYSICS
CHARLES UNIVERSITY

VISCOELASTIC RESPONSE OF THE EARTH: INITIAL-VALUE APPROACH

Ph.D. THESIS

LADISLAV HANYK

PRAGUE 1999

Supervisor: Doc. RNDr. Ondřej Čadek, CSc.

Consultants: Doc. RNDr. Ctirad Matyska, DrSc.
Prof. Dr. David A. Yuen

Author's address: Department of Geophysics
Faculty of Mathematics and Physics
Charles University
V Holešovičkách 2
180 00 Praha 8 – Libeň
Czech Republic

e-mail: Ladislav.Hanyk@mff.cuni.cz

Prvnímu geofyzikovi v rodině . . .
mé mamince

Vydávaje první tuto částku díla již od dávna i chystaného i očekávaného, nemohu opominouti, abych neosvědčil se o něm veřejně aspoň několika slovy.
Ode mládi neznal sem tužby vřelejší ani vyšší pro vezdejší život svůj, nežli abych posloužil milovanému národu svému . . .
K otevřenému vyznání tomuto však bez odkladu přidati musím také osvědčení druhé, a to neméně upřímné: že jakkoli věrně snažil sem se, aby dílo mé národu k užitku a mně samému ke cti sloužiti mohlo, předce s bolestí vidím a cítím, že jen velmi nedokonale podařilo se mi, nedostatečné jsouc téměř ve každé své stránce; aniž pak mi již zbývalo jiné volení, nežli aneb odříci se navždy nejmilejší své tužby a čáky, a potlačiti tudíž naprosto dílo nespokojující, — aneb podati je národu, jakéžkoli jest.

FRANTIŠEK PALACKÝ, *Dějiny národu českého v Čechách a v Moravě* (1848)

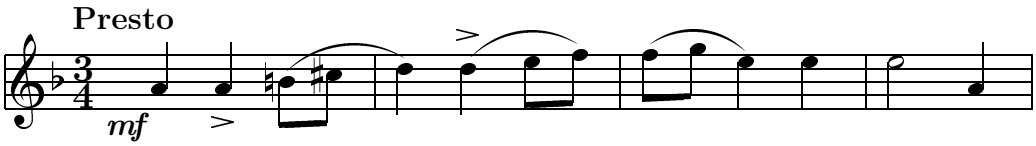

ANTONÍN DVOŘÁK, *Czech Suite in D major, Op. 39. V. Finale (Furiant). Presto* (1879)

Contents

List of Abbreviations

1-D	one-dimensional, here: spherically symmetric
2-D	two-dimensional, here: axially symmetric
3-D	three-dimensional
BV	boundary value
DAE	differential-algebraic equation
FD	finite difference
GIA	glacial isostatic adjustment
GPS	global positioning system
IV	initial value
l.h.s.	left-hand side
LM	lower mantle
LVZ	low-viscosity zone
MOL	method of lines
MOR	method of Rothe
NM	normal mode
ODE	ordinary differential equation
PDE	partial differential equation
PREM	preliminary reference Earth model
r.h.s.	right-hand side
SNREI	spherically symmetric, non-rotating, elastic, isotropic
VLBI	very long baseline interferometry

$\dot{f}$	a partial derivative of function f with respect to time t
f'	a partial derivative of function f with respect to the radius r

Summary

The relevance of the viscoelastic approximation of the Earth responses emerges in the context of processes operating on the transient temporal scales, between the domains of purely elastic and viscous modelling. Modelling of the uplift of regions deglaciated during the late Pleistocene epoch is the leading application. The forward problem of the postglacial rebound consists of the evaluation of response functions to the unit load and of the convolution of the responses with models of glacial-oceanic loading in time and space. It is a long-standing tradition to evade the time dependence of the responses by reformulation of the problem in the Laplace domain and to express the Laplace spectra of the responses in terms of normal modes. However, the messy structure of the Laplace spectra of spherical compressible models with realistic distribution of physical parameters poses the serious obstacle for the inverse transformation of the responses back into the time domain. For this reason, the application of the normal-mode approach to these compressible Earth models becomes rather ineffective, if not impossible.

We have derived a new approach based on the direct solution to the viscoelastic responses in time. Mathematically it is a reformulation of evolutional partial differential equations governing the infinitesimal response of the pre-stressed viscoelastic continuum in the form of an initial-value problem for ordinary differential equations. In Part I we derive the initial-value formulation in full detail. We begin from the field partial differential equations, continue with the spherical harmonic decomposition and the spatial semi-discretization via the method of lines and discuss routines appropriate for numerical solution to resulting stiff ordinary differential equations. We also touch our older initial-value formulation based on an alternative technique of discretization. We concentrate on models with spherically symmetric distribution of physical parameters, although a set of differential equations for the case of axisymmetric viscosity is derived, too. In Part II we collect our publications on the initial-value approach. We focus on characteristic features of responses of realistic models with complex viscosity profiles. In particular, the influences of elastic compressibility, of the thickness of the lithosphere, of the nature of internal mantle boundaries and of the structure of the asthenosphere are studied. The comparison of results obtained by the both approaches is conducted for simplified as well as for realistic models. We demonstrate the gravitational instability of a compressible homogeneous sphere, the fact forgettable and sometime being forgotten in the framework of the normal-mode approach.

The initial-value approach offers the alternative fundamentals for the numerical modelling of the viscoelastic responses. Besides its applicability to arbitrarily stratified spherical Earth models, it provides the possibility of being generalized for models with 2-D and 3-D viscosity distribution. Due to the efficiency of numerical procedures applicable to the forward problem, it can eventually extend the throughput of the inverse modelling.

Chapter 1

Introduction

1.1 Glacial Isostatic Adjustment

In the presented thesis we treat a subject of the global response of the Earth to surface loading. The *global response* is characterized in accordance with observations by fast perturbations of an initial state during progressive changes of a surface load, followed by a slower relaxation towards a new state of isostatic equilibrium after stabilization of the load. This behaviour can be well described by viscoelastic rheologies with the preference given to that of the Maxwell solid. By the term *the Earth* we mean a model of the Earth, specifically the particular case of a non-rotating, self-gravitating, spherically or axially symmetric sphere, responding in time as an elastic, viscoelastic or viscous body, or a combination of these. *Surface loading*, large enough and not too distant in the past to initiate the global response observable at present of the body of the Earth, has been achieved by glaciers during the late Pleistocene epoch and, hence, it is customary to refer to the whole process as the *glacial isostatic adjustment* (GIA). From the physical point of view, modelling of GIA consists of two complementary problems:

the *forward problem*: from prescribed parameters of the Earth (e.g., density, elastic parameters and viscosity) and from a prescribed model of a surface load, observable response functions (e.g., amplitudes and rates of surface vertical and horizontal deformations and of gravitational anomalies) are evaluated;

the *inverse problem*: from observed data (e.g., recent long-term surface movements monitored by geodetic techniques, secular changes of parameters of rotational dynamics, gravitational anomalies in both deglaciated areas and surrounding regions and past sea-level changes projected into coral lines) and from a priori information (e.g., seismological models of density and elastic parameters and evidences of spatial distribution of past glaciers), depth distribution of viscosity and a refined load history are inferred.

As far as the modelling of the viscoelastic Earth is concerned, the field is dominated by the normal-mode (NM) approach developed by Prof. W.R. Peltier and his colleagues (Peltier 1974, 1976; Peltier & Andrews 1976; Wu & Peltier 1982; Yuen & Peltier 1982; Peltier 1982, 1985; Mitrovica & Peltier 1989, 1991) and further elaborated and extended also by other teams (Sabadini et al. 1982; Yuen et al. 1982, 1986; Wolf 1984; Nakada & Lambeck 1987; Wolf 1991, 1994; Han &

Wahr 1995; Fang & Hager 1995; Johnston et al. 1997; Tromp & Mitrovica 1999a, 1999b). The basic idea is the decomposition of the response into a set of normal modes. Field partial differential equations (PDEs) governing the viscoelastic response of the Earth are transformed into the Laplace domain and are subjected to spherical harmonic decomposition what leads to a system of ordinary differential equations (ODEs) with respect to the radius, similar to those known from the theory of free oscillations (e.g., Pekeris & Jarosch 1958) and the theory of Earth tides (e.g., Melchior 1978). Time dependence of the PDEs in the case of viscoelasticity results in that that the ODEs are parametrized by the Laplace variable s.

The ability to solve the forward problem with the maximal efficiency appears to be the primary requisite for the valuable treatment of the inverse problem. Although the theory of the forward problem has been available for more than 25 years and a lot was done in the inverse modelling and data interpretation, an effort pointing to the forward-problem fundamentals has been continuing with permanent intensity. Let us mention publications on analytical solutions to relaxation of simplified Earth models (Wolf 1985a, 1985b; Wu & Ni 1996; Vermeersen et al. 1996b; Martinec & Wolf 1999), designing matrix-propagator methods as the alternative to numerical integrators of the ODEs (Sabadini et al. 1982; Spada et al. 1990), improvement of numerical techniques of the inverse transformation back from the Laplace domain (Mitrovica & Peltier 1992; Han & Wahr 1995; Fang & Hager 1994, 1995, 1996; Boschi et al. 1999) and applicability of simplified incompressible models to modelling of the realistic Earth response (Vermeersen et al. 1996a; Vermeersen & Sabadini 1997).

In recent years an increasing effort has been devoted to generalization of the forward-problem formulation to an axially symmetric (2-D) and a general (3-D) Earth, at least in terms of viscosity distribution. Besides iterative methods applicable to small perturbations of the radial viscosity (Sabadini et al. 1986; Gasperini & Sabadini 1989, 1990; D'Agostino et al. 1997), a branch built on the application of the finite-element software has been emerging with the noticeable vitality (Wu & Johnston 1998; Wu et al. 1998; Kaufmann & Wu 1998; Ni & Wu 1998); although presently being applied within the planar geometry, it allows for both large contrasts of the mantle viscosity and variations of density and elastic parameters. Eventually, a theory of the viscoelastic relaxation of the spherical Earth with the 3-D viscosity in terms of scalar, vector and tensor spherical harmonics has been developed (Martinec 1999), and the analytically solved case of eccentrically nested spheres (Martinec & Wolf 1999) provides the prerequisite for testing the 2-D and 3-D numerical codes.

1.2 History of the Initial-Value Approach

Although the forward problem of the glacial isostatic adjustment had already been attacked by initial-value (IV) techniques (Cathles 1971, 1975; Ivins et al. 1993), the first attempt to formulate the forward problem as the IV problem on the basis consistent with Peltier (1974) and completely in the time domain appeared no earlier than around 1993. At that time an extensive discussion of positive and negative features of the NM approach was in progress (Han & Wahr 1995; Fang & Hager 1994, 1995). A frequent question was how to accurately invert the complex, apparently continuous, Laplace spectra of compressible realistic Earth models back into the time domain. In the framework of the NM approach, no obvious possibility, e.g., employing few-layered models, crude numerical treatment of the Laplace spectra or spending too much resources in the process of inversion, ensured a sufficient satisfaction.

With these difficulties, the idea of numerical solution to the forward problem entirely in the time domain appeared quite naturally. As the obvious elaboration of this idea, time derivatives in the constitutive relation of Maxwell viscoelasticity had been replaced by finite-difference (FD) formulas. With the effort to preserve as much of the traditional technique as possible, most other features had been kept, especially that the problem takes the form of a series of boundary-value (BV) problems with respect to the radius. Specifically, the system of ODEs to be solved in the NM approach forms the BV problem parametrized by the Laplace variable. The task is to scan the parameter space to find certain values of the parameter that are subsequently associated with the modal relaxation times. While obtaining solutions to the individual BV problems is a tractable procedure, the scanning of the parameter space—in principle, a root-finding problem—can become very intricate due to a high density of clustering of roots. A problem is to catch as much modes as possible, and more importantly, to locate accurately the strong modes among all the weak modes. It is rather difficult within the NM approach to estimate the number of the BV problems to be solved in advance. In our original formulation of the IV approach replacement of time derivatives by the FD formulas leads to a system of linear non-homogeneous ODEs. A vector on the right-hand side (r.h.s.) of the ODEs is time-dependent and can be computed at each time level from the previous values of the solution. Physically, the r.h.s. vector expresses the memory of the viscoelastic model. The IV problem is again decomposed into a series of BV problems, now of a limited number which can be assessed a priori.

The ODEs of the both approaches can be formally described as follows, cf. Peltier (1974) and (7.17) & (7.35), respectively,

$$\textit{NM Approach:} \qquad \frac{d}{dr}\mathbf{y}(s,r) = \boldsymbol{A}(s,r)\ \mathbf{y}(s,r)\,, \tag{1.1}$$

$$\textit{IV Approach:} \qquad \frac{d}{dr}\mathbf{y}(t,r) = \boldsymbol{A}(r)\ \mathbf{y}(t,r) + \mathbf{q}(t,r)\,, \tag{1.2}$$

$$\frac{d}{dt}\mathbf{q}(t,r) = \frac{\mu(r)}{\eta(r)}\left[\tilde{\boldsymbol{Q}}(r)\ \mathbf{y}(t,r) + \tilde{\tilde{\boldsymbol{Q}}}(r)\ \mathbf{q}(t,r)\right], \tag{1.3}$$

with r denoting the radius, s the Laplace variable, t time, μ the shear modulus and η the viscosity. The solution vector $\mathbf{y}$ incorporates coefficients of scalar representations of the unknown physical quantities, i.e., the displacement vector, the incremental stress tensor and the incremental gravitational potential. Matrix $\boldsymbol{A}$, cf. (2.50), (6.38) or (7.14), is formally identical in the both approaches, although, in the NM approach, it is implicitly parametrized by the s-dependence of the shear modulus $\mu(r,s)$; matrices $\tilde{\boldsymbol{Q}}$ and $\tilde{\tilde{\boldsymbol{Q}}}$ are given by (7.36) and eq. (1.3) is actually (6.39).

In the first numerical tests, we reached a perfect coincidence of the response curves found by the IV approach with responses obtained by the NM approach for simple incompressible models, both analytically (for the homogeneous sphere) and numerically (for stratified models). Serious discrepancies emerged in the relaxation curves of realistic compressible models, but these could be attributed to the incompleteness of the numerical inversion of the overfull spectra of the realistic models. However, a rapidly emerging secular instability appeared in the response of the homogeneous compressible model, and the tantalizing question about the origin of this instability remained unexplained. The original formulation of the IV approach and the just described results were first presented by the Czech-American team, members of which were Prof. D.A. Yuen, Dr. C. Matyska and my classmate J. Moser, on the memorable *Workshop on Global Geodynamics*, held in the Pístina village in southern Bohemia in 1993. It was Prof. W.R. Peltier who had been kept at the authors' poster and forced to listen to the tales on all the unsuccessful numerical attempts

which should have eliminated the instability of the response of simple compressible models.

The first paper on our formulation of the IV approach[1] was a letter by Hanyk et al. (1995), internally referred to as *The Paratrooper* (invented by the coauthor, Prof. D.A. Yuen). A primary mission of *The Paratrooper* was to prepare a battlefield for the companion paper, Hanyk et al. (1996), with the code-name *The Tank*. While the former briefly introduced the IV approach and showed for a realistic compressible model differences in relaxation obtained by the both approaches, the latter provided equations (1.2)–(1.3) explicitly and demonstrated on a set of 144 panels both the complexity of the Laplace spectra and temporal responses of a large family of realistic compressible Earth models with complex viscosity profiles. (For that number of presented window-like panels, the paper received another nickname, *The Apartment Building*.) Meanwhile, a new acronym for the IV approach emerged, *FLT*, with the meaning of *Forget the Laplace Transform*. Perhaps, these three letters well express the atmosphere, developed by the two papers on the IV approach, impaired by a concept of the non-modal contribution employed by *The Paratrooper* in the explanation of the differences in the responses obtained by the both approaches, and also intesified by reactions of others to this concept. Here we mention papers announcing derivation of analytical solutions to the response of the compressible models (Vermeersen et al. 1996a, 1996b) or exposing some examples on reliability of the description of the Earth response by simple incompressible models (Vermeersen & Sabadini 1997; 143 panels were laboured in this paper). The present state is not—we believe—a state of war; perhaps, it has also been documented in the prominent milestone among publications on the topic of GIA, the book *Dynamics of the Ice Age Earth: A Modern Perspective*, where Vermeersen & Sabadini (1998) and Hanyk et al. (1998) lie alongside without noticeable shots over the borderline.

New advances appeared in the theory and the numerical practice of the NM approach applied to incompressible models, however, opening up the topic of the response of simple compressible models brought back the old doubts. At least the concept of the homogeneous compressible model, being both the initial state and the final isostatic state, must have been the object of a suspicion as actually follows from the vast discussion on the stability of the liquid core (e.g., Longman 1963, 1975; Fang 1998). Indeed, Plag & Jüttner (1995) found and discussed the unstable response of realistic compressible models and attributed it to the Rayleigh-Taylor instabilities implied by unstable density distribution of the model they considered (PREM by Dziewonski & Anderson 1981). Wolf & Kaufmann (1999) explicitly discriminate between the compressional and compositional density stratification of compressible initial models. Effects of a non-adiabatic density gradient on the stability of the viscoelastic response are also studied by Nakada (1999). The topic of the viscoelastic response of the homogeneous compressible sphere is addressed by Hanyk et al. (1999). In this paper, the NM approach has been applied to prove analytically the existence of growing modes in the response of the homogeneous model, and the fact that compressible models which consist of few homogeneous layers exhibit the fast gravitational collapse has been demonstrated.

Meanwhile, an effort to improve our numerical implementation of the IV formulation has been under way. There was the only but the essential reason for this endeavour: to overcome the limit imposed on the maximal stepsize in time to keep the integration numerically stable. Here, the numerical stability of the relaxation is concerned, not the physical stability of the initial models. This limit on the stepsize corresponds to a minimal Maxwell time (the ratio of viscosity and the shear modulus) of any solid layer of the initial model, and is particularly painful when models

[1] A reader not interested in the military aspects of the IV approach should skip this paragraph.

with low-viscosity zones are taken into account. Actually, this is the expectable behaviour of ODE solvers built on explicit integration schemes when applied to stiff sets of ODEs (e.g., Ascher & Petzold 1998), and the ODEs resulting from the application of the IV approach to models with physical parameters spanning over a broad range are the stiff systems. A cure is simple, at least virtually: one should use the integrators designed for the stiff ODEs. However, this poses a problem in the original IV formulation. Utilization of stiff integrators requires a knowledge of the Jacobian matrix of the system which can not be expressed from (1.3) explicitly. The new formulation of the IV approach presented in Chapters 3 and 4 overcomes this difficulty. The system (1.2)–(1.3) is replaced by the differential system with respect to both time and the radius which allows to make use of the method of lines (MOL) (e.g., Schiesser 1991), cf. (3.23),

$$\textit{IV/MOL Approach:} \qquad \frac{d}{dt}\left[\frac{d}{dr}\mathbf{y}(t,r) - \boldsymbol{A}(r)\ \mathbf{y}(t,r)\right] \;=\; \frac{\mu(r)}{\eta(r)}\left[\boldsymbol{D}(r)\frac{d}{dr}\mathbf{y}(t,r) + \boldsymbol{E}(r)\ \mathbf{y}(t,r)\right]. \quad (1.4)$$

In accord with the idea of MOL, we only apply FD formulas to the derivatives with respect to r. The number of obtained ODEs is proportional to the density of spatial discretization, and therefore might be very large, but the matrix of the system is both band-diagonal and prepared for the immediate application of stiff integrators. These features are the two prerequisities for the numerical efficiency of the new formulation.

1.3 Overview of the Thesis

In the presented thesis we provide a review of our formulations of the IV approach to the modelling of viscoelastic responses of the Earth, from the original version by Hanyk et al. (1995, 1996) through the integro-differential formulation by Hanyk et al. (1998) up to recently discovered and here first published formulation based on the method of lines. However, the thesis is arranged in the reverse order: the new material is supplied in Part I to allow the detailed understanding of the IV machinery, and the publications presenting the physical results obtained by the IV approach are placed in Part II.

Part I contains a complete derivation of the new formulation of the IV/MOL approach. In Chapter 2 we collect a system of field PDEs governing the global response of a spherically symmetric, gravitating, compressible Earth model to surface loading. With the elastic constitutive relation considered first, the field PDEs are converted into a system of ODEs with respect to the radius by means of the spherical harmonic analysis and the technique of scalar representation of both vectors and second-order tensors. In Chapter 3 we switch to the constitutive relation of the Maxwell viscoelasticity which introduces the time evolution into the system. To convert the field PDEs into the PDEs (1.4), we carefully reproduce the procedure given for the case of the elastic rheology. We derive related PDEs for the standard linear solid and for the axisymmetric viscosity distribution, too. In Chapter 4 we discretize the PDEs (1.4) in the spatial dimension and obtain a system of ODEs with respect to time, suitable for efficient numerical implementation of stiff integrators. The Rosenbrock and the semi-implicit extrapolating stiff integrators are discussed and adapted for the band-diagonal structure of the matrix of the system. Numerical properties of the new formulation are demonstrated on some examples. References relevant to the presented material are included at the end of Part I. The new formulation has been initiated rather recently and is still a kind of

work in progress[2]; the reader is asked to withstand the presented glimmer of numerical outputs as well as no further elaboration of the PDEs for the 2-D viscosity. Part II incorporates (in the chronological order) four publications which apply the IV approach to a large family of viscoelastic Earth models. We keep the text as was originally published, perhaps with some typing errors corrected. Consequently, the notation used in Part II might be different from that used in Part I, and may even differ between the separate chapters. In Chapters 5, 6 and 7 we focus on characteristic features of responses of realistic models with complex viscosity profiles. In particular, the influence of elastic compressibility, the thickness of the lithosphere, the nature of internal mantle boundaries and the viscosity structure of the asthenosphere are studied. The comparison of results obtained by the both approaches is conducted for simplified as well as for realistic models. Chapter 6 contains our first formulation of the IV approach, Chapter 7 presents another one, the integro-differential formulation. The gravitational instability of a compressible homogeneous sphere is examined in Chapter 8. A survey of features of scalar spherical harmonics is given in Appendix A, where efficient numerical procedures for computation of coefficients of scalar-field expansions are also described. To make it easier for a reader to trace Chapters 2 and 3, we recall scalar representation of scalar, vector and second-order tensor fields subjected to differential operators in Appendix B; expressions for scalar components of strain and elastic stress tensors are also derived. Excerpts of Fortran routines referenced in the text and perhaps of general applicability are attached in Appendix C.

At this point I want to express my gratitude to people without ceaseless encouragement of whose this work would hardly appear at the surface of the Earth. I begin the list with my supervisor O. Čadek for his patient treatment of myself. Without any doubt the crucial significance for the existence of the presented results, the existence of this work as a whole and the existence of myself in the field of geophysics have C. Matyska and D.A. Yuen. I express my thank to Z. Martinec and J. Zahradník, the former providing me with a living paradigm for a Researcher, and the latter for exactly the same. Discussions and suggestions proposed by D. Wolf, P. Johnston, M. Fang, G. Ranalli and others (see sectional acknowledgements in Part II) helped substantially. My appreciation spreads over the people I have met at the Department of Geophysics: J. Moser who brought initial ideas of the initial-value approach, H. Čížková for a thousand of things, J. Matas for inventing the trip to Morocco, and a dozen others. *The only worth in this world is a family*[3]. Without my wife Lenka and my daughter Martina, everything, with the probability equal to 1, would be else. And last, and of course not least, I affirm that the thesis has been prepared with the financial support provided by the Grant Agency of Charles University (Nos 1/97/B-GEO-MFF and 170/98/B-GEO/MFF). The thesis has been composed with TEX, LATEX 2$_\varepsilon$, MusiXTEX and MPP, the incredibly powerful typesetting system.

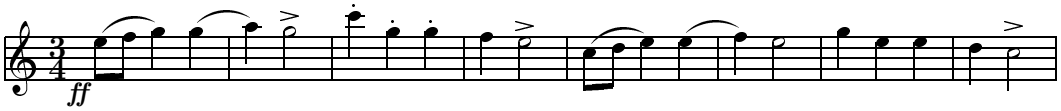

ANTONÍN DVOŘÁK, *Slavonic Dances, Op. 46. No. 1 in C major. Presto* (1878)

[2]The term used by director F.F. Coppola presenting his still unfinished film *Apocalypse Now* to the Festival International du Film at Cannes in May, 1979.

[3]The paraphrase of Don Michael Corleone's sentence in *The Godfather, Part III* by F.F. Coppola.

Part I

Initial-Value Approach via the Method of Lines

Chapter 2

Elastic Response of the Earth

In this chapter we collect a fundamental set of field partial differential equations (PDEs) of gravitational viscoelastodynamics for incremental field variables, describing the response of the Earth model to the unit surface load. For the special case of the spherically symmetric, non-rotating, elastic and isotropic (SNREI) Earth model, we deduce from the field PDEs a system of ordinary differential equations (ODEs) for coefficients of spherical harmonic expansions of field variables. We apply a similar procedure to PDEs for viscoelastic Earth models in Chapter 3.

2.1 Field Partial Differential Equations

We consider a gravitating, compressible, non-rotating continuum initially in hydrostatic equilibrium. It is conventional to decompose total fields, such as the stress tensor and the gravitational potential, into initial and incremental parts. The incremental fields are employed for description of infinitesimal, quasi-static, gravitational-viscoelastic perturbations of the initial fields. Physical quantities and field equations given below conform to the standard form of gravitational viscoelastodynamics (Peltier 1974), also referred to as the material-local form of the linearized field theory (Wolf 1997). Since all necessary expansions of field variables and related expressions are collected in Appendix B, the main deal here is to substitute these expansions into the field PDEs.

The initial state of the above qualified continuum is described, in terms of the initial (Cauchy) stress tensor $\boldsymbol{\tau}_0$, the initial gravitational potential φ_0, the initial density distribution ϱ_0 and the forcing term $\boldsymbol{f}_0$, by the momentum equation and the Poisson equation, respectively,

$$\nabla \cdot \boldsymbol{\tau}_0 + \boldsymbol{f}_0 = \boldsymbol{0}\,, \tag{2.1}$$

$$\nabla^2 \varphi_0 - 4\pi G \varrho_0 = 0\,, \tag{2.2}$$

where G is the Newton gravitational constant. The boundary conditions required at the surface and all internal boundaries are the continuity of the normal initial stress, $[\boldsymbol{n} \cdot \boldsymbol{\tau}_0]^+_- = 0$, of the gravitational potential, $[\varphi_0]^+_- = 0$, and of the normal component of its gradient, $[\boldsymbol{n} \cdot \nabla \varphi_0]^+_- = 0$, where $\boldsymbol{n}$ is the outward unit normal with respect to the boundary; moreover, the tangential stress should vanish at liquid boundaries and at the surface, $\boldsymbol{n} \cdot \boldsymbol{\tau}_0 = (\boldsymbol{n} \cdot \boldsymbol{\tau}_0 \cdot \boldsymbol{n})\boldsymbol{n}$. The premise of the hydrostatic initial stress requires no deviatoric stresses, $\boldsymbol{\tau}_0 = -p_0 \boldsymbol{I}$, with p_0 the mechanical pressure and $\boldsymbol{I}$ the unit diagonal tensor. We take the force $\boldsymbol{f}_0$ equal to the gravity force per unit volume,

$\boldsymbol{f}_0 = -\rho_0 \nabla \varphi_0$. In the case of the spherically symmetric density, $\varrho_0(r)$, where r is the radius, all initial fields also become spherically symmetric. Introducing the gravitational acceleration $g_0(r)$ by the relation $g_0 \boldsymbol{e}_r = \nabla \varphi_0$, eqs (2.1)–(2.2) reduce to

$$p_0' + \varrho_0 g_0 = 0\,, \tag{2.3}$$
$$g_0' + 2g_0/r - 4\pi G \varrho_0 = 0\,, \tag{2.4}$$

where (B.23) and (B.24) have been used. The prime $'$ denotes differentiation with respect to r.

The incremental fields include the displacement $\mathbf{u}$, the incremental (Cauchy) stress tensor $\boldsymbol{\tau}$, the incremental gravitational potential φ_1 and the incremental density ϱ_1. Note that the incremental potential φ_1 under the presence of a surface load is due to both the gravitational forcing of the load and the internal mass redistribution of the model. For incremental fields the adoption of the concept of Lagrangian or Eulerian formulations of a field becomes necessary, the former relating the current value of a field at the material point to the initial position of that point, the latter relating the field to the current, local position. Leaving derivation of the following equations for specialized monographs (e.g., Wolf 1997[1]), we state that if $\boldsymbol{\tau}$ is in Lagrangian description and φ_1 and ϱ_1 are in Eulerian description, then, within this conventional casting (as stated above, the material-local form), the incremental field equations for infinitesimal, quasi-static perturbations, i.e., the momentum equation and the Poisson equation, will take the form as follows:

$$\nabla \cdot \boldsymbol{\tau} + \boldsymbol{f} = \mathbf{0}\,, \tag{2.5}$$
$$\nabla^2 \varphi_1 - 4\pi G \varrho_1 = 0\,. \tag{2.6}$$

The forcing term $\boldsymbol{f}$ and the Eulerian incremental density ϱ_1 are

$$\boldsymbol{f} = -\varrho_0 \nabla \varphi_1 - \varrho_1 \nabla \varphi_0 - \nabla(\varrho_0 \mathbf{u} \cdot \nabla \varphi_0)\,, \tag{2.7}$$
$$\varrho_1 = -\nabla \cdot (\varrho_0 \mathbf{u})\,. \tag{2.8}$$

Introducing the strain tensor $\boldsymbol{e}$ with the first invariant $\bar{e}$, cf. (B.49) and (B.52),

$$\boldsymbol{e} = \frac{1}{2}\left[\nabla \mathbf{u} + (\nabla \mathbf{u})^T\right], \qquad \bar{e} = \nabla \cdot \mathbf{u}\,, \tag{2.9}$$

we can write the linearized elastic constitutive relation in the form

$$\boldsymbol{\tau}^E = \lambda \bar{e}\, \boldsymbol{I} + 2\mu\, \boldsymbol{e} = \lambda \nabla \cdot \mathbf{u} \boldsymbol{I} + \mu \left[\nabla \mathbf{u} + (\nabla \mathbf{u})^T\right] \tag{2.10}$$

with λ and μ the elastic Lamé parameters, the latter also referred to as the shear modulus or rigidity; they are related to the bulk modulus or isentropic incompressibility K through $K = \lambda + \frac{2}{3}\mu$. We apply symbol $\boldsymbol{\tau}^E$ for the "elastic part" of any stress tensor, if it can be written in the form of (2.10). Thus, the constitutive relation of Maxwell viscoelasticity (Peltier 1974) can be rewritten as

$$\dot{\boldsymbol{\tau}} + \frac{\mu}{\eta}\left(\boldsymbol{\tau} - \frac{1}{3}\bar{\boldsymbol{\tau}} \boldsymbol{I}\right) = \dot{\boldsymbol{\tau}}^E\,, \tag{2.11}$$

where η is the dynamic viscosity and the dots denote differentiation with respect to time t. The first invariants of both the Maxwell and the elastic stress tensors coincide, cf. (B.61),

$$\bar{\boldsymbol{\tau}} = \bar{\boldsymbol{\tau}}^E = (3\lambda + 2\mu) \nabla \cdot \mathbf{u} = 3K \nabla \cdot \mathbf{u}\,. \tag{2.12}$$

[1]Correspondence between the notation used here (l.h.s.) and that by Wolf (1997) (r.h.s.) is as follows: $\tau_{0,ij} = t_{ij}^{(0)}$, $\tau_{ij} = t_{ij}^{(\delta)}$, $\varphi_0 = -\phi^{(0)}$, $\varphi_1 = -\phi^{(\Delta)}$; other relations are obvious.

The internal boundary conditions for the incremental fields require continuity of the displacement, the incremental stress, the incremental gravitational potential and its gradient, $[\mathbf{u}]_-^+ = \mathbf{0}$, $[\boldsymbol{\tau}]_-^+ = \mathbf{0}$, $[\varphi_1]_-^+ = 0$ and $[\nabla\varphi_1]_-^+ = \mathbf{0}$, and zero tangential stress at liquid boundaries, $\boldsymbol{n}\cdot\boldsymbol{\tau} = (\boldsymbol{n}\cdot\boldsymbol{\tau}\cdot\boldsymbol{n})\boldsymbol{n}$. Under the presence of the load prescribed by the interface density γ_L, the surface boundary conditions for the incremental stress and gradient of the incremental gravitational potential balance the applied load, $[\boldsymbol{n}\cdot\boldsymbol{\tau}]_-^+ = -g_0\gamma_L\boldsymbol{n}$ and $[\boldsymbol{n}\cdot(\nabla\varphi_1 + 4\pi G\rho_0\mathbf{u})]_-^+ = -4\pi G\gamma_L$.

To summarize the equations, the fundamental system of the field PDEs for the incremental fields $\mathbf{u}$, φ_1 and $\boldsymbol{\tau}$ in the continuum with the Maxwell viscoelastic rheology and the spherically symmetric density distribution $\varrho_0(r)$ takes the form

$$\nabla\cdot\boldsymbol{\tau} + \boldsymbol{f} = 0\,, \qquad \boldsymbol{f} = -\varrho_0\nabla\varphi_1 + \nabla\cdot(\varrho_0\mathbf{u})g_0\boldsymbol{e}_r - \nabla(\varrho_0 g_0\boldsymbol{e}_r\cdot\mathbf{u})\,, \tag{2.13}$$

$$\nabla\cdot(\nabla\varphi_1 + 4\pi G\varrho_0\mathbf{u}) = 0\,, \tag{2.14}$$

$$\dot{\boldsymbol{\tau}} = \dot{\boldsymbol{\tau}}^E - \frac{\mu}{\eta}\left(\boldsymbol{\tau} - K\nabla\cdot\mathbf{u}\boldsymbol{I}\right)\,. \tag{2.15}$$

This system of field PDEs is to be further elaborated. We adopt the spherically symmetric distribution of density and elastic Lamé parameters. For this case, the spherical harmonic analysis is applied to (2.13)–(2.14) with the constitutive relation of elasticity, $\boldsymbol{\tau} = \boldsymbol{\tau}^E$, in the following section.

2.2 Spherical Harmonic Decomposition

Let $\boldsymbol{e}_r$, $\boldsymbol{e}_\vartheta$ and $\boldsymbol{e}_\varphi$ be the unit basis vectors of the spherical coordinates r, ϑ and φ, denoting the radius, the colatitude and the longitude, respectively. We introduce the scalar spherical harmonics $Y_{nm}(\vartheta,\varphi)$,

$$Y_{nm}(\vartheta,\varphi) = (-1)^m N_{nm} P_n^m(\cos\vartheta)e^{im\varphi}\,, \tag{2.16}$$

cf. (A.12), where $P_n^m(\cos\vartheta)$ are the associated Legendre functions and N_{nm} the norm factors; for details see Appendix A.2. We also introduce the vector spherical harmonics $\boldsymbol{S}_{nm}^{(-1)}$, $\boldsymbol{S}_{nm}^{(1)}$ and $\boldsymbol{S}_{nm}^{(0)}$,

$$\boldsymbol{S}_{nm}^{(-1)}(\vartheta,\varphi) = Y_{nm}\boldsymbol{e}_r\,, \tag{2.17}$$

$$\nabla_\Omega Y_{nm} \equiv \boldsymbol{S}_{nm}^{(1)}(\vartheta,\varphi) = \frac{\partial Y_{nm}}{\partial\vartheta}\boldsymbol{e}_\vartheta + \frac{1}{\sin\vartheta}\frac{\partial Y_{nm}}{\partial\varphi}\boldsymbol{e}_\varphi\,, \tag{2.18}$$

$$\boldsymbol{e}_r\times\nabla_\Omega Y_{nm} \equiv \boldsymbol{S}_{nm}^{(0)}(\vartheta,\varphi) = -\frac{1}{\sin\vartheta}\frac{\partial Y_{nm}}{\partial\varphi}\boldsymbol{e}_\vartheta + \frac{\partial Y_{nm}}{\partial\vartheta}\boldsymbol{e}_\varphi\,, \tag{2.19}$$

cf. (B.28)–(B.30). This orthogonal set of vector functions allows for expanding a vector field into the radial and tangent parts, the latter represented in terms of the surface gradient ∇_Ω and the surface curl $\boldsymbol{e}_r\times\nabla_\Omega$ (the Helmholtz representation); Dahlen & Tromp (1998) can be consulted for more details. The normalization of the vector spherical harmonics has been chosen to conform with Martinec (1999), as is the case of the used notation as well. In the space of square-integrable vector functions defined on the unit sphere, $\boldsymbol{S}_{nm}^{(-1)}$ and $\boldsymbol{S}_{nm}^{(1)}$ form the spheroidal basis (further separable into the radial and consoidal parts), whereas $\boldsymbol{S}_{nm}^{(0)}$ create the toroidal basis.

Since we are confined to the spherically symmetric distribution of density and elastic Lamé parameters, $\varrho_0(r)$, $\lambda(r)$ and $\mu(r)$, the gravitational acceleration is also spherically symmetric, $g_0(r)$. We can write the following expansions of the scalar and vector functions $\mathbf{u}$, φ_1 and $\boldsymbol{e}_r\cdot\boldsymbol{\tau}$,

$$\mathbf{u}(\boldsymbol{r}) = \sum_{nm}\left[U_{nm}(r)\boldsymbol{S}^{(-1)}_{nm} + V_{nm}(r)\boldsymbol{S}^{(1)}_{nm} + W_{nm}(r)\boldsymbol{S}^{(0)}_{nm}\right], \tag{2.20}$$

$$\varphi_1(\boldsymbol{r}) = \sum_{nm} F_{nm}(r)Y_{nm}, \tag{2.21}$$

$$\boldsymbol{e}_r\cdot\boldsymbol{\tau} \equiv \boldsymbol{T}_r(\boldsymbol{r}) = \sum_{nm}\left[T_{rr,nm}(r)\boldsymbol{S}^{(-1)}_{nm} + T_{r\vartheta,nm}(r)\boldsymbol{S}^{(1)}_{nm} + T_{r\varphi,nm}(r)\boldsymbol{S}^{(0)}_{nm}\right]. \tag{2.22}$$

Employing these expansions and expressions given in Appendix B, the following expansions of $\nabla\cdot\mathbf{u}$, $\boldsymbol{e}_r\cdot\boldsymbol{\tau}^E$, $\nabla\cdot\boldsymbol{\tau}^E$, $\boldsymbol{f}$ and $\nabla\cdot(\nabla\varphi_1 + 4\pi G\varrho_0\mathbf{u})$ can be found:

$$\nabla\cdot\mathbf{u} = \sum_{nm} X_{nm}Y_{nm}, \tag{2.23}$$

$$\boldsymbol{e}_r\cdot\boldsymbol{\tau}^E \equiv \boldsymbol{T}^E_r = \sum_{nm}\left[T^E_{rr,nm}\boldsymbol{S}^{(-1)}_{nm} + T^E_{r\vartheta,nm}\boldsymbol{S}^{(1)}_{nm} + T^E_{r\varphi,nm}\boldsymbol{S}^{(0)}_{nm}\right], \tag{2.24}$$

$$\begin{aligned}\nabla\cdot\boldsymbol{\tau}^E = \sum_{nm}\Bigg[&\left(T^{E\,\prime}_{rr,nm} - \frac{4\gamma}{r^2}U_{nm} + \frac{2N\gamma}{r^2}V_{nm} + \frac{4\mu}{r\beta}T^E_{rr,nm} - \frac{N}{r}T^E_{r\vartheta,nm}\right)\boldsymbol{S}^{(-1)}_{nm}\\ &+\left(T^{E\,\prime}_{r\vartheta,nm} + \frac{2\gamma}{r^2}U_{nm} - \frac{N\gamma+(N-2)\mu}{r^2}V_{nm} + \frac{\lambda}{r\beta}T^E_{rr,nm} + \frac{3}{r}T^E_{r\vartheta,nm}\right)\boldsymbol{S}^{(1)}_{nm}\\ &+\left(T^{E\,\prime}_{r\varphi,nm} - \frac{(N-2)\mu}{r^2}W_{nm} + \frac{3}{r}T^E_{r\varphi,nm}\right)\boldsymbol{S}^{(0)}_{nm}\Bigg],\end{aligned} \tag{2.25}$$

$$\begin{aligned}\boldsymbol{f} = \sum_{nm}\Bigg[&\left(\frac{4\varrho_0 g_0}{r}U_{nm} - \frac{N\varrho_0 g_0}{r}V_{nm} + \frac{(n+1)\varrho_0}{r}F_{nm} - \varrho_0 Q_{nm}\right)\boldsymbol{S}^{(-1)}_{nm}\\ &-\left(\frac{\varrho_0 g_0}{r}U_{nm} + \frac{\varrho_0}{r}F_{nm}\right)\boldsymbol{S}^{(1)}_{nm}\Bigg],\end{aligned} \tag{2.26}$$

$$\nabla\cdot(\nabla\varphi_1 + 4\pi G\varrho_0\mathbf{u}) = \sum_{nm}\left[Q'_{nm} + 4\pi G\frac{(n+1)\varrho_0}{r}U_{nm} - 4\pi G\frac{N\varrho_0}{r}V_{nm} - \frac{n-1}{r}Q_{nm}\right]Y_{nm}, \tag{2.27}$$

where the following relations hold,

$$X_{nm} = U'_{nm} + \frac{2U_{nm} - NV_{nm}}{r}, \tag{2.28}$$

$$T^E_{rr,nm} = \lambda X_{nm} + 2\mu U'_{nm} = \beta U'_{nm} + \frac{\lambda}{r}\left(2U_{nm} - NV_{nm}\right), \tag{2.29}$$

$$T^E_{r\vartheta,nm} = \mu\left(V'_{nm} + \frac{U_{nm} - V_{nm}}{r}\right), \tag{2.30}$$

$$T^E_{r\varphi,nm} = \mu\left(W'_{nm} - \frac{W_{nm}}{r}\right), \tag{2.31}$$

$$Q_{nm} = F'_{nm} + \frac{n+1}{r}F_{nm} + 4\pi G\varrho_0 U_{nm}, \tag{2.32}$$

with $\beta = \lambda + 2\mu$, $\gamma = \mu(3\lambda + 2\mu)/\beta$ and $N = n(n+1)$. None of expressions (2.23)–(2.32) contains the second (or higher) derivatives of coefficients in (2.20)–(2.22).

2.3 Ordinary Differential Equations for the SNREI Earth

The spherically symmetric, non-rotating, elastic, isotropic Earth model is considered in this section. We have already collected all necessary spherical harmonic expansions, (2.20)–(2.32), for decomposition of the system of field PDEs (2.13)–(2.14) accompanied with the elastic constitutive relation (2.10), i.e., $\boldsymbol{\tau} = \boldsymbol{\tau}^E$.

We introduce vector $\mathbf{y}^E_{nm}$ with 8 elements,

$$\mathbf{y}^E_{nm} = \left(U_{nm}, V_{nm}, T^E_{rr,nm}, T^E_{r\vartheta,nm}, F_{nm}, Q_{nm}, W_{nm}, T^E_{r\varphi,nm}\right)^T , \tag{2.33}$$

and an 8×8 matrix $\boldsymbol{A}_{nm} \equiv (a_{nm,ik})$, to be expressed later. The elements of $\mathbf{y}^E_{nm}$ are collected in a way allowing trivial decomposition into the spheroidal (elements 1..6) and toroidal (elements 7..8) parts; the spheroidal elements are ordered in accord with, e.g., Peltier (1974). As all the expansions (2.23)–(2.32) are decoupled with respect to both degree n and order m, we suppress these subscripts throughout this section when referring to the elements $y^E_{nm,k}$ and $a_{nm,ik}$ of $\mathbf{y}^E_{nm}$ and $\boldsymbol{A}_{nm}$, respectively.

By substitution of $\mathbf{y}^E_{nm}$ into (2.29)–(2.32) we arrive at

$$y_1^{E\prime} = \textstyle\sum_k a_{1k} y_k^E , \qquad a_{1,1..8} = \left(-\frac{2\lambda}{r\beta}, \frac{N\lambda}{r\beta}, \frac{1}{\beta}, 0, 0, 0, 0, 0\right) , \tag{2.34}$$

$$y_2^{E\prime} = \textstyle\sum_k a_{2k} y_k^E , \qquad a_{2,1..8} = \left(-\frac{1}{r}, \frac{1}{r}, 0, \frac{1}{\mu}, 0, 0, 0, 0\right) , \tag{2.35}$$

$$y_5^{E\prime} = \textstyle\sum_k a_{5k} y_k^E , \qquad a_{5,1..8} = \left(-4\pi G\varrho_0, 0, 0, 0, -\frac{n+1}{r}, 1, 0, 0\right) , \tag{2.36}$$

$$y_7^{E\prime} = \textstyle\sum_k a_{7k} y_k^E , \qquad a_{7,1..8} = \left(0, 0, 0, 0, 0, 0, \frac{1}{r}, \frac{1}{\mu}\right) \tag{2.37}$$

with $\sum_k$ abbreviating $\sum_{k=1}^{8}$. Next we rewrite (2.25)–(2.26) into the form

$$\nabla \cdot \boldsymbol{\tau}^E = \textstyle\sum_{nm} \left[\left(y_3^{E\prime} - \sum_k b_{3k} y_k^E\right) \boldsymbol{S}^{(-1)}_{nm} + \left(y_4^{E\prime} - \sum_k b_{4k} y_k^E\right) \boldsymbol{S}^{(1)}_{nm} + \left(y_8^{E\prime} - \sum_k b_{8k} y_k^E\right) \boldsymbol{S}^{(0)}_{nm} \right] , \tag{2.38}$$

$$\boldsymbol{f} = \textstyle\sum_{nm} \left[-\sum_k c_{3k} y_k^E \boldsymbol{S}^{(-1)}_{nm} - \sum_k c_{4k} y_k^E \boldsymbol{S}^{(1)}_{nm} \right] , \tag{2.39}$$

with the auxiliary coefficients, b_{ik} and c_{ik}, given by

$$b_{3,1..8} = \left(\frac{4\gamma}{r^2}, -\frac{2N\gamma}{r^2}, -\frac{4\mu}{r\beta}, \frac{N}{r}, 0, 0, 0, 0\right) , \tag{2.40}$$

$$b_{4,1..8} = \left(-\frac{2\gamma}{r^2}, \frac{N\gamma + (N-2)\mu}{r^2}, -\frac{\lambda}{r\beta}, -\frac{3}{r}, 0, 0, 0, 0\right) , \tag{2.41}$$

$$b_{8,1..8} = \left(0, 0, 0, 0, 0, \frac{(N-2)\mu}{r^2}, -\frac{3}{r}\right) , \tag{2.42}$$

$$c_{3,1..8} = \left(-\frac{4\varrho_0 g_0}{r}, \frac{N\varrho_0 g_0}{r}, 0, 0, -\frac{(n+1)\varrho_0}{r}, \varrho_0, 0, 0\right) , \tag{2.43}$$

$$c_{4,1..8} = \left(\frac{\varrho_0 g_0}{r}, 0, 0, 0, \frac{\varrho_0}{r}, 0, 0, 0\right) . \tag{2.44}$$

With (2.38)–(2.39) and $\boldsymbol{\tau} = \boldsymbol{\tau}^E$ we can convert momentum equation (2.13) into the three scalar equations,

$$y_3^{E\prime} = \textstyle\sum_k a_{3k} y_k^E , \qquad a_{3,1..8} = b_{3,1..8} + c_{3,1..8} , \tag{2.45}$$

$$y_4^{E\prime} = \textstyle\sum_k a_{4k} y_k^E , \qquad a_{4,1..8} = b_{4,1..8} + c_{4,1..8} , \tag{2.46}$$

$$y_8^{E\prime} = \textstyle\sum_k a_{8k} y_k^E , \qquad a_{8,1..8} = b_{8,1..8} . \tag{2.47}$$

Finally the Poisson equation (2.14) combined with (2.27) gives

$$y_6^{E\prime} = \textstyle\sum_k a_{6k} y_k^E , \qquad a_{6,1..8} = \left(-4\pi G\frac{(n+1)\varrho_0}{r}, 4\pi G\frac{N\varrho_0}{r}, 0, 0, 0, \frac{n-1}{r}, 0, 0\right) . \tag{2.48}$$

We have arrived at the linear first-order system of ODEs with respect to r for the solution vector $\mathbf{y}^E_{nm}$, assembled from (2.34)–(2.37) and (2.45)–(2.48),

$$\mathbf{y}^{E\,\prime}_{nm}(r) \;=\; \boldsymbol{A}_n(r)\mathbf{y}^E_{nm}(r)\,, \tag{2.49}$$

with matrix $\boldsymbol{A}_n(r)$ equal to

$$\boldsymbol{A}_n = \begin{pmatrix}
-\frac{2\lambda}{r\beta} & \frac{N\lambda}{r\beta} & \frac{1}{\beta} & 0 & 0 & 0 & 0 & 0 \\
-\frac{1}{r} & \frac{1}{r} & 0 & \frac{1}{\mu} & 0 & 0 & 0 & 0 \\
\frac{4\gamma}{r^2}-\frac{4\varrho_0 g_0}{r} & -\frac{2N\gamma}{r^2}+\frac{N\varrho_0 g_0}{r} & -\frac{4\mu}{r\beta} & \frac{N}{r} & -\frac{(n+1)\varrho_0}{r} & \varrho_0 & 0 & 0 \\
-\frac{2\gamma}{r^2}+\frac{\varrho_0 g_0}{r} & \frac{N\gamma+(N-2)\mu}{r^2} & -\frac{\lambda}{r\beta} & -\frac{3}{r} & \frac{\varrho_0}{r} & 0 & 0 & 0 \\
-4\pi G\varrho_0 & 0 & 0 & 0 & -\frac{n+1}{r} & 1 & 0 & 0 \\
-4\pi G\frac{(n+1)\varrho_0}{r} & 4\pi G\frac{N\varrho_0}{r} & 0 & 0 & 0 & \frac{n-1}{r} & 0 & 0 \\
0 & 0 & 0 & 0 & 0 & 0 & \frac{1}{r} & \frac{1}{\mu} \\
0 & 0 & 0 & 0 & 0 & 0 & \frac{(N-2)\mu}{r^2} & -\frac{3}{r}
\end{pmatrix}, \tag{2.50}$$

and, let us recall, $\beta = \lambda + 2\mu$, $\gamma = \mu(3\lambda + 2\mu)/\beta = 3\mu K/\beta$ and $N = n(n+1)$. For the case of material incompressibility, $K \to \infty$, the following expressions should be considered instead:

$$1/\beta \to 0\,, \quad \lambda/\beta \to 1\,, \quad \text{and} \quad \gamma \to 3\mu\,. \tag{2.51}$$

System (2.49) is decoupled with respect to both degree n and order m, and for each n and m consists of two independent systems, one with 6×6 matrix $(a_{1..6,1..6})$, connecting the spheroidal coefficients of $\mathbf{u}$ and $\boldsymbol{\tau}^E$, and another with 2×2 matrix $(a_{7..8,7..8})$, containing the toroidal coefficients. Moreover, matrix $\boldsymbol{A}_n(r)$ is independent of m. The spherical harmonic representation of the surface boundary conditions for the point mass load, $\gamma_L(\vartheta) = \sum_n \Gamma_n P_{n0}(\cos\vartheta)$ (Farrell 1972), reads

$$\begin{pmatrix} y_3(a) \\ y_4(a) \\ y_6(a) \\ y_8(a) \end{pmatrix} = \frac{1}{N_n}\begin{pmatrix} -g_0\Gamma_n \\ 0 \\ -4\pi G\Gamma_n \\ 0 \end{pmatrix}, \quad N_n = \sqrt{\frac{2n+1}{4\pi}}\,, \quad \Gamma_n = \frac{2n+1}{4\pi a^2}\,, \tag{2.52}$$

where a is the radius of the Earth and the norm factors N_n come from (2.16).

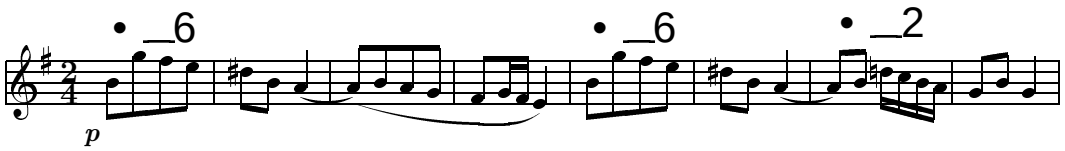

ANTONÍN DVOŘÁK, *Slavonic Dances, Op. 46. No. 2 in E minor. Allegretto scherzando* (1878)

Chapter 3

Viscoelastic Response of the Earth

The main result of Chapter 2, the boundary-value problem (2.49) for the linear first-order ODEs, has been known for four decades in the field of gravitational elastodynamics. Peltier (1974) reformulated the problem of gravitational viscoelastodynamics within the Laplace domain and obtained a set of ODEs formally identical with (2.49) but implicitly parametrized by the Laplace variable s. In this chapter we reformulate the problem of gravitational viscoelastodynamics within the time domain. For the spherically symmetric (1-D), Maxwell Earth model we derive a linear first-order system of PDEs (3.23) with respect to both time and the radius for a time-dependent solution vector $\mathbf{y}_{nm}(t,r)$, constructed from coefficients of spherical harmonic expansions of field variables. We derive similar PDEs (3.56) for the case of the constitutive relation of the standard linear solid and find a generalized set of PDEs (3.104) for the case of axially symmetric (2-D) viscosity distribution. PDEs (3.23), however, become the major outcome of this chapter, further elaborated in Chapter 4.

To establish a starting point, we recall the field PDEs (2.13)–(2.15) in the form appropriate for further advance. The constitutive relation of the Maxwell rheology reads

$$\dot{\boldsymbol{\tau}} \;=\; \dot{\boldsymbol{\tau}}^E - \xi\,(\boldsymbol{\tau} - K\nabla\cdot\mathbf{u}\boldsymbol{I})\;, \tag{3.1}$$

where, for brevity, the auxiliary parameter ξ equal to the ratio of the shear modulus and viscosity, i.e., the inverse Maxwell time,

$$\xi \;=\; \frac{\mu}{\eta}\,, \tag{3.2}$$

has been introduced. The field equations combined with (3.1) can be written in the form

$$\nabla\cdot\dot{\boldsymbol{\tau}}^E + \dot{\boldsymbol{f}} \;=\; \nabla\cdot\left[\xi\,(\boldsymbol{\tau} - K\nabla\cdot\mathbf{u}\boldsymbol{I})\right]\;, \tag{3.3}$$

$$\nabla\cdot(\nabla\varphi_1 + 4\pi G\varrho_0\mathbf{u}) \;=\; 0\,. \tag{3.4}$$

Let us recall that $\boldsymbol{\tau}^E$ is the elastic part of the stress tensor $\boldsymbol{\tau}$ given by (2.10) and that the dots denote time differentiation. The steps to be undertaken are similar to those made in Chapter 2. In addition we have to consider a new form of (3.1) and (3.3) and express a resulting system of PDEs in terms of $\mathbf{y}_{nm}$ instead of $\mathbf{y}^E_{nm}$.

3.1 Differential Equations for the Spherical Viscoelastic Earth

3.1.1 Partial Differential Equations for the Maxwell Solid

A system of PDEs with respect to time and the radius for the viscoelastic response of the spherically symmetric, non-rotating, Maxwell Earth model is to be derived. We consider the spatial distribution of the parameters and field variables as follows:

$$\varrho_0 = \varrho_0(r)\,, \quad \lambda = \lambda(r)\,, \quad \mu = \mu(r)\,, \quad K = K(r)\,, \quad g_0 = g_0(r)\,, \quad \eta = \eta(r)\,, \quad \xi = \xi(r)\,, \tag{3.5}$$

$$\mathbf{u} = \mathbf{u}(r,\vartheta,\varphi)\,, \quad \varphi_1 = \varphi_1(r,\vartheta,\varphi)\,, \quad \boldsymbol{\tau} = \boldsymbol{\tau}(r,\vartheta,\varphi)\,. \tag{3.6}$$

We construct the solution vector $\mathbf{y}_{nm}(t,r)$ from the coefficients of the spherical harmonic expansions of $\mathbf{u}$, φ_1 and $\boldsymbol{\tau}$,

$$\mathbf{y}_{nm}(t,r) \;=\; (U_{nm}, V_{nm}, T_{rr,nm}, T_{r\vartheta,nm}, F_{nm}, Q_{nm}, W_{nm}, T_{r\varphi,nm})^T\,. \tag{3.7}$$

We see that $\mathbf{y}_{nm}$ only differs from the elastic solution vector $\mathbf{y}^E_{nm}$ given by (2.33),

$$\mathbf{y}^E_{nm}(r) \;=\; \big(U_{nm}, V_{nm}, T^E_{rr,nm}, T^E_{r\vartheta,nm}, F_{nm}, Q_{nm}, W_{nm}, T^E_{r\varphi,nm}\big)^T\,, \tag{3.8}$$

in the coefficients of the spherical harmonic expansions of the stress vector $\boldsymbol{T}_r \equiv \boldsymbol{e}_r \cdot \boldsymbol{\tau}$, connected with the stress vector $\boldsymbol{T}^E_r \equiv \boldsymbol{e}_r \cdot \boldsymbol{\tau}^E$ through the relation following from (3.1),

$$\dot{\boldsymbol{T}}_r \;=\; \dot{\boldsymbol{T}}^E_r - \xi\,(\boldsymbol{T}_r - K\nabla\cdot\mathbf{u}\,\boldsymbol{e}_r)\,. \tag{3.9}$$

We remark that the stress vector $\boldsymbol{T}_r$ is only needed for the evaluation of the response in the 1-D case; using other stress vectors becomes necessary later. From (3.7)–(3.9) we obtain the following relations between the corresponding elements of $\mathbf{y}_{nm}$ and $\mathbf{y}^E_{nm}$,

$$\begin{aligned} &\dot y^E_1 = \dot y_1\,, \qquad \dot y^E_2 = \dot y_2\,, \qquad \dot y^E_5 = \dot y_5\,, \qquad \dot y^E_6 = \dot y_6\,, \qquad \dot y^E_7 = \dot y_7\,, \\ &\dot y^E_3 = \dot y_3 + \xi(y_3 - KX)\,, \qquad \dot y^E_4 = \dot y_4 + \xi y_4\,, \qquad \dot y^E_8 = \dot y_8 + \xi y_8\,, \qquad X = y_1' + (2y_1 - Ny_2)/r\,. \end{aligned} \tag{3.10}$$

We suppress the subscripts n, m throughout this section when referring to the elements $y_{nm,k}$ and $a_{nm,ik}$ of $\mathbf{y}_{nm}$ and $\boldsymbol{A}_{nm}$, respectively; matrix $\boldsymbol{A}_{nm}$ is as in (2.50) as will be shown. Symbol X stands for X_{nm}, the coefficients of the spherical harmonic expansion (2.23) of $\nabla\cdot\mathbf{u}$. In the 1-D case the resulting system of PDEs remains decoupled with respect to both n and m which will justify this policy.

In (2.34)–(2.37) the four relations containing the first derivatives of the coefficients of $\mathbf{u}$ and φ_1, namely $y^{E\prime}_1$, $y^{E\prime}_2$, $y^{E\prime}_5$ and $y^{E\prime}_7$, are collected. These relations remain valid in the viscoelastic case, and the only necessary arrangement is the change of variables from $\mathbf{y}^E_{nm}$ to $\mathbf{y}_{nm}$ in accordance with (3.10). This results in the four equations for elements of $\mathbf{y}_{nm}$,

$$\dot y_1' - \textstyle\sum_k a_{1k}\dot y_k \;=\; \xi\,[a_{13}(y_3 - KX) + a_{14}y_4 + a_{18}y_8] \;=\; \xi a_{13}(y_3 - KX)\,, \tag{3.11}$$

$$\dot y_2' - \textstyle\sum_k a_{2k}\dot y_k \;=\; \xi\,[a_{23}(y_3 - KX) + a_{24}y_4 + a_{28}y_8] \;=\; \xi a_{24}y_4\,, \tag{3.12}$$

$$\dot y_5' - \textstyle\sum_k a_{5k}\dot y_k \;=\; \xi\,[a_{53}(y_3 - KX) + a_{54}y_4 + a_{58}y_8] \;=\; 0\,, \tag{3.13}$$

$$\dot y_7' - \textstyle\sum_k a_{7k}\dot y_k \;=\; \xi\,[a_{73}(y_3 - KX) + a_{74}y_4 + a_{78}y_8] \;=\; \xi a_{78}y_8\,, \tag{3.14}$$

where $\sum_k$ stands for $\sum_{k=1}^8$ and the zero terms (i.e., those with a_{14}, a_{18}, a_{23}, a_{28}, a_{53}, a_{54}, a_{58}, a_{73} and a_{74}) have been discarded.

The next step is to express the momentum equation (3.3) in terms of $\mathbf{y}_{nm}$. We need to substitute $\mathbf{y}_{nm}$ into the l.h.s. of (3.3), expressed in terms of $\mathbf{y}^E_{nm}$ in (2.38)–(2.39), and to evaluate the r.h.s. of (3.3). We substitute (3.10) into (2.38)–(2.39), differentiated with respect to time,

$$\begin{aligned}
\nabla\cdot\dot{\boldsymbol{\tau}}^E &= \textstyle\sum_{nm}[\dot{y}_3' + (\xi(y_3-KX))' - \sum_k b_{3k}\dot{y}_k - b_{33}\xi(y_3-KX) - b_{34}\xi y_4]\boldsymbol{S}^{(-1)}_{nm} \qquad (3.15)\\
&+ \textstyle\sum_{nm}[\dot{y}_4' + (\xi y_4)' - \sum_k b_{4k}\dot{y}_k - b_{43}\xi(y_3-KX) - b_{44}\xi y_4]\boldsymbol{S}^{(1)}_{nm}\\
&+ \textstyle\sum_{nm}[\dot{y}_8' + (\xi y_8)' - \sum_k b_{8k}\dot{y}_k - b_{88}\xi y_8]\boldsymbol{S}^{(0)}_{nm}\,,\\
\dot{\boldsymbol{f}} &= \textstyle\sum_{nm}[-\sum_k c_{3k}\dot{y}_k\boldsymbol{S}^{(-1)}_{nm} - \sum_k c_{4k}\dot{y}_k\boldsymbol{S}^{(1)}_{nm}]\,, \qquad (3.16)
\end{aligned}$$

where the zero terms (those with b_{38}, b_{48}, b_{83}, b_{84}, c_{33}, c_{34}, c_{38}, c_{43}, c_{44} and c_{48}) have been discarded. For the r.h.s. of (3.3) we can write

$$\begin{aligned}
\nabla\cdot[\xi\,(\boldsymbol{\tau} - K\nabla\cdot\mathbf{u}\boldsymbol{I})] &= \xi\,[\nabla\cdot\boldsymbol{\tau} - \nabla(K\nabla\cdot\mathbf{u})] + \nabla\xi\cdot[\boldsymbol{\tau} - K\nabla\cdot\mathbf{u}\boldsymbol{I}]\\
&= \xi\,[-\boldsymbol{f} - \nabla(K\nabla\cdot\mathbf{u})] + \xi'\,[\boldsymbol{T}_r - K\nabla\cdot\mathbf{u}\boldsymbol{e}_r]\\
&= \textstyle\sum_{nm}\,[\xi\sum_k c_{3k}y_k - \xi(KX)' + \xi'(y_3 - KX)]\,\boldsymbol{S}^{(-1)}_{nm} \qquad (3.17)\\
&+ \textstyle\sum_{nm}\,[\xi\sum_k c_{4k}y_k - \xi KX/r + \xi' y_4]\,\boldsymbol{S}^{(1)}_{nm}\\
&+ \textstyle\sum_{nm}\,[\xi' y_8]\,\boldsymbol{S}^{(0)}_{nm}\,,
\end{aligned}$$

where (B.36) has been used for representation of $\nabla(K\nabla\cdot\mathbf{u})$. With (3.15)–(3.17) we can extract the three scalar components of (3.3). Removing terms which appear on the both sides, we obtain the following equations,

$$\begin{aligned}
\dot{y}_3' - \textstyle\sum_k a_{3k}\dot{y}_k &= \xi\,[-y_3' + b_{33}(y_3 - KX) + b_{34}y_4 + \textstyle\sum_k c_{3k}y_k] \qquad (3.18)\\
&= \xi\,[-y_3' + \textstyle\sum_k a_{3k}y_k - b_{31}y_1 - b_{32}y_2 - b_{33}KX]\,,\\
\dot{y}_4' - \textstyle\sum_k a_{4k}\dot{y}_k &= \xi\,[-y_4' + b_{43}(y_3 - KX) + b_{44}y_4 + \textstyle\sum_k c_{4k}y_k - KX/r] \qquad (3.19)\\
&= \xi\,[-y_4' + \textstyle\sum_k a_{4k}y_k - b_{41}y_1 - b_{42}y_2 - (b_{43} + 1/r)KX]\,,\\
\dot{y}_8' - \textstyle\sum_k a_{8k}\dot{y}_k &= \xi\,[-y_8' + b_{88}y_8] \quad = \quad \xi\,[-y_8' + \textstyle\sum_k a_{8k}y_k - b_{87}y_7]\,. \qquad (3.20)
\end{aligned}$$

We recall that $a_{3k} = b_{3k} + c_{3k}$, $a_{4k} = b_{4k} + c_{4k}$ and $a_{8k} = b_{8k}$, $k = 1,\ldots,8$, according to (2.45)–(2.47).

The last step is accomplished by substitution of the elements of $\mathbf{y}_{nm}$ into the spherical harmonic expansion of the Poisson equation given by (2.48) and differentiated with respect to time. Due to the zero values of a_{63}, a_{64} and a_{68}, we obtain

$$\dot{y}_6' - \textstyle\sum_k a_{6k}\dot{y}_k \;=\; 0\,. \qquad (3.21)$$

With (3.11)–(3.14) and (3.18)–(3.21) we have arrived at a linear system of PDEs with respect to time and the radius for the solution vector $\mathbf{y}_{nm}$,

$$\dot{\mathbf{y}}'_{nm}(t,r) - \boldsymbol{A}_n(r)\dot{\mathbf{y}}_{nm}(t,r) \;=\; \xi\begin{pmatrix}
a_{13}(y_3 - KX)\\
a_{24}y_4\\
-y_3' + \sum_k a_{3k}y_k - b_{31}y_1 - b_{32}y_2 - b_{33}KX\\
-y_4' + \sum_k a_{4k}y_k - b_{41}y_1 - b_{42}y_2 - (b_{43} + 1/r)KX\\
0\\
0\\
a_{78}y_8\\
-y_8' + \sum_k a_{8k}y_k - b_{87}y_7
\end{pmatrix}, \qquad (3.22)$$

which can be rewritten into the form

$$\dot{\mathbf{y}}'_{nm}(t,r) - \boldsymbol{A}_n(r)\dot{\mathbf{y}}_{nm}(t,r) \;=\; \xi(r)\left[\boldsymbol{D}_n(r)\mathbf{y}'_{nm}(t,r) + \boldsymbol{E}_n(r)\mathbf{y}_{nm}(t,r)\right]. \tag{3.23}$$

Matrix $\boldsymbol{A}_n(r)$ keeps the form of (2.50) and the explicit expressions of the matrices $\boldsymbol{D}_n(r)$ and $\boldsymbol{E}_n(r)$ follow from (3.22) after substitution for a_{13}, …, b_{87} from (2.50) and for X from (2.23),

$$\boldsymbol{D}_n = \begin{pmatrix} -\frac{K}{\beta} & 0 & 0 & 0 & 0 & 0 & 0 & 0 \\ 0 & 0 & 0 & 0 & 0 & 0 & 0 & 0 \\ \frac{4\gamma}{3r} & 0 & -1 & 0 & 0 & 0 & 0 & 0 \\ -\frac{2\gamma}{3r} & 0 & 0 & -1 & 0 & 0 & 0 & 0 \\ 0 & 0 & 0 & 0 & 0 & 0 & 0 & 0 \\ 0 & 0 & 0 & 0 & 0 & 0 & 0 & 0 \\ 0 & 0 & 0 & 0 & 0 & 0 & 0 & 0 \\ 0 & 0 & 0 & 0 & 0 & 0 & 0 & -1 \end{pmatrix}, \tag{3.24}$$

$$\boldsymbol{E}_n = \begin{pmatrix} -\frac{2K}{r\beta} & \frac{NK}{r\beta} & \frac{1}{\beta} & 0 & 0 & 0 & 0 & 0 \\ 0 & 0 & 0 & \frac{1}{\mu} & 0 & 0 & 0 & 0 \\ \frac{8\gamma}{3r^2} - \frac{4\varrho_0 g_0}{r} & -\frac{4N\gamma}{3r^2} + \frac{N\varrho_0 g_0}{r} & -\frac{4\mu}{r\beta} & \frac{N}{r} & -\frac{(n+1)\varrho_0}{r} & \varrho_0 & 0 & 0 \\ -\frac{4\gamma}{3r^2} + \frac{\varrho_0 g_0}{r} & \frac{2N\gamma}{3r^2} & -\frac{\lambda}{r\beta} & -\frac{3}{r} & \frac{\varrho_0}{r} & 0 & 0 & 0 \\ 0 & 0 & 0 & 0 & 0 & 0 & 0 & 0 \\ 0 & 0 & 0 & 0 & 0 & 0 & 0 & 0 \\ 0 & 0 & 0 & 0 & 0 & 0 & 0 & \frac{1}{\mu} \\ 0 & 0 & 0 & 0 & 0 & 0 & 0 & -\frac{3}{r} \end{pmatrix}. \tag{3.25}$$

We recall that $\beta = \lambda + 2\mu$, $\gamma = \mu(3\lambda + 2\mu)/\beta = 3\mu K/\beta$ and $N = n(n+1)$, or, in the case of material incompressibility, $1/\beta \to 0$, $\lambda/\beta \to 1$, $K/\beta \to 1$ and $\gamma \to 3\mu$. Similarly to the elastic case, system (3.23) is separated with respect to both n and m and matrices $\boldsymbol{A}_n$, $\boldsymbol{D}_n$ and $\boldsymbol{E}_n$ from (3.23) remain independent of m and consist of 6×6 spheroidal and 2×2 toroidal blocks. Note that with the surface boundary conditions evoked by the point mass load, the spheroidal part of the system only needs to be solved. An appropriate procedure of numerical solution to this system is discussed in Chapter 4.

3.1.2 Initial and Boundary Conditions

To treat PDEs (3.23) as an IV problem, one needs to specify the initial condition, e.g., the value of $\mathbf{y}_{nm}(t,r)$ for $t = 0$. From now on we consider the point mass load with the Heaviside dependence in time, i.e., the point mass load applied at the surface, $r = a$, in the time instant $t = 0$ and effecting continuously for $t > 0$. The Maxwell Earth responds elastically in the time instant of the load application, thus, the appropriate initial condition is $\mathbf{y}_{nm}(0,r) = \mathbf{y}^E_{nm}(r)$.

Surface boundary conditions for this load keep the form of (2.52),

$$\begin{pmatrix} y_3(a) \\ y_4(a) \\ y_6(a) \\ y_8(a) \end{pmatrix} = \frac{1}{N_n} \begin{pmatrix} -g_0\Gamma_n \\ 0 \\ -4\pi G\Gamma_n \\ 0 \end{pmatrix}, \quad N_n = \sqrt{\frac{2n+1}{4\pi}}, \quad \Gamma_n = \frac{2n+1}{4\pi a^2}, \tag{3.26}$$

uniformly for $t \geq 0$. At internal solid boundaries (i.e., between two layers of non-zero shear modulus μ), the continuity of all elements of $\mathbf{y}_{nm}(t,r)$ is required, and at liquid boundaries (between a solid layer, $\mu \neq 0$, and a liquid layer, $\mu = 0$) the boundary conditions are according to, e.g., Wu & Peltier (1982). At $r = 0$, finite values of $\mathbf{y}_{nm}$ are expected.

To find the initial condition for a spherically symmetric model with arbitrary distribution of density and elastic parameters, ODEs (2.49) must be solved numerically. However, for the homogeneous Earth model the solutions are known analytically. Moreover, these solutions can be employed in numerical integration for arbitrarily stratified models as the starting solutions, as is described in Section 6.2.2. Hence, it makes sense to rewrite here explicitly three independent solutions to (2.49) for a compressible model (λ finite) with constant values of ϱ_0, λ and μ (e.g., Wu & Peltier 1982),

$$\mathbf{y}_1 = \begin{pmatrix} -\dfrac{NCj_n(kr) + krj_n'(kr)}{k^2 r} \\ -\dfrac{(1+C)j_n(kr) + Ckrj_n'(kr)}{k^2 r} \\ \lambda j_n(kr) + 2\mu\left[\dfrac{NC}{kr}\left(\dfrac{j_n(kr)}{kr} - j_n'(kr)\right) - j_n''(kr)\right] \\ -\mu C j_n(kr) + 2\mu\left[\dfrac{1+C}{kr}\left(\dfrac{j_n(kr)}{kr} - j_n'(kr)\right) - Cj_n''(kr)\right] \\ \dfrac{3\varsigma j_n(kr)}{k^2} \\ \dfrac{3\varsigma(1-nC)(1+n)j_n(kr)}{k^2 r} \end{pmatrix}, \quad \mathbf{y}_3 = \begin{pmatrix} nr^{n-1} \\ r^{n-1} \\ 2\mu n(n-1)r^{n-2} \\ 2\mu(n-1)r^{n-2} \\ -n\varsigma r^n \\ -2n(n-1)\varsigma r^{n-1} \end{pmatrix}, \tag{3.27}$$

where $\varsigma = \frac{4}{3}\pi G\varrho_0$, $N = n(n+1)$ and j_n, j_n' and j_n'' are the spherical Bessel functions and their first and second derivatives, respectively. Solution vector $\mathbf{y}_2$ preserves the form of $\mathbf{y}_1$ with k replaced by q and C by D where

$$2k^2 = \frac{4\varsigma\varrho_0}{\beta} + \sqrt{\left(\frac{4\varsigma\varrho_0}{\beta}\right)^2 + \frac{4N\varsigma^2\varrho_0^2}{\mu\beta}}, \qquad 2q^2 = \frac{4\varsigma\varrho_0}{\beta} - \sqrt{\left(\frac{4\varsigma\varrho_0}{\beta}\right)^2 + \frac{4N\varsigma^2\varrho_0^2}{\mu\beta}}, \tag{3.28}$$

$$C = -\frac{\varsigma\varrho_0}{\mu k^2}, \qquad D = -\frac{\varsigma\varrho_0}{\mu q^2}, \tag{3.29}$$

with $\beta = \lambda + 2\mu$.

3.1.3 Partial Differential Equations for the Standard Linear Solid

We have found the system of evolutional PDEs (3.23) which governs the response of the spherically symmetric, Maxwell Earth. To demonstrate the applicability of the IV approach to other viscoelastic rheologies, we derive a similar system of PDEs for the spherically symmetric Earth responding as the standard linear solid. In popular conventional analogy, which expresses various viscoelastic rheologies by means of springs and dashpots (e.g., Peltier 1982; Dahlen & Tromp 1998),

the Maxwell solid is the serial connection of a spring (μ) and a dashpot (η), the Kelvin-Voight solid is the parallel connection of a spring (μ) and a dashpot (η), and the standard linear solid is either the parallel connection of a spring and a Maxwell element or the serial connection of a spring (μ_1) and a Kelvin-Voight element (μ_2, η).

We consider the constitutive relation of the standard linear solid (e.g., Peltier 1982) in the form which conforms with the latter, serial analogy of standard linear solid mentioned above,

$$\dot{\boldsymbol{\tau}} + \frac{\mu 1 + \mu 2}{\eta}\left(\boldsymbol{\tau} - \frac{1}{3}\bar{\boldsymbol{\tau}}\,\boldsymbol{I}\right) = \lambda\,\dot{\bar{e}}\,\boldsymbol{I} + 2\mu_1\,\dot{\boldsymbol{e}} + \frac{2\mu_1\mu_2}{\eta}\left(\boldsymbol{e} - \frac{1}{3}\bar{\boldsymbol{e}}\,\boldsymbol{I}\right), \tag{3.30}$$

where λ and μ_1 are the elastic Lamé parameters and μ_2 and η are the shear modulus and the viscosity associated with the Kelvin-Voight element, respectively. For brevity, we invoke the auxiliary parameters

$$\xi_1 = \frac{\mu_1 + \mu_2}{\eta}\,, \qquad \xi_2 = \frac{2\mu_1\mu_2}{\eta} \tag{3.31}$$

with the physical units s^{-1} and $\mathrm{Pa\,s}^{-1}$, respectively. The constitutive relation (3.30) and the field PDEs (2.13)–(2.14) take the form

$$\begin{aligned}
\dot{\boldsymbol{\tau}} &= \dot{\boldsymbol{\tau}}^E - \xi_1(\boldsymbol{\tau} - K\nabla\cdot\mathbf{u}\boldsymbol{I}) + \xi_2(\boldsymbol{e} - \tfrac{1}{3}\nabla\cdot\mathbf{u}\boldsymbol{I})\,, && (3.32)\\
\nabla\cdot\dot{\boldsymbol{\tau}}^E + \dot{\boldsymbol{f}} &= \nabla\cdot\left[\xi_1(\boldsymbol{\tau} - K\nabla\cdot\mathbf{u}\boldsymbol{I}) - \xi_2(\boldsymbol{e} - \tfrac{1}{3}\nabla\cdot\mathbf{u}\boldsymbol{I})\right], && (3.33)\\
\nabla\cdot(\nabla\varphi_1 + 4\pi G\varrho_0\mathbf{u}) &= 0\,. && (3.34)
\end{aligned}$$

We have substituted $\boldsymbol{\tau}^E = \lambda\,\bar{\boldsymbol{e}}\,\boldsymbol{I} + 2\mu_1\,\boldsymbol{e}$ and the first invariants of the strain and stress tensors, $\bar{e} = \nabla\cdot\mathbf{u}$ and $\bar{\tau} = (3\lambda + 2\mu_1)\nabla\cdot\mathbf{u} = 3K\nabla\cdot\mathbf{u}$, with the latter obtained from (3.30).

The following steps repeat those made for the Maxwell Earth, so we comment on them briefly. It follows from (3.32) for the stress vector $\boldsymbol{T}_r \equiv \boldsymbol{e}_r\cdot\boldsymbol{\tau}$ that

$$\dot{\boldsymbol{T}}_r = \dot{\boldsymbol{T}}_r^E - \xi_1(\boldsymbol{T}_r - K\nabla\cdot\mathbf{u}\,\boldsymbol{e}_r) + \xi_2(\boldsymbol{E}_r - \tfrac{1}{3}\nabla\cdot\mathbf{u}\,\boldsymbol{e}_r)\,, \tag{3.35}$$

where the spherical harmonic expansion of $\boldsymbol{E}_r \equiv \boldsymbol{e}_r\cdot\boldsymbol{e} = \sum_{nm}[E_r\boldsymbol{S}_{nm}^{(-1)} + E_\vartheta\boldsymbol{S}_{nm}^{(1)} + E_\varphi\boldsymbol{S}_{nm}^{(0)}]$ is given by (B.53). We make use of both definitions (3.7)–(3.8) of $\mathbf{y}_{nm}(t,r)$ and $\mathbf{y}_{nm}^E(t,r)$ for expressing the scalar components of $\boldsymbol{T}_r$,

$$\dot{y}_3^E = \dot{y}_3 + \xi_1(y_3 - KX) - \xi_2(E_r - X/3)\,, \quad \dot{y}_4^E = \dot{y}_4 + \xi_1 y_4 - \xi_2 E_\vartheta\,, \quad \dot{y}_8^E = \dot{y}_8 + \xi_1 y_8 - \xi_2 E_\varphi\,. \tag{3.36}$$

Equations similar to (3.11)–(3.14) then take the form

$$\begin{aligned}
\dot{y}_1' - \textstyle\sum_k a_{1k}\dot{y}_k &= a_{13}\left[\xi_1(y_3 - KX) - \xi_2(E_r - X/3)\right], && (3.37)\\
\dot{y}_2' - \textstyle\sum_k a_{2k}\dot{y}_k &= a_{24}\left[\xi_1 y_4 - \xi_2 E_\vartheta\right], && (3.38)\\
\dot{y}_5' - \textstyle\sum_k a_{5k}\dot{y}_k &= 0\,, && (3.39)\\
\dot{y}_7' - \textstyle\sum_k a_{7k}\dot{y}_k &= a_{78}\left[\xi_1 y_8 - \xi_2 E_\varphi\right]. && (3.40)
\end{aligned}$$

For the expressions on the l.h.s. of (3.33) we obtain

$$\begin{aligned}
\nabla\cdot\dot{\boldsymbol{\tau}}^E &= \textstyle\sum_{nm}\big[\dot{y}_3' + (\xi_1(y_3 - KX) - \xi_2(E_r - X/3))' - \sum_k b_{3k}\dot{y}_k && (3.41)\\
&\qquad - b_{33}(\xi_1(y_3 - KX) - \xi_2(E_r - X/3)) - b_{34}(\xi_1 y_4 - \xi_2 E_\vartheta)\big]\boldsymbol{S}_{nm}^{(-1)}\\
&+ \textstyle\sum_{nm}\big[\dot{y}_4' + (\xi_1 y_4 - \xi_2 E_\vartheta)' - \sum_k b_{4k}\dot{y}_k\\
&\qquad - b_{43}(\xi_1(y_3 - KX) - \xi_2(E_r - X/3)) - b_{44}(\xi_1 y_4 - \xi_2 E_\vartheta)\big]\boldsymbol{S}_{nm}^{(1)}\\
&+ \textstyle\sum_{nm}\big[\dot{y}_8' + (\xi_1 y_8 - \xi_2 E_\varphi)' - \sum_k b_{8k}\dot{y}_k - b_{88}(\xi_1 y_8 - \xi_2 E_\varphi)\big]\boldsymbol{S}_{nm}^{(0)}\,,\\
\dot{\boldsymbol{f}} &= \textstyle\sum_{nm}\big[-\sum_k c_{3k}\dot{y}_k\boldsymbol{S}_{nm}^{(-1)} - \sum_k c_{4k}\dot{y}_k\boldsymbol{S}_{nm}^{(1)}\big]\,, && (3.42)
\end{aligned}$$

while the r.h.s. of (3.33) is equal to

$$\begin{aligned}
&\nabla\cdot\left[\xi_1(\boldsymbol{\tau}-K\nabla\cdot\mathbf{u}\boldsymbol{I})-\xi_2(\boldsymbol{e}-\tfrac{1}{3}\nabla\cdot\mathbf{u}\boldsymbol{I})\right]\\
&\quad=\ \xi_1\left[\nabla\cdot\boldsymbol{\tau}-\nabla(K\nabla\cdot\mathbf{u})\right]+\nabla\xi_1\cdot\left[\boldsymbol{\tau}-K\nabla\cdot\mathbf{u}\boldsymbol{I}\right]-\xi_2\left[\nabla\cdot\boldsymbol{e}-\tfrac{1}{3}\nabla\nabla\cdot\mathbf{u}\right]-\nabla\xi_2\cdot\left[\boldsymbol{e}-\tfrac{1}{3}\nabla\cdot\mathbf{u}\boldsymbol{I}\right]\\
&\quad=\ \xi_1\left[-\boldsymbol{f}-\nabla(K\nabla\cdot\mathbf{u})\right]+\xi_1'\left[\boldsymbol{T}_r-K\nabla\cdot\mathbf{u}\boldsymbol{e}_r\right]-\xi_2\left[\nabla\cdot\boldsymbol{e}-\tfrac{1}{3}\nabla\nabla\cdot\mathbf{u}\right]-\xi_2'\left[\boldsymbol{E}_r-\tfrac{1}{3}\nabla\cdot\mathbf{u}\boldsymbol{e}_r\right]\\
&\quad=\ \textstyle\sum_{nm}\left[\xi_1\sum_k c_{3k}y_k-\xi_1(KX)'+\xi_1'(y_3-KX)-\xi_2D_r-\xi_2'(E_r-X/3)\right]\boldsymbol{S}_{nm}^{(-1)} \qquad (3.43)\\
&\quad+\ \textstyle\sum_{nm}\left[\xi_1\sum_k c_{4k}y_k-\xi_1KX/r+\xi_1'y_4-\xi_2D_\vartheta-\xi_2'E_\vartheta\right]\boldsymbol{S}_{nm}^{(1)}\\
&\quad+\ \textstyle\sum_{nm}\left[\xi_1'y_8-\xi_2D_\varphi-\xi_2'E_\varphi\right]\boldsymbol{S}_{nm}^{(0)}
\end{aligned}$$

with $\nabla\cdot\boldsymbol{e}-\frac{1}{3}\nabla\nabla\cdot\mathbf{u}=\sum_{nm}[D_r\boldsymbol{S}_{nm}^{(-1)}+D_\vartheta\boldsymbol{S}_{nm}^{(1)}+D_\varphi\boldsymbol{S}_{nm}^{(0)}]$; the coefficients D_r, D_ϑ and D_φ can be found from (B.40) and (B.56). Thus, the spherical harmonic expansions of the scalar components of (3.33) read

$$\begin{aligned}
\dot y_3'-\textstyle\sum_k a_{3k}\dot y_k &= \xi_1\left[-y_3'+\sum_k a_{3k}y_k-b_{31}y_1-b_{32}y_2-b_{33}KX\right] &(3.44)\\
&+\ \xi_2\left[(E_r-X/3)'-D_r-b_{33}(E_r-X/3)-b_{34}E_\vartheta\right], &\\
\dot y_4'-\textstyle\sum_k a_{4k}\dot y_k &= \xi_1\left[-y_4'+\sum_k a_{4k}y_k-b_{41}y_1-b_{42}y_2-(b_{43}+1/r)KX\right] &(3.45)\\
&+\ \xi_2\left[E_\vartheta'-D_\vartheta-b_{43}(E_r-X/3)-b_{44}E_\vartheta\right], &\\
\dot y_8'-\textstyle\sum_k a_{8k}\dot y_k &= \xi_1\left[-y_8'+\sum_k a_{8k}y_k-b_{87}y_7\right]+\xi_2\left[E_\varphi'-D_\varphi-b_{88}E_\varphi\right]. &(3.46)
\end{aligned}$$

The Poisson equation (3.34) remains as in (3.21),

$$\dot y_6'-\textstyle\sum_k a_{6k}\dot y_k \;=\; 0\,. \qquad (3.47)$$

We can finalize the PDEs with respect to time and the radius for the solution vector $\mathbf{y}_{nm}$,

$$\dot{\mathbf{y}}_{nm}'(t,r)-\boldsymbol{A}_n(r)\dot{\mathbf{y}}_{nm}(t,r) \;=\; \qquad (3.48)$$

$$\xi_1\begin{pmatrix}
a_{13}(y_3-KX)\\
a_{24}y_4\\
-y_3'+\sum_k a_{3k}y_k-b_{31}y_1-b_{32}y_2-b_{33}KX\\
-y_4'+\sum_k a_{4k}y_k-b_{41}y_1-b_{42}y_2-(b_{43}+\frac{1}{r})KX\\
0\\
0\\
a_{78}y_8\\
-y_8'+\sum_k a_{8k}y_k-b_{87}y_7
\end{pmatrix}+\xi_2\begin{pmatrix}
-a_{13}(E_r-\frac{X}{3})\\
-a_{24}E_\vartheta\\
(E_r-\frac{X}{3})'-D_r-b_{33}(E_r-\frac{X}{3})-b_{34}E_\vartheta\\
E_\vartheta'-D_\vartheta-b_{43}(E_r-\frac{X}{3})-b_{44}E_\vartheta\\
0\\
0\\
-a_{78}E_\varphi\\
E_\varphi'-D_\varphi-b_{88}E_\varphi
\end{pmatrix}.$$

Some algebra with (B.40), (B.53) and (B.56) yields

$$\begin{aligned}
E_r-\frac{X}{3} &= \frac{2y_1'}{3}+\frac{-2y_1+Ny_2}{3r}\,, &(3.49)\\
E_\vartheta &= \frac{y_2'}{2}+\frac{y_1-y_2}{2r}\,, &(3.50)\\
E_\varphi &= \frac{y_7'}{2}-\frac{y_7}{2r}\,, &(3.51)\\
\left(E_r-\frac{X}{3}\right)'-D_r &= \frac{-4y_1'+Ny_2'}{2r}+\frac{(N+4)y_1-3Ny_2}{2r^2}\,, &(3.52)\\
E_\vartheta'-D_\vartheta &= \frac{2y_1'-9y_2'}{6r}+\frac{-11y_1+(4N+3)y_2}{r^2}\,, &(3.53)\\
E_\varphi'-D_\varphi &= -\frac{3y_7'}{2r}+\frac{(N+1)y_7}{2r^2}\,. &(3.54)
\end{aligned}$$

We recall (see p. 13) that

$$a_{13} = \frac{1}{\beta}\,, \quad a_{24} = \frac{1}{\mu_1}\,, \quad a_{78} = \frac{1}{\mu_1}\,, \quad b_{33} = -\frac{4\mu_1}{r\beta}\,, \quad b_{34} = \frac{N}{r}\,, \quad b_{43} = -\frac{\lambda}{r\beta}\,, \quad b_{44} = -\frac{3}{r}\,, \quad b_{88} = -\frac{3}{r} \tag{3.55}$$

with $\beta = \lambda + 2\mu_1$. From that we see that it is possible to obtain the PDEs for the spherically symmetric Earth model with the rheology of the standard linear solid in the form essentially identical with (3.23),

$$\begin{aligned} \dot{\mathbf{y}}'_{nm}(t,r) - \boldsymbol{A}_n(r)\dot{\mathbf{y}}_{nm}(t,r) &= \xi_1(r)\left[\boldsymbol{D}_n(r)\mathbf{y}'_{nm}(t,r) + \boldsymbol{E}_n(r)\mathbf{y}_{nm}(t,r)\right] \\ &+ \xi_2(r)\left[\boldsymbol{F}_n(r)\mathbf{y}'_{nm}(t,r) + \boldsymbol{G}_n(r)\mathbf{y}_{nm}(t,r)\right]. \end{aligned} \tag{3.56}$$

Matrices $\boldsymbol{A}_n$, $\boldsymbol{D}_n$ and $\boldsymbol{E}_n$ (with μ replaced by μ_1) are given by (2.50), (3.24) and (3.25), respectively, and explicit expressions for matrices $\boldsymbol{F}_n$ and $\boldsymbol{G}_n$ follow from (3.48)–(3.55).

3.1.4 Older Formulation of the Initial-Value Approach

We demonstrate here the compatibility of the IV/MOL approach with the older formulation of the IV approach, employed in Part II. In Chapter 7 the spheroidal and the toroidal systems of ODEs (7.17), (7.21), (7.35) and (7.38) are derived in the form, respectively,

$$\mathbf{y}'_n(t,r) = \tilde{\boldsymbol{A}}_n(r)\mathbf{y}_n(t,r) + \mathbf{q}_n(t,r)\,, \qquad \mathbf{q}_n(t,r) = \int_0^t \xi\left[\tilde{\boldsymbol{Q}}_n(r)\mathbf{y}_n(t',r) + \tilde{\tilde{\boldsymbol{Q}}}_n(r)\mathbf{q}_n(t',r)\right] dt'\,, \tag{3.57}$$

$$\mathbf{z}'_n(t,r) = \tilde{\boldsymbol{B}}_n(r)\mathbf{z}_n(t,r) + \mathbf{p}_n(t,r)\,, \qquad \mathbf{p}_n(t,r) = \int_0^t \xi\left[\tilde{\boldsymbol{P}}_n(r)\mathbf{z}_n(t',r) + \tilde{\tilde{\boldsymbol{P}}}_n(r)\mathbf{p}_n(t',r)\right] dt'\,, \tag{3.58}$$

with $\xi = \mu/\eta$. The difference between (3.23) and (3.57)–(3.58) is that, for instance, vector $\mathbf{q}$ is expressed in terms of $\mathbf{y}$ and $\mathbf{q}$, while the r.h.s. of (3.23) is expressed in terms of $\mathbf{y}$ and $\mathbf{y}'$.

We denote the 6×6 spheroidal blocks of matrices $\boldsymbol{A}_n$, $\boldsymbol{D}_n$ and $\boldsymbol{E}_n$ from (3.23) by the subscript $_{6\times6}$, and the 2×2 toroidal blocks by the subscript $_{2\times2}$. It is straightforward to write relations between $\tilde{\boldsymbol{A}}_n$, $\tilde{\boldsymbol{B}}_n$ from (3.57)–(3.58) and $\boldsymbol{A}_n$ from (3.23),

$$\tilde{\boldsymbol{A}}_n = (\boldsymbol{A}_n)_{6\times6}\,, \qquad \tilde{\boldsymbol{B}}_n = (\boldsymbol{A}_n)_{2\times2}\,. \tag{3.59}$$

After time differentiation of the left two equations of (3.57)–(3.58), we can obtain the relation between $\mathbf{q}$, $\mathbf{p}$ and the r.h.s. of (3.23). By substitution for $\mathbf{y}'_n$ and $\mathbf{z}'_n$ back from (3.57)–(3.58), the expressions for $\dot{\mathbf{q}}_n$ and $\dot{\mathbf{p}}_n$ read

$$\dot{\mathbf{q}}_n = \xi\left[(\boldsymbol{D}_n)_{6\times6}\mathbf{y}'_n + (\boldsymbol{E}_n)_{6\times6}\mathbf{y}_n\right] = \xi\left[(\boldsymbol{D}_n\boldsymbol{A}_n + \boldsymbol{E}_n)_{6\times6}\,\mathbf{y}_n + (\boldsymbol{D}_n)_{6\times6}\mathbf{q}_n\right], \tag{3.60}$$

$$\dot{\mathbf{p}}_n = \xi\left[(\boldsymbol{D}_n)_{2\times2}\mathbf{z}'_n + (\boldsymbol{E}_n)_{2\times2}\mathbf{z}_n\right] = \xi\left[(\boldsymbol{D}_n\boldsymbol{A}_n + \boldsymbol{E}_n)_{2\times2}\,\mathbf{z}_n + (\boldsymbol{D}_n)_{2\times2}\mathbf{p}_n\right]. \tag{3.61}$$

We see from (3.60)–(3.61) and the right two equations of (3.57)–(3.58) that

$$\tilde{\boldsymbol{Q}}_n = (\boldsymbol{D}_n\boldsymbol{A}_n + \boldsymbol{E}_n)_{6\times6}\,, \qquad \tilde{\tilde{\boldsymbol{Q}}}_n = (\boldsymbol{D}_n)_{6\times6}\,, \tag{3.62}$$

$$\tilde{\boldsymbol{P}}_n = (\boldsymbol{D}_n\boldsymbol{A}_n + \boldsymbol{E}_n)_{2\times2}\,, \qquad \tilde{\tilde{\boldsymbol{P}}}_n = (\boldsymbol{D}_n)_{2\times2}\,, \tag{3.63}$$

expressed explicitly as follows:

$$\tilde{\boldsymbol{Q}}_n = \begin{pmatrix} -\frac{4\gamma}{3r\beta} & \frac{2N\gamma}{3r\beta} & \frac{4\mu}{3\beta^2} & 0 & 0 & 0 \\ 0 & 0 & 0 & \frac{1}{\mu} & 0 & 0 \\ -\frac{4\gamma K}{r^2\beta} & \frac{2N\gamma K}{r^2\beta} & \frac{4\gamma}{3r\beta} & 0 & 0 & 0 \\ \frac{2\gamma K}{r^2\beta} & \frac{2\mu - N(\frac{\gamma K}{\beta}+\mu)}{r^2} & -\frac{2\gamma}{3r\beta} & 0 & 0 & 0 \\ 0 & 0 & 0 & 0 & 0 & 0 \\ 0 & 0 & 0 & 0 & 0 & 0 \end{pmatrix}, \quad \tilde{\tilde{\boldsymbol{Q}}}_n = \begin{pmatrix} -\frac{K}{\beta} & 0 & 0 & 0 & 0 & 0 \\ 0 & 0 & 0 & 0 & 0 & 0 \\ \frac{4\gamma}{3r} & 0 & -1 & 0 & 0 & 0 \\ -\frac{2\gamma}{3r} & 0 & 0 & -1 & 0 & 0 \\ 0 & 0 & 0 & 0 & 0 & 0 \\ 0 & 0 & 0 & 0 & 0 & 0 \end{pmatrix}, \tag{3.64}$$

$$\tilde{\boldsymbol{P}}_n = \begin{pmatrix} 0 & \frac{1}{\mu} \\ -\frac{(N-2)\mu}{r^2} & 0 \end{pmatrix}, \quad \tilde{\tilde{\boldsymbol{P}}}_n = \begin{pmatrix} 0 & 0 \\ 0 & -1 \end{pmatrix}. \tag{3.65}$$

The expressions are identical with those for $\tilde{\boldsymbol{Q}}_n$ and $\tilde{\tilde{\boldsymbol{Q}}}_n$ given by (7.36), and correct those for $\tilde{\boldsymbol{P}}_n$ and $\tilde{\tilde{\boldsymbol{P}}}_n$ by (7.39).

3.2 Differential Equations for the Axisymmetric Viscoelastic Earth

The derivation of the PDEs (3.23) for the viscoelastic response of the spherically symmetric, Maxwell Earth model to a surface load can be generalized to conform with the axially symmetric (2-D) distribution of viscosity; on the contrary, the restrictive assumption of the axial geometry of the load, with identical axes of symmetry of both the viscosity and the load, is enforced. Then, the spatial dependence of the viscoelastic response of this system is axisymmetric as well. The below developed approach for the 2-D viscosity is scalar by nature, i.e., purely scalar representation of the field quantities is only employed.

We consider the following spatial distribution of the parameters and the field variables,

$$\varrho_0 = \varrho_0(r)\,, \quad \lambda = \lambda(r)\,, \quad \mu = \mu(r)\,, \quad K = K(r)\,, \quad g_0 = g_0(r)\,, \quad \eta = \eta(r,\vartheta)\,, \quad \xi = \xi(r,\vartheta)\,, \tag{3.66}$$

$$\mathbf{u} = \mathbf{u}(r,\vartheta)\,, \quad \varphi_1 = \varphi_1(r,\vartheta)\,, \quad \boldsymbol{\tau} = \boldsymbol{\tau}(r,\vartheta)\,. \tag{3.67}$$

Let us remind that, in accord with (3.2), $\xi = \mu/\eta$. We introduce the scalar and vector zonal spherical harmonics, Y_n and $\boldsymbol{S}_n^{(-1)}$, $\boldsymbol{S}_n^{(1)}$, $\boldsymbol{S}_n^{(0)}$, respectively, and the derivatives Z_n of Y_n, all only the functions of the colatitude ϑ,

$$\begin{array}{lllllllll} Y_n(\vartheta) & = & Y_{n0}(\vartheta)\,, & & Z_n(\vartheta) & = & \dfrac{\partial Y_{n0}(\vartheta)}{\partial\vartheta}\,, & & \\ \boldsymbol{S}_n^{(-1)}(\vartheta) & = & Y_n(\vartheta)\boldsymbol{e}_r\,, & & \boldsymbol{S}_n^{(1)}(\vartheta) & = & Z_n(\vartheta)\boldsymbol{e}_\vartheta\,, & \boldsymbol{S}_n^{(0)}(\vartheta) & = & Z_n(\vartheta)\boldsymbol{e}_\varphi\,, \end{array} \tag{3.68}$$

cf. (2.16)–(2.19). With (3.68), the spherical harmonic expansions (2.20)–(2.22) of $\mathbf{u}$, φ_1 and $\boldsymbol{T}_r$ are reduced to

$$\mathbf{u}(r,\vartheta) = \sum_n \Big[U_n(r)Y_n(\vartheta)\boldsymbol{e}_r + V_n(r)Z_n(\vartheta)\boldsymbol{e}_\vartheta + W_n(r)Z_n(\vartheta)\boldsymbol{e}_\varphi\Big]\,, \tag{3.69}$$

$$\varphi_1(r,\vartheta) = \sum_n F_n(r)Y_n(\vartheta)\,, \tag{3.70}$$

$$\boldsymbol{e}_r\cdot\boldsymbol{\tau} \equiv \boldsymbol{T}_r(r,\vartheta) = \sum_n \Big[T_{rr,n}(r)Y_n(\vartheta)\boldsymbol{e}_r + T_{r\vartheta,n}(r)Z_n(\vartheta)\boldsymbol{e}_\vartheta + T_{r\varphi,n}(r)Z_n(\vartheta)\boldsymbol{e}_\varphi\Big]\,. \tag{3.71}$$

It will emerge later, cf. (3.89), that, in the case of the 2-D viscosity distribution, it is necessary to employ not only the stress vector $\boldsymbol{T}_r$ but also the stress vector $\boldsymbol{T}_\vartheta \equiv \boldsymbol{e}_\vartheta \cdot \boldsymbol{\tau}$. The spherical harmonic expansion of $\boldsymbol{T}_\vartheta$ can be written analogically to (3.71),

$$\boldsymbol{e}_\vartheta \cdot \boldsymbol{\tau} \quad \equiv \quad \boldsymbol{T}_\vartheta(r,\vartheta) \quad = \quad \sum_n \left[T_{\vartheta r,n}(r) Y_n(\vartheta) \boldsymbol{e}_r + T_{\vartheta\vartheta,n}(r) Z_n(\vartheta) \boldsymbol{e}_\vartheta + T_{\vartheta\varphi,n}(r) Z_n(\vartheta) \boldsymbol{e}_\varphi \right] . \tag{3.72}$$

Expansions of the elastic parts of the stress vectors, $\boldsymbol{T}_r^E \equiv \boldsymbol{e}_r \cdot \boldsymbol{\tau}^E$ and $\boldsymbol{T}_\vartheta^E \equiv \boldsymbol{e}_\vartheta \cdot \boldsymbol{\tau}^E$, correspond to (3.71) and (3.72), respectively. The relations between the stress vectors and the corresponding elastic parts $\boldsymbol{T}_r^E$ and $\boldsymbol{T}_\vartheta^E$ follow from the Maxwell constitutive relation (3.1),

$$\dot{\boldsymbol{T}}_r \quad = \quad \dot{\boldsymbol{T}}_r^E - \xi(r,\vartheta) \left(\boldsymbol{T}_r - K \nabla \cdot \mathbf{u}\, \boldsymbol{e}_r \right) , \tag{3.73}$$

$$\dot{\boldsymbol{T}}_\vartheta \quad = \quad \dot{\boldsymbol{T}}_\vartheta^E - \xi(r,\vartheta) \left(\boldsymbol{T}_\vartheta - K \nabla \cdot \mathbf{u}\, \boldsymbol{e}_\vartheta \right) . \tag{3.74}$$

However, it will also emerge later that we can get a system of PDEs more appropriate for numerical solution with an alternative set of coefficients, $\bar{T}_{\vartheta r,n}$, $\bar{T}_{\vartheta\vartheta,n}$, $\bar{T}_{\vartheta\varphi,n}$, $\bar{T}^E_{\vartheta r,n}$, $\bar{T}^E_{\vartheta\vartheta,n}$ and $\bar{T}^E_{\vartheta\varphi,n}$, introduced by the conversion relations

$$\begin{aligned}
\textstyle\sum_n \bar{T}_{\vartheta r,n} Z_n \sin^2\vartheta &= \textstyle\sum_n T_{\vartheta r,n} Y_n , & \qquad \textstyle\sum_n \bar{T}^E_{\vartheta r,n} Z_n \sin^2\vartheta &= \textstyle\sum_n T^E_{\vartheta r,n} Y_n , \\
\textstyle\sum_n \bar{T}_{\vartheta\vartheta,n} Y_n &= \textstyle\sum_n T_{\vartheta\vartheta,n} Z_n , & \qquad \textstyle\sum_n \bar{T}^E_{\vartheta\vartheta,n} Y_n &= \textstyle\sum_n T^E_{\vartheta\vartheta,n} Z_n , \\
\textstyle\sum_n \bar{T}_{\vartheta\varphi,n} Y_n &= \textstyle\sum_n T_{\vartheta\varphi,n} Z_n , & \qquad \textstyle\sum_n \bar{T}^E_{\vartheta\varphi,n} Y_n &= \textstyle\sum_n T^E_{\vartheta\varphi,n} Z_n .
\end{aligned} \tag{3.75}$$

We have collected all the coefficients necessary for the definition of the 11-element solution vector $\mathbf{y}_n(t,r)$ for the case of the 2-D viscosity distribution,

$$\mathbf{y}_n(t,r) \quad = \quad \left(U_n, V_n, T_{rr,n}, T_{r\vartheta,n}, F_n, Q_n, W_n, T_{r\varphi,n}, \bar{T}_{\vartheta r,n}, \bar{T}_{\vartheta\vartheta,n}, \bar{T}_{\vartheta\varphi,n} \right)^T , \tag{3.76}$$

and of the corresponding vector $\mathbf{y}_n^E(r)$,

$$\mathbf{y}_n^E(r) \quad = \quad \left(U_n, V_n, T^E_{rr,n}, T^E_{r\vartheta,n}, F_n, Q_n, W_n, T^E_{r\varphi,n}, \bar{T}^E_{\vartheta r,n}, \bar{T}^E_{\vartheta\vartheta,n}, \bar{T}^E_{\vartheta\varphi,n} \right)^T . \tag{3.77}$$

At this point we introduce a notation for coefficients of spherical harmonic expansions of products of two scalar fields. It makes sense to employ these coefficients in what follows since efficient procedures for their numerical evaluation are available (see Appendices A.4, A.5 and C.3). Namely, we denote $\langle a; B_{n'} \rangle_{YY,n}$, $\langle a; B_{n'} \rangle_{ZY,n}$, $\langle a; B_{n'} \rangle_{YZ,n}$ and $\langle a; B_{n'} \rangle_{ZZ,n}$ the coefficients of the product $a(r,\vartheta) b(r,\vartheta)$, where $a(r,\vartheta)$ is a prescribed function and $b(r,\vartheta)$ is a function known by coefficients of its expansions in terms of either Y_n or $Z_n \sin\vartheta$, in accordance with

$$\begin{aligned}
a(r,\vartheta) \textstyle\sum_n B_n(r) Y_n(\vartheta) &= \textstyle\sum_n \langle a; B_{n'} \rangle_{YY,n}(r) Y_n(\vartheta) , \\
a(r,\vartheta) \textstyle\sum_n B_n(r) Z_n(\vartheta) \sin\vartheta &= \textstyle\sum_n \langle a; B_{n'} \rangle_{ZY,n}(r) Y_n(\vartheta) , \\
a(r,\vartheta) \textstyle\sum_n B_n(r) Y_n(\vartheta) &= \textstyle\sum_n \langle a; B_{n'} \rangle_{YZ,n}(r) Z_n(\vartheta) \sin\vartheta , \\
a(r,\vartheta) \textstyle\sum_n B_n(r) Z_n(\vartheta) \sin\vartheta &= \textstyle\sum_n \langle a; B_{n'} \rangle_{ZZ,n}(r) Z_n(\vartheta) \sin\vartheta .
\end{aligned} \tag{3.78}$$

Let us state in advance that $\xi(r,\vartheta)$ will be casted into $a(r,\vartheta)$ and that expressions involving expansion coefficients of the field variables will appear in place of $B_n(r)$. The relations between the scalar components of the stress vectors $\boldsymbol{T}_r$ and $\boldsymbol{T}_r^E$ follow from (3.73) and (2.23),

$$\begin{aligned}
\textstyle\sum_n \dot{T}_{rr,n} Y_n &= \textstyle\sum_n \dot{T}^E_{rr,n} Y_n - \xi(r,\vartheta) \sum_n \left(T_{rr,n} - K X_n \right) Y_n &= \textstyle\sum_n (\dot{T}^E_{rr,n} - \langle \xi; T_{rr,n'} - K X_{n'} \rangle_{YY,n}) Y_n , \\
\textstyle\sum_n \dot{T}_{r\vartheta,n} Z_n &= \textstyle\sum_n \dot{T}^E_{r\vartheta,n} Z_n - \xi(r,\vartheta) \sum_n T_{r\vartheta,n} Z_n &= \textstyle\sum_n (\dot{T}^E_{r\vartheta,n} - \langle \xi; T_{r\vartheta,n'} \rangle_{ZZ,n}) Z_n , \\
\textstyle\sum_n \dot{T}_{r\varphi,n} Z_n &= \textstyle\sum_n \dot{T}^E_{r\varphi,n} Z_n - \xi(r,\vartheta) \sum_n T_{r\varphi,n} Z_n &= \textstyle\sum_n (\dot{T}^E_{r\varphi,n} - \langle \xi; T_{r\varphi,n'} \rangle_{ZZ,n}) Z_n ,
\end{aligned} \tag{3.79}$$

the relations between corresponding pairs of $T_{\vartheta r,n}$, ..., $T^E_{\vartheta\varphi,n}$ follow from (3.74),

$$\begin{aligned}
\textstyle\sum_n \dot{T}_{\vartheta r,n} Y_n &= \textstyle\sum_n \dot{T}^E_{\vartheta r,n} Y_n - \xi(r,\vartheta) \sum_n T_{\vartheta r,n} Y_n \,, \\
\textstyle\sum_n \dot{T}_{\vartheta\vartheta,n} Z_n &= \textstyle\sum_n \dot{T}^E_{\vartheta\vartheta,n} Z_n - \xi(r,\vartheta) \sum_n \left(T_{\vartheta\vartheta,n} Z_n - K X_n Y_n\right) \,, \\
\textstyle\sum_n \dot{T}_{\vartheta\varphi,n} Z_n &= \textstyle\sum_n \dot{T}^E_{\vartheta\varphi,n} Z_n - \xi(r,\vartheta) \sum_n T_{\vartheta\varphi,n} Z_n \,,
\end{aligned} \tag{3.80}$$

and the corresponding relations for $\bar{T}_{\vartheta r,n}$, ..., $\bar{T}^E_{\vartheta\varphi,n}$, follow from (3.80), (3.75) and (3.78),

$$\begin{aligned}
\textstyle\sum_n \dot{\bar{T}}_{\vartheta r,n} Z_n \sin^2\vartheta &= \textstyle\sum_n (\dot{\bar{T}}^E_{\vartheta r,n} Z_n - \xi \sum_n \bar{T}_{\vartheta r,n} Z_n) \sin^2\vartheta &&= \textstyle\sum_n (\dot{\bar{T}}^E_{\vartheta r,n} - \langle \xi; \bar{T}_{\vartheta r,n'} \rangle_{ZZ,n}) Z_n \sin^2\vartheta \,, \\
\textstyle\sum_n \dot{\bar{T}}_{\vartheta\vartheta,n} Y_n &= \textstyle\sum_n \dot{\bar{T}}^E_{\vartheta\vartheta,n} Y_n - \xi \sum_n \left(\bar{T}_{\vartheta\vartheta,n} - K X_n\right) Y_n &&= \textstyle\sum_n (\dot{\bar{T}}^E_{\vartheta\vartheta,n} - \langle \xi; \bar{T}_{\vartheta\vartheta,n'} - K X_{n'} \rangle_{YY,n}) Y_n \,, \\
\textstyle\sum_n \dot{\bar{T}}_{\vartheta\varphi,n} Y_n &= \textstyle\sum_n \dot{\bar{T}}^E_{\vartheta\varphi,n} Y_n - \xi \sum_n \bar{T}_{\vartheta\varphi,n} Y_n &&= \textstyle\sum_n (\dot{\bar{T}}^E_{\vartheta\varphi,n} - \langle \xi; \bar{T}_{\vartheta\varphi,n'} \rangle_{YY,n}) Y_n \,.
\end{aligned} \tag{3.81}$$

Relations (3.79) and (3.81) expressed in terms of elements of $\mathbf{y}_n$ and $\mathbf{y}^E_n$ lead to the relations

$$\begin{aligned}
&\dot{y}^E_{1,n} = \dot{y}_{1,n}, \quad \dot{y}^E_{2,n} = \dot{y}_{2,n}, \quad \dot{y}^E_{5,n} = \dot{y}_{5,n}, \quad \dot{y}^E_{6,n} = \dot{y}_{6,n}, \quad \dot{y}^E_{7,n} = \dot{y}_{7,n}, \\
&\dot{y}^E_{3,n} = \dot{y}_{3,n} + \langle \xi; y_{3,n'} - K X_{n'} \rangle_{YY,n}, \quad \dot{y}^E_{4,n} = \dot{y}_{4,n} + \langle \xi; y_{4,n'} \rangle_{ZZ,n}, \quad \dot{y}^E_{8,n} = \dot{y}_{8,n} + \langle \xi; y_{8,n'} \rangle_{ZZ,n}, \\
&\dot{y}^E_{9,n} = \dot{y}_{9,n} + \langle \xi; y_{9,n'} \rangle_{ZZ,n}, \quad \dot{y}^E_{10,n} = \dot{y}_{10,n} + \langle \xi; y_{10,n'} - K X_{n'} \rangle_{YY,n}, \quad \dot{y}^E_{11,n} = \dot{y}_{11,n} + \langle \xi; y_{11,n'} \rangle_{YY,n}.
\end{aligned} \tag{3.82}$$

Now we are ready to collect the PDEs we are looking for. To obtain the first four, we substitute (3.82) into the relations (2.34)–(2.37) for $y^{E\prime}_{1,n}$, $y^{E\prime}_{2,n}$, $y^{E\prime}_{5,n}$ and $y^{E\prime}_{7,n}$, cf. (3.11)–(3.14),

$$\dot{y}'_{1,n} - \textstyle\sum_k a_{1k,n} \dot{y}_{k,n} = a_{13,n} \langle \xi; y_{3,n'} - K X_{n'} \rangle_{YY,n} \,, \tag{3.83}$$

$$\dot{y}'_{2,n} - \textstyle\sum_k a_{2k,n} \dot{y}_{k,n} = a_{24,n} \langle \xi; y_{4,n'} \rangle_{ZZ,n} \,, \tag{3.84}$$

$$\dot{y}'_{5,n} - \textstyle\sum_k a_{5k,n} \dot{y}_{k,n} = 0 \,, \tag{3.85}$$

$$\dot{y}'_{7,n} - \textstyle\sum_k a_{7k,n} \dot{y}_{k,n} = a_{78,n} \langle \xi; y_{8,n'} \rangle_{ZZ,n} \,. \tag{3.86}$$

Secondly, we express the scalar components of the momentum equation (3.3). We substitute (3.82) into the l.h.s. terms by (2.38)–(2.39),

$$\begin{aligned}
\nabla \cdot \dot{\boldsymbol{\tau}}^E &= \textstyle\sum_n [\dot{y}'_{3,n} + \langle \xi; (y_{3,n'} - K X_{n'})' \rangle_{YY,n} + \langle \xi'; y_{3,n'} - K X_{n'} \rangle_{YY,n} \\
&\quad - \textstyle\sum_k b_{3k,n} \dot{y}_{k,n} - b_{33,n} \langle \xi; y_{3,n'} - K X_{n'} \rangle_{YY,n} - b_{34,n} \langle \xi; y_{4,n'} \rangle_{ZZ,n}] \boldsymbol{S}^{(-1)}_n \\
&+ \textstyle\sum_n [\dot{y}'_{4,n} + \langle \xi; y'_{4,n'} \rangle_{ZZ,n} + \langle \xi'; y_{4,n'} \rangle_{ZZ,n} \\
&\quad - \textstyle\sum_k b_{4k,n} \dot{y}_{k,n} - b_{43,n} \langle \xi; y_{3,n'} - K X_{n'} \rangle_{YY,n} - b_{44,n} \langle \xi; y_{4,n'} \rangle_{ZZ,n}] \boldsymbol{S}^{(1)}_n \\
&+ \textstyle\sum_n [\dot{y}'_{8,n} + \langle \xi; y'_{8,n'} \rangle_{ZZ,n} + \langle \xi'; y_{8,n'} \rangle_{ZZ,n} - \sum_k b_{8k,n} \dot{y}_{k,n} - b_{88,n} \langle \xi; y_{8,n'} \rangle_{ZZ,n}] \boldsymbol{S}^{(0)}_n \,,
\end{aligned} \tag{3.87}$$

$$\dot{\boldsymbol{f}} = \textstyle\sum_n [-\sum_k c_{3k,n} \dot{y}_{k,n} \boldsymbol{S}^{(-1)}_n - \sum_k c_{4k,n} \dot{y}_{k,n} \boldsymbol{S}^{(1)}_n] \,, \tag{3.88}$$

and arrange the r.h.s. term as follows,

$$\begin{aligned}
\nabla \cdot [\xi (\boldsymbol{\tau} - K \nabla \cdot \mathbf{u} \boldsymbol{I})] &= \xi [\nabla \cdot \boldsymbol{\tau} - \nabla (K \nabla \cdot \mathbf{u})] + \nabla \xi \cdot [\boldsymbol{\tau} - K \nabla \cdot \mathbf{u} \boldsymbol{I}] \\
&= \xi [-\boldsymbol{f} - \nabla (K \nabla \cdot \mathbf{u})] + \xi' [\boldsymbol{T}_r - K \nabla \cdot \mathbf{u} \boldsymbol{e}_r] + \frac{\zeta}{r \sin\vartheta} [\boldsymbol{T}_\vartheta - K \nabla \cdot \mathbf{u} \boldsymbol{e}_\vartheta] \,,
\end{aligned} \tag{3.89}$$

where the auxiliary function $\zeta(r,\vartheta)$, $\nabla\xi = \xi' \boldsymbol{e}_r + \zeta/(r\sin\vartheta)\boldsymbol{e}_\vartheta$, has been introduced. The spherical harmonic expansion of $\zeta(r,\vartheta)$ can be deduced from (B.36) and (A.21), rewritten as

$$\nabla \xi = \textstyle\sum_n \left[\xi'_n Y_n \boldsymbol{e}_r + \frac{\xi_n}{r} Z_n \boldsymbol{e}_\vartheta \right] , \qquad Z_n \sin\vartheta = \omega^+_n Y_{n+1} + \omega^-_n Y_{n-1} \,; \tag{3.90}$$

having $\xi(r,\vartheta)$ prescribed, the expansion coefficients of $\zeta(r,\vartheta)$ can be found from the expansion coefficients of $\xi(r,\vartheta)$, as follows from the relations

$$\begin{aligned}\zeta(r,\vartheta) &= \textstyle\sum_n \xi_n(r) Z_n(\vartheta)\sin\vartheta &= \textstyle\sum_n \xi_n \left[\omega_n^+ Y_{n+1} + \omega_n^- Y_{n-1}\right] \\ &= \textstyle\sum_n \left[\omega_{n-1}^+ \xi_{n-1} + \omega_{n+1}^- \xi_{n+1}\right] Y_n &= \textstyle\sum_n \left[\frac{n(n-1)\xi_{n-1}}{\sqrt{(2n-1)(2n+1)}} - \frac{(n+1)(n+2)\xi_{n+1}}{\sqrt{(2n+1)(2n+3)}}\right] Y_n\,.\end{aligned} \tag{3.91}$$

Taking into account expansion (3.72) of $\boldsymbol{T}_\vartheta$ and the conversion relations (3.75), we have for the r.h.s. term by (3.89)

$$\begin{aligned}\nabla\cdot[\xi\,(\boldsymbol{\tau} - K\nabla\cdot\mathbf{u}\boldsymbol{I})] &= \xi\textstyle\sum_n[(\sum_k c_{3k,n} y_{k,n} - (KX_n)')\boldsymbol{S}_n^{(-1)} + (\sum_k c_{4k,n} y_{k,n} - KX_n/r)\boldsymbol{S}_n^{(1)}] \\ &+ \xi'\textstyle\sum_n[(y_{3,n} - KX_n)\boldsymbol{S}_n^{(-1)} + y_{4,n}\boldsymbol{S}_n^{(1)} + y_{8,n}\boldsymbol{S}_n^{(0)}] \\ &+ \zeta/(r\sin\vartheta)\textstyle\sum_n[y_{9,n} Z_n \sin^2\vartheta\,\boldsymbol{e}_r + (y_{10,n} - KX_n) Y_n \boldsymbol{e}_\vartheta + y_{11,n} Y_n \boldsymbol{e}_\varphi]\end{aligned} \tag{3.92}$$

and with the notation by (3.78), the r.h.s. of (3.3) takes the final form,

$$\begin{aligned}&\nabla\cdot[\xi(\boldsymbol{\tau} - K\nabla\cdot\mathbf{u}\boldsymbol{I})] \quad = \\ &= \textstyle\sum_n[\langle\xi; \sum_k c_{3k,n'} y_{k,n'} - (KX_{n'})'\rangle_{YY,n} + \langle\xi'; y_{3,n'} - KX_{n'}\rangle_{YY,n} + \langle\zeta/r; y_{9,n'}\rangle_{ZY,n}]\boldsymbol{S}_n^{(-1)} \\ &+ \textstyle\sum_n[\langle\xi; \sum_k c_{4k,n'} y_{k,n'} - KX_{n'}/r\rangle_{ZZ,n} + \langle\xi'; y_{4,n'}\rangle_{ZZ,n} + \langle\zeta/r; y_{10,n'} - KX_{n'}\rangle_{YZ,n}]\boldsymbol{S}_n^{(1)} \\ &+ \textstyle\sum_n[\langle\xi'; y_{8,n'}\rangle_{ZZ,n} + \langle\zeta/r; y_{11,n'}\rangle_{YZ,n}]\boldsymbol{S}_n^{(0)}\,.\end{aligned} \tag{3.93}$$

From (3.87), (3.88) and (3.93) we extract three scalar components of (3.3) which lead to the three sets of PDEs, cf. (3.18)–(3.20),

$$\begin{aligned}\dot{y}'_{3,n} - \textstyle\sum_k a_{3k,n}\dot{y}_{k,n} &= -\langle\xi; y'_{3,n'}\rangle_{YY,n} + b_{33,n}\langle\xi; y_{3,n'} - KX_{n'}\rangle_{YY,n} + b_{34,n}\langle\xi; y_{4,n'}\rangle_{ZZ,n} \\ &\quad + \langle\xi; \textstyle\sum_k c_{3k,n'} y_{k,n'}\rangle_{YY,n} + \langle\zeta/r; y_{9,n'}\rangle_{ZY,n}\,,\end{aligned} \tag{3.94}$$

$$\begin{aligned}\dot{y}'_{4,n} - \textstyle\sum_k a_{4k,n}\dot{y}_{k,n} &= -\langle\xi; y'_{4,n'}\rangle_{ZZ,n} + b_{43,n}\langle\xi; y_{3,n'} - KX_{n'}\rangle_{YY,n} + b_{44,n}\langle\xi; y_{4,n'}\rangle_{ZZ,n} \\ &\quad + \langle\xi; \textstyle\sum_k c_{4k,n'} y_{k,n'} - KX_{n'}/r\rangle_{ZZ,n} + \langle\zeta/r; y_{10,n'} - KX_{n'}\rangle_{YZ,n}\,,\end{aligned} \tag{3.95}$$

$$\dot{y}'_{8,n} - \textstyle\sum_k a_{8k,n}\dot{y}_{k,n} = -\langle\xi; y'_{8,n'}\rangle_{ZZ,n} + b_{88,n}\langle\xi; y_{8,n'}\rangle_{ZZ,n} + \langle\zeta/r; y_{11,n'}\rangle_{YZ,n}\,. \tag{3.96}$$

Thirdly, the spherical harmonic expansion of the Poisson equation (3.4) expressed in terms of elements of $\mathbf{y}_n$ reads, cf. (3.21),

$$\dot{y}'_{6,n} - \textstyle\sum_k a_{6k,n}\dot{y}_{k,n} = 0\,. \tag{3.97}$$

Fourthly, we have three equations for $\dot{y}_{9,n}$, $\dot{y}_{10,n}$ and $\dot{y}_{11,n}$ in the bottom line of (3.82). However, we still need expressions for $y^E_{9,n}$, $y^E_{10,n}$ and $y^E_{11,n}$. Appendix B.5 can be consulted for the spherical harmonic expansion of $\boldsymbol{T}^E_\vartheta$, given in terms the zonal spherical harmonics by (B.77),

$$\begin{aligned}\textstyle\sum_n T^E_{\vartheta r,n} Y_n &= \textstyle\sum_n \left[\mu\left(V'_n + \frac{U_n - V_n}{r}\right) Z_n\right]\,, \\ \textstyle\sum_n T^E_{\vartheta\vartheta,n} Z_n &= \textstyle\sum_n \left[\left(\lambda X_n + 2\mu\frac{U_n - NV_n}{r}\right) Y_n - 2\mu\frac{V_n}{r}\frac{\cos\vartheta}{\sin\vartheta} Z_n\right]\,, \\ \textstyle\sum_n T^E_{\vartheta\varphi,n} Z_n &= \textstyle\sum_n \left[-N\mu\frac{W_n}{r} Y_n - 2\mu\frac{W_n}{r}\frac{\cos\vartheta}{\sin\vartheta} Z_n\right]\,.\end{aligned} \tag{3.98}$$

In combination with the conversion relations (3.75) we obtain

$$\begin{aligned}\textstyle\sum_n \bar{T}^E_{\vartheta r,n} Z_n \sin^2\vartheta &= \textstyle\sum_n \left[\mu\left(V'_n + \frac{U_n - V_n}{r}\right) Z_n\right]\,, \\ \textstyle\sum_n \bar{T}^E_{\vartheta\vartheta,n} Y_n \sin^2\vartheta &= \textstyle\sum_n \left[\left(\lambda X_n + 2\mu\frac{U_n - NV_n}{r}\right) Y_n \sin^2\vartheta - 2\mu\frac{V_n}{r} Z_n \sin\vartheta\cos\vartheta\right]\,, \\ \textstyle\sum_n \bar{T}^E_{\vartheta\varphi,n} Y_n \sin^2\vartheta &= \textstyle\sum_n \left[-N\mu\frac{W_n}{r} Y_n \sin^2\vartheta - 2\mu\frac{W_n}{r} Z_n \sin\vartheta\cos\vartheta\right]\,.\end{aligned} \tag{3.99}$$

Taking into account relations (A.25)–(A.27), respectively,

$$\begin{aligned} Y_n \sin^2\vartheta &= s_n^+ Y_{n+2} + s_n^0 Y_n + s_n^- Y_{n-2}\,, \\ Z_n \sin^2\vartheta &= t_n^+ Z_{n+2} + t_n^0 Z_n + t_n^- Z_{n-2}\,, \\ Z_n \sin\vartheta\cos\vartheta &= z_n^+ Y_{n+2} + z_n^0 Y_n + z_n^- Y_{n-2}\,, \end{aligned} \tag{3.100}$$

with the coefficients s_n^+, …, z_n^- dependent on n, we arrive at

$$t_{n-2}^+ \bar{T}^E_{\vartheta r,n-2} + t_n^0 \bar{T}^E_{\vartheta r,n} + t_{n+2}^- \bar{T}^E_{\vartheta r,n+2} = \mu\left(V_n' + \frac{U_n - V_n}{r}\right), \tag{3.101}$$

$$s_{n-2}^+ \bar{T}^E_{\vartheta\vartheta,n-2} + s_n^0 \bar{T}^E_{\vartheta\vartheta,n} + s_{n+2}^- \bar{T}^E_{\vartheta\vartheta,n+2} = \tag{3.102}$$

$$\begin{aligned} &= s_{n-2}^+\left[\lambda X_{n-2} + \frac{2\mu}{r}\left(U_{n-2} - (n-2)(n-1)V_{n-2}\right)\right] + s_n^0\left[\lambda X_n + \frac{2\mu}{r}\left(U_n - n(n+1)V_n\right)\right] \\ &+ s_{n+2}^-\left[\lambda X_{n+2} + \frac{2\mu}{r}\left(U_{n+2} - (n+2)(n+3)V_{n+2}\right)\right] - \frac{2\mu}{r}\left[z_{n-2}^+ V_{n-2} + z_n^0 V_n + z_{n+2}^- V_{n+2}\right], \end{aligned}$$

$$s_{n-2}^+ \bar{T}^E_{\vartheta\varphi,n-2} + s_n^0 \bar{T}^E_{\vartheta\varphi,n} + s_{n+2}^- \bar{T}^E_{\vartheta\varphi,n+2} = \tag{3.103}$$

$$\begin{aligned} &= -\frac{\mu}{r}\left[s_{n-2}^+(n-2)(n-1)W_{n-2} + s_n^0 n(n+1)W_n + s_{n+2}^-(n+2)(n+3)W_{n+2}\right] \\ &- \frac{2\mu}{r}\left[z_{n-2}^+ W_{n-2} + z_n^0 W_n + z_{n+2}^- W_{n+2}\right]. \end{aligned}$$

Thus, the coefficients $y^E_{9,n}$, $y^E_{10,n}$ and $y^E_{11,n}$ can be found from $y_{1,n}$, $y_{2,n}$, $y_{7,n}$, $y'_{1,n}$ and $y'_{2,n}$ by solution to the band-diagonal systems of linear algebraic equations (3.101)–(3.103).

We can summarize eqs (3.83)–(3.86), (3.94)–(3.97) and bottom three eqs from (3.82) into the linear system of PDEs with respect to time and the radius for the solution vector $\mathbf{y}_n$,

$$\dot{\mathbf{y}}'_{1..8,n} - \boldsymbol{A}_n \dot{\mathbf{y}}_{1..8,n} = \begin{pmatrix} a_{13,n}\langle\xi; y_{3,n'} - KX_{n'}\rangle_{YY,n} \\ a_{24,n}\langle\xi; y_{4,n'}\rangle_{ZZ,n} \\ -\langle\xi; y'_{3,n'}\rangle_{YY,n} + b_{33,n}\langle\xi; y_{3,n'} - KX_{n'}\rangle_{YY,n} + b_{34,n}\langle\xi; y_{4,n'}\rangle_{ZZ,n} \\ \quad + \langle\xi; \sum_k c_{3k,n'} y_{k,n'}\rangle_{YY,n} + \langle\zeta/r; y_{9,n'}\rangle_{ZY,n} \\ -\langle\xi; y'_{4,n'}\rangle_{ZZ,n} + b_{43,n}\langle\xi; y_{3,n'} - KX_{n'}\rangle_{YY,n} + b_{44,n}\langle\xi; y_{4,n'}\rangle_{ZZ,n} \\ \quad + \langle\xi; \sum_k c_{4k,n'} y_{k,n'} - KX_{n'}/r\rangle_{ZZ,n} + \langle\zeta/r; y_{10,n'} - KX_{n'}\rangle_{YZ,n} \\ 0 \\ 0 \\ a_{78,n}\langle\xi; y_{8,n'}\rangle_{ZZ,n} \\ -\langle\xi; y'_{8,n'}\rangle_{ZZ,n} + b_{88,n}\langle\xi; y_{8,n'}\rangle_{ZZ,n} + \langle\zeta/r; y_{11,n'}\rangle_{YZ,n} \end{pmatrix}, \tag{3.104}$$

$$\dot{\mathbf{y}}_{9..11,n} - \dot{\mathbf{y}}^E_{9..11,n} = \begin{pmatrix} -\langle\xi; y_{9,n'}\rangle_{ZZ,n} \\ -\langle\xi; y_{10,n'} - KX_{n'}\rangle_{YY,n} \\ -\langle\xi; y_{11,n'}\rangle_{YY,n} \end{pmatrix}, \tag{3.105}$$

supplemented by the three band-diagonal systems of linear algebraic equations (3.101)–(3.103) for $y^E_{9,n}$, $y^E_{10,n}$ and $y^E_{11,n}$,

$$t^+_{n-2}\, y^E_{9,n-2} \; + t^0_n y^E_{9,n} \; + t^-_{n+2}\, y^E_{9,n+2} \quad = \quad \mu\left[y'_{2,n} + (y_{1,n} - y_{2,n})/r\right] , \tag{3.106}$$

$$s^+_{n-2} y^E_{10,n-2} + s^0_n y^E_{10,n} + s^-_{n+2} y^E_{10,n+2} \quad = \tag{3.107}$$

$$= \; s^+_{n-2}\left[\lambda X_{n-2} + 2\mu/r\,(y_{1,n-2} - (n-2)(n-1)y_{2,n-2})\right] + s^0_n\left[\lambda X_n + 2\mu/r\,(y_{1,n} - n(n+1)y_{2,n})\right]$$

$$+ \; s^-_{n+2}\left[\lambda X_{n+2} + 2\mu/r\,(y_{1,n+2} - (n+2)(n+3)y_{2,n+2})\right] - 2\mu/r\left[z^+_{n-2}y_{2,n-2} + z^0_n y_{2,n} + z^-_{n+2}y_{2,n+2}\right] ,$$

$$s^+_{n-2} y^E_{11,n-2} + s^0_n y^E_{11,n} + s^-_{n+2} y^E_{11,n+2} \quad = \tag{3.108}$$

$$= \; -\mu/r\left[s^+_{n-2}(n-2)(n-1)y_{7,n-2} + s^0_n n(n+1)y_{7,n} + s^-_{n+2}(n+2)(n+3)y_{7,n+2}\right]$$

$$- \; 2\mu/r\left[z^+_{n-2}y_{7,n-2} + z^0_n y_{7,n} + z^-_{n+2}y_{7,n+2}\right] .$$

This is the differential-algebraic system of 11 PDEs and 3 algebraic equations for each degree considered; coupling among systems of close degrees is maintained through both the r.h.s. of the PDEs and the band-diagonal shape of the algebraic equations. Differential-algebraic systems are shortly discussed in the next chapter, however, we do not intend to deal here with the 2-D case further. We only remark that this 2-D system seems to be a good basis for application of stiff integrating routines (described in the next chapter as well) and that it also allows for implementation of other efficient algorithms, e.g., the one for the evaluation of expansion coefficients of products of two scalar fields (see Appendices A.4, A.5 and C.3). For now—let us switch back to the 1-D case.

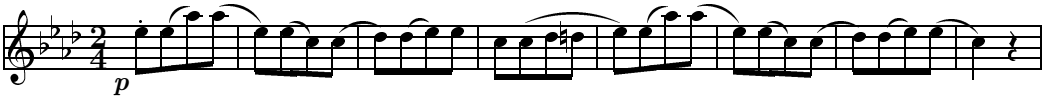

ANTONÍN DVOŘÁK, *Slavonic Dances, Op. 46. No. 3 in A flat major. Poco allegro* (1878)

Chapter 4

Numerical Methods

In Chapter 3 we have derived the linear system of PDEs (3.23) with respect to time t and the radius r,

$$\dot{\mathbf{y}}'(t,r) - \boldsymbol{A}(r)\dot{\mathbf{y}}(t,r) \quad = \quad \xi(r)\left[\boldsymbol{D}(r)\mathbf{y}'(t,r) + \boldsymbol{E}(r)\mathbf{y}(t,r)\right], \tag{4.1}$$

for the solution vector $\mathbf{y}(t,r)$ describing the response of the spherically symmetric, viscoelastic, Maxwell Earth model. (The degree and order subscripts, n and m, respectively, of $\mathbf{y}_{nm}$, $\boldsymbol{A}_n$, $\boldsymbol{D}_n$ and $\boldsymbol{E}_n$ are suppressed throughout this chapter.) Now we are concerned with numerical methods applicable to this system. We begin with a rather terminological remark on differential-algebraic equations which, in fact, precede (4.1). Among several possible techniques of solution to (4.1), we prefer and elaborate the semi-discretizing method of lines (MOL). We discuss two essences of MOL: semi-discretization of the system in the spatial dimension and a choice of methods for time integration of intermediate ODEs, often possessing a high degree of numerical stiffness. We adopt two stiff integrators based on Press et al. (1996)[1]. We also discuss another semi-discretizing method, the method of Rothe, employed in publications collected in Part II. Finally, numerical examples demonstrate the efficiency of the presented approach.

4.1 Differential-Algebraic Equations

Differential-algebraic equations (DAEs), features of DAEs and numerical techniques applicable to DAEs have been a subject of an intensive research over the recent years (see, e.g., Ascher & Petzold 1998 for thorough introduction and a bibliography). Since one of below mentioned techniques for dealing with DAEs has already been applied in Chapter 3, we bring a brief introduction into the terminology of DAEs. Our intent is to emphasize that the system of PDEs (4.1) is essentially based on a system of DAEs, and that techniques available within the DAE methodology should be examined in future works on the IV approach.

The system of DAEs for the solution vector $\boldsymbol{y}(t)$ can be written in the general form as

[1] Our reference to Press et al. (1996) stands for either of Press et al. (1996a) and Press et al. (1996b). The former should be consulted for more details on theoretical background, more references and routines coded in Fortran 77, the latter for the same routines translated into Fortran 90.

$$\boldsymbol{F}(t, \boldsymbol{y}, \dot{\boldsymbol{y}}) \;=\; \mathbf{0}\,, \tag{4.2}$$

where $\boldsymbol{F}$ is a vector function with, possibly, a singular Jacobian matrix $\partial\boldsymbol{F}/\partial\dot{\boldsymbol{y}}$. (The dot means differentiation with respect to t. Within this chapter, the italicized $\boldsymbol{y}$ is casted as an arbitrary vector in rather general statements; the solution vector $\mathbf{y}$ to (4.1) is, however, the intended target.) The minimal number of differentiations of (4.2) which would be required to solve for $\dot{\boldsymbol{y}}(t)$ uniquely in terms of $\boldsymbol{y}(t)$ and t is referred to as the index along the solution $\boldsymbol{y}(t)$. In other words, the index of a system of DAEs is equal to a number of differentiations needed to obtain an explicit system of ODEs for $\boldsymbol{y}(t)$; ODEs are index-0 DAEs. It should be noted that the classification of DAEs is still in evolution; e.g., the above defined index gives a partial insight as it can depend not only on the form of DAEs but also on local features of the solution $\boldsymbol{y}(t)$.

Most DAEs encountered in practice can be written in the form

$$\boldsymbol{f}(t, \boldsymbol{u}, \dot{\boldsymbol{u}}, \boldsymbol{v}, \dot{\boldsymbol{v}}) \;=\; \mathbf{0}\,, \tag{4.3}$$

$$\boldsymbol{g}(t, \boldsymbol{u}, \boldsymbol{v}) \;=\; \mathbf{0}\,. \tag{4.4}$$

This system can also be referred to as the ODEs (4.3) with the algebraic constraints (4.4). The general treatment of DAEs usually begins by some reformulation. For the particular case of (4.3)–(4.4), at least two techniques are conceivable: substitution of, e.g., $\boldsymbol{v}(t)$ from (4.4) into (4.3), which would yield ODEs for $\boldsymbol{u}(t)$, and analytical differentiation of (4.4). The former technique can be applied when $\boldsymbol{v}(t)$ is explicitly expressible from (4.4), the latter is eligible for low-index DAEs. The number of differentiations of (4.4) equal to the index leads to the elimination of the algebraic part in the sense that the system of DAEs takes the form of a system of ODEs. The technique of analytical differentiation is referred to as index reduction.

From comparison of (4.3)–(4.4) with our system of the field PDEs (3.3)–(3.4) we see that the momentum equation forms a differential part of DAEs similar to (4.3), while the Poisson equation gives an algebraic part in the form of (4.4). (The spatial dependence is irrelevant in this context.) Thus, we can obtain the system of DAEs,

$$\begin{aligned}
\dot{\mathbf{y}}'_{1..4,7..8}(t,r) - \boldsymbol{A}_{1..4,7..8\times 1..8}(r)\dot{\mathbf{y}}_{1..8}(t,r) - \\
- \xi(r)\left[\boldsymbol{D}_{1..4,7..8\times 1..8}(r)\mathbf{y}'_{1..8}(t,r) + \boldsymbol{E}_{1..4,7..8\times 1..8}(r)\mathbf{y}_{1..8}(t,r)\right] &= \mathbf{0}\,, \qquad (4.5)\\
\mathbf{y}'_{5..6}(t,r) - \boldsymbol{A}_{5..6\times 1..8}(r)\mathbf{y}_{1..8}(t,r) &= \mathbf{0}\,, \qquad (4.6)
\end{aligned}$$

where the subscripts nm have been suppressed and the remaining subscripts denote the ranges of rows and columns. Differentiation of (4.6) with respect to t gives (3.13) and (3.21) and leads consequently, with (4.5), to the PDEs (4.1).

We conclude that the field PDEs (3.3)–(3.4) give rise to the time-dependent linear index-1 system of DAEs (4.5)–(4.6) which in turn leads to the system of PDEs (4.1) by application of index reduction.

4.2 Method of Lines. Step 1: Discretization in Space

We describe the method of discretization of the PDEs (4.1). It is known that the solution vector $\mathbf{y}(t,r)$ can be characterized by the exponential-like development in time and by the spatial distribution which can be expressed in terms of the spherical Bessel functions. In other words, the

behaviour of $\mathbf{y}(t,r)$ is considerably different in the directions of each independent variable. For this kind of PDEs, methods based on semi-discretization are of a great benefit. Here we discuss the semi-discretizing method referred to as the method of lines. Applying the spatial discretization to (4.1), the intermediate system of ODEs (4.14) is derived. In this context, we point out to a procedure for the evaluation of weights of finite-difference (FD) formulas on arbitrarily spaced grids (Fornberg 1996). We briefly discuss (4.14) from the viewpoint of the eigenvalue analysis.

More or less detailed mentions of the MOL idea can be found in several textbooks (e.g., Dahlquist & Björck 1974; Ascher & Petzold 1998). Monographs concentrated on MOL appeared as well (e.g., Schiesser 1991).

4.2.1 Preliminary Notes on the Semi-discretizing Methods

Semi-discretizing methods for solution to the time- and spatially-dependent PDEs are based on decomposition of the process of discretization into two steps: discretization in space and discretization in time. Either of these steps leads first to intermediate ODEs, and second to algebraic equations. The actual sequence of the steps determines whether the intermediate ODEs form an initial-value (IV) problem or a boundary-value (BV) problem. The intent of the two-step discretization is to allow for utilization of specialized techniques designed for solution to the intermediate ODEs. These techniques accomplish the second, often trickier, or at least too routine, step of the process of solution.

Let us consider a system of K PDEs for the K-element vector $\boldsymbol{y}(t,r)$,

$$\boldsymbol{F}(t,r,\boldsymbol{y},\dot{\boldsymbol{y}}(t,r),\boldsymbol{y}'(t,r),\dot{\boldsymbol{y}}'(t,r))=\boldsymbol{0}\,, \tag{4.7}$$

with initial and boundary conditions $\boldsymbol{y}(0,r)=\boldsymbol{y}_0(r)$ and, e.g., $\boldsymbol{y}(t,a)=\boldsymbol{y}_a(t)$, $\boldsymbol{y}(t,b)=\boldsymbol{y}_b(t)$, respectively. The spatial discretization on the grid $r_0=b<r_1<\ldots<r_J=a$ and the substitution of FD formulas for the spatial derivatives converts (4.7) into the IV problem for ODEs,

$$\boldsymbol{F}^{\mathrm{IV}}(t,\boldsymbol{y}^{\mathrm{IV}}(t),\dot{\boldsymbol{y}}^{\mathrm{IV}}(t))=\boldsymbol{0}\,, \tag{4.8}$$

which is, in fact, a set of scalar IV problems to be integrated along the lines of constant grid points: we have arrived at the reason why MOL is called MOL (sometimes also the numerical method of lines, NUMOL). The $K\times(J+1)$-element solution vector $\boldsymbol{y}^{\mathrm{IV}}(t)$ is composed of $\boldsymbol{y}(t,r_0)$, …, $\boldsymbol{y}(t,r_J)$; the initial condition for $\boldsymbol{y}^{\mathrm{IV}}(0)$ is constructed from $\boldsymbol{y}_0(r_0)$, …, $\boldsymbol{y}_0(r_J)$ in the same manner. The actual number of the ODEs (4.8) depends on the character of the boundary conditions. For the Dirichlet boundary conditions, i.e., those imposed on $\boldsymbol{y}(t,a)$ and $\boldsymbol{y}(t,b)$, the number of scalar unknowns is in fact $K\times(J-1)$, and the same number of equations is necessary: ODEs (4.7) in the $J-1$ interior grid points are to be employed. For the Neumann boundary conditions, i.e., those imposed on $\boldsymbol{y}'(t,a)$ and $\boldsymbol{y}'(t,b)$, the number of scalar unknowns remains $K\times(J+1)$ and the discretized boundary conditions must be added to the $K\times(J-1)$ equations in the interior points to reach the necessary number of equations, $K\times(J+1)$. In the second step, numerical routines appropriate for solution to the IV problems for ODEs (the IV integrators) are applied to (4.8) what results in the above mentioned algebraic equations. It is the advance in the field of IV integrators what makes this approach particularly attractive. Essential prerequisities for efficiency of the integration, namely the adoption of stable integrators and adaptive stepsize control guided by required accuracy, are ensured on a user's behalf by more or less standardized ODE packages.

Table 4.1. Weights for centered FD formulas on an equally spaced grid (Fornberg 1996)

order	w_{j-4}	w_{j-3}	w_{j-2}	w_{j-1}	w_j	w_{j+1}	w_{j+2}	w_{j+3}	w_{j+4}
1st derivative, $f'_j \approx \sum_{k=-4}^{4} w_{j+k} f_{j+k}/h$									
2				$-\frac{1}{2}$	0	$\frac{1}{2}$			
4			$\frac{1}{12}$	$-\frac{2}{3}$	0	$\frac{2}{3}$	$-\frac{1}{12}$		
6		$-\frac{1}{60}$	$\frac{3}{20}$	$-\frac{3}{4}$	0	$\frac{3}{4}$	$-\frac{3}{20}$	$\frac{1}{60}$	
8	$\frac{1}{280}$	$-\frac{4}{105}$	$\frac{1}{5}$	$-\frac{4}{5}$	0	$\frac{4}{5}$	$-\frac{1}{5}$	$\frac{4}{105}$	$-\frac{1}{280}$
2nd derivative, $f''_j \approx \sum_{k=-4}^{4} w_{j+k} f_{j+k}/h^2$									
2				1	-2	1			
4			$-\frac{1}{12}$	$\frac{4}{3}$	$-\frac{5}{2}$	$\frac{4}{3}$	$-\frac{1}{12}$		
6		$\frac{1}{90}$	$-\frac{3}{20}$	$\frac{3}{2}$	$-\frac{49}{18}$	$\frac{3}{2}$	$-\frac{3}{20}$	$\frac{1}{90}$	
8	$-\frac{1}{560}$	$\frac{8}{315}$	$-\frac{1}{5}$	$\frac{8}{5}$	$-\frac{205}{72}$	$\frac{8}{5}$	$-\frac{1}{5}$	$\frac{8}{315}$	$-\frac{1}{560}$

On the other hand, the idea of another semi-discretizing method, called the method of Rothe, is to discretize the PDEs (4.7) in time, $t_0 = 0 < t_1 < \ldots < t_i < \ldots$ It results in a series of BV problems for ODEs parametrized by the time index i,

$$\boldsymbol{F}^{\mathrm{BV}}(i, r, \boldsymbol{y}^{\mathrm{BV}}(i,r), \boldsymbol{y}^{\mathrm{BV}\,\prime}(i,r)) = \boldsymbol{0}\,, \tag{4.9}$$

for the K-element solution vector $\boldsymbol{y}^{BV}(i,r)$, with the boundary conditions $\boldsymbol{y}^{\mathrm{BV}}(i,a) = \boldsymbol{y}_a(i)$ and $\boldsymbol{y}^{\mathrm{BV}}(i,b) = \boldsymbol{y}_b(i)$. Since $\boldsymbol{F}^{\mathrm{BV}}$ depends, at least implicitly, on the integration history, eq. (4.9) is to be solved successively for $i = 0, 1, \ldots$ For the apparent "orthogonality" to MOL, the method of Rothe is occasionaly referred to as the transverse method of lines.

We have already stated that MOL will be particularly suitable if the solution behaves considerably different along the directions of each dimension. Following Ascher & Petzold (1998), another feature of the solution should also signal the advisable application of MOL: if no sharp fronts move rapidly in both space and time, i.e., if these fronts, if they exist, can be reasonably well decoupled in the both dimensions. Hence, MOL is thought to be more suitable for the parabolic PDEs than for the hyperbolic ones, although successful MOL applications are developed for the both classes of PDEs (and—not only as a curiosity—MOL applications for solving to the elliptic PDEs have also been proposed, e.g., Schiesser 1991). We remind that PDEs (4.1) involve the first derivatives with respect to time explicitly and the second derivatives with respect to the radius implicitly, through the stress components of $\mathbf{y}$. Thus, PDEs (4.1) can be characterized as the parabolic PDEs.

A final preliminary note: beside the semi-discretizing methods, universal FD techniques for discretization in the both dimensions in parallel can be applied to (4.1). However, the standard FD schemes lack the efficiency for the stiff problems. To our present knowledge, the IV integrators are the only methods which appear to be capable for solution to the stiff problems. Thus, we adhere to them in what follows.

Table 4.2. Weights for one-sided FD formulas on an equally spaced grid (Fornberg 1996)

order	w_j	w_{j+1}	w_{j+2}	w_{j+3}	w_{j+4}	w_{j+5}	w_{j+6}	w_{j+7}	w_{j+8}
1st derivative, $f'_j \approx \sum_{k=0}^{8} w_{j+k} f_{j+k}/h$									
1	-1	1							
2	$-\frac{3}{2}$	2	$-\frac{1}{2}$						
3	$-\frac{11}{6}$	3	$-\frac{3}{2}$	$\frac{1}{3}$					
4	$-\frac{25}{12}$	4	-3	$\frac{4}{3}$	$-\frac{1}{4}$				
5	$-\frac{137}{60}$	5	-5	$\frac{10}{3}$	$-\frac{5}{4}$	$\frac{1}{5}$			
6	$-\frac{49}{20}$	6	$-\frac{15}{2}$	$\frac{20}{3}$	$-\frac{15}{4}$	$\frac{6}{5}$	$-\frac{1}{6}$		
7	$-\frac{363}{140}$	7	$-\frac{21}{2}$	$\frac{35}{3}$	$-\frac{35}{4}$	$\frac{21}{5}$	$-\frac{7}{6}$	$\frac{1}{7}$	
8	$-\frac{761}{280}$	8	-14	$\frac{56}{3}$	$-\frac{35}{2}$	$\frac{56}{5}$	$-\frac{14}{3}$	$\frac{8}{7}$	$-\frac{1}{8}$
2nd derivative, $f''_j \approx \sum_{k=0}^{8} w_{j+k} f_{j+k}/h^2$									
1	1	-2	1						
2	2	-5	4	-1					
3	$\frac{35}{12}$	$-\frac{26}{3}$	$\frac{19}{2}$	$-\frac{14}{3}$	$\frac{11}{12}$				
4	$\frac{15}{4}$	$-\frac{77}{6}$	$\frac{107}{6}$	-13	$\frac{61}{12}$	$-\frac{5}{6}$			
5	$\frac{203}{45}$	$-\frac{87}{5}$	$\frac{117}{4}$	$-\frac{254}{9}$	$\frac{33}{2}$	$-\frac{27}{5}$	$\frac{137}{180}$		
6	$\frac{469}{90}$	$-\frac{223}{10}$	$\frac{879}{20}$	$-\frac{949}{18}$	41	$-\frac{201}{10}$	$\frac{1019}{180}$	$-\frac{7}{10}$	
7	$\frac{29531}{5040}$	$-\frac{962}{35}$	$\frac{621}{10}$	$-\frac{4006}{45}$	$\frac{691}{8}$	$-\frac{282}{5}$	$\frac{2143}{90}$	$-\frac{206}{35}$	$\frac{363}{560}$

4.2.2 Finite-Difference Formulas on Arbitrarily Spaced Grids

The derivatives can be approximated by FD formulas which weights are either tabulated a priori or are evaluated by means of a numerical routine. The former eventuality is reasonably applicable to equally spaced grids, while the latter is general and can be applied to arbitrarily spaced grids. In the latter case, the weights are dependent on the grid-point locations.

In Table 4.1 we gather the weights of the centered FD formulas of various orders of accuracy for the first and the second derivatives of $f(x)$ at the point x_j, $f'_j \equiv f'(x_j)$ and similarly for f''_j, in terms of values $f_{j+k} \equiv f(x_{j+k})$, $k = 0, \pm 1, \ldots$, in adjacent, equally spaced grid points x_{j+1}, x_{j-1}, x_{j+2}, x_{j-2} etc. In Table 4.2 the one-sided approximations in terms of values of $f(x)$ at x_j, x_{j+1}, x_{j+2} etc. are collected. To give an example, the second-order FD formulas for the first derivative of $f(x)$ take the form as follows,

$$f'_j \approx \frac{-f_{j-1} + f_{j+1}}{2h} \approx \frac{-3f_j + 4f_{j+1} - f_{j+2}}{2h} \approx \frac{f_{j-2} - 4f_{j-1} - 3f_j}{2h}\,, \tag{4.10}$$

with $h = x_{j+1} - x_j = x_j - x_{j-1}$.

An efficient algorithm for the evaluation of the weights of the FD formulas for arbitrary derivatives of $f(x)$ was discovered and first published by Fornberg in 1988. The weights are obtained by

differentiation of the Lagrange interpolating polynomial fitting a set of arbitrary nonrepeated points and by utilization of some recursion relations. The algorithm has been described in both a symbolic language and Fortran 77 in Fornberg (1996) and we rewrite it in Fortran 90 in Appendix C.1.

4.2.3 Discretized System of Ordinary Differential Equations

In order to present a compact numerical formulation of the IV/MOL approach, we discretize the PDEs (4.1) in the spatial dimension using the second-order FD formulas. However, FD formulas of higher orders could be employed in a similar manner.

On the arbitrarily spaced grid, $x_0 = b < x_1 < \ldots < x_J = a$, we can write the second-order FD formulas for the first derivative of $f(x)$ in the general form,

$$f'_0 \approx \beta_0 f_0 + \gamma_0 f_1 + \alpha_0 f_2 \,, \tag{4.11}$$

$$f'_j \approx \alpha_j f_{j-1} + \beta_j f_j + \gamma_j f_{j+1} \,, \qquad j = 1, 2, \ldots, J-1 \,, \tag{4.12}$$

$$f'_J \approx \gamma_J f_{J-2} + \alpha_J f_{J-1} + \beta_J f_J \,, \tag{4.13}$$

where α_j, β_j and γ_j, $j = 0, \ldots, J$, are the weights discussed above. For $x_{j+1} - x_j = x_j - x_{j-1}$, eqs (4.11)–(4.13) reduce to (4.10).

Let us consider (4.1) in an interior point x_j. With FD formulas by (4.11)–(4.13), the term $\dot{\mathbf{y}}'$ is approximated by $\alpha_j \dot{\mathbf{y}}_{j-1} + \beta_j \dot{\mathbf{y}}_j + \gamma_j \dot{\mathbf{y}}_{j+1}$, similarly $\boldsymbol{D}\mathbf{y}' \approx \boldsymbol{D}_j(\alpha_j \mathbf{y}_{j-1} + \beta_j \mathbf{y}_j + \gamma_j \mathbf{y}_{j+1})$, etc. It becomes apparent that (4.1) discretized with respect to r can be expressed in the form of the ODEs for the solution vector $\mathbf{y}(t)$,

$$\boldsymbol{P}\dot{\mathbf{y}}(t) \;=\; \boldsymbol{Q}\mathbf{y}(t) + \mathbf{q} \,. \tag{4.14}$$

Vector $\mathbf{y}(t)$ consists of $8 \times (J+1)$ elements,

$$\mathbf{y}(t) = \left(\boxed{\mathbf{y}_0}, \boxed{\mathbf{y}_1}, \ldots, \boxed{\mathbf{y}_J} \right) \,, \tag{4.15}$$

where each block represents one 8-element vector $\mathbf{y}_j \equiv \mathbf{y}(t, r_j)$, $j = 0, \ldots, J$. Matrix $\boldsymbol{P}$ is band-diagonal with constant coefficients and made from 8×8 blocks. It can be schematically sketched in the form of $J+1$ block-rows and the same number of block-columns, as follows:

$$\boldsymbol{P} = \begin{pmatrix} \boxed{\beta_0 \boldsymbol{I} - \boldsymbol{A}_0} & \boxed{\gamma_0 \boldsymbol{I}} & \boxed{\alpha_0 \boldsymbol{I}} & & 0 \\ \boxed{\alpha_1 \boldsymbol{I}} & \boxed{\beta_1 \boldsymbol{I} - \boldsymbol{A}_1} & \boxed{\gamma_1 \boldsymbol{I}} & & \\ & \boxed{\alpha_2 \boldsymbol{I}} & \boxed{\beta_2 \boldsymbol{I} - \boldsymbol{A}_2} & \boxed{\gamma_2 \boldsymbol{I}} & \\ & \ddots & \ddots & \ddots & \\ & & \boxed{\alpha_{J-1} \boldsymbol{I}} & \boxed{\beta_{J-1} \boldsymbol{I} - \boldsymbol{A}_{J-1}} & \boxed{\gamma_{J-1} \boldsymbol{I}} \\ 0 & & \boxed{\gamma_J \boldsymbol{I}} & \boxed{\alpha_J \boldsymbol{I}} & \boxed{\beta_J \boldsymbol{I} - \boldsymbol{A}_J} \end{pmatrix} , \tag{4.16}$$

where $\boldsymbol{I}$ is the diagonal matrix and $\boldsymbol{A}_j \equiv \boldsymbol{A}(r_j)$, $j = 0, \ldots, J$. Focussing the attention to the specific, i.e., diagonal shape of the two thinly framed blocks, $\alpha_0 \boldsymbol{I}$ and $\gamma_J \boldsymbol{I}$, these blocks can be eliminated

by subtraction of the appropriately multiplied adjacent block-rows, i.e., those with $\gamma_1 \boldsymbol{I}$ and $\alpha_{J-1}\boldsymbol{I}$, respectively. Matrix $\boldsymbol{Q}$ is band-diagonal, too, and can be sketched in the similar manner,

$$\boldsymbol{Q} = \begin{pmatrix} \boxed{\beta_0\boldsymbol{D}_0 + \boldsymbol{E}_0} & \boxed{\gamma_0\boldsymbol{D}_0} & \boxed{\alpha_0\boldsymbol{D}_0} & & 0 \\ \boxed{\alpha_1\boldsymbol{D}_1} & \boxed{\beta_1\boldsymbol{D}_1 + \boldsymbol{E}_1} & \boxed{\gamma_1\boldsymbol{D}_1} & & \\ & \boxed{\alpha_2\boldsymbol{D}_2} & \boxed{\beta_2\boldsymbol{D}_2 + \boldsymbol{E}_2} & \boxed{\gamma_2\boldsymbol{D}_2} & \\ & \ddots & \ddots & \ddots & \\ & & \boxed{\alpha_{J-1}\boldsymbol{D}_{J-1}} & \boxed{\beta_{J-1}\boldsymbol{D}_{J-1} + \boldsymbol{E}_{J-1}} & \boxed{\gamma_{J-1}\boldsymbol{D}_{J-1}} \\ 0 & & \boxed{\gamma_J\boldsymbol{D}_J} & \boxed{\alpha_J\boldsymbol{D}_J} & \boxed{\beta_J\boldsymbol{D}_J + \boldsymbol{E}_J} \end{pmatrix}, \quad (4.17)$$

where (sic) $\boldsymbol{D}_j \equiv \xi(r_j)\boldsymbol{D}(r_j)$ and $\boldsymbol{E}_j \equiv \xi(r_j)\boldsymbol{E}(r_j)$, $j = 0, \ldots, J$. The elimination of the off-diagonal blocks is only feasible if all corresponding elements of the adjacent blocks are mutually proportional. This has been the case of the diagonally-shaped blocks, but it might not be the case of the blocks $\alpha_0\boldsymbol{D}_0$ and $\gamma_J\boldsymbol{D}_J$ versus $\gamma_1\boldsymbol{D}_1$ and $\alpha_{J-1}\boldsymbol{D}_{J-1}$. However, setting $\boldsymbol{D}_0 = \boldsymbol{D}_1$ and $\boldsymbol{D}_J = \boldsymbol{D}_{J-1}$ seems to be a satisfactory approximation; a possibility to discretize more densely near the boundaries is congenial in this context.

The r.h.s. vector $\mathbf{q}$ has the same block structure as is shown in (4.15). A description of the explicit shape of $\mathbf{q}$ must be preceded by some remarks on the treatment of the boundary conditions. At $r = r_J = a$, a is the radius of the Earth, we employ the boundary conditions by (3.26), i.e., those by Farrell (1972) with the Heaviside dependence in time. In the Jth and $(J-1)$th block-rows, we (i) eliminate the 3rd, 4th, 6th and 8th elements of $\mathbf{y}_J$ from the solution vector $\mathbf{y}(t)$, shortening so its length, (ii) substitute the eliminated elements of $\mathbf{y}_J$ into the $\boldsymbol{Q}\mathbf{y}(t)$ term, (iii) eliminate the 3rd, 4th, 6th and 8th rows of the Jth block-row in (4.14); preserved equations correspond, in fact, to the discretized Neumann boundary conditions (cf. p. 31). Steps (i) and (ii) result in some constant terms which emerge in the equations of the Jth and $(J-1)$th block-rows and must be moved to the r.h.s. Thus, we receive 12 elements of $\mathbf{q}$, 8 in the block $\mathbf{q}_{J-1}$ and 4 in the truncated block $\mathbf{q}_J$. The boundary conditions at $r = r_0 = b$, i.e., at the core-mantle boundary, should be deduced from the general requirements for the liquid boundaries, see p. 11 and 19. A special treatment would require the case of $b = 0$ which is examined in Section 4.5. For now we skip further discussion of the boundary conditions at $r = b$, leaving the only note that they may contribute to the blocks $\mathbf{q}_0$ and $\mathbf{q}_1$. The other blocks $\mathbf{q}_j$, $j = 2, \ldots, J-2$, are zero identically.

In (4.14) we have arrived at the linear, band-diagonal ODEs with constant coefficients. Note that the spheroidal and toroidal parts of (4.14) remain decoupled and that it is necessary only to solve the spheroidal part if the boundary conditions (3.26) are considered. The form of (4.14) is appropriate for the application of standard IV integrators. This is discussed in detail in Section 4.3.

4.2.4 Eigenvalue Analysis

We make an ancillary note on the role of the eigenvalue analysis for studying relaxation spectra of the Earth models. For the linear homogeneous system of ODEs with constant coefficients,

$$\dot{\boldsymbol{y}}(t) = \boldsymbol{B}\boldsymbol{y}(t)\,, \quad (4.18)$$

with $\boldsymbol{B}$ the constant matrix, a solution, referred to as the fundamental system, can be written as a linear combination of the constituents

$$e^{\lambda_p t} \quad \text{or} \quad R_q e^{\lambda_q t}\,, \tag{4.19}$$

where λ_p is any nondegenerated eigenvalue of $\boldsymbol{B}$, λ_q any Q-degenerated eigenvalue of $\boldsymbol{B}$ and R_q a polynomial of the maximal degree $Q-1$. For the nonhomogeneous system of ODEs,

$$\dot{\boldsymbol{y}}(t) = \boldsymbol{B}\boldsymbol{y}(t) + \boldsymbol{b}\,, \tag{4.20}$$

a solution is the sum of the fundamental system and a particular solution; for constant $\boldsymbol{b}$ the particular solution is constant, too. If there is any (complex) eigenvalue λ_r of $\boldsymbol{B}$ with a positive real part, the fundamental system of (4.20) will contain a term with $e^{\mathrm{Re}\,\lambda_r t}$, and the solution will be exponentially growing with increasing t.

The ODEs (4.14) form the linear nonhomogeneous system with constant coefficients and, for the surface boundary conditions (3.26), with the constant r.h.s. vector $\mathbf{q}$. In comparison with (4.20) we see that

$$\boldsymbol{y}(t) = \mathbf{y}(t)\,, \quad \boldsymbol{B} = \boldsymbol{P}^{-1}\boldsymbol{Q}\,, \qquad \boldsymbol{b} = \boldsymbol{P}^{-1}\mathbf{q}\,. \tag{4.21}$$

It follows from the statements given above that it is possible to study the properties of the solution to (4.14) by means of the eigenvalue analysis applied to $\boldsymbol{B} = \boldsymbol{P}^{-1}\boldsymbol{Q}$. This technique is certainly related to the traditional normal-mode technique by Peltier (1974). However, if the relaxation times—or stability of the initial model—are only concerned, it might be convenient to construct matrices $\boldsymbol{P}$ and $\boldsymbol{Q}$ and to subject $\boldsymbol{B} = \boldsymbol{P}^{-1}\boldsymbol{Q}$ to some routines from standard eigenvalue packages. Unfortunately, numerical routines for the evaluation of eigenvalues are only efficient for symmetric or Hermitian matrices. For nonsymmetric matrices, the numerical demands, in terms of the processing time, are growing with the third power of the size of matrices. The reasonable bound on J, the total number of layers of the spatial grid discussed above, could not exceed few hundreds.

The appropriate routines for solution to eigenvalues of real nonsymmetric matrices are `balanc`, `elmhes` and `hqr` by Press et al. (1996). It might be profitable to browse other, specialized libraries (e.g., LAPACK/EISPACK[2]).

4.3 Method of Lines. Step 2: Integration in Time

In the previous section the intermediate system of ODEs (4.14) with respect to time has been derived by application of the spatial discretization to PDEs (4.1). It is a general feature of MOL that the intermediate ODEs possess a high degree of numerical stiffness. We begin this section by the illumination of the concept of stiffness. Then, two methods appropriate for integrating stiff ODEs (referred to as the stiff integrators) are introduced and adapted for the band-diagonal structure of the ODEs (4.14). Numerical routines for solution to the underlying linear algebraic equations with the band-diagonal structure are proposed.

[2] In *http://www.netlib.org*.

4.3.1 Concept of Stiffness

Stiffness occurs in a problem where there are two or more very different scales of the independent variable on which the dependent variables are changing[3]. We encounter two sources of numerical stiffness within the IV/MOL approach: (i) that of the physical origin which appears when physical parameters (viscosity, in particular) of the Earth model under consideration span over several orders of magnitude, and (ii) that somehow intrinsic to MOL applications, emergent from the spatial discretization. While the time scale of a problem is determined by the smallest eigenvalue, the largest eigenvalue multiplied by the stepsize in time must lie in the region of the absolute stability of the integration scheme. These regions of explicit integration schemes are generally substantially smaller than those of implicit schemes. It is a problem of stability rather than accuracy what handicaps the explicit schemes in stiff problems.

The origin of stiffness can be demonstrated by the classic example (e.g., Press et al. 1996a). Let us consider the single ODE

$$\dot{y} = -cy \tag{4.22}$$

with constant $c > 0$ and the solution $y(t) = Ae^{-ct}$ with A given by an initial value. The explicit Euler scheme leads to

$$y_{n+1} = y_n + hy'_n = (1 - ch)y_n \,, \tag{4.23}$$

with $h = t_{n+1} - t_n$, while the implicit Euler scheme gives

$$y_{n+1} = y_n + hy'_{n+1} = \frac{y_n}{1 + ch} \,. \tag{4.24}$$

While the former scheme becomes unstable for $h > 2/c$, since $|y_{n+1}| > -|y_n|$ for any n and y_n and $\lim_{n\to\infty} y_n \to \infty$, the latter formula gives the correct value of $\lim_{n\to\infty} y_n$ even for $h \to \infty$. Analogically for the linear system of ODEs with constant coefficients,

$$\dot{\boldsymbol{y}} = -\boldsymbol{C}\boldsymbol{y} \,, \tag{4.25}$$

with $\boldsymbol{C}$ the positive definite matrix (i.e., with positive eigenvalues), the condition of stability imposed on the largest allowed step of explicit Euler differencing is $h < 2/\lambda_{\max}$, where $\lambda_{\max}$ is the largest eigenvalue of $\boldsymbol{C}$. The long-time character of the relaxation of $\boldsymbol{y}$, proportional to $\exp(-\lambda_{\min} t)$, can only be traced by explicit schemes with stepsizes given above. The shortcomings of this constraint for the stiff problems, with the ratio of $\lambda_{\max}/\lambda_{\min}$ being large, are apparent. On the other hand, implicit Euler differencing applied to (4.25) retains stability for all stepsizes h.

Turning to the implicit schemes, a question of accuracy receives the priority. For instance, the implicit Euler scheme, with the region of absolute stability spanning over the complex plane with the exception of the unit circle around the point (1,0), is only first-order accurate. In the following we introduce efficient higher-order methods for integrating IV problems for stiff ODEs in the general form of

$$\dot{\boldsymbol{y}} = \boldsymbol{f}(t, \boldsymbol{y}) \,, \qquad \boldsymbol{y}(t_0) = \boldsymbol{y}_0 \,. \tag{4.26}$$

Several classes of higher-order methods have been proposed (e.g., Ascher & Petzold 1998). First we describe generalizations of the Runge-Kutta method, namely the Rosenbrock methods (also called

[3]Press et al. (1996a), p. 727.

the Kaps-Rentrop methods). Second, we turn to generalizations of the Bulirsch-Stoer methods referred to as the semi-implicit extrapolation methods. The other class (from the historical point of view, the first one) covers predictor-corrector methods usually based on the Gear multistep backward differentiation formulas. Press et al. (1996) confine themselves to the single-step methods of the first two classes, and so do we. A particular reason for this choice is the larger memory consumption of the multistep methods what can become prohibitive in 2-D and 3-D modelling.

4.3.2 Rosenbrock Method

Let us remind the general scheme of the Runge-Kutta methods for integrating ODEs (4.26), e.g., Ascher & Petzold (1998),

$$\boldsymbol{y}(t_0+h)=\boldsymbol{y}_0+\sum_{i=1}^{s}c_i\boldsymbol{k}_i\,,\qquad \boldsymbol{k}_i=h\boldsymbol{f}\left(\boldsymbol{y}_0+\sum_{j=1}^{i-1}\alpha_{ij}\boldsymbol{k}_j\right)\,,\quad i=1,\ldots,s\,, \tag{4.27}$$

with h the stepsize and c_i and α_{ij} constants of a particular member of the Runge-Kutta family. In the Rosenbrock methods, vectors $\boldsymbol{k}_i$ are the solutions to s linear algebraic equations

$$(\boldsymbol{I}-\gamma h\boldsymbol{f}')\cdot\boldsymbol{k}_i=h\boldsymbol{f}\left(\boldsymbol{y}_0+\sum_{j=1}^{i-1}\alpha_{ij}\boldsymbol{k}_j\right)+h\boldsymbol{f}'\cdot\sum_{j=1}^{i-1}\gamma_{ij}\boldsymbol{k}_j\,,\quad i=1,\ldots,s\,, \tag{4.28}$$

where $\boldsymbol{f}'\equiv\partial\boldsymbol{f}/\partial\boldsymbol{y}$ denotes the Jacobian matrix and the coefficients c_i, γ, α_{ij} and γ_{ij} are constants of a particular member of the Rosenbrock family. Note that for $\gamma=\gamma_{ij}=0$, eqs (4.28) reduce to the Runge-Kutta scheme (4.27). The algorithm for the automatic stepsize adjustment in the Rosenbrock methods became available by the Kaps-Rentrop (or, later, Shampine) implementation of the embedded, Runge-Kutta-Fehlberg schemes (and is also implemented by Press et al. 1996).

Let us recall that the ODEs (4.14) can be casted into (4.26) with

$$\boldsymbol{f} = \boldsymbol{P}^{-1}(\boldsymbol{Q}\mathbf{y}+\mathbf{q})\,, \tag{4.29}$$
$$\boldsymbol{f}' = \boldsymbol{P}^{-1}\boldsymbol{Q}\,. \tag{4.30}$$

For (4.29)–(4.30), it is advisable to rewrite the Rosenbrock scheme (4.28) into the form

$$(\boldsymbol{P}-\gamma h\boldsymbol{Q})\cdot\boldsymbol{k}_i=h\left[\boldsymbol{Q}\left(\mathbf{y}_0+\sum_{j=1}^{i-1}\alpha_{ij}\boldsymbol{k}_j\right)+\mathbf{q}\right]+h\boldsymbol{Q}\cdot\sum_{j=1}^{i-1}\gamma_{ij}\boldsymbol{k}_j\,,\quad i=1,\ldots,s\,, \tag{4.31}$$

where the band-diagonal matrices appear on the both sides. Press et al. (1996) have implemented the Rosenbrock stiff integrator for (4.28) by the routine `stiff`. We need a modified implementation for the special, band-diagonal form of both sides of (4.31). This can be found in Appendix C.2.

4.3.3 Semi-implicit Extrapolation Method

The original Bulirsch-Stoer extrapolation method based on the modified midpoint rule and the idea of Richardson extrapolation has been accommodated to the stiff problems by inventing a new, semi-implicit midpoint rule. Press et al. (1996a) give details, references and the implementation. We adjust here this method to the ODEs (4.14).

First, we give in two sentences the outline of the Bulirsch-Stoer method. The method extrapolates a value of $\boldsymbol{y}(t+H)$ from estimations of $\boldsymbol{y}(t+H)$, obtained by the evaluation of a series of n-step progressions of $\boldsymbol{y}_k \equiv \boldsymbol{y}(t+kh)$, $h = H/n$, $k = 1, \ldots, n$. In other words, one computes an estimate of $\boldsymbol{y}(t+H)$ using the midpoint rule with n_1 equidistant steps $h_1 = H/n_1$, then another estimate of $\boldsymbol{y}(t+H)$ with n_2 equidistant steps $h_2 = H/n_2$, $h_2 < h_1$, etc., as far as the method asks for, and then an estimate corresponding to $h \to 0$ is extrapolated. Second, we show the implementation of the semi-implicit midpoint rule by Press et al. (1996). With $\Delta_k \equiv \boldsymbol{y}_{k+1} - \boldsymbol{y}_k$ and $h = H/m$, the implementation for the general ODEs (4.26) takes the following form,

$$\begin{array}{rclcrcl}
\Delta_0 &=& \left(\boldsymbol{I} - h\boldsymbol{f}'\right)^{-1} \cdot h\boldsymbol{f}(\boldsymbol{y}_0)\,, & & \boldsymbol{y}_1 &=& \boldsymbol{y}_0 + \Delta_0\,, \\
\Delta_k &=& \Delta_{k-1} + 2\left(\boldsymbol{I} - h\boldsymbol{f}'\right)^{-1} \cdot \left[h\boldsymbol{f}(\boldsymbol{y}_k) - \Delta_{k-1}\right]\,, & & \boldsymbol{y}_{k+1} &=& \boldsymbol{y}_k + \Delta_k\,, \quad k = 1, \ldots, m-1, \\
\Delta_m &=& \left(\boldsymbol{I} - h\boldsymbol{f}'\right)^{-1} \cdot \left[h\boldsymbol{f}(\boldsymbol{y}_m) - \Delta_{m-1}\right]\,, & & \bar{\boldsymbol{y}}_m &=& \boldsymbol{y}_m + \Delta_m\,.
\end{array} \tag{4.32}$$

Third, we rewrite (4.32) for the ODEs (4.14), i.e., we substitute for $\boldsymbol{f}$ and $\boldsymbol{f}'$ from (4.29)–(4.30):

$$\begin{array}{rclcrcl}
(\boldsymbol{P} - h\boldsymbol{Q})\Delta_0 &=& h(\boldsymbol{Q}\mathbf{y}_0 + \mathbf{q})\,, & & \mathbf{y}_1 &=& \mathbf{y}_0 + \Delta_0\,, \\
(\boldsymbol{P} - h\boldsymbol{Q})\Delta_k &=& (\boldsymbol{P} - h\boldsymbol{Q})\Delta_{k-1} + 2\left[h(\boldsymbol{Q}\mathbf{y}_k + \mathbf{q}) - \boldsymbol{P}\Delta_{k-1}\right]\,, & & & & \\
& & & & \mathbf{y}_{k+1} &=& \mathbf{y}_k + \Delta_k\,, \quad k = 1, \ldots, m-1, \\
(\boldsymbol{P} - h\boldsymbol{Q})\Delta_m &=& \left[h(\boldsymbol{Q}(\mathbf{y}_m) + \mathbf{q}) - \boldsymbol{P}\Delta_{m-1}\right]\,, & & \bar{\mathbf{y}}_m &=& \mathbf{y}_m + \Delta_m\,.
\end{array} \tag{4.33}$$

Note that we refer here by $\mathbf{y}_k$, $k = 0, \ldots, m$, to the values of $\mathbf{y}(t)$ at the internal stages of the Bulirsch-Stoer method, not to the block components of $\mathbf{y}(t)$ in (4.15). The implementation of the semi-implicit extrapolation stiff integrator is available in Press et al. (1996) by the routine `stiffbs`. To adapt `stifbs` to (4.33), a part of the routine for solution to (4.32) has to be rewritten; a part controlling the automatic stepsize adjustment can be preserved without any change.

4.3.4 Linear Algebraic Equations

We have arrived at the systems of linear algebraic equations (4.31) and (4.33) to which the Rosenbrock and the semi-implicit extrapolation stiff integrators, respectively, reduce the ODEs (4.14). We see that at each time step, one algebraic system with the matrix $\boldsymbol{P} - h\boldsymbol{Q}$ must be solved repeatedly for several different r.h.s. (Multiplier γ from (4.31) is irrelevant here.) Matrices $\boldsymbol{P}$ and $\boldsymbol{Q}$ are constant and given by (4.16) and (4.17), respectively, vector $\mathbf{q}$ depends on imposed boundary conditions. It is a crucial property of this algebraic system that $\boldsymbol{P} - h\boldsymbol{Q}$ is a band-diagonal matrix and that band-diagonal solvers may be applied. Numerical characteristics (both processing time and required memory) thus become linear functions of the number of spatial grid points.

Each block-row of $\boldsymbol{P} - h\boldsymbol{Q}$ consists of three non-zero 8×8 blocks, so the maximal width of the diagonal band is bounded by $15 + 1 + 15 = 31$ elements at the most. For the spheroidal subsystem, which consists of 6×6 blocks, the maximal width is bounded by $11 + 1 + 11 = 23$ elements. Moreover, the off-diagonal blocks, essentially matrices $\boldsymbol{I}$ and $\boldsymbol{D}_j$, are either diagonal or sparse, cf. (3.24), so the actual width for the spheroidal subsystem amounts to $9 + 1 + 6 = 16$ elements. In this context we remind the necessity of the reduction of the "off-off-diagonal" blocks $\alpha_0\boldsymbol{I}$, $\gamma_J\boldsymbol{I}$, $\alpha_0\boldsymbol{D}_0$ and $\gamma_J\boldsymbol{D}_J$, see p. 34, otherwise the maximal width would be spuriously increased. Solvers to the algebraic band-diagonal equations are available anywhere (e.g., LAPACK[4]). We adhere to

[4] In *http://www.netlib.org*.

the pivoting solver by Press et al. (1996), `bandec` & `banbks`, accompanied with the routine `banmul` for multiplication of a band-diagonal matrix by a vector to carry out the evaluation of the r.h.s. of (4.31) or (4.33).

The block structure of the diagonal band of $\boldsymbol{P} - h\boldsymbol{Q}$ allures to employ solvers which would exploit this feature. Matrices of this structure are referred to as block-diagonal and emerge commonly when FD formulas are applied to differential equations; the resulting algebraic equations are called the finite-difference equations. An appropriate solver based on Gaussian elimination can be found in Press et al. (1996) in the context of solving BV problems of ODEs by relaxation methods. Their routine `solvde` is designed for a rather special kind of finite-difference equations, the key internal routines `pinvs` and `red`, however, are applicable and, on account of the detailed description of this solver in the referenced source, the generalization (not presented here) is conceivable.

The part of the Rosenbrock stiff integrator, which solves to the algebraic system (4.31) by the band-diagonal solver `bandec` & `banbks` and is intended as the replacement of the corresponding part of the routine `stiff` by Press et al. (1996), is presented in Appendix C.2.

4.4 Method of Rothe

Our older formulation of the IV approach is not based on MOL. In Section 3.1.4 we have demonstrated the compatibility of certain relations of both the older and the IV/MOL formulations. We show now that the older formulation is equivalent to the application of the method of Rothe (MOR) to the PDEs (4.1). MOR is favoured in theoretical studies on stability, uniqueness etc. of various kinds of evolutional PDEs (e.g., Rektorys 1982). The characteristic feature of MOR is that discretization od PDEs in time is performed at first. This kind of discretization in time can not devote too much attention to the nature of PDEs, and, typically, MOR is not a particularly effective method for numerical solution to differential systems with a higher degree of stiffness. However, results presented in Chapters 5–8 have been computed using the older formulation, and we present here how it can be derived via MOR.

We consider the PDEs (4.1) in the form of (3.22) and without indicating the r-dependence of the quantities,

$$\dot{\mathbf{y}}'(t) - \boldsymbol{A}\dot{\mathbf{y}}(t) \;=\; \xi \begin{pmatrix} a_{13}(y_3(t) - KX(t)) \\ a_{24}y_4(t) \\ -y_3'(t) + \sum_k a_{3k}y_k(t) - b_{31}y_1(t) - b_{32}y_2(t) - b_{33}KX(t) \\ -y_4'(t) + \sum_k a_{4k}y_k(t) - b_{41}y_1(t) - b_{42}y_2(t) - (b_{43} + 1/r)KX(t) \\ 0 \\ 0 \\ a_{78}y_8(t) \\ -y_8'(t) + \sum_k a_{8k}y_k(t) - b_{87}y_7(t) \end{pmatrix} . \quad (4.34)$$

In Chapters 5 and 6 we have employed the first-order (Euler) explicit FD formula for the first derivative of the function $f(t)$, $f^i \equiv f(t^i)$,

$$\dot{f}(t^i) \equiv \dot{f}^i \approx \frac{f^{i+1} - f^i}{\Delta t^i}\,, \qquad \Delta t^i \equiv t^{i+1} - t^i\,, \tag{4.35}$$

cf. (5.3) and (6.3). Applying (4.35) to the time derivatives in (4.34), we obtain at $t = t^i$

$$(\mathbf{y}^{i+1})' - \boldsymbol{A}\mathbf{y}^{i+1} = (\mathbf{y}^i)' - \boldsymbol{A}\mathbf{y}^i - \xi\Delta t^i \begin{pmatrix} 0 \\ 0 \\ (y_3^i)' - \sum_k a_{3k} y_k^i \\ (y_4^i)' - \sum_k a_{4k} y_k^i \\ 0 \\ 0 \\ 0 \\ (y_8^i)' - \sum_k a_{8k} y_k^i \end{pmatrix} + \xi\Delta t^i \begin{pmatrix} a_{13}(y_3^i - KX^i) \\ a_{24} y_4^i \\ -b_{31} y_1^i - b_{32} y_2^i - b_{33} KX^i \\ -b_{41} y_1^i - b_{42} y_2^i - (b_{43} + 1/r) KX^i \\ 0 \\ 0 \\ a_{78} y_8^i \\ -b_{87} y_7^i \end{pmatrix}.$$

With $a_{13}, \ldots, b_{87}$ substituted from (2.34)–(2.47), we arrive at the relation for $\mathbf{q}^i = (\mathbf{y}^{i+1})' - \boldsymbol{A}\mathbf{y}^{i+1}$, cf. (6.22),

$$\mathbf{q}^i = \mathbf{q}^{i-1} \begin{pmatrix} 1 \\ 1 \\ 1 - \xi\Delta t^i \\ 1 - \xi\Delta t^i \\ 0 \\ 0 \\ 1 \\ 1 - \xi\Delta t^i \end{pmatrix} + \xi\Delta t^i \begin{pmatrix} \frac{1}{\beta}(y_3^i - KX^i) \\ \frac{1}{\mu} y_4^i \\ -\frac{4\gamma}{r^2} y_1^i + \frac{2N\gamma}{r^2} y_2^i + \frac{4\gamma}{3r} X^i \\ \frac{2\gamma}{r^2} y_1^i - \frac{N\gamma + (N-2)\mu}{r^2} y_2^i - \frac{2\gamma}{3r} X^i \\ 0 \\ 0 \\ \frac{1}{\mu} y_8^i \\ -\frac{(N-2)\mu}{r^2} y_7^i \end{pmatrix}, \tag{4.36}$$

which conforms with (6.39).

Finally we discuss the integro-differential formulation presented in Chapter 7. We discretize (4.1) in time using the FD formula corresponding to (7.40), rewritten in the differential form as

$$\omega\dot{f}^i + (1-\omega)\dot{f}^{i+1} \approx \frac{f^{i+1} - f^i}{\Delta t^i}\,, \quad \Delta t^i \equiv t^{i+1} - t^i\,, \quad 0 \le \omega \le 1\,. \tag{4.37}$$

Let us restrict ourselves to the special case of $\omega = 0$, i.e., the purely implicit scheme. We obtain at the time level $t = t^{i+1}$

$$(\mathbf{y}^{i+1})' - \boldsymbol{A}\mathbf{y}^{i+1} = (\mathbf{y}^i)' - \boldsymbol{A}\mathbf{y}^i + \xi\Delta t^i \left[\boldsymbol{D}(\mathbf{y}^{i+1})' + \boldsymbol{E}\mathbf{y}^{i+1}\right], \tag{4.38}$$

from what the relation for vector $\mathbf{q}^{i+1} = (\mathbf{y}^{i+1})' - \boldsymbol{A}\mathbf{y}^{i+1}$ follows immediately,

$$\begin{aligned} \mathbf{q}^{i+1} &= \mathbf{q}^i + \xi\Delta t^i \left[\boldsymbol{D}(\boldsymbol{A}\mathbf{y}^{i+1} + \mathbf{q}^{i+1}) + \boldsymbol{E}\mathbf{y}^{i+1}\right] \\ &= \mathbf{q}^i + \xi\Delta t^i \left[(\boldsymbol{D}\boldsymbol{A} + \boldsymbol{E})\mathbf{y}^{i+1} + \boldsymbol{D}\mathbf{q}^{i+1}\right]. \end{aligned} \tag{4.39}$$

With the relations (3.62) for $\tilde{\boldsymbol{Q}}_n$ and $\tilde{\tilde{\boldsymbol{Q}}}_n$, we have arrived at (7.43) with $\omega = 0$, and, hence, at (7.45), the final expression of Chapter 7.

Table 4.3. Physical Parameters of the Homogeneous Earth Model and Other Constants

radius a	6371 km
density ϱ_0	5517 $\mathrm{kg\,m^{-3}}$
Lamé elastic parameter λ	3.5288×10^{11} Pa
shear modulus μ	1.4519×10^{11} Pa
bulk modulus K	4.4967×10^{11} Pa
viscosity η	10^{21} Pa s
β	$\lambda + 2\mu$
γ	$3\mu K/\beta$
ξ	μ/η
Newton gravitational constant G	6.6732×10^{-11} $\mathrm{m^3 s^{-2} kg^{-1}}$
year	$3600 \times 24 \times 365.25$ s
π in `REAL(8)` data type of Fortran 90	3.141592653589793_8

4.5 Numerical Implementation

We illustrate the IV/MOL formulation by some output of the numerical modelling. Our current implementation targets on the homogeneous, spherically symmetric, Maxwell viscoelastic Earth models, both incompressible and compressible. We are not ready to release results for viscoelastic Maxwell models with realistic profiles of parameters or for models with the axially symmetric viscosity for the time being, the results below are, however, still worth to be presented since analytical solutions are known for the response of the homogeneous models. With what is given below, the means of validation of the new formulation is provided and the potential of the new code can be appraised.

The code solves to the spheroidal part of the ODEs (4.14) with constant matrices $\boldsymbol{P}$, $\boldsymbol{Q}$ and vector $\mathbf{q}$, all evaluated from $\boldsymbol{A}(r_j)$, $\boldsymbol{D}(r_j)$ and $\boldsymbol{E}(r_j)$ by (2.50), (3.24) and (3.25), respectively. Spatial grid points may be distributed arbitrarily, $r_0 = b < r_1 < \ldots < r_J = a$, with a the radius of the model and b the radius of the elastic "core", underlying the viscoelastic "mantle". The boundary conditions at $r = a$ have been imposed on $\mathbf{y}(t, a) = \mathbf{y}_J(t)$ in accord with (3.26). A temporary shortage of the code resides in the adoption of the boundary conditions at $r = b$. The outputs below have been obtained with the ad hoc choice of $b = 0$ and $\mathbf{y}(t, b) \equiv \mathbf{y}_0(t) = \mathbf{0}$, which partially complies with the initial elastic solution (3.27). It is apparent from Fig. 4.4 that this choice is essentially correct for $\mathbf{y}_0(t)$ at degrees $n > 2$ and for the non-stress components of $\mathbf{y}_0(t)$ at $n = 2$. The ODEs (4.14) have been solved by both the Rosenbrock and the semi-implicit extrapolation stiff integrators adapted for solution to (4.31) and (4.33), respectively. We have employed the Earth model defined by the constant values of initial density ϱ_0, elastic Lamé parameters λ and μ, and viscosity η, according to Table 4.3. The gravitational acceleration can be deduced from (2.4), $g_0(r) = \frac{4}{3}\pi G \varrho_0 r$. Let us also recall that, in the case of material incompressibility, $\lambda \to \infty$, $K \to \infty$, $1/\beta \to 0$, $\lambda/\beta \to 1$ and $\gamma \to 3\mu$.

In Fig. 4.1 we demonstrate the time evolution of the surface values of the Love numbers h_n, l_n and k_n, $n = 2$, 6, 15, 60 and 120, for the first 10^6 yr after the onset of the Heaviside (in time) point mass load at the surface. The surface Love numbers are related to the 1st, 2nd and 5th elements of $\mathbf{y}_J(t)$ by the definition (Farrell 1972)

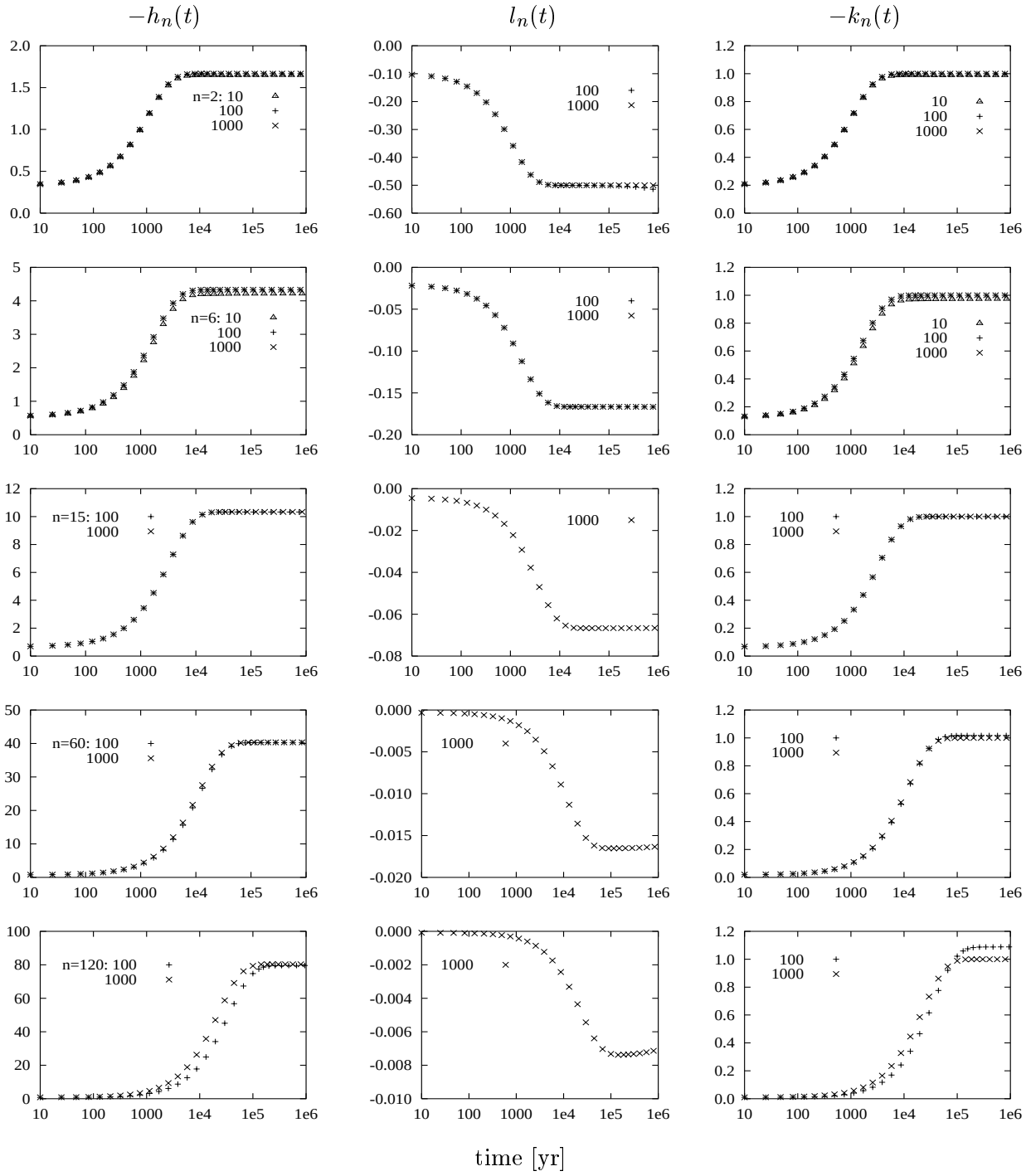

Fig. 4.1. Time evolution of the surface Love numbers h_n, l_n and k_n, $n = 2$, 6, 15, 60 and 120, of the homogeneous incompressible model evaluated by the IV/MOL approach. One symbol represents one time step made by the Rosenbrock stiff integrator. The responses have been calculated with various density of the spatial discretization: symbols $\triangle$ denote values obtained with 11 equidistant spatial grid points (!), + pertain to 101 grid points and $\times$ to 1001 grid points ($J = 10$, 100 and 1000, respectively). The equilibrium state is reached with less than 20 time steps; with 101 grid points, recent Pentium processors generate 20 time steps per second.

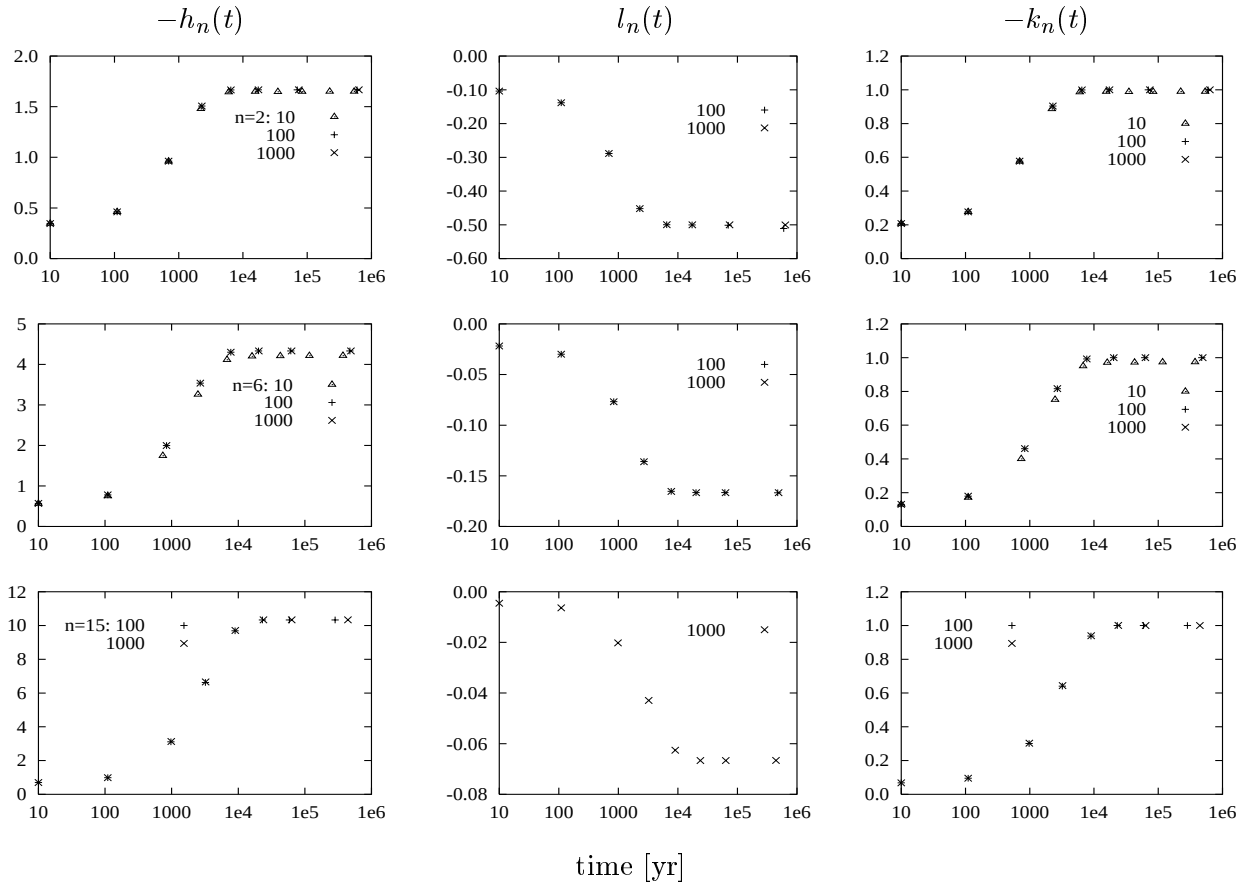

Fig. 4.2. Time evolution of the surface Love numbers h_n, l_n and k_n, $n = 2$, 6 and 15, of the homogeneous incompressible model calculated by the semi-implicit extrapolation stiff integrator. One symbol represents one time step. The stepsizes are more than three times longer than in Fig. 4.1, the total evaluation time amounts to half.

$$\begin{pmatrix} y_{J,1} \\ y_{J,2} \\ y_{J,5} \end{pmatrix} = \frac{\Phi_n}{N_n} \begin{pmatrix} h_n/g_0 \\ l_n/g_0 \\ -k_n \end{pmatrix}, \quad \Phi_n = \frac{4\pi G a \Gamma_n}{2n+1}, \quad N_n = \sqrt{\frac{2n+1}{4\pi}}, \quad \Gamma_n = \frac{2n+1}{4\pi a^2}, \tag{4.40}$$

with Φ_n the coefficients of the spherical harmonic expansion of the surface potential of the point mass load and N_n the norm factors of the spherical harmonics, cf. (2.52). Let us remind that the 3rd, 4th and 6th elements of $\mathbf{y}_J(t)$ are prescribed by the surface boundary conditions (3.26) and that we refrain from solution to the toroidal subsystem (7th and 8th elements). Symbols $\triangle$, $+$ and $\times$ in Fig. 4.1 and others represent the time instants, chosen automatically by the stiff integrators; each time instant is depicted. We have employed 11, 101 and 1001 equally spaced grid points in the spatial dimension (i.e., $J = 10$, 100 and 1000, respectively). The Rosenbrock stiff integrator has been launched for generating Fig. 4.1 and the semi-implicit extrapolation stiff integrator has been employed to compute responses in Fig. 4.2. Adaptive stepsize control of the both stiff integrators works satisfactorily: by the Rosenbrock stiff integrator the state of the isostatic equilibrium has been reached within 20 time steps, and the time instant of 10^6 yr within 30 time steps. The speed of the integration is governed by the number of spatial grid points. Due to the band-diagonal structure of the underlying algebraic equations, the dependence of both the processor time and the allocated memory is a linear function of the number of spatial grid points. As an example

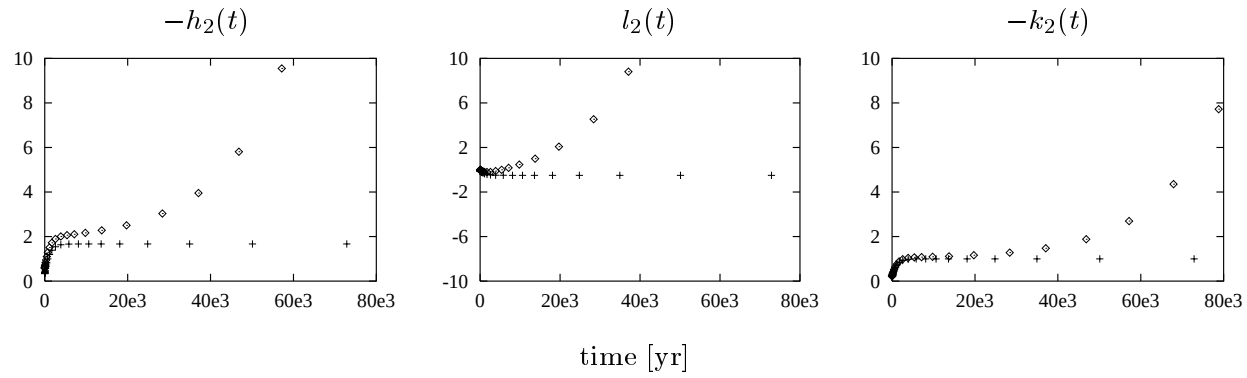

Fig. 4.3. Surface Love numbers h_2, l_2 and k_2 of the homogeneous compressible model (symbols $\diamondsuit$) by the Rosenbrock stiff integrator. The response of the homogeneous incompressible model is shown, too (symbols $+$). Actually, the same as Fig. 8.1.

we can say that the Pentium/350 processor generates 20 time steps per second with 101 spatial grid points. For $n \leq 6$, even the grid of 11 equidistant points reveals satisfactory h_n and k_n; for higher n, similar savings could be achieved by redistributing the grid points towards the surface. Actually, this is the case of 101 grid points for $n \geq 120$, too. Time steps produced by the both stiff integrators exhibit even distribution in the logarithmic scale. The Rosenbrock stiff integrator yields denser time-stepping which is rather universal: the Rosenbrock method by `stiff` utilizes just four intermediate functional evaluations per step, while the number of internal stages (i.e., the steps by h) per step (i.e., the step by H, cf. p. 39) employed by the semi-implicit extrapolation method by `stiffbs` is, in general, higher. The results from the interior points can not, unfortunately, be consistently employed due to the extrapolating character of the latter method. Let us remind that the expected isostatic limits are known analytically (Wu & Peltier 1982),

$$\lim_{t\to\infty} h_n(t) = -\frac{2n+1}{3}\,, \quad \lim_{t\to\infty} k_n(t) = -1\,. \tag{4.41}$$

The long-time values of the surface Love numbers fit these values accurately.

The surface Love numbers of the compressible homogeneous model for $n = 2$ are shown in Fig. 4.3. We see the fast onset of the exponential-like instability of the all three Love numbers. This is the indication of the gravitational collapse of the compressible homogeneous spheres which is discussed in greater detail in Chapter 8; in particular, Fig. 8.1 and Table 8.2 may be confronted.

In Fig. 4.4 we demonstrate the relaxation of the incompressible model again. Now we monitor not only the surface values of $\mathbf{y}_J(t)$, but the depth dependence of the whole $\mathbf{y}(t)$. The time evolution of the physical components of $\mathbf{y}(t)$ has been plotted in the "one time step—one curve" manner. We meet a credible shape of the plotted curves with the amplitudes moving towards the surface with increasing n. We may also confirm the general acceptability of the boundary condition $\mathbf{y}_0(t) = \mathbf{0}$, as has been announced above; in particular, the stress components $T_{rr,2}$ and $T_{r\vartheta,2}$ are the only non-zero components at $r = 0$.

The small number of time steps per degree required in order to obtain the response within the first 10^6 yr appears to be the promising feature of the numerical implementation of the IV/MOL approach. However, other numerical features of the presented code must still be understood. In Fig. 4.5 we present the same content as in Fig. 4.1, now for the time interval of 10^{18} yr. We see the tendency of the horizontal Love numbers $l_n(t)$ to move away from the values reached within

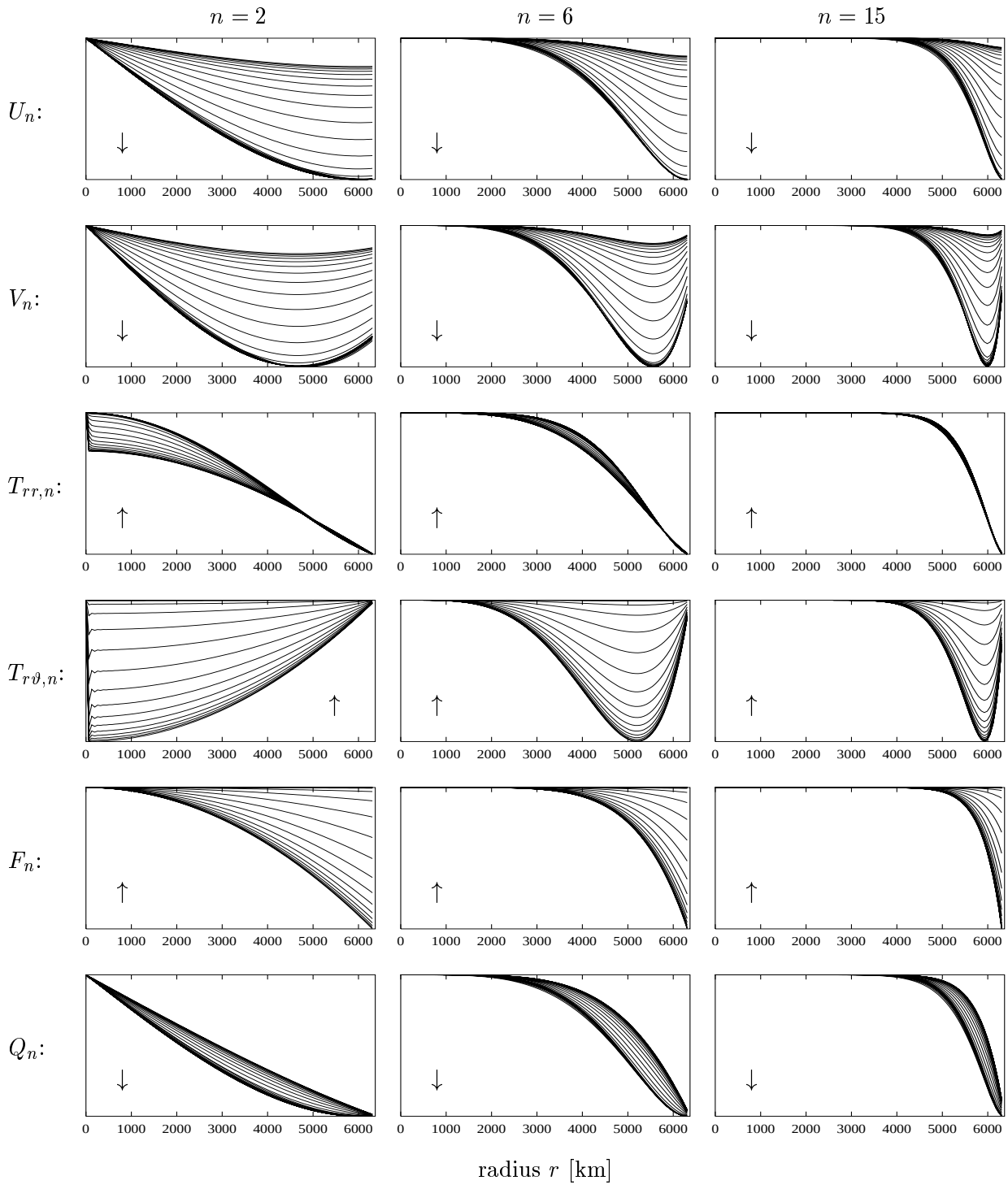

Fig. 4.4. Time evolution of the physical components of the discretized solution vector $\mathbf{y}(t)$ of the homogeneous incompressible model from the elastic response at $t = 0$ up to $t = 10^6$ yr. The direction of the progress in time is depicted by the arrows; timing of the particular time instants can be revealed by comparison with the surface values given in Fig. 4.1. Spatial dimension of 6371 km has been discretized by 101 grid points. Vertical labelling is relative and has been suppressed.

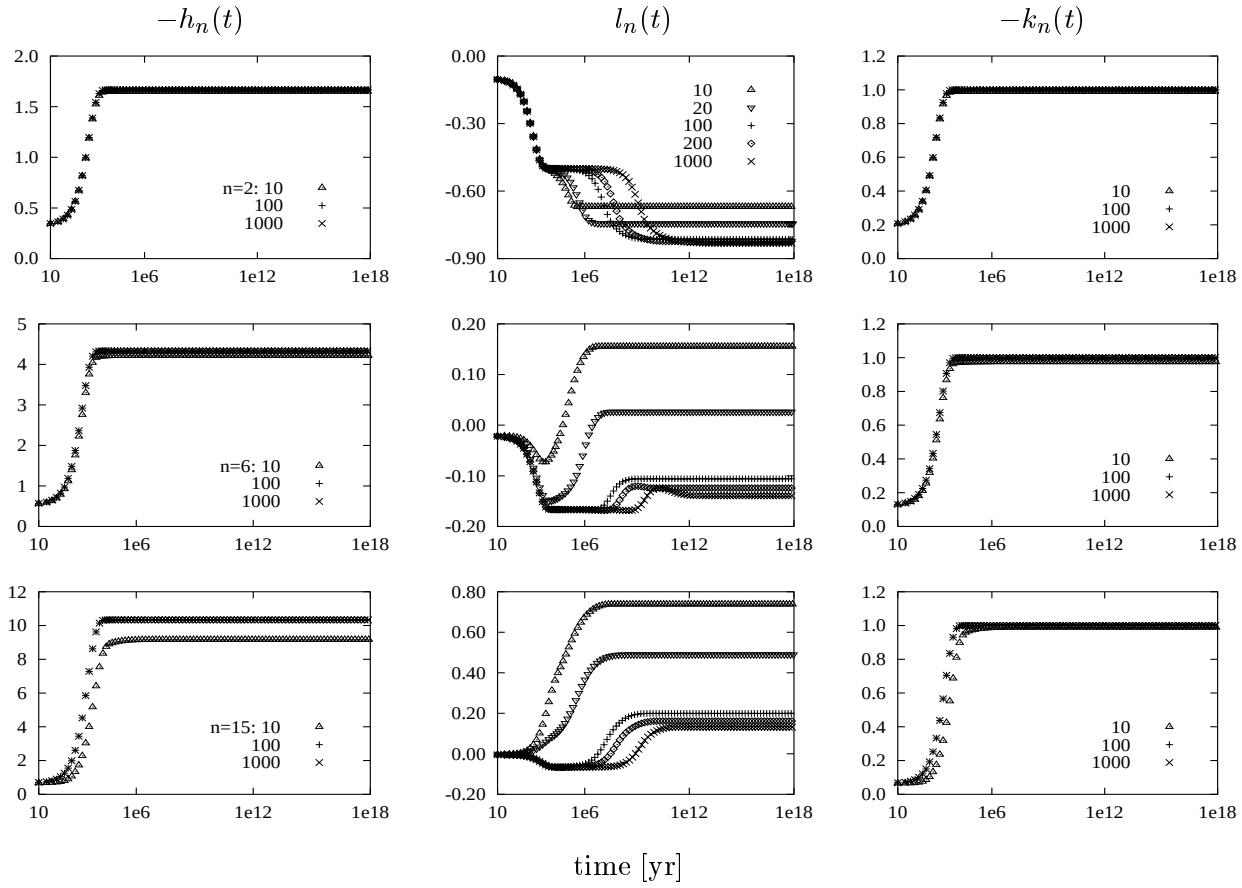

Fig. 4.5. Time evolution of the surface Love numbers h_n, l_n and k_n of the homogeneous incompressible model evaluated by the IV/MOL approach. Similar to Fig. 4.1, but the time period of 10^{18} yr is shown. Various densities of the spatial discretization are considered: 11, 21, 101, 201 and 1001 grid points. See the text for the discussion (but not for the explanation) of the behaviour of $l_n(t)$.

the first 10^6 yr. The time of the onset of this transition to other, somehow arbitrary, but constant values depends on the density of the spatial discretization; the higher density, the latter onset. In Fig. 4.6 we reveal the depth-dependence of the physical components of $\mathbf{y}(t)$ that we have obtained for 101 equidistant grid points. Some of the computed field variables undergo a kind of overturning within the time scale of 10^6–10^{12} yr. This holds a sign of a numerically dependent effect, sensitive not to the choice of the stiff integrator or its internal parameters, but rather to the spatial-grid distribution. At the present moment we do not have a satisfactory explanation of this behaviour on hand. Note, however, that at the limit of $t \to \infty$, from the viewpoint of the NM approach, V_n ought to become undefined.

The generalization of the tested code to process arbitrarily stratified 1-D models will require (i) preparation of appropriate values of $\boldsymbol{P}$, $\boldsymbol{Q}$ and $\mathbf{q}$, (ii) evaluation of the initial elastic solution vector $\mathbf{y}(0)$, and (iii) implementation of proper boundary conditions at the core-mantle boundary. A report on the further development is postponed for a future work[5].

[5] *Ph.D. thesis is considered to be a limited project, and a finite amount of time should only be spent with its preparation* (A. van den Berg, personal communication).

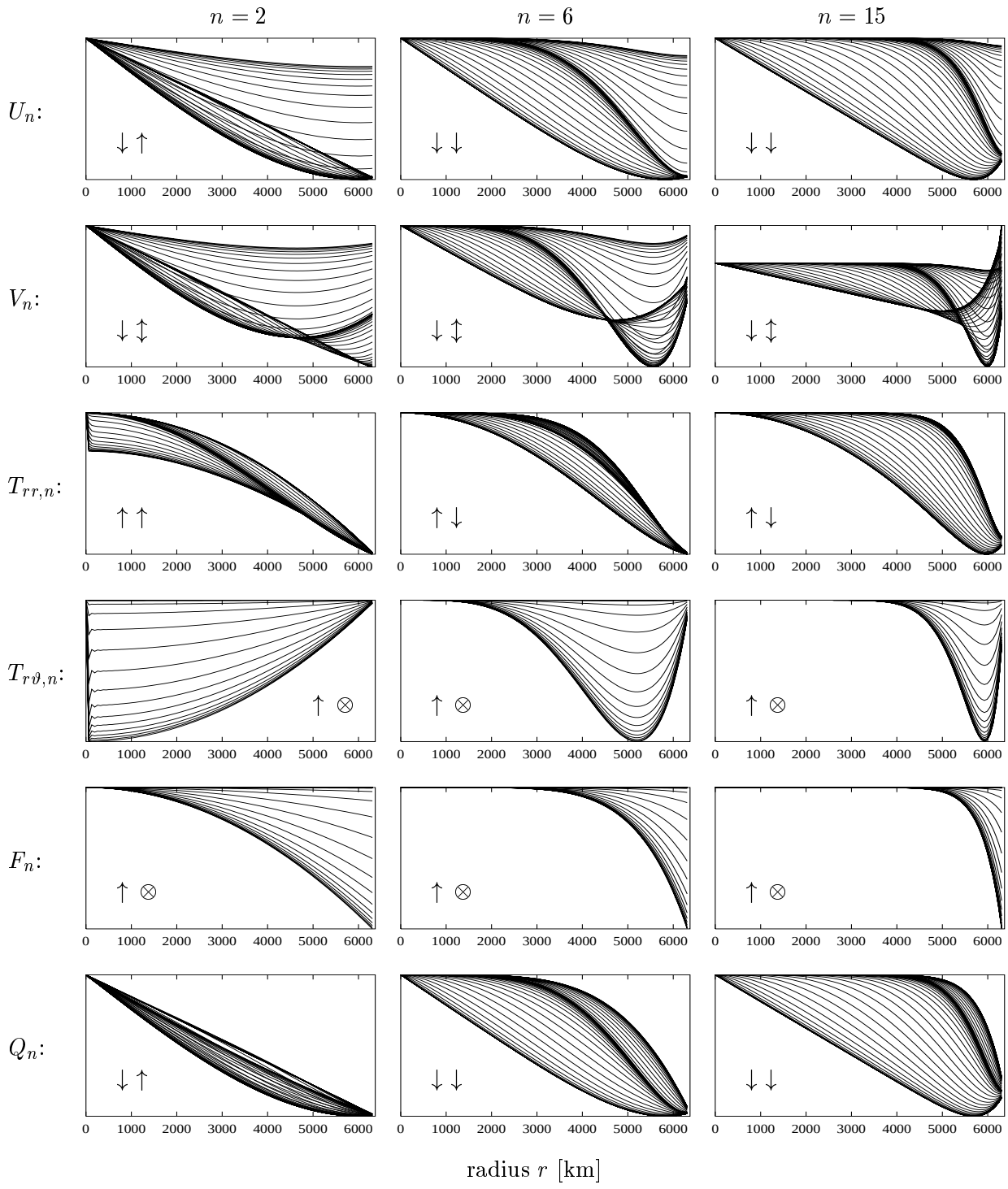

Fig. 4.6. Time evolution of the physical components of the discretized solution vector $\mathbf{y}(t)$ of the homogeneous incompressible model from the elastic response at $t = 0$ to $t = 10^{12}$ yr. The direction of the progress in time is depicted by the arrows; the left arrows direct the evolution of the appropriate field variable for $t \leq 10^6$ yr (identical with Fig. 4.4), the right arrows show the progress during the overturning. No temporal development of the field variable for $t > 10^6$ yr is denoted by the symbol $\otimes$.

4.6 Conclusion to Part I

We have finalized the formulation of the initial-value approach via the method of lines. The field partial differential equations (2.13)–(2.14) in the material-local form have been subjected to the spectral harmonic decomposition. With the elastic constitutive relation (2.10) being considered first, the procedure of derivation of the boundary-value problem for the ordinary differential equations (2.49) with respect to the radius has been exposed. The similar procedure, generalized for the Maxwell viscoelastic constitutive relation (2.15), has been introduced to derive the partial differential equations (3.23) with respect to both time and the radius. Similar differential systems, (3.56) and (3.104), respectively, have been derived with the constitutive relation of the standard linear solid and for the axially symmetric viscosity distribution. The partial differential equations (3.23) for the Maxwell solid have been further elaborated. In accordance with the idea of the method of lines, the spatial semi-discretization has been enforced. This has led to the ordinary differential equations (4.14) with respect to time in the form appropriate for the application of stiff integrators. We have adapted the Rosenbrock and the semi-implicit extrapolation stiff integrators, (4.31) and (4.33), respectively, to exploit the band-diagonal structure of the underlying linear differential equations. The efficiency of the derived formulation has been examined on the analytically tractable relaxation of the homogeneous, Maxwell viscoelastic sphere.

Another formulation of the IV approach has been derived from the partial differential equations (2.13)–(2.15) via the alternative semi-discretizing method of Rothe in Section 4.4. It is this formulation which has been employed in our published papers on the initial-value approach, collected in the following Part II.

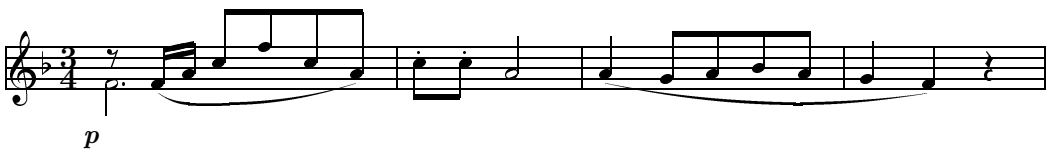

ANTONÍN DVOŘÁK, *Slavonic Dances, Op. 46. No. 4 in F major. Tempo di Minuetto* (1878)

References

Ascher, U.M. & Petzold, L.R., 1998. *Computer Methods for Ordinary Differential Equations and Differential-Algebraic Equations*, SIAM, Philadelphia.

Backus, G.E., 1967. Converting vector and tensor equations to scalar equations in spherical coordinates, *Geophys. J. R. astr. Soc.*, **13**, 71–101.

Boschi, L., Tromp, J. & O'Connell, R.J., 1999. On Maxwell singularities in postglacial rebound, *Geophys. J. Int.*, **136**, 492–498.

Cathles, L.M., 1971. The viscosity of the Earth's mantle, *PhD thesis*, Princeton University, Princeton, New Jersey.

Cathles, L.M., 1975. *The Viscosity of the Earth's Mantle*, Princeton University Press, Princeton, New Jersey.

D'Agostino, G., Spada, G. & Sabadini, R., 1997. Postglacial rebound and lateral viscosity variations: a semi-analytical approach based on a spherical model with Maxwell rheology, *Geophys. J. Int.*, **129**, F9–F13.

Dahlen, F.A. & Tromp, J., 1998. *Theoretical Global Seismology*, Princeton University Press, Princeton, New Jersey.

Dahlquist, G. & Björck, Å., 1974. *Numerical Methods*, Prentice-Hall, New Jersey.

Dziewonski, A.M. & Anderson, D.L., 1981. Preliminary reference Earth model, *Phys. Earth Planet. Inter.*, **25**, 297–356.

Fang, M., 1998. Static deformation of the outer core, in *Dynamics of the Ice Age Earth: A Modern Perspective*, ed. by P. Wu, pp. 155–190, Trans Tech Publ., Zürich, Switzerland.

Fang, M. & Hager, B.H., 1994. A singularity free approach to post glacial rebound calculations, *Geophys. Res. Lett.*, **21**, 2131–2134.

Fang, M. & Hager, B.H., 1995. The singularity mystery associated with a radially continuous Maxwell viscoelastic structure, *Geophys. J. Int.*, **123**, 849–865.

Fang, M. & Hager, B.H., 1996. The sensitivity of post-glacial sea level to viscosity structure and ice-load history for realistically parametrized viscosity profiles, *Geophys. Res. Lett.*, **23**, 3787–3790.

Farrell, W.E., 1972. Deformation of the earth by surface loads, *Rev. Geophys. Space Phys.*, **10**, 761–797.

Fornberg, B., 1996. *A Practical Guide to Pseudospectral Methods*, Cambridge University Press, New York.

Gasperini, P. & Sabadini, R., 1989. Lateral heterogeneities in mantle viscosity and post-glacial rebound, *Geophys. J. Int.*, **98**, 413–428.

Gasperini, P. & Sabadini, R., 1990. Finite element modeling of lateral viscosity heterogeneities and post-glacial rebound, *Tectonophysics*, **179**, 141–149.

Han, D. & Wahr, J., 1995. The viscoelastic relaxation of a realistically stratified earth, and a further analysis of postglacial rebound, *Geophys. J. Int.*, **120**, 287–311.

Hanyk, L., Matyska, C. & Yuen, D.A., 1998. Initial-value approach for viscoelastic responses of the Earth's mantle, in *Dynamics of the Ice Age Earth: A Modern Perspective*, ed. by P. Wu, pp. 135–154, Trans Tech Publ., Zürich, Switzerland.

Hanyk, L., Matyska, C. & Yuen, D.A., 1999. Secular gravitational instability of a compressible viscoelastic sphere, *Geophys. Res. Lett.*, **26**, 557–560.

Hanyk, L., Moser, J., Yuen, D.A. & Matyska, C., 1995. Time-domain approach for the transient responses in stratified viscoelastic Earth models, *Geophys. Res. Lett.*, **22**, 1285–1288.

Hanyk, L., Yuen, D.A. & Matyska, C., 1996. Initial-value and modal approaches for transient viscoelastic responses with complex viscosity profiles, *Geophys. J. Int.*, **127**, 348–362.

Ivins, E.R., Sammis, C.G. & Yoder, C.F., 1993. Deep mantle viscous structure with prior estimate and satellite constraint, *J. Geophys. Res.*, **98**, 4579–4609.

Johnston, P., Lambeck, K. & Wolf, D., 1997. Material versus isobaric internal boundaries in the Earth and their influence on postglacial rebound, *Geophys. J. Int.*, **129**, 252–268.

Jones, M.N., 1985. *Spherical Harmonics and Tensors for Classical Field Theory*, Research Studies Press, Letchworth.

Kaufmann, G. & Wu, P., 1998. Lateral asthenospheric viscosity variations and postglacial rebound: a case study for the Barents Sea, *Geophys. Res. Lett.*, **25**, 1963–1966.

Longman, I.M., 1963. A Green's function for determining the deformation of the earth under surface mass loads, 2. Computations and numerical results, *J. Geophys. Res.*, **68**, 485–496.

Longman, I.M., 1975. On the stability of a spherical gravitating compressible liquid planet without spin, *Geophys. J. R. astr. Soc.*, **42**, 621–635.

Martinec, Z., 1984. Free oscillations of the Earth, *Travaux Géophys.*, **591**, 117–236.

Martinec, Z., 1989. Program to calculate the spectral harmonic expansion coefficients of the two scalar fields product, *Comput. Phys. Commun.*, **54**, 177–182.

Martinec, Z., 1999. Spectral, initial value approach for viscoelastic relaxation of a spherical earth with a three-dimensional viscosity–I. Theory, *Geophys. J. Int.*, **137**, 469–488.

Martinec, Z. & Wolf, D., 1999. Gravitational viscoelastic relaxation of eccentrically nested spheres, *Geophys. J. Int.*, **138**, 45–66.

Melchior, P., 1978. *The Tides of the Planet Earth*, Pergamon Press, Oxford.

Metcalf, M. & Reid, J., 1997. *Fortran 90/95 Explained*, Oxford University Press, New York.

Mitrovica, J.X. & Peltier, W.R., 1989. Pleistocene deglaciation and the global gravity field, *J. Geophys. Res.*, **94**, 13651–13671.

Mitrovica, J.X. & Peltier, W.R., 1991. A complete formalism for the inversion of post-glacial rebound data: resolving power analysis, *Geophys. J. Int.*, **104**, 267–288.

Mitrovica, J.X. & Peltier, W.R., 1992. A comparison of methods for the inversion of viscoelastic relaxation spectra, *Geophys. J. Int.*, **108**, 410–414.

Morse, P.M. & Feshbach, H., 1953. *Methods of Theoretical Physics*, Part I, McGraw-Hill, New York.

Nakada, M., 1999. Implications of a non-adiabatic density gradient for the Earth's viscoelastic response to surface loading, *Geophys. J. Int.*, **137**, 663–674.

Nakada, M. & Lambeck, K., 1987. Glacial rebound and relative sea-level variations: A new appraisal, *Geophys. J. R. astr. Soc.*, **90**, 171–224.

Ni, Z. & Wu, P., 1998. Effects of removing concentric positioning on postglacial vertical displacement in the presence of lateral variation in lithospheric thickness, *Geophys. Res. Lett.*, **25**, 3209–3212.

Pekeris, C.L. & Jarosch, H., 1958. The free oscillations of the Earth, in *Contributions in Geophysics in Honor on Beno Gutenberg*, ed. by H. Benioff, M. Ewing, B.F. Howell, Jr. & F. Press, pp. 171–192, Pergamon Press, New York.

Peltier, W.R., 1974. The impulse response of a Maxwell earth, *Rev. Geophys. Space Phys.*, **12**, 649–669.

Peltier, W.R., 1976. Glacial-isostatic adjustment–II. The inverse problem, *Geophys. J. R. astr. Soc.*, **46**, 669–706.

Peltier, W.R., 1982. Dynamics of the Ice Age earth, *Adv. Geophys.*, **24**, 1–146.

Peltier, W.R., 1985. The LAGEOS constraint on deep mantle viscosity: results from a new normal mode method for the inversion of viscoelastic relaxation spectra, *J. Geophys. Res.*, **90**, 9411–9421.

Peltier, W.R. & Andrews, J.T., 1976. Glacial-isostatic adjustment–I. The forward problem, *Geophys. J. R. astr. Soc.*, **46**, 605–646.

Plag, H.-P. & Jüttner, H.-U., 1995. Rayleigh-Taylor instabilities of a self-gravitating Earth, *J. Geodynamics*, **20**, 267–288.

Press, W.H., Teukolsky, S.A., Vetterling, W.T. & Flannery, B.P., 1996a. *Numerical Recipes in Fortran 77: The Art of Scientific Computing*, second edition, Cambridge University Press, New York.

Press, W.H., Teukolsky, S.A., Vetterling, W.T. & Flannery, B.P., 1996b. *Numerical Recipes in Fortran 90: The Art of Parallel Scientific Computing*, Cambridge University Press, New York.

Rektorys, K., 1982. *The Method of Discretization in Time and Partial Differential Equations*, Reidel Publ., Dortrecht-Boston-London.

Sabadini, R., Yuen, D.A. & Boschi, E., 1982. Polar wandering and the forced responses of a rotating, multilayered, viscoelastic planet, *J. Geophys. Res.*, **87**, 2885–2903.

Sabadini, R., Yuen, D.A. & Portney, M., 1986. The effects of upper-mantle lateral heterogeneities on postglacial rebound, *Geophys. Res. Lett.*, **13**, 337–340.

Schiesser, W.E., 1991. *The Numerical Method of Lines: Integration of Partial Differential Equations*, Academic Press, San Diego.

Spada, G., Yuen, D.A., Sabadini, R., Morin, P.J. & Gasperini, P., 1990. A computer-aided, algebraic approach to the post-glacial rebound problem, *Mathematica Journal*, **1**, 65–69.

Tromp, J. & Mitrovica, J.X., 1999a. Surface loading of a viscoelastic earth–I. General theory, *Geophys. J. Int.*, **137**, 847–855.

Tromp, J. & Mitrovica, J.X., 1999b. Surface loading of a viscoelastic earth–II. Spherical models, *Geophys. J. Int.*, **137**, 856–872.

Varshalovich, D.A., Moskalev, A.N. & Khersonskii, V.K., 1988. *Quantum Theory of Angular Momentum*, World Scientific Publ., London.

Vermeersen, L.L.A. & Sabadini, R., 1997. A new class of stratified viscoelastic models by analytical techniques, *Geophys. J. Int.*, **129**, 531–570.

Vermeersen, L.L.A. & Sabadini, R., 1998. Effects of compressibility and stratification on viscoelastic relaxation: the analytical perspective, in *Dynamics of the Ice Age Earth: A Modern Perspective*, ed. by P. Wu, pp. 123–134, Trans Tech Publ., Zürich, Switzerland.

Vermeersen, L.L.A., Sabadini, R. & Spada, G., 1996a. Analytical visco-elastic relaxation models, *Geophys. Res. Lett.*, **23**, 697–700.

Vermeersen, L.L.A., Sabadini, R. & Spada, G., 1996b. Compressible rotational deformation, *Geophys. J. Int.*, **126**, 735–761.

Wolf, D., 1984. The relaxation of spherical and flat Maxwell Earth models and effects due to the presence of the lithosphere, *J. Geophys.*, **56**, 24–33.

Wolf, D., 1985a. The normal modes of a uniform, compressible Maxwell half-space, *J. Geophys.*, **56**, 100–105.

Wolf, D., 1985b. The normal modes of a layered, incompressible Maxwell half-space, *J. Geophys.*, **57**, 106–117.

Wolf, D., 1991. Viscoelastodynamics of a stratified, compressible planet: incremental field equations and short- and long-time asymptotes, *Geophys. J. Int.*, **104**, 401–417.

Wolf, D., 1994. Lamé's problem of gravitational viscoelasticity: the isochemical, incompressible planet, *Geophys. J. Int.*, **116**, 321–348.

Wolf, D., 1997. Gravitational viscoelastodynamics for a hydrostatic planet, *Habilitation thesis*, Bayerische Akademie der Wissenschaften, München, Germany.

Wolf, D. & Kaufmann, G., 1999. Effects due to compressional and compositional density stratification on load-induced Maxwell-viscoelastic perturbations, *Geophys. J. Int.*, in press.

Wu, P. & Johnston, P., 1998. Validity of using flat-earth finite element models in the study of postglacial rebound, in *Dynamics of the Ice Age Earth: A Modern Perspective*, ed. by P. Wu, pp. 191–202, Trans Tech Publ., Zürich, Switzerland.

Wu, P. & Ni, Z., 1996. Some analytical solutions for the viscoelastic gravitational relaxation of a two-layer non-self-gravitating incompressible spherical earth, *Geophys. J. Int.*, **126**, 413–436.

Wu, P., Ni, Z. & Kaufmann, G., 1998. Postglacial rebound with lateral heterogeneities: from 2D to 3D modeling, in *Dynamics of the Ice Age Earth: A Modern Perspective*, ed. by P. Wu, pp. 557–582, Trans Tech Publ., Zürich, Switzerland.

Wu, P. & Peltier, W.R., 1982. Viscous gravitational relaxation, *Geophys. J. R. astr. Soc.*, **70**, 435–485.

Yuen, D.A. & Peltier, W.R., 1982. Normal modes of the viscoelastic earth, *Geophys. J. R. astr. Soc.*, **69**, 495–526.

Yuen, D.A., Sabadini, R. & Boschi, E., 1982. Viscosity of the lower mantle as inferred from rotational data, *J. Geophys. Res.*, **87**, 10745–10762.

Yuen, D.A., Sabadini, R., Gasperini, P. & Boschi, E., 1986. On transient rheology and glacial isostasy, *J. Geophys. Res.*, **91**, 11420–11438.

Part II

Publications on the Initial-Value Approach

Chapter 5

Time-Domain Approach for the Transient Responses in Stratified Viscoelastic Earth Models[1]

We have developed the numerical algorithm for the computation of transient viscoelastic responses in the time domain for a radially stratified Earth model. Stratifications in both the elastic parameters and the viscosity profile have been considered. The particular viscosity profile employed has a viscosity maximum with a contrast of $O(10^2)$ in the mid lower mantle. The distribution of relaxation times reveals the presence of a continuous spectrum situated between $O(10^2)$ and $O(10^4)$ years. The principal mode is embedded within this continuous spectrum. From this initial-value approach we have found that for the low-degree harmonics the non-modal contributions are comparable to the modal contributions. For this viscosity model the differences between the time-domain and normal-mode results are found to decrease strongly with increasing angular order. These calculations also show that a time-dependent effective relaxation time can be defined, which can be bounded by the relaxation times of the principal modes.

5.1 Introduction

The normal-mode approach for studying the viscoelasic responses to postglacial and postseismic rebound problems (Peltier 1974; Boschi et al. 1985) has been the traditional way. Recent papers by Fang & Hager (1994, 1995) have pointed out the intrinsic mathematical difficulties associated with the normal-mode approach. This problem becomes more serious with the introduction of both continuous viscosity profiles and realistic elastic structures. In this report we will show that these mathematical difficulties associated with the usage of normal-mode expansion in the Laplace domain can be eliminated by employing instead initial-value techniques. We will also study the contaminating influence of the non-modal contributions to the regular normal-mode expansion.

[1]Original reference: Hanyk, L., Moser, J., Yuen, D.A. & Matyska, C., 1995. Time-domain approach for the transient responses in stratified viscoelastic Earth models, *Geophys. Res. Lett.*, **22**, 1285–1288. (Received December 29, 1994; accepted February 25, 1995.)

5.2 Mathematical Formulation

The linear responses of the Earth to a surface load are described in a spherical non-rotating self-gravitating model by the momentum and the gravitational equations (e.g., Farrell 1972) and an appropriate constitutive relation, for instance, that of a viscoelastic Maxwell model commonly used in postglacial studies,

$$\dot{\boldsymbol{\tau}}^M = \dot{\boldsymbol{\tau}}^E - \frac{\mu}{\eta}\left(\boldsymbol{\tau}^M - \frac{1}{3}\bar{\boldsymbol{\tau}}^M \boldsymbol{I}\right), \tag{5.1}$$

where $\mathbf{u}$ is the small-amplitude displacement and $\boldsymbol{\tau}^M$ the incremental Cauchy stress tensor of the Maxwell model with the trace $\bar{\boldsymbol{\tau}}^M = 3K\nabla\cdot\mathbf{u}$. The dots denote time derivation. The elastic contribution to the Maxwell stress tensor is

$$\boldsymbol{\tau}^E = \left(K - \frac{2}{3}\mu\right)\nabla\cdot\mathbf{u}\boldsymbol{I} + \mu\left(\nabla\mathbf{u} + \nabla\mathbf{u}^T\right). \tag{5.2}$$

Rheology of the earth model is thus sufficiently parametrized by the shear and bulk moduli, $\mu(r)$ and $K(r)$, and the viscosity $\eta(r)$.

The classical approach to the problem consists in the application of the Laplace transform that converts the rheological relationship into Hooke's law with Lamé's coefficients dependent on the Laplace-transformed variable s. It was proposed by Peltier (1974) that for a simple layered Earth models the solution may be expressed by a short sum of normal modes. Such a solution can be inversely transformed into the time domain easily as it uses only discrete points on the real axis in the spectral domain. It represented great computer savings, when it was first introduced. Recently, attention has been focused to the omitted part of the Laplacian spectrum for more realistic depth-dependences of viscosities. Han & Wahr (1995) pointed out to the continuous part in the spectrum of the normal modes and Fang & Hager (1994, 1995) dealt with the singularities associated with the shear modulus and the viscosity depth-dependence. The solution thus becomes more and more diverse, which complicates the inversion into the time domain.

We propose to avoid the mathematical problems inherent in the spectral approach by using the constitutive equations in the time domain. With greater computational speed available in 1990's, the task of engaging in time-domain integration is not as daunting as before and, in fact, is quite feasible. We integrate the relation (5.1) at time $t = t^{i+1}$ in terms of the time step Δt^i by the classical Euler method:

$$\boldsymbol{\tau}^{M,i+1} = \boldsymbol{\tau}^{E,i+1} + \boldsymbol{\tau}^{M,i} - \boldsymbol{\tau}^{E,i} - \frac{\mu\Delta t^i}{\eta}(\boldsymbol{\tau}^{M,i} - K\nabla\cdot\mathbf{u}^i\boldsymbol{I}), \tag{5.3}$$

$$\boldsymbol{\tau}^{M,0} = \boldsymbol{\tau}^{E,0}. \tag{5.4}$$

The divergence of $\boldsymbol{\tau}^{M,i+1}$ can be now split into the two terms

$$\nabla\cdot\boldsymbol{\tau}^{M,i+1} = \nabla\cdot\boldsymbol{\tau}^{E,i+1} - \mathbf{h}(t^i), \tag{5.5}$$

where the second one is the contribution from the past history to the time t^i. Finally, the momentum and the Poisson equations yield the time-discretized system at the time t^{i+1} as

$$\left[\varrho_0\nabla\varphi_1 - \nabla\cdot(\varrho_0\mathbf{u})\nabla\varphi_0 + \nabla(\varrho_0\mathbf{u}\cdot\nabla\varphi_0) - \nabla\cdot\boldsymbol{\tau}^E\right]^{i+1} = -\mathbf{h}(t^i), \tag{5.6}$$

$$\left[\nabla^2\varphi_1 + 4\pi G\nabla\cdot(\varrho_0\mathbf{u})\right]^{i+1} = 0, \tag{5.7}$$

where ϱ_0 and φ_0 are the original density and gravitational potential, respectively. The self-gravitation is then described by means of the perturbation of the potential φ_1. The new quantity $-\mathbf{h}(t^i)$ on the right-hand side—in contrast to the well-known left-hand-side quantities—is not related to the actual time level t^{i+1} but to the previous time. This is the crucial point of this approach; we can determine time-dependent displacement and perturbation potential simply by adding some additional terms, obtained from previous time steps, into the momentum equation. The components of displacements and the perturbation potential are used to be expressed by means of their dimensionless counterparts—the Love numbers.

After expansion of unknowns into the series of spherical harmonics, the equations (5.6)–(5.7) are converted into a system of ordinary differential equations, decomposed with respect to the angular order n,

$$\frac{d}{dr}\mathbf{y}_n^{i+1}(r) = \boldsymbol{A}_n(r) + \mathbf{q}_n^i(r)\,, \tag{5.8}$$

in which the non-zero right-hand side $\mathbf{q}_n^i(r)$ is due to the non-zero right-hand side $-\mathbf{h}(t^i)$ of (5.6). The vector $\mathbf{y}_n(r)$ is the six-component solution of the elastic-gravitational problem (e.g., Farrell 1972). The system (5.8) with $\mathbf{q}_n^i(r) = \mathbf{0}$ is identical to that known from the elastic problem.

The system (5.8) has been discretized in the radial direction into 607 levels with 114 points in the first 220 km, 92 points between 220 and 670 km, 224 points in the lower mantle and 177 point in the core. The physical parameters of the PREM model (Dziewonski & Anderson 1981) have been interpolated at the assigned grid points. We have employed an analytical form for the viscosity profile, given below in the equation (5.9), in integrating the system of equations (5.8). With time-integration it is quite straightforward today to catch all of the dynamical timescales and amplitudes of the normal modes and continuous spectra.

5.3 Results

We have employed the following formula for describing a possible viscosity profile in the lower mantle. It is given by

$$\eta(z) = \left[1 + 214.3\, z\, e^{-16.7(0.7 - z)^2}\right] \times 10^{21}\ \mathrm{Pa\,s} \tag{5.9}$$

where z is the depth non-dimensionalized with respect to the thickness of the mantle. The viscosity is assumed twenty orders higher of magnitude to account for the elastic rheology of the lithosphere ($z < 0.042$). This profile is shown in Fig. 5.1 along with a discrete layered viscous structure, which is similar to those traditionally used for parameterizing viscosity profiles in viscoelastic problems (e.g., Sabadini et al. 1984). Additional layers will produce new normal modes. This would mean more complicated modal structures for increasingly finer discretized models. This particular viscosity profile with a distinct viscosity maximum in the mid-lower mantle is similar to that derived by inversion of geoid anomalies and plate velocities (Ricard & Wuming 1991). The presence of the viscosity "hill" has also been found in numerical convection calculations by van Keken & Yuen (1995) based on the rheology obtained by parameterizing the high melting curves of perovskite (Zerr & Boehler 1993).

The spectra of relaxation times versus degree harmonic depend sensitively on the style of stratification. For continuous profiles involving the PREM model Han & Wahr (1995) have shown the

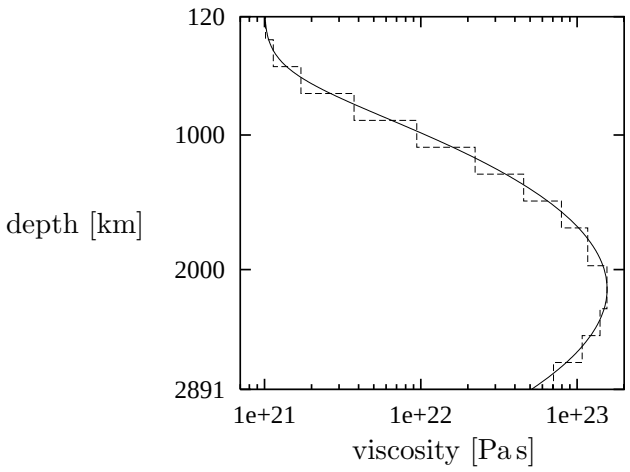

Fig. 5.1. A continuous viscosity profile (5.9) and a layered viscosity approximation. Each discrete viscosity layer creates additional relaxation modes. This viscosity profile has been used in conjunction with the PREM model, which provides the elastic parameters and the density distribution.

clustering of the relaxation times within a certain time window, leading to the formation of a continuous spectrum. For the continuous viscosity profile shown in Fig. 5.1 we have calculated the relaxation spectra using a standard Laplace-transform normal-mode code, e.g., searching for the poles of the Laplace transforms of $\mathbf{y}_n(r,t)$ on the negative half of the real axis. The modal strength coefficients have been determined from the secular determinant with respect to the Laplace variable s, following the prescription given in Han & Wahr (1995). The relaxation spectrum up to an angular order of 60 is displayed in Fig. 5.2. The continuous spectrum appears as the vertical line spanning between the logarithmic inverse relaxation times of -2 and 1. The range of the continuous

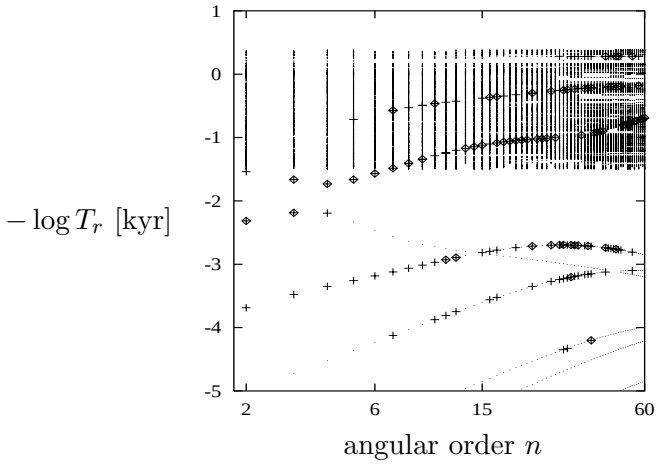

Fig. 5.2. Relaxation spectra of the continuous viscosity profile (5.9). The logarithm of the inverse relaxation time of each class of modes is plotted as a function of the angular order n. Diamond and cross signs indicate modes whose contributions are respectively more than 25% and 5% of the total modal contributions at each angular order. The vertical lines represent the continuous spectra.

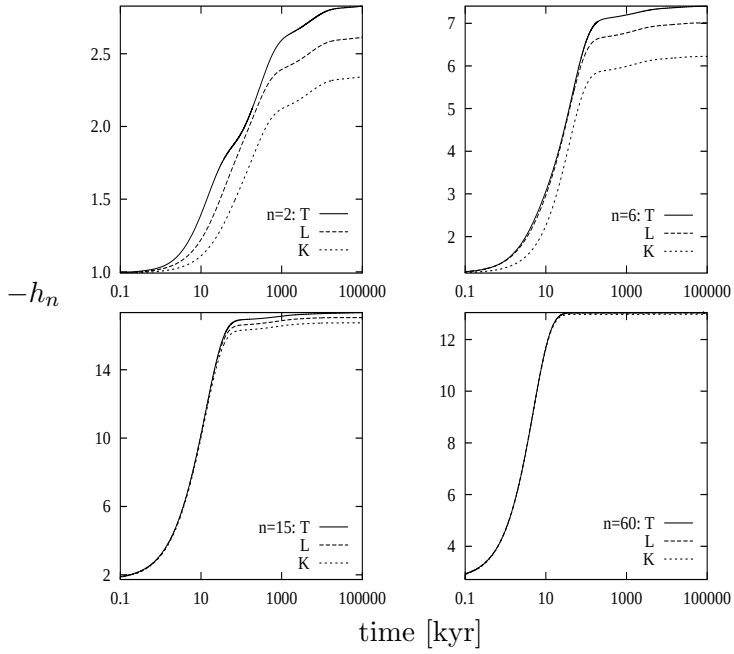

Fig. 5.3. Time-dependent vertical Love numbers h_n as a function of time. The initial-value result is labeled by T, L denotes the sum of all modes we were able to find and K stands for the sum of four dominating modes. Angular orders 2, 6, 15 and 60 have been considered. Lower and upper ordinates indicate respectively the elastic and viscous limits in the response.

spectrum depends on the magnitude of the viscosity "hill" in the lower mantle, as it controls the extrema of the local Maxwell times. The major contributing modes are designated by the diamond signs. The major modes, lying within the band of continuous spectrum, indicate the potential of additional contribution from the continuous spectrum.

In Fig. 5.3 we compare the time-dependent responses between the the time-domain calculations, those obtained from normal-mode expansion in which we have kept just the top four dominating modes that we have found quickly during s-adaptive stepwise searching on the negative real half-axis. The response obtained by adding all modes that we were able to find is displayed, too. The load function is a point source in space and has a Heaviside functional dependence in time. A comparison is made for angular orders 2, 6, 15 and 60. For this model in which the maximum deviation of the viscosity lies in the lower mantle, the most significant differences between the time-domain and the normal-mode results are found for the lowest angular order $n = 2$. There in the transient regime, discrepancies up to 100% can be found in the transient viscous responses. This result would have very dire consequences for using viscoelastic normal-mode theory with its usual resolution of modes in rotational problems (Yuen & Sabadini 1985) involving stratifed viscoelastic structure in the lower mantle. The differences between the time-domain and normal-mode calculations are found to decrease strongly with increasing angular order or shorter wavelength. This can be explained on physical grounds, because the higher-degree eigenfunctions cannot sample the lower mantle, where the maximum negative convexity of the viscosity is located. These results concur with the recent finding by Fang & Hager (1995), who have found that the normal-mode technique becomes increasingly invalid for viscosity profiles displaying a degree of negative convexity, as in the case

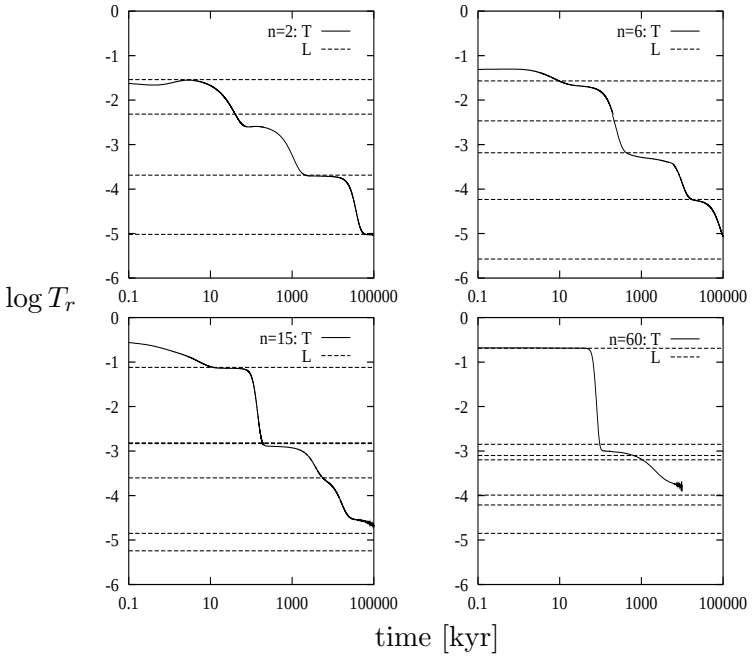

Fig. 5.4. Effective time-dependent relaxation time T_r in kyr as a function of time for the cases given in Fig. 5.3. The relaxation times of the major modes from the Laplace-transform theory are given as dashed lines. Otherwise, same symbols as in Fig. 5.3.

of the viscosity profile shown in Fig. 5.1. For other types of viscosity profile, such as those with a low-viscosity zone (Boschi et al. 1985), the situation would be reversed to where higher-degree responses would become more contaminated with non-modal contributions.

From the time-dependence of the responses shown in Fig. 5.3, an effective time-dependent relaxation time may be constructed by sampling locally the time series. This was done by conducting a least-squares fit for a moving window spanning 10 points in the time series. The results for the degrees shown in Fig. 5.3 are now displayed in Fig. 5.4. We have shown the relaxation times associated with the major modes (horizontal bars at the vertical edge of the figure) of each degree. The effective relaxation times are fast in the beginning and become longer with time. They are bounded by the relaxation times associated with the major modes. These results show that there is a correspondence between relaxation times in normal mode theory and the evolving timescales in viscoelastic responses.

5.4 Conclusion

We have presented here an efficient method for conducting time-domain analysis of transient viscoelastic responses in geophysical problems. The big payoff in this approach will be realized for more complicated viscosity models and for models with lateral viscosity variations. In this study we have found that normal mode theory fails for long wavelengths for a viscosity profile displaying a large negative convexity in the lower mantle. This result has very important implications for the usage of conventional normal-mode theory without the usage of branch-cut integration (Fang &

Hager 1995) in realistic viscously stratified situations. Other types of viscosity stratification, such as an asthenosphere, can cause problems for conventional normal-mode decomposition at shorter wavelengths.

Acknowledgements. We thank Drs. M. Fang and J. Wahr for discussions, Drs. D. Han, P. Machetel and D. Wolf for their comments. This research has been supported by D.O.E. Geosciences Program, Lageos-II program of N.A.S.A., the U.S.–Czechoslovak Science and Technology Joint Fund in cooperation with the Ministry of Education of the Czech Republic, USGS and NSF under Project No. 202/93/0450 and the Czech national grant GAČR No. 0450.

References

Boschi, E.V., Sabadini, R. & Yuen, D.A., 1985. The transient polar motions and the nature of the asthenosphere for short time scales, *J. Geophys. Res.*, **90**, 3559–3568.

Dziewonski, A.M. & Anderson, D.L., 1981. Preliminary reference Earth model, *Phys. Earth Planet. Inter.*, **25**, 297–356.

Fang, M. & Hager, B.H., 1994. A singularity free approach to post glacial rebound calculations, *Geophys. Res. Lett.*, **21**, 2131–2134.

Fang, M. & Hager, B.H., 1995. The singularity mystery associated with a radially continuous Maxwell viscoelastic structure, *Geophys. J. Int.*, **123**, 849–865.

Farrell, W.E., 1972. Deformation of the earth by surface loads, *Rev. Geophys. Space Phys.*, **10**, 761–797.

Han, D. & Wahr, J., 1995. The viscoelastic relaxation of a realistically stratified earth, and a further analysis of postglacial rebound, *Geophys. J. Int.*, **120**, 287–311.

Peltier, W.R., 1974. The impulse response of a Maxwell earth, *Rev. Geophys. Space Phys.*, **12**, 649–669.

Ricard, Y. & Wuming, B., 1991. Inferring the viscosity and the 3-D density structure of the mantle from geoid, topography and plate velocities, *Geophys. J. Int.*, **105**, 561–571.

van Keken, P. & Yuen, D.A., 1995. Dynamical influences of high viscosity in the lower mantle induced by the steep melting curve of perovskite: Effects of curvature and time dependence, *J. Geophys. Res.*, **100**, 15233–15248.

Yuen, D.A. & Sabadini, R., 1985. Viscosity stratification of the lower mantle as inferred from the $\dot{J}_2$ observation, *Ann. Geophys.*, **3**, 647–654.

Zerr, A. & Boehler, R., 1993. Melting of (Mg,Fe)SiO_3-perovskite under hydrostatic, inert conditions to 580 kbar: indication of very high melting temperatures in the lower mantle, *Science*, **262**, 663–665.

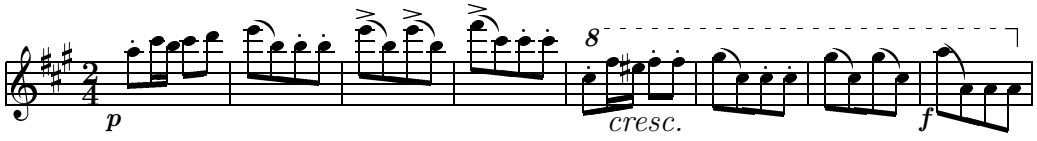

ANTONÍN DVOŘÁK, *Slavonic Dances, Op. 46. No. 5 in A major. Allegro vivace* (1878)

Chapter 6

Initial-Value and Modal Approaches for Transient Viscoelastic Responses with Complex Viscosity Profiles[1]

An initial-value theory is proposed for studying viscoelastic responses of compressible earth models with complex viscosity profiles. Continuous spectra are caused by both compressibility and the viscosity stratification, and they can cause numerical difficulties for the modal approach. We have studied the different responses for various types of viscosity profiles and found that there are differences in the responses at short wavelengths for viscosity profiles with sharp low-viscosity zones. We found that many modes are required to match the full initial-value solutions in the presence of sharp viscosity stratifications in both the upper and lower mantles. The normal-mode approach is best suited for simple layered models, long wavelengths and timescales greater than several thousand years, while the initial-value approach is indispensable in treating short-timescale problems with sharp low-viscosity zones in the upper mantle and viscosity stratification in the lower mantle.

6.1 Introduction

Postglacial rebound was first studied with simple viscous models (Haskell 1935; Vening-Meinesz 1937). These initial investigations were then followed by methods using relaxation time spectra (e.g., McConnell 1968) for estimating the upper-mantle viscosity from the rate of uplift (Crittenden 1963). Viscoelastic models were introduced by Cathles (1971) and Peltier (1974) because of the availability of more precise uplift data with more extensive geographical coverage. Rapid progress in modelling postglacial rebound has been made by means of the correspondence principle and use of the viscoelastic normal-mode approach (e.g., Peltier 1974; Yuen & Peltier 1982; Sabadini et al. 1984a). This type of spectral expansion has also been applied to other transient viscoelastic phenomena, such as postseismic relaxation (Sabadini et al. 1984b; Boschi et al. 1985). The initial-

[1]Original reference: Hanyk, L., Yuen, D.A. & Matyska, C., 1996. Initial-value and modal approaches for transient viscoelastic responses with complex viscosity profiles, *Geophys. J. Int.*, **127**, 348–362. (Received July 17, 1995; revised June 26, 1996; accepted June 26, 1996.)

value approach for the viscoelastic relaxation problem has been employed by Cathles (1971), Ivins et al. (1993) and most recently by Hanyk et al. (1995).

In the past year there has been a flurry of activity following the recognition that new problems arise with the application of normal modes in the presence of complicated stratified earth models (Han & Wahr 1995; Fang & Hager 1994, 1995; Peltier 1995; Hanyk et al. 1995). Han & Wahr (1995) were the first to recognize the problem of the continuous spectrum due to the use of the PREM model (Dziewonski & Anderson 1981) for describing the elastic stratification, and they recognized the need to classify the different types of modes, the normal modes and the continuous spectrum. Fang & Hager (1994, 1995) found that, by deforming the contour of integration, contributions from the continuous spectrum were obtained for an incompressible model with stratified viscosity. Hanyk et al. (1995) developed an initial-value technique and compared the initial-value results with the normal-mode findings. Differences were found for the long-wavelength component due to the lower-mantle viscosity stratification if only the principal normal modes were taken into account. Recently, Mitrovica & Davis (1995) and Peltier (1995) found that many normal modes are needed to capture correctly the horizontal displacements. Steinberger (1996) employed an initial-value approach for integrating the viscoelastic equations in the Earth rotation problem. The issues ensuing from the need to employ both the normal modes and continuous spectrum are by no means restricted to viscoelasticity, but are also of crucial importance in the atmospheric sciences for the baroclinic instability problem (Pierrehumbert & Swanson 1995).

Recently, Piersanti et al. (1995) and Sabadini et al. (1995) studied the short-timescale problem of postseismic deformation with an incompressible model consisting of a few viscoelastic layers. This regime, involving both short timescales and wavelengths, may be especially vulnerable to contributions from the continuous spectrum, as this lies within the transient regime, where the contributions from the continuous spectrum are likely to be substantial. Therefore, it is especially important to assess the validity of the viscoelastic models used for short timescales. The purposes of this paper are (1) to set down the theory for the initial-value approach in detail; (2) to examine the effects of compressibility and various viscosity stratifications on the transient responses; and (3) to understand better the relationship between the initial-value and the modal approaches.

6.2 Formulation

6.2.1 Theory

The Maxwell viscoelastic rheology can be expressed as

$$\dot{\boldsymbol{\tau}}^M = \dot{\boldsymbol{\tau}}^E - \frac{\mu}{\eta}(\boldsymbol{\tau}^M - K\nabla\cdot\mathbf{u}\boldsymbol{I})\,, \tag{6.1}$$

$$\boldsymbol{\tau}^E = (K - 2/3\mu)\nabla\cdot\mathbf{u}\boldsymbol{I} + \mu(\nabla\mathbf{u} + \nabla\mathbf{u}^T)\,, \tag{6.2}$$

with the ordinary casting of variables, i.e., $\boldsymbol{\tau}^M$ for the stress tensor, $\mathbf{u}$ for the displacement vector, μ, K for the shear-stress and bulk moduli, respectively, and η for the dynamic viscosity; $\boldsymbol{I}$ is the identity tensor and dots above quantities denote time derivatives. The approximation of the time integration of eq. (6.1), by employing the first-order one-sided scheme on the successive time levels $t^0 < t^1 < \ldots < t^{i+1}$, yields

$$\boldsymbol{\tau}^M\Big|_{t^0}^{t^{i+1}} = \boldsymbol{\tau}^E\Big|_{t^0}^{t^{i+1}} - \sum_{j=0}^{i} \frac{\mu\left(t^{j+1}-t^j\right)}{\eta}\left(\boldsymbol{\tau}^{M,j} - K\nabla\cdot\mathbf{u}^j\boldsymbol{I}\right)\,, \tag{6.3}$$

which justifies the following decomposition of the stress tensor $\boldsymbol{\tau}^{M,i+1}$ into

$$\boldsymbol{\tau}^{M,i+1} = \boldsymbol{\tau}^{E,i+1} + \boldsymbol{\tau}^{V,i} \tag{6.4}$$

with the initial-value condition $\boldsymbol{\tau}^{M,0} = \boldsymbol{\tau}^{E,0}$; additional superscripts indicate the time level of a given quantity. The "memory" term $\boldsymbol{\tau}^{V,i}$ contains—whether explicitly or implicitly—contributions of all time levels $t^j < t^{i+1}$. It is advantageous to manipulate the non-elastic contribution $\boldsymbol{\tau}^{V,i}$ to the Maxwell stress tensor into the form

$$\boldsymbol{\tau}^{V,i} = \boldsymbol{\tau}^{V,i-1} - M^i(\boldsymbol{\tau}^{M,i} - K\nabla\cdot\mathbf{u}^i\boldsymbol{I})\,, \tag{6.5}$$

where $M^i = (t^{i+1}-t^i)\mu/\eta$, the dimensionless factor proportional to the ith time step, is introduced.

The set of partial differential equations describing the perturbations of the pre-stressed self-gravitating continuum in a non-rotating reference system has been a subject of long-standing interest to geophysicists, who deal with short-term applications such as tidal or free oscillation excitation. In the context of elasticity, we write the momentum and the gravitational Poisson equations

$$\begin{aligned} \nabla\cdot\boldsymbol{\tau}^E - \mathbf{f} &= \mathbf{0}\,, & (6.6)\\ \nabla^2\varphi_1 + 4\pi G\nabla\cdot(\varrho_0\mathbf{u}) &= 0\,, & (6.7) \end{aligned}$$

where $\mathbf{f} = \varrho_0\nabla\varphi_1 - \nabla\cdot(\varrho_0\mathbf{u})\nabla\varphi_0 + \nabla(\varrho_0\mathbf{u}\cdot\nabla\varphi_0)$ means that inertial forces are neglected. For earth models with spherically symmetric physical parameters, $\varrho_0 = \varrho_0(r)$, $\mu = \mu(r)$, $K = K(r)$, this and similar systems can be solved by means of spherical decomposition. The displacement and gravitational potential perturbations, $\mathbf{u} = \mathbf{u}(r,\Omega)$ and $\varphi_1 = \varphi_1(r,\Omega)$, can be decomposed into expansions of the spherical harmonic functions $Y_n(\Omega)$ (see Appendix 6.A), and the following expansions of eqs (6.6), (6.7), henceforth for spheroidal motion only, can be written as

$$\begin{aligned} \textstyle\sum_n\left[\alpha_n(r)Y_n(\Omega)\boldsymbol{e}_r + \beta_n(r)\nabla_\Omega Y_n(\Omega)\right] &= \mathbf{0}\,, & (6.8)\\ \textstyle\sum_n \varepsilon_n(r)Y_n(\Omega) &= 0\,. & (6.9) \end{aligned}$$

Choosing the solution vector as

$$\mathbf{y}_n^E(r) = \left(U_n, V_n, T^E_{rr,n}, T^E_{r\vartheta,n}, F_n, Q_n\right)^T\,, \tag{6.10}$$

where U_n, V_n represent respectively the radial and tangential displacements, $T^E_{rr,n}$, $T^E_{r\vartheta,n}$ are the normal and shear stress-tensor elements, and Q_n is the gravitational traction (Farrell 1972), the particular requirements

$$\alpha_n(r) = 0\,, \quad \beta_n(r) = 0\,, \quad \varepsilon_n(r) = 0 \tag{6.11}$$

form exactly the 3rd, 4th, and 6th rows, respectively, of the well-known system of ordinary differential equations (ODEs),

$$\frac{d}{dr}\mathbf{y}_n^E(r) = \boldsymbol{A}_n^E(r)\mathbf{y}_n^E(r)\,. \tag{6.12}$$

For the sake of completeness, the other rows of eq. (6.12), the 1st, 2nd, and 5th, arise directly from the definitions of the stress-like elements $T^E_{rr,n}$, $T^E_{r\vartheta,n}$ and Q_n, respectively.

Next, we consider the momentum equation with the Maxwell stress tensor, although any viscoelastic stress tensor is acceptable, if the decomposition (6.4) can be applied. We note that the same procedure for decomposition can be applied for the Burgers' body rheology (e.g., Yuen & Peltier 1982). Such a viscoelastic stress tensor $\boldsymbol{\tau}^M$ gives rise to a non-zero right-hand side in the viscoelastic counterparts of eqs (6.6), (6.7):

$$\nabla \cdot \boldsymbol{\tau}^{E,i+1} - \mathbf{f}^{i+1} = -\nabla \cdot \boldsymbol{\tau}^{V,i}\,, \tag{6.13}$$

$$\nabla^2 \varphi_1^{i+1} + 4\pi G \nabla \cdot (\varrho_0 \mathbf{u}^{i+1}) = 0\,. \tag{6.14}$$

For a spherical decomposition of the right-hand side of eq. (6.13), we can write

$$-\nabla \cdot \boldsymbol{\tau}^{V,i} = \textstyle\sum_n \left[\gamma_n^i(r) Y_n(\Omega)\boldsymbol{e}_r + \delta_n^i(r)\nabla_\Omega Y_n(\Omega)\right]\,. \tag{6.15}$$

Then we can repeat the procedure described for the elastic case by insisting that

$$\alpha_n^{i+1}(r) - \gamma_n^i(r) = 0\,, \quad \beta_n^{i+1}(r) - \delta_n^i(r) = 0\,, \quad \varepsilon_n^{i+1}(r) = 0\,. \tag{6.16}$$

This will result in the spheroidal system of ODEs

$$\frac{d}{dr}\mathbf{y}_n^{E,i+1}(r) = \boldsymbol{A}_n^E(r)\mathbf{y}_n^{E,i+1}(r) + \mathbf{q}_n^{E,i}(r)\,, \tag{6.17}$$

where $\mathbf{y}_n^{E,i+1}(r)$ and $\boldsymbol{A}_n^E(r)$ are the same as in eq. (6.12), and

$$\mathbf{q}_n^{E,i}(r) = \left(0, 0, \gamma_n^i, \delta_n^i, 0, 0\right)^T\,, \tag{6.18}$$

an inhomogeneous term on the right-hand side of eq. (6.17), is a new "viscoelastic" term consisting of a linear combination of components of the already known vector $\mathbf{y}_n^{E,i}(r)$.

As the last step, we substitute the solution vector $\mathbf{y}_n^E(r)$ of eq. (6.17) by the viscoelastic solution vector $\mathbf{y}_n^M(r)$,

$$\mathbf{y}_n^M(r) = \left(U_n, V_n, T^M_{rr,n}, T^M_{r\vartheta,n}, F_n, Q_n\right)^T\,, \tag{6.19}$$

which differs from the elastic solution vector $\mathbf{y}_n^E(r)$ by its stress components analogously to the decomposition of $\boldsymbol{\tau}^M$ in (6.4). This decomposition takes the form

$$\mathbf{y}_n^{M,i+1}(r) = \mathbf{y}_n^{E,i+1}(r) + \mathbf{y}_n^{V,i}(r) \tag{6.20}$$

with $\mathbf{y}_n^{M,0}(r) = \mathbf{y}_n^{E,0}(r)$. We note here that one needs only to apply the viscoelastic stress boundary conditions on $T^M_{rr,n}(r)$, $T^M_{r\vartheta,n}(r)$ in order to reduce the number of terms in $\mathbf{q}_n^M(r)$. Eq. (6.20), for Maxwell rheology, together with

$$\mathbf{y}_n^{V,i}(r) = \mathbf{y}_n^{V,i-1}(r) - M^i\left(0, 0, T^{M,i}_{rr,n} - KX_n^i, T^{M,i}_{r\vartheta,n}, 0, 0\right)^T\,, \tag{6.21}$$

where X_n^i are the spherical coefficients of $\nabla \cdot \mathbf{u}$, turns the system (6.17) into a system which is formally identical but more suitable for numerical implementation. This system now reads

$$\frac{d}{dr}\mathbf{y}_n^{M,i+1}(r) = \boldsymbol{A}_n^E(r)\mathbf{y}_n^{M,i+1}(r) + \mathbf{q}_n^{M,i}(r)\,. \tag{6.22}$$

Elements of the propagator matrix $\boldsymbol{A}_n^E(r)$ and the "Maxwellian" vector

$$\mathbf{q}_n^{M,i}(r) = \mathbf{q}_n^{E,i}(r) + \frac{d}{dr}\mathbf{y}_n^{V,i}(r) - \boldsymbol{A}_n^E(r)\mathbf{y}_n^{V,i}(r) \tag{6.23}$$

can be found in Appendix 6.A.

Toroidal equivalents of the spheroidal terms $\boldsymbol{A}_n^E(r)$ and $\mathbf{q}_n^{M,i}(r)$ can be derived with the same procedure with toroidal expansions of eqs (6.13), (6.14). They are left out here, as this work is only concerned with the problem of viscoelastic relaxation of a spherically symmetric earth model excited by a vertical surface load, i.e., a problem involving purely spheroidal deformation.

6.2.2 Numerical Aspects

First, we will review the key steps used by the normal-mode (NM) technique (e.g., Wu & Peltier 1982). The correspondence principle and the Laplace transform are employed to replace the viscoelastic constitutive relation (6.1) by one formally the same as relation (6.2) but with the shear modulus dependent on the Laplacian variable s: $\mu(s,r) = \mu/(s + \mu/\eta)$. For selected (real and negative) s, three separate solution vectors $\mathbf{y}_n^E$ are propagated from inside the model upwards, using standard propagator matrix techniques. The surface values of $T_{rr,n}^E(s)$, $T_{r\vartheta,n}^E(s)$ and $Q_n(s)$ of each solution constitute a 3×3 matrix whose determinant (the secular determinant) is evaluated. Time-dependent relaxation curves from normal modes are expected to be a finite sum of exponentially decaying functions. A crossing at $s = -s_n^j$ of the secular determinant curve and the negative real axis in the Laplacian plane implies the existence of the exponential mode $h_n^V \exp(-s_n^j t)$ with a relaxation time $T_n^j = (s_n^j)^{-1}$. The strength coefficient h_n^V can be found by calculating the residuals. A useful formula for this is given in Han & Wahr (1995).

If either the shear modulus μ or viscosity η vary with the radius in such a way that $s + \mu/\eta = 0$ for at least one r, the Laplacian shear modulus $\mu(s,r)$ becomes singular. The minimal and maximal s of singularities $\mu(s,r)$ define the singular bound, as introduced by Fang & Hager (1995). To maintain numerical accuracy in the propagator scheme, we have made the continuous profiles of the shear modulus and viscosity discrete, while keeping in mind that $s + \mu/\eta \neq 0$ for any r. Such a discretization of continuous $\mu(r)$ and $\eta(r)$ allows us to find a discrete approximation to the continuous spectrum.

A high-resolution scanning over the negative real axis of the Laplacian plane for the zero-crossings is necessary for determining the normal modes of an earth model embedded in a continuous spectrum. This procedure is adequate for incompressible layered models, which is not surprising since the boundary conditions can be expressed by means of an analytical secular determinant (Sabadini et al. 1982). However, when more than two layers are used, the analytical treatment requires numerical root-finding procedures to solve the secular equation (Vermeersen et al. 1996). Moreover, accounting for elastic compressibility would produce denumerably infinite sets of relaxation modes, which represents a further obstacle to the precise determination of the relaxation curves. In our computations, the total number of s-samples has been of the order of tens for models with bare modal branches (models A1, B1 in Fig. 6.1) or as many as a few thousands for complex viscosity profiles (discretized models B2, B3, C2, C3 in Fig. 6.1) during the course of accurately fitting the isostatic ($s = 0$) relaxation limit. It is clear that the number of modes increases with the decreasing thickness of layers, and thus the study of the continuous spectrum becomes extremely cumbersome.

The initial-value (IV) approach is simpler in its application because no singularities are present in the propagator matrix in the time domain. We have employed the standard technique for solving systems similar to eq. (6.22). A solution of the system with $\mathbf{q}_n^M = 0$ (i.e., the elastic one) with prescribed boundary conditions is found by first propagating three linearly independent solutions through the earth interior. Then, at each time step, a particular solution of eq. (6.22) with $\mathbf{q}_n^M \neq 0$ is propagated through the mantle and adjusted (with the help of the three elastic solutions) to the zero values of $T_{rr,n}^M$, $T_{r\vartheta,n}^M$ and Q_n on the outer boundary. A superposition of all the homogeneous and inhomogeneous solution vectors constitutes the complete solution of eq. (6.22) at each time step.

Some of the advantages of the IV technique are obvious. While a user of the modal technique must pay attention to the number of normal modes already registered, the user of the IV approach only needs to take care of the length of the time step in marching forward in time. We have employed the time-step criterion

$$t^{i+1} - t^i \leq A\eta(r)/\mu(r) \quad \text{for} \quad r_{\rm CMB} \leq r \leq r_0\,, \tag{6.24}$$

where $r_{\rm CMB}$ and r_0 are the depths of the lower and upper boundaries of the mantle, respectively and A is a constant ~ 1. This criterion can be used as a starting point for further fine-tuning of the time step.

We have not found any numerical problems for realistic earth models with the spheroidal elastic matrix $\boldsymbol{A}_n^E(r)$ derived from the PREM model. We have tested not only models with the viscosity profiles from Fig. 6.1 but also similar models without the elastic lithosphere. This numerical scheme has also worked well for incompressible models. However, some compressible models with density and elastic parameters very different from the real earth parameters, for example a compressible homogeneous sphere, do not converge easily to isostatic equilibrium. The scheme formally resembles both an implicit-like and an explicit-like time integration, as it is necessary to solve an elliptic problem at each time step but part of the momentum equation is evaluated from the quantities obtained from the previous step. Moreover, the operator in the momentum equation, containing many different time derivatives, is too complicated for a standard mathematical classification of the system of equations.

To show a specific example of the computational costs, we consider an arbitrary case taken from models without a low-viscosity zone (LVZ), A1–A4, B1 or C1, shown in Fig. 6.1. A uniform time step of 100 yr can be chosen because the mantle Maxwell time $\eta/\mu > 107$ yr is valid for the PREM model and each of the viscosity models. Single Love numbers $h_n(t)$, $l_n(t)$, $k_n(t)$ for a fixed n and for the first 20 kyr can be computed using 200 time steps with a total CPU time of 3 s (evaluated on the HP 735/125 workstation). In other words, the parallel evaluation of Love numbers in 200 spectral layers also takes (on the same single-processor system) 3 s per time step with a total memory of 32 MB (for a radial discretization of 600 levels). A decrease of viscosity in the models with a LVZ demands a smaller time step, according to eq. (6.24).

We define here the effective relaxation times $T_{{\rm ef},n}$ of the vertical Love numbers $h_n(t)$. The values of the relaxation times are computed by the formula

$$T_{{\rm ef},n}(t) = -\dot{h}_n(t)/\ddot{h}_n(t)\,, \tag{6.25}$$

based on its validity for a single exponential $h_n(t) = h_n^E + h_n^V[1 - \exp(-t/T_{{\rm ef},n})]$, where h_n^E and h_n^V are constants. The double dot represents the second derivative with respect to time. We have used this formula instead of the straightforward least-squares method because it displays a sharper sensitivity to a few particular modes.

6.3 Results

There is a substantial difference between our knowledge of the elastic and viscous stratification. Whereas the spherically symmetric seismic models yield compressional and shear velocities with the accuracy of a few per cent, the uncertainty in the viscosity can reach an order of magnitude in the

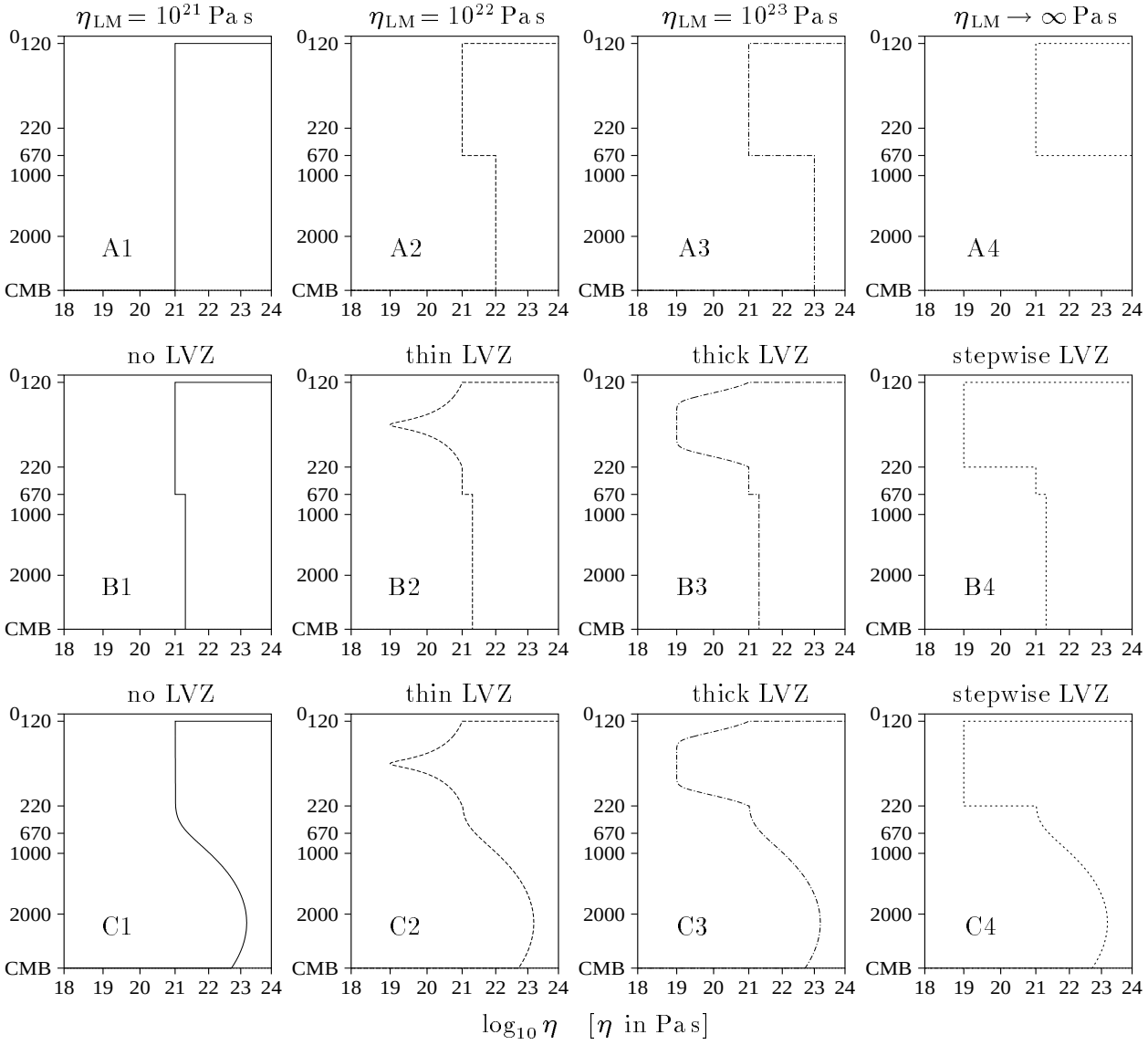

Fig. 6.1. Families A, B and C of the depth-dependent viscosity profiles used in the calculations. Family A is employed to demonstrate the relaxation features between the isoviscous and the elastic bound of lower-mantle viscosity. The profiles for family B are based on a model suggested by previous postglacial studies (e.g., Tushingham & Peltier 1992) and modulated by various shapes of a low-viscosity zone. Family C is composed of profiles with a "viscosity hill" in the lower mantle combined with a LVZ like the ones in family B. The upper-mantle viscosity of families A and B is $\eta_{UM} = 10^{21}$ Pa s, and the elastic lithosphere is taken to be 120 km thick. The depth range of the LVZ has been exaggerated.

asthenosphere and at least the same in the lower mantle. This is the reason why we have employed the elastic moduli based on values provided by the PREM model (Dziewonski & Anderson 1981), in order to concentrate on the influences of the changes of the viscosity. We have incorporated a fully elastic lithosphere ($\eta \to \infty$) of 120 km thickness, and a liquid core ($\eta \to 0$) ranging from a depth of 2891 km to the centre of the Earth in all of the models. The models are divided into three families (Fig. 6.1). Family A consists of simple four-layer viscosity profiles (core, lower mantle, upper

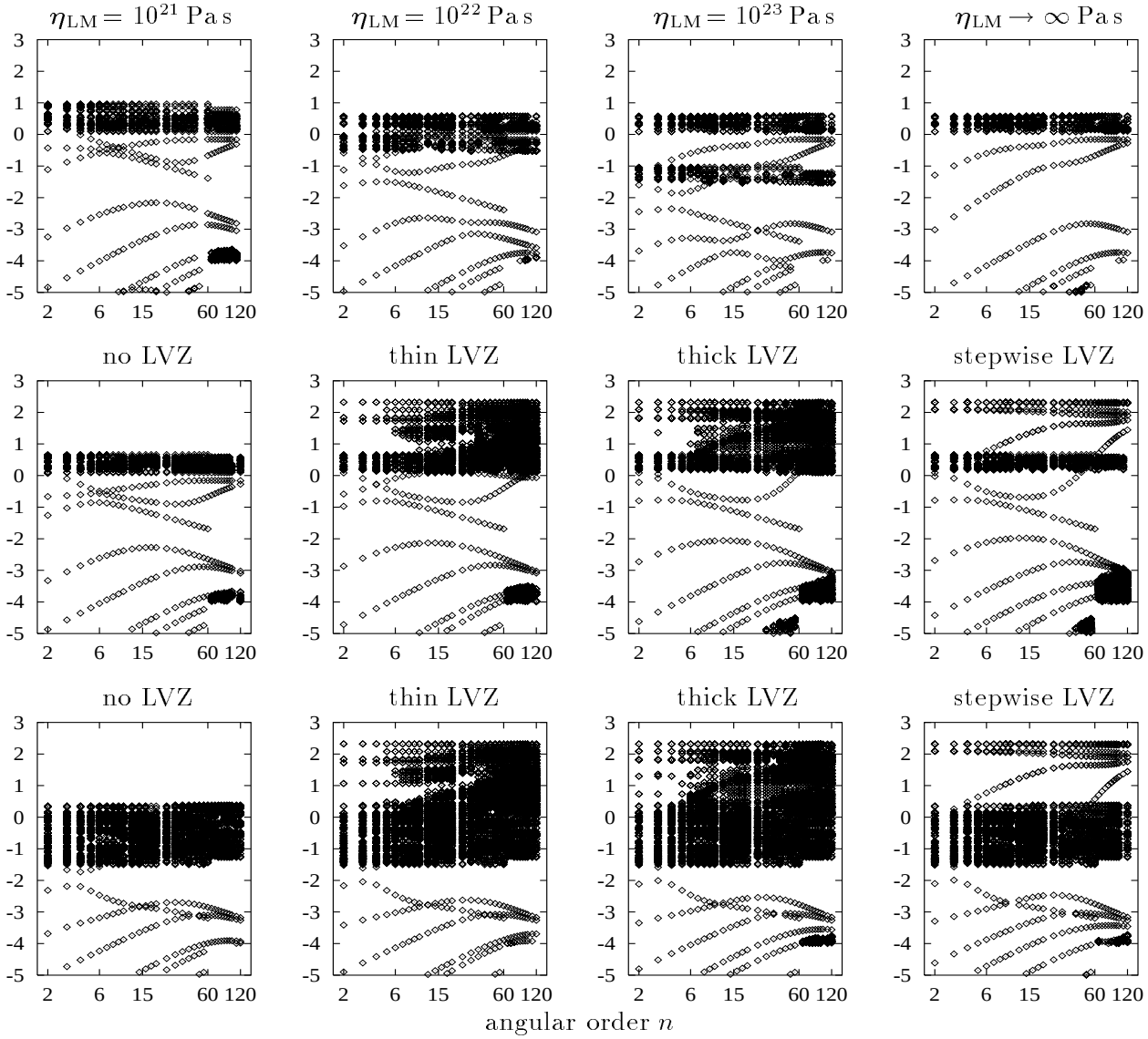

Fig. 6.2. Modal relaxation times for the viscosity profiles shown in Fig. 6.1. Relaxation times, found by the NM technique, are plotted in the angular order versus the logarithmic inverse relaxation time (in kyr) plane, and constitute both characteristic branches, called M0, L0, C0, M1, M2 etc., and overfilled areas, known as the continuous spectrum. Notice the splitting of continuous spectra in models that include layers (A3, B4, C4) in contrast to the spreading of continuous spectra of models with rather sharp continuous profiles (B2, B3, C2, C3).

mantle, lithosphere), with the fixed upper-mantle viscosity $\eta_{UM} = 10^{21}$ Pa s and the lower-mantle viscosity changing between the bounds 10^{21} Pa s (model A1) and infinity (model A4). Family B concentrates on the influence of the LVZ beneath the lithosphere; the viscosities in the upper and the lower mantle are taken from the model by Tushingham & Peltier (1992) based on postglacial studies. Models B2 and B3 are characterized by the continuous Gaussian-like profiles of viscosity through the LVZ. Family C differs from family B by the presence of the "viscosity hill" in the lower mantle derived from geodynamical modelling (Ricard & Wuming 1991). An approximate viscosity formula used for the "hill" is given in Hanyk et al. (1995).

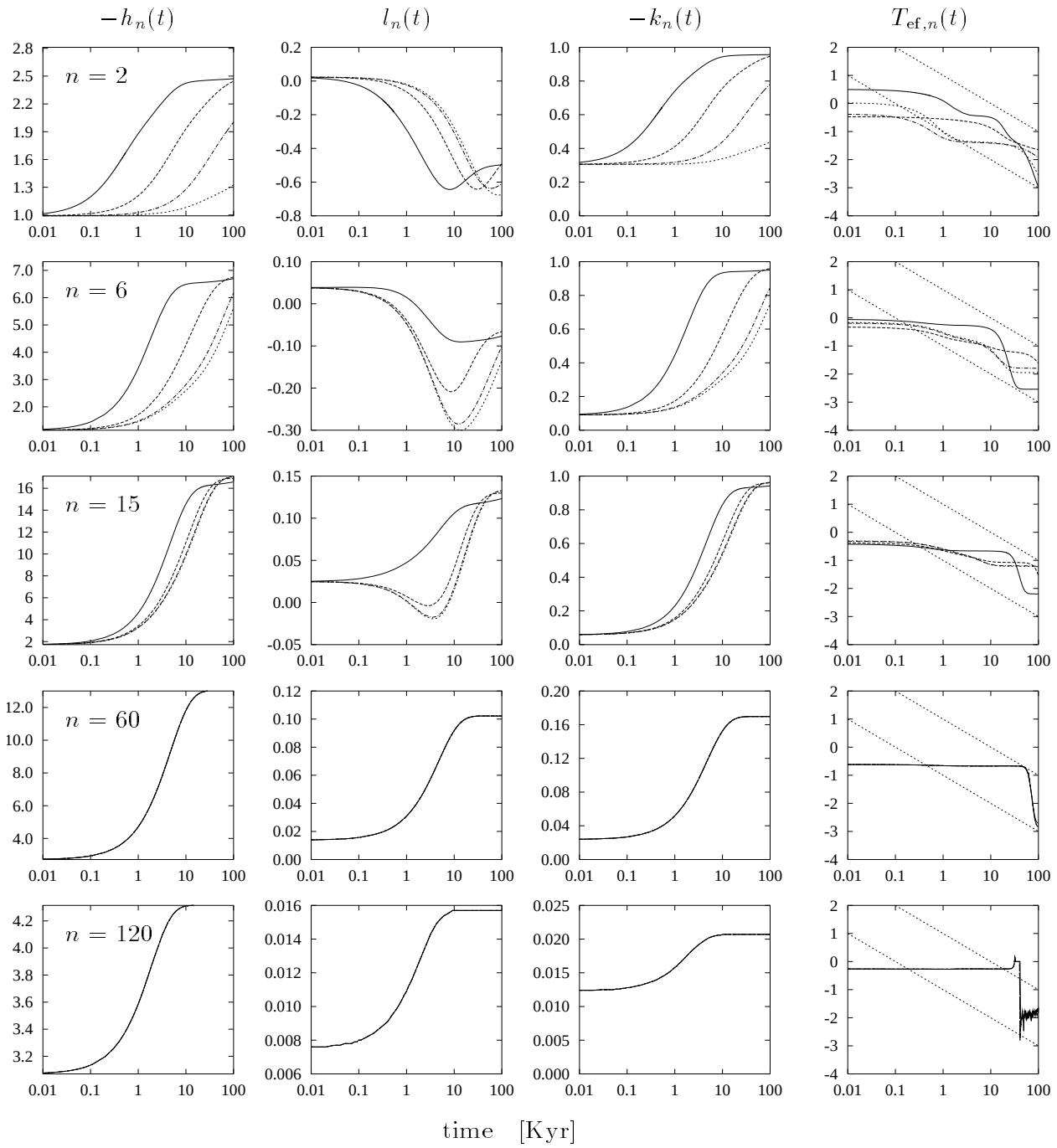

Fig. 6.3. Time-dependent vertical, horizontal and potential Love numbers, h_n, l_n and k_n, respectively, and the effective relaxation times $T_{\mathrm{ef},n}$ (n = 2, 6, 15, 60, 120) of the family A viscosity profiles found by the initial-value approach. The horizontal axes are given in terms of the logarithm of time (in kyr), and the vertical axes are dimensionless for the first three columns and the logarithmic inverse relaxation time (in kyr) for the last column. The vertical axes of the h_n-panels are bounded by the elastic and isostatic limits. Solid, dashed, dashed-dotted and dotted lines correspond, respectively, to the models A1, A2, A3 and A4 (in the same way as in Fig. 6.1).

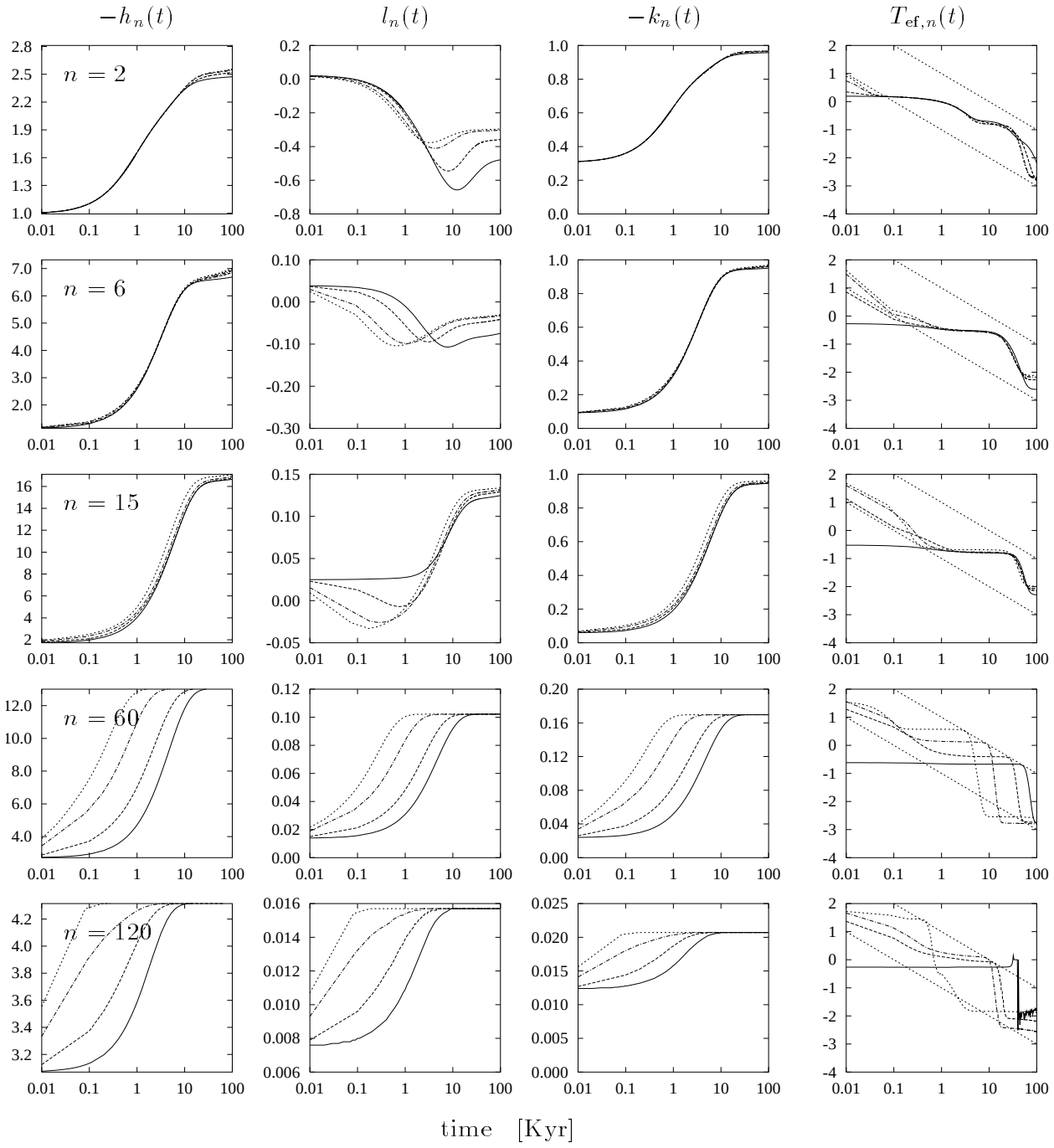

Fig. 6.4. As Fig. 6.3, but for the family B viscosity profiles. Vertical Love numbers of lower angular orders are not sensitive to the existence of the LVZ. This is not the case for the horizontal displacements. The essential role of the details in the shape of the LVZ on short-time responses can clearly be seen from higher-angular-order Love numbers.

We have applied the NM algorithm as outlined in the previous section to find the response of all the models to a surface load of Heaviside time history for angular orders $n \leq 120$. The result of this effort, i.e., values of s where the secular determinant changes sign as a function of n, is

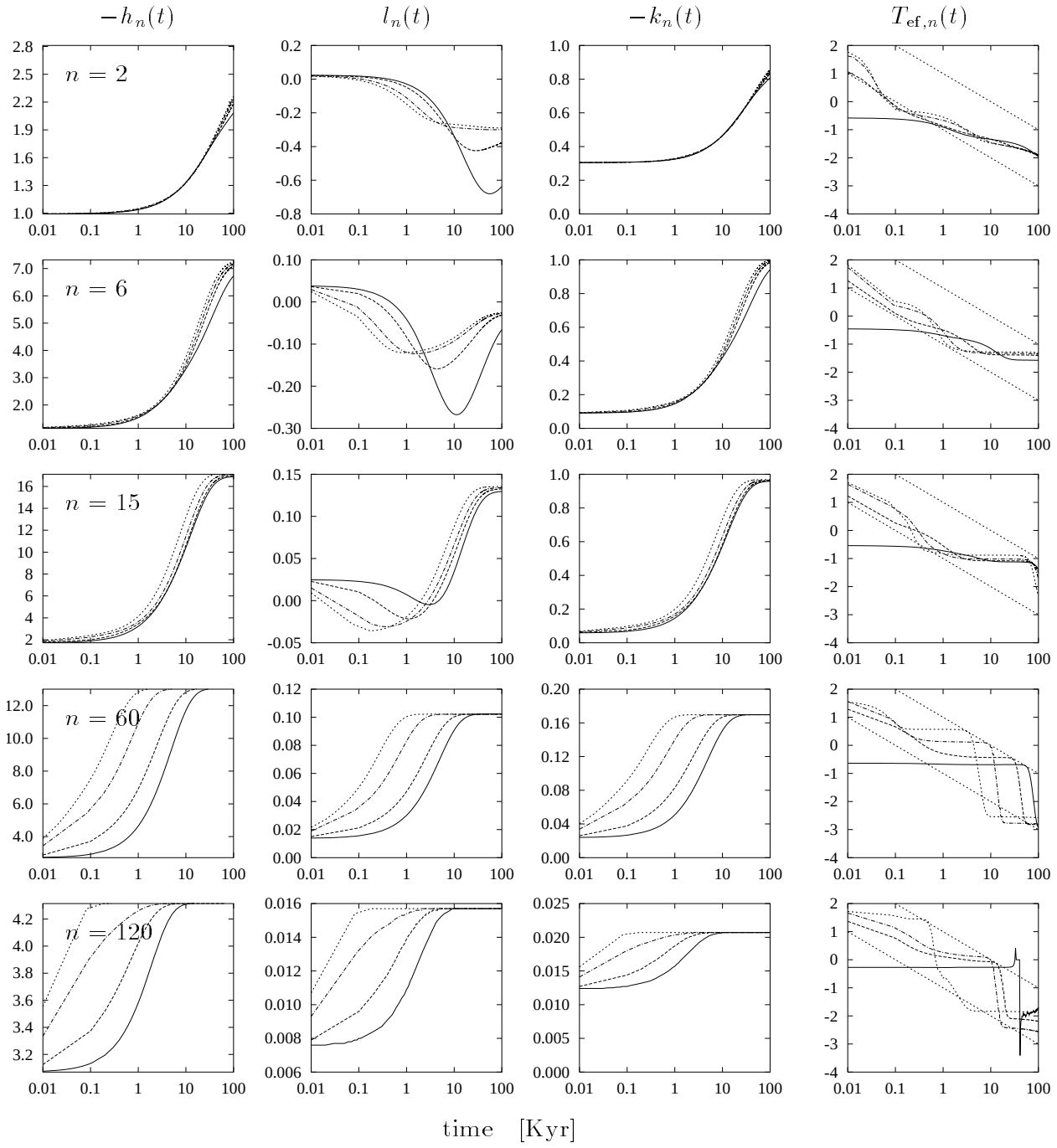

Fig. 6.5. As Fig. 6.3, but for the family C viscosity profiles. Compared with Fig. 6.4, the influence of the lower-mantle "viscosity hill" is distinct for lower-angular-order Love numbers.

shown in Fig. 6.2. Some of the points depicted might not represent true relaxation modes, as they could be so-called false zero crossings (Han & Wahr 1995). The discrete approximations of the continuous spectra lie inside the singular bound (Fang & Hager 1995), i.e., the interval defined by the minimal and maximal s for which $\mu(s, r)$ becomes singular for at least one position in r. Even

in the case of the simplest viscosity profile, A1, the singular bound (SB) spreads over 10^2 yr $< s^{-1}$ $< 10^3$ yr with the well-developed continuous spectrum inside it, which is a consequence of both the continuity and the compressibility of PREM. The layers with higher viscosity in the profiles A2–A4 split the SB, and also shift one part towards the longer relaxation times. The spreading of the SB of the profiles B and C towards 1 yr and/or 10^4 yr is due to the continuous viscosity profiles in the LVZ (profiles B2, B3, C2, C3) and/or in the lower mantle (all profiles C). The SB of the "fully continuous" profiles C2, C3 spreads over four orders of magnitude and covers the whole extent of the effective relaxation times $T_{\mathrm{ef},n}$ (Fig. 6.5).

Figs 6.3–6.5 show the time histories computed by the IV approach of the vertical h_n, horizontal l_n and potential k_n Love numbers of the model families for selected angular orders. The lower and upper horizontal axes of the h_n-panels are the elastic and isostatic limits, respectively, the latter one computed independently by means of Wu & Peltier's (1982) approach. Plots demonstrating the time dependence of the effective relaxation times $T_{\mathrm{ef},n}$ (6.25) associated with the vertical Love number are also shown. The diagonal band in the $T_{\mathrm{ef},n}$ panels marks the area of the effective Deborah number, $\mathrm{De}(t) = T_{\mathrm{ef},n}(t)/t$ where $0.1 \leq \mathrm{De}(t) \leq 10$ (cf. Poirier 1985 where the Deborah number represents the ratio of the viscoelastic relaxation time to the timescales of the flow). The sensitivity of the Love numbers to the viscosity variations at various depth coinsides with our general expectation. The influence of the lower mantle (LM) variations is substantial for low n. Specifically, the higher the LM viscosity, the slower the relaxation; see h_n and k_n of A1–A4, B1, and C1 models for $n \leq 15$. The relaxation delay is saturated for LM viscosities of about 10^{23} Pa s, as is demonstrated by the negligible difference between the relaxation curves of the A3 and A4 models (except for $n = 2$). The long-wavelength values for l_n are non-monotonic. This has been interpreted by Mitrovica & Davis (1995) as a consequence of modal amplitudes involving either sign. Similarly, they explained the purely monotonic short-wavelength l_n as a dominance of the M0 mode with increasing n. The depth-dependent viscosity in both the LM and LVZ hinders this phenomenon (for an example, see l_{15} in Figs 6.3–6.5).

The LVZ mostly influences the short-wavelength relaxation. The wider the LVZ, the faster the relaxation. For $n = 60$, the effective relaxation time of the B4 and C4 models is shortened by two orders of magnitude of 10^2 yr. The presence of the LVZ is clearly visible even in the long-wavelength l_n, which is in agreement with Fang & Hager's (1994) statement that the horizontal motion is more sensitive to the viscosity structure below the lithosphere. The dominance of fast short-wavelength relaxations (for example shorter than 10^2 yr for $n = 120$, or 10^3 yr for $n = 60$) indicates that there is a considerable LVZ in a model. Moreover, the existence of the LVZ filters out the influence of the LM variations in the whole spectrum of l_n. The appearance of any substantial slow short-wavelength relaxation (lasting, for example, 10^4 yr or more) points to the weakening of the LVZ. If there is no LVZ in a model, then all long-wavelength l_n respond similarly to the LM viscosity, as the h_n and k_n do, i.e., the relaxation becomes slower with the LM viscosity increase (again, compare the families B and C). Note also the strongest sensitivity of l_n-amplitudes of the B1 and C1 models to the LM viscosity when $n = 6$.

The effective relaxation time $T_{\mathrm{ef},n}(t)$ is a suitable quantity to desribe the instantaneous character of relaxation. Plateaus in the curves $T_{\mathrm{ef},n}(t)$ reveal the subsequent domination by a few strong modes; at each time a dominant mode determines the effective relaxation time. Piecewise-constant curves of $T_{\mathrm{ef},n}(t)$ obtained mainly in layered models of family A and in the models B1, C1 thus suggest that the NM method is suitable in these cases. Note that comparison of the plateaus if

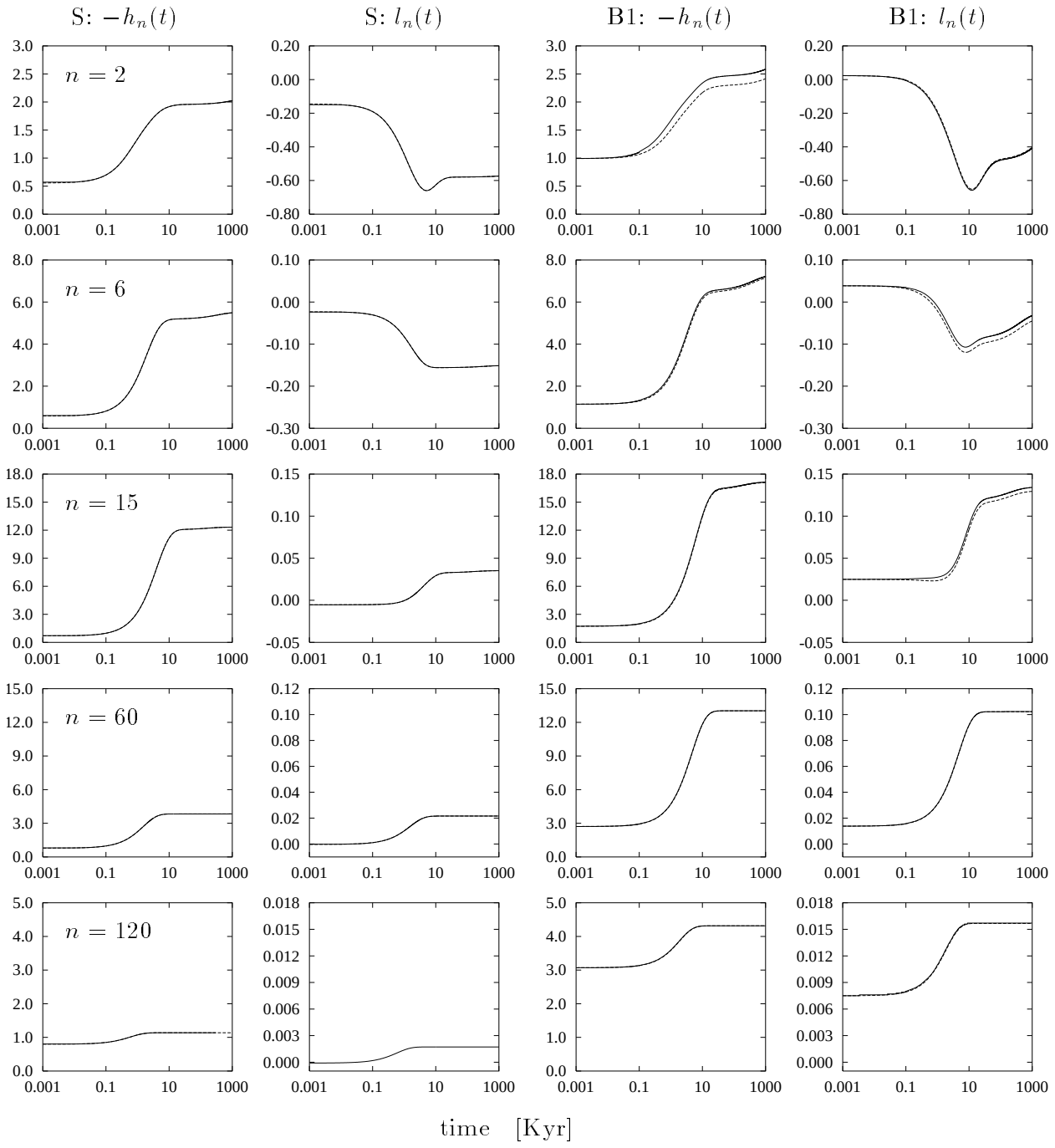

Fig. 6.6. A comparison of the vertical (h_n) and horizontal (l_n) Love numbers (n = 2, 6, 15, 60, 120) by both the initial-value (solid lines) and the modal (dashed lines) approaches. The left two columns were computed for an elastically incompressible four-layer earth model, and the right two columns are results of the viscosity profile B1 with elastic parameters given by PREM. No differences between the results for the two methods are found for the simple incompressible case, and only minor differences are noticeable in the Love numbers with lower n for the B1 profile. The number of modes included is six for the S model and five for the B1 model. The vertical scales are chosen to be the same for both models in order to show the extent to which Earth features, based on simple incompressible models, can be accurately modelled.

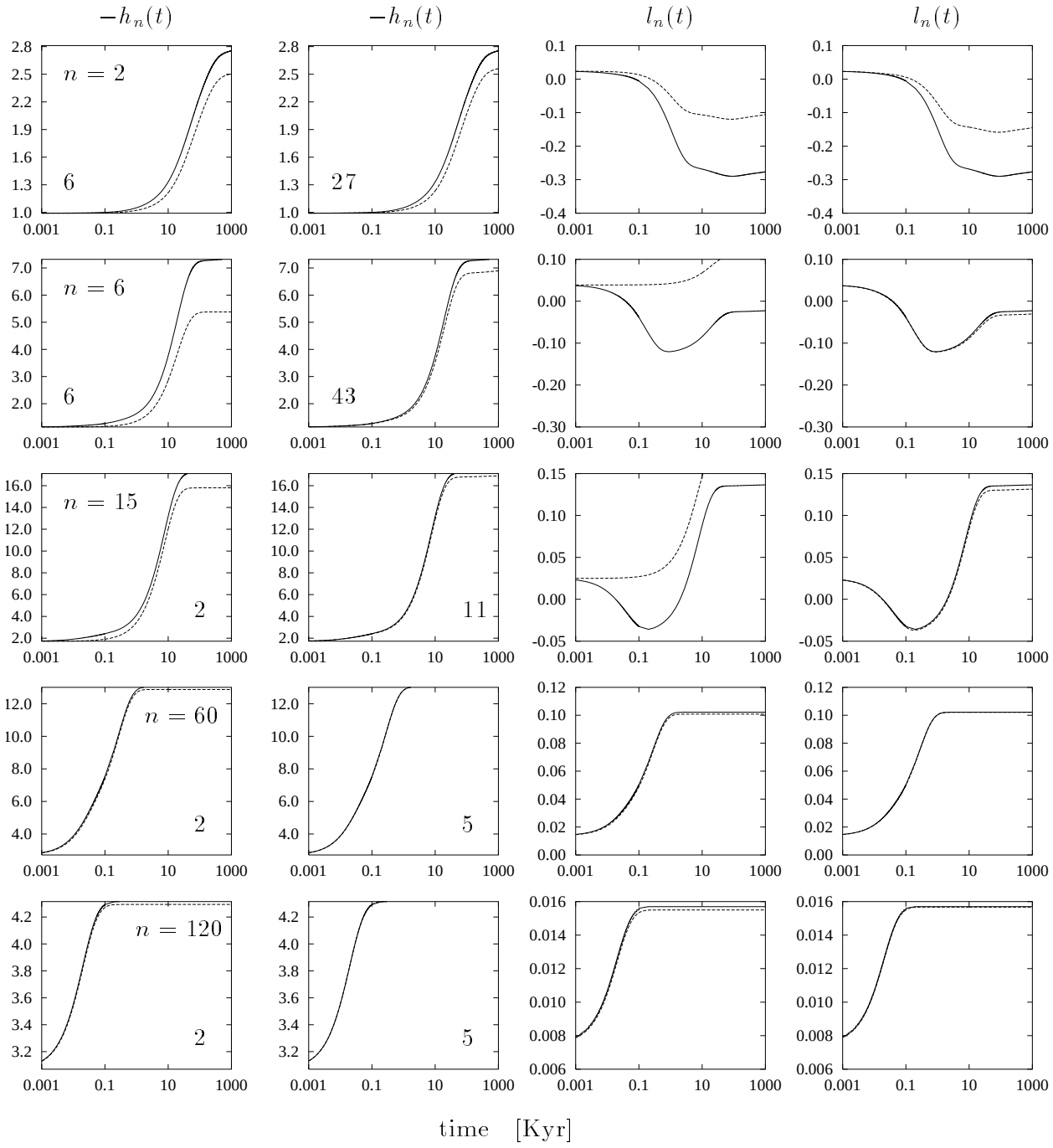

Fig. 6.7. A comparison of the vertical (h_n, left two columns) and the horizontal (l_n, right two columns) Love numbers ($n = 2, 6, 15, 60, 120$) obtained by the initial-value (solid lines) and the modal (dashed lines) approaches for the viscosity profile C4. Various numbers of modes were included in the modal expansions (given at the bottom of the panels for h_n) to demonstrate the necessity of large modal expansion in order to fit accurately the Love numbers accurately (represented here by results of the initial-value approach).

Figs 6.3–6.5 with the relaxation spectra in Fig. 6.2 may serve as a numerical test of the correspondence between the two methods. Models with the LVZ (B2–B4, C2–C4) exhibit a different

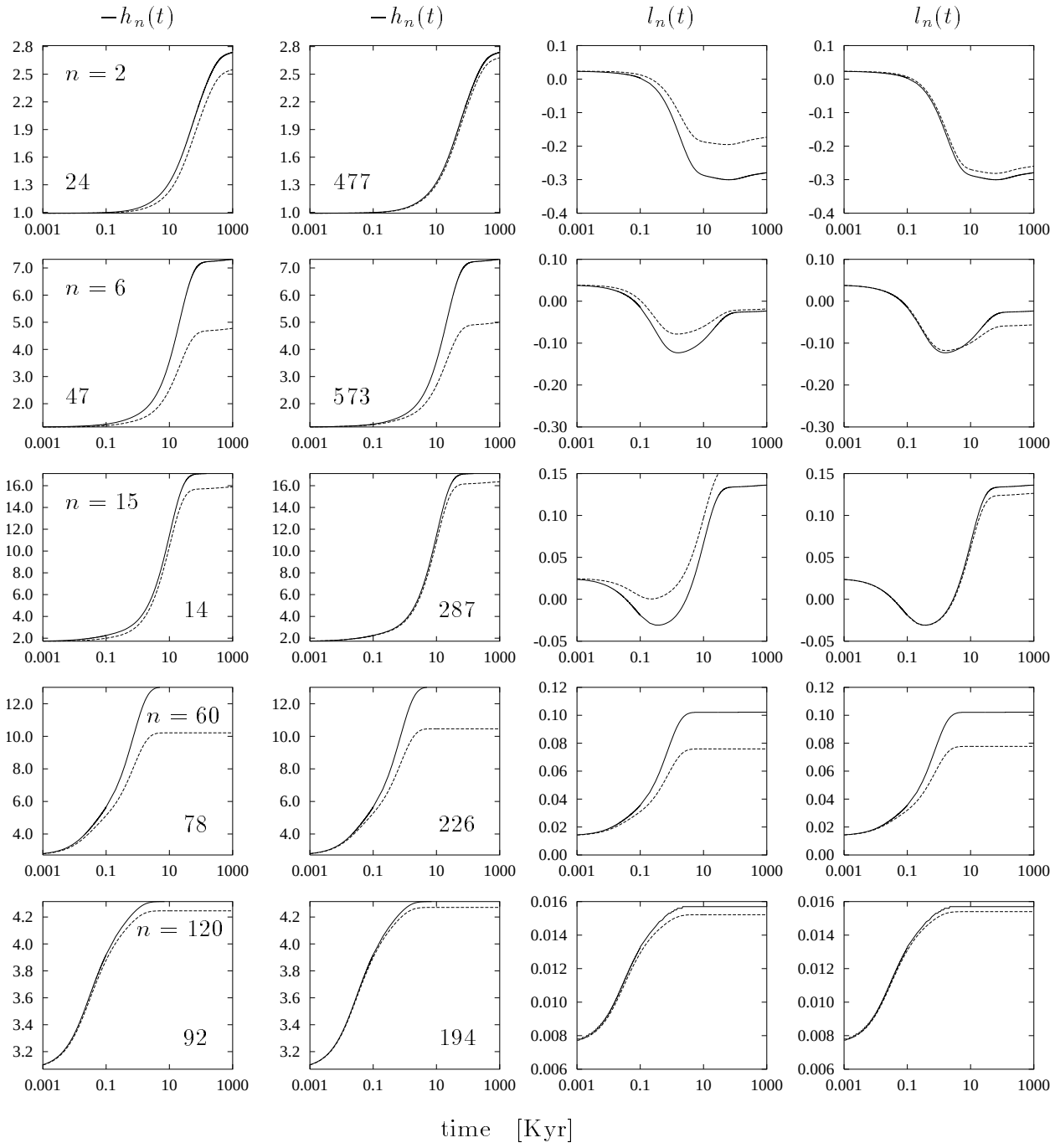

Fig. 6.8. As Fig. 6.7, but for the C3 viscosity profile. Larger modal expansions are required to fit Love numbers well than for the C4 profile. At high n, the Love numbers, derived from the IV approach, are difficult to match, even with many modes included.

behaviour for short times. The curves of $T_{\mathrm{ef},n}(t)$ continuously decrease for thousands ($n \leq 15$) or tens of thousands ($n \geq 60$) of years along the diagonal corresponding to the fixed Deborah number $\mathrm{De}(t) = 1$. The short-time relaxation of the models with the LVZ can thus be characterized

by setting the effective relaxation times equal to the actual time. This points to the necessity of taking the short-time continuous spectrum (in the terminology of the NM method) into account for short-time and short-wavelength phenomena, such as post-seismic relaxation (e.g., Boschi et al. 1985).

Fig. 6.6 shows the time histories of Love numbers for the model by Piersanti et al. (1995), labeled S here, and the B1 model, obtained by the IV and the NM approaches. The simple model S is the elastically incompressible four-layer model called C1 in the original paper. The popularity of incompressible models with a small number of layers (Sabadini et al. 1982; Spada et al. 1990; Vermeersen et al. 1996) stems from the fact that their responses can be well described by a small number of normal modes, which makes the computations easier. During the course of solving responses of incompressible layered models, we have not discovered any differences between the results of the two approaches. In principle, the recent work by Vermeersen et al. (1996) arrives at the same conclusion by their advocating the validity of the NM approach. The reliability of this technique for incompressible models with rather rough radial discretization is a direct consequence of the simple nature of the discrete relaxation spectrum of such models. However, the models themselves are inappropriate for studies with shorter wavelengths because of the weak amplitudes of the Love numbers in this part of the spectrum.

It is interesting to assess the number of normal modes needed to replicate the time history predicted by the IV method, especially in the presence of complex viscosity stratifications. The two right-hand columns of Fig. 6.6 show an acceptable coincidence of the relaxation curves for the B1 model obtained by the IV and NM approaches. Figs 6.7 and 6.8 compare the time histories of the vertical and horizontal Love numbers computed for the models C4 and C3 respectively. The number of normal modes employed for each case is given inside the panel for each angular order in the two left-hand columns, describing the vertical displacements. The same numbers of modes were also used for the corresponding horizontal displacements in the two right-hand columns. The isostatic limits of the vertical Love numbers (the upper horizontal axes of the h_n-panels in Figs 6.7 and 6.8) were satisfactorily reached by the IV technique for all angular orders, while our NM computations may exhibit substantial differences from the isostatic limit, even when hundreds of modes have been included, especially in the case of the C3 model with the thick LVZ.

6.4 Discussion and Concluding Remarks

It is a matter of debate whether the asthenosphere is characterized by a layer of partial melting (Anderson 1995) which may cause a dramatic decrease of viscosity. Our results clearly demonstrate that even a thin layer with a viscosity decrease by two orders of magnitude can substantially influence the viscoelastic response for high degrees of the spherical harmonic decomposition. Modelling of the viscoelastic responses is thus able to provide new insights into the lithospheric-sublithospheric structure. The influence of compressibility as given by PREM increases strongly with increasing degree, since the incompressible models strongly dampen the higher-order Love numbers. The most sensitive part of the high-degree part of the harmonic spectrum to the changes of viscosity in the LVZ comes mainly from short responses, up to about one thousand years. As this part of the spectrum must be taken into account in local or regional problems, the use of elastically incompressible models is questionable, for example in the modelling of short-timescale post-seismic deformation processes (e.g., Piersanti et al. 1995) or the analysis of transient and intermediate

relaxation regimes (Vermeersen et al. 1996).

The key role is played by the horizontal Love numbers, since they can be directly used to compare the models with plate deformations observed by VLBI because of their sensitivity to the viscosity profiles (James & Lambert 1993; Mitrovica et al. 1993, 1994a, 1994b; Peltier 1995). It is clear that spherically symmetric models represent an oversimplification of the situation in shallow structures. Recently, the deep roots of oceanic ridges and continental shields have been recognized in global tomographic models (Su et al. 1994). This accounts for the reason why viscoelastic modelling combined with the precise new-generation geodetic methods will be capable of bringing new constraints to the lithospheric-asthenospheric system. The modelling with fully 3-D viscosity fields is a topic for future research. The normal-mode approach would involve the coupling between different orders in the propagator matrix in the Laplace domain. However, the method based on direct integration in the time domain can remains, basically, unchanged. There are two steps here—the equations for toroidal motions must be added, and at each time step it is necessary to carry out the spherical harmonic decomposition of the additional right-hand-side vector of the momentum equation.

With the advent of precise regional GPS networks (Ware & Businger 1995), we can expect the development of more precise models of plate deformations, which can describe both postseismic and postglacial responses. These forward modelling improvements will be vital for progress in viscoelastic inverse problems. The skin-effect of viscoelastic responses to shallow sources could, in principle, be the starting point of viscoelastic tomography going from high to low degrees and producing, in due course, mantle viscosity models from shallow to great depths.

Acknowledgements. We thank M. Fang for his constructive critical comments and efforts in comparing results and J. X. Mitrovica for stimulating discussions. Multidisciplinary discussions with O. Čadek are gratefully acknowledged. This research has been supported by the US-Czechoslovak Science and Technology Joint Fund in cooperation with the Ministry of Education of the Czech Republic, USGS, NSF under Project No. 93 002, by the Grant Agency of the Czech Republic under Project No. 205/96/0212, and by the Geosciences Program, Department of Energy, USA.

References

Anderson, D.L., 1995. Lithosphere, asthenosphere, and perisphere, *Rev. Geophys.*, **33**, 125–149.

Boschi, E.V., Sabadini, R. & Yuen, D.A., 1985. The transient polar motions and the nature of the asthenosphere for short time scales, *J. Geophys. Res.*, **90**, 3559–3568.

Cathles, L.M., 1971. The viscosity of the Earth's mantle, *PhD thesis*, Princeton University, Princeton, NJ.

Crittenden, M.D., 1963. Effective viscosity of the Earth derived from isostatic loading of Pleistocene Lake Bonneville, *J. Geophys. Res.*, **68**, 1865–1880.

Dziewonski, A.M. & Anderson, D.L., 1981. Preliminary reference Earth model, *Phys. Earth Planet. Inter.*, **25**, 297–356.

Fang, M. & Hager, B.H., 1994. A singularity free approach to post glacial rebound calculations, *Geophys. Res. Lett.*, **21**, 2131–2134.

Fang, M. & Hager, B.H., 1995. The singularity mystery associated with a radially continuous Maxwell viscoelastic structure, *Geophys. J. Int.*, **123**, 849–865.

Farrell, W.E., 1972. Deformation of the earth by surface loads, *Rev. Geophys. Space Phys.*, **10**, 761–797.

Han, D. & Wahr, J., 1995. The viscoelastic relaxation of a realistically stratified earth, and a further analysis of postglacial rebound, *Geophys. J. Int.*, **120**, 287–311.

Hanyk, L., Moser, J., Yuen, D.A. & Matyska, C., 1995. Time-domain approach for the transient responses in stratified viscoelastic Earth models, *Geophys. Res. Lett.*, **22**, 1285–1288.

Haskell, N.A., 1935. The motion of a viscous fluid under a surface load, *Physics*, **6**, 265–269.

Ivins, E.R., Sammis, C.G. & Yoder, C.F., 1993. Deep mantle viscous structure with prior estimate and satellite constraint, *J. Geophys. Res.*, **98**, 4579–4609.

James, T.S. & Lambert, A., 1993. A comparison of VLBI data with the ICE-3G glacial rebound model, *Geophys. Res. Lett.*, **20**, 871–874.

Jones, M.N., 1985. *Spherical Harmonics and Tensors for Classical Field Theory*, Research Studies Press Ltd, Letchworth.

McConnell, R.K., 1968. Viscosity of the mantle from relaxation time spectra of isostatic adjustment, *J. Geophys. Res.*, **73**, 7089–7105.

Mitrovica, J.X. & Davis, J.L., 1995. Some comments on the 3-D impulse response of a Maxwell viscoelastic earth, *Geophys. J. Int.*, **120**, 227–234.

Mitrovica, J.X., Davis, J.L. & Shapiro, I.I., 1993. Constraining proposed combinations of ice history and Earth rheology using VLBI determined baseline length rates in North America, *Geophys. Res. Lett.*, **20**, 2387–2390.

Mitrovica, J.X., Davis, J.L. & Shapiro, I.I., 1994a. A spectral formalism for computing three-dimensional deformations due to surface loads, 1. Theory, *J. Geophys. Res.*, **99**, 7057–7073.

Mitrovica, J.X., Davis, J.L. & Shapiro, I.I., 1994b. A spectral formalism for computing three dimensional deformations due to surface loads, 2. Present-day glacial isostatic adjustment, *J. Geophys. Res.*, **99**, 7075–7101.

Peltier, W.R., 1974. The impulse response of a Maxwell earth, *Rev. Geophys. Space Phys.*, **12**, 649–669.

Peltier, W.R., 1995. VLBI baseline variations from the ICE-4G model of postglacial rebound, *Geophys. Res. Lett.*, **22**, 465–468.

Pierrehumbert, R.T. & Swanson, K.L., 1995. Baroclinic instability, *An. Rev. Fluid. Mech.*, **27**, 419–467.

Piersanti, A., Spada, G., Sabadini, R. & Bonafede, M., 1995. Global post-seismic deformation, *Geophys. J. Int.*, **120**, 544–566.

Poirier, J.P., 1985. *Creep of Crystals—High-temperature Deformation Processes in Metals, Ceramics and Minerals*, Cambridge University Press, Cambridge.

Ricard, Y. & Wuming, B., 1991. Inferring the viscosity and the 3-D density structure of the mantle from geoid, topography and plate velocities, *Geophys. J. Int.*, **105**, 561–571.

Sabadini, R., Yuen, D.A. & Boschi, E., 1982. Polar wandering and the forced responses of a rotating, multilayered, viscoelastic planet, *J. Geophys. Res.*, **87**, 2885–2903.

Sabadini, R., Yuen, D.A. & Boschi, E., 1984a. A comparison of the complete and truncated versions of the polar wander equations, *J. Geophys. Res.*, **89**, 7609–7620.

Sabadini, R., Yuen, D.A. & Boschi, E., 1984b. The effects of postseismic motions on the moment of inertia of a stratified viscoelastic Earth with an asthenosphere, *Geophys. J. R. astr. Soc.*, **79**, 727–746.

Sabadini, R., Piersanti, A. & Spada, G., 1995. Toroidal/poloidal partitioning of global post-seismic deformation, *Geophys. Res. Lett.*, **22**, 985–988.

Spada, G., Yuen, D.A., Sabadini, R., Morin, P.J. & Gasperini, P., 1990. A computer-aided, algebraic approach to the post-glacial rebound problem, *Mathematica Journal*, **1**, 65–69.

Steinberger, B.M., 1996. Motion of hotspots and changes of the Earth's rotation axis caused by a convecting mantle, *PhD thesis*, Harvard University, Cambridge, Massachusetts.

Su, W.J., Woodward, R.L. & Dziewonski, A.M., 1994. Degree 12 model of shear velocity heterogeneity in the mantle, *J. Geophys. Res.*, **99**, 6945–6980.

Tushingham, A.M. & Peltier, W.R., 1992. Validation of the ICE-3G model of Wurm-Wisconsin deglaciation using a global data base of relative sea level histories, *J. Geophys. Res.*, **97**, 3285–3304.

Vening-Meinesz, F.A., 1937. The determination of the Earth's plasticity from the postglacial uplift of Scandinavia: Isostatic Adjustment, *Koninklijke Akademie Van Wettenschapen Te Amsterdam*, **40**, 654–662.

Vermeersen, L.L.A., Sabadini, R. & Spada, G., 1996. Analytical visco-elastic relaxation models, *Geophys. Res. Lett.*, **23**, 697–700.

Ware, R. & Businger, S., 1995. Global positioning finds applications in geosciences research, *EOS, Trans. Am. Geophys. Un.*, **76**, 187.

Wu, P. & Peltier, W.R., 1982. Viscous gravitational relaxation, *Geophys. J. R. astr. Soc.*, **70**, 435–485.

Yuen, D.A. & Peltier, W.R., 1982. Normal modes of the viscoelastic earth, *Geophys. J. R. astr. Soc.*, **69**, 495–526.

Appendix 6.A: Expressions for a Spherically Symmetric Earth

A brief survey of the definitions and the expressions derived for the spheroidal components of $\mathbf{y}_n^E$, $\mathbf{y}_n^M$, $\boldsymbol{A}_n^E$ and $\mathbf{q}_n^M$ follows.

The solution vectors $\mathbf{y}_n^E(r)$ and $\mathbf{y}_n^M(r)$, with the elements ordered as usual in the postglacial rebound theory (Peltier 1974), are defined by

$$\mathbf{y}_n^{E|M,i}(r) = (U_n^i, V_n^i, T_{rr,n}^{E|M,i}, T_{r\vartheta,n}^{E|M,i}, F_n^i, Q_n^i)^T\,, \tag{6.26}$$

with the elements originated from spherical decomposition:

$$\begin{aligned}
\mathbf{u}(r,\Omega,t^i) &= \textstyle\sum_n [U_n^i(r) Y_n(\Omega)\boldsymbol{e}_r + V_n^i(r)\nabla_\Omega Y_n(\Omega)]\,, && (6.27)\\
\boldsymbol{\tau}_{rr}^{E|M}(r,\Omega,t^i) &= \textstyle\sum_n T_{rr,n}^{E|M,i}(r) Y_n(\Omega)\,, && (6.28)\\
\boldsymbol{\tau}_{r\vartheta}^{E|M}(r,\Omega,t^i) &= \textstyle\sum_n T_{r\vartheta,n}^{E|M,i}(r)\dfrac{dY_n(\Omega)}{d\vartheta}\,, && (6.29)\\
\varphi_1(r,\Omega,t^i) &= \textstyle\sum_n F_n^i(r) Y_n(\Omega)\,, && (6.30)\\
\nabla\cdot\mathbf{u}(r,\Omega,t^i) &= \textstyle\sum_n X_n^i(r) Y_n(\Omega)\,, && (6.31)
\end{aligned}$$

where $Y_n(\Omega)$ is any linear combination of the spherical harmonics $Y_{nm}(\vartheta,\varphi) = P_{nm}(\cos\vartheta)\exp(im\varphi)$, and $P_{nm}(\cos\vartheta)$ are the associated Legendre functions (Jones 1985). In the following expressions, the angular-order subscript n has mostly been omitted, the time superscripts are given only for those other than i, and the prime denotes the spatial derivative d/dr. The abbreviations

$$N = n(n+1)\,,\quad \beta = K + \frac{4}{3}\mu\,,\quad \gamma = \frac{3\mu K}{\beta}\,,\quad \lambda = K - \frac{2}{3}\mu \tag{6.32}$$

have been heavily used; we note also that $M^i = (t^{i+1} - t^i)\mu/\eta$ is used in the time-stepping and that $g_0 = \nabla\varphi_0$ is the gravitational acceleration. The limit of incompressibility (Wu & Peltier 1982) can be reached by setting

$$K \to \infty\,, \quad \frac{1}{\beta} \to 0\,, \quad \frac{\lambda}{\beta} \to 1\,, \quad \text{and} \quad \gamma \to 3\mu\,. \tag{6.33}$$

The coefficients of spherical decompositions are related by

$$\begin{aligned} Q &= F' + (n+1)F/r + 4\pi G\varrho_0 U\,, && (6.34)\\ X &= U' + 2U/r - NV/r\,, && (6.35)\\ T^E_{rr} &= \lambda X + 2\mu U'\,, && (6.36)\\ T^E_{r\vartheta} &= \mu(V' + U/r - V/r)\,. && (6.37) \end{aligned}$$

The elastic propagator matrix $\boldsymbol{A}^E_n(r)$ of both eqs (6.12) and (6.17) in the main text is given by

$$\begin{pmatrix} -\dfrac{2\lambda}{r\beta} & \dfrac{N\lambda}{r\beta} & \dfrac{1}{\beta} & 0 & 0 & 0 \\ -\dfrac{1}{r} & \dfrac{1}{r} & 0 & \dfrac{1}{\mu} & 0 & 0 \\ \dfrac{4(\gamma - r\varrho_0 g_0)}{r^2} & \dfrac{N(-2\gamma + r\varrho_0 g_0)}{r^2} & -\dfrac{4\mu}{r\beta} & \dfrac{N}{r} & -\dfrac{\varrho_0(n+1)}{r} & \varrho_0 \\ \dfrac{-2\gamma + r\varrho_0 g_0}{r^2} & \dfrac{-2\mu + N(\gamma+\mu)}{r^2} & -\dfrac{\lambda}{r\beta} & -\dfrac{3}{r} & \dfrac{\varrho_0}{r} & 0 \\ -4\pi G\varrho_0 & 0 & 0 & 0 & -\dfrac{n+1}{r} & 1 \\ -\dfrac{4\pi G\varrho_0(n+1)}{r} & \dfrac{4\pi G\varrho_0 N}{r} & 0 & 0 & 0 & \dfrac{n-1}{r} \end{pmatrix}. \tag{6.38}$$

The "Maxwellian" vector $\mathbf{q}^{M,i}_n(r)$ is

$$\mathbf{q}^{M,i}_n = \mathbf{q}^{M,i-1}_n \begin{pmatrix} 1 \\ 1 \\ 1 - M^i \\ 1 - M^i \\ 0 \\ 0 \end{pmatrix} + M^i \begin{pmatrix} \dfrac{1}{\beta}\left(T^M_{rr} - KX\right) \\ \dfrac{1}{\mu} T^M_{r\vartheta} \\ \dfrac{2\gamma}{r^2}\left(\dfrac{2rX}{3} - 2U + NV\right) \\ \dfrac{2\gamma}{r^2}\left(-\dfrac{rX}{3} + U\right) + \dfrac{2\mu - N(\gamma+\mu)}{r^2} V \\ 0 \\ 0 \end{pmatrix}, \tag{6.39}$$

where the components U, V, T^M_{rr}, $T^M_{r\vartheta}$ are obtained by $\mathbf{y}^{M,i}_n(r)$ in the last time step, and X, following (6.35) with U' substituted by the right-hand side of the first row of eq. (6.17), can be expressed as

$$X = \frac{1}{r}\left(1 - \frac{\lambda}{\beta}\right)(2U - NV) + \frac{1}{\beta} T^M_{rr} + q^{M,i-1}_1\,. \tag{6.40}$$

Finally, we include the spectral representation of the Heaviside boundary condition $\mathbf{b}^i_n(a) = \mathbf{B}^H_n$ for the point-mass load (Farrell 1972):

$$\mathbf{b}_n^i(a) \equiv \begin{pmatrix} T_{rr,n}^{M,i}(a) \\ T_{r\vartheta,n}^{M,i}(a) \\ Q_n^i(a) \end{pmatrix} = \mathbf{B}_n^H \equiv \begin{pmatrix} -g_0\Gamma_n \\ 0 \\ -4\pi G\Gamma_n \end{pmatrix}, \quad \Gamma_n = \frac{2n+1}{4\pi a^2}, \tag{6.41}$$

where a is the Earth's radius and Γ_n are spectral coefficients of the Legendre series for the Dirac delta function, $\delta(\vartheta) = \sum_n \Gamma_n P_{n0}(\cos\vartheta)$.

Appendix 6.B: Remarks on Expressions for 3-D Viscosity Models

In the following, we sketch the basic steps of application of the initial-value approach for the 3-D viscosity distribution. First, we consider spherical decompositions, similar to (6.27)–(6.31), but for both the spheroidal and toroidal components, for example

$$\mathbf{u}(r,\Omega,t^i) = \sum_n [U_n^i(r)Y_n(\Omega)\boldsymbol{e}_r + V_n^i(r)\nabla_\Omega Y_n(\Omega) + W_n^i(r)\boldsymbol{e}_r \times \nabla_\Omega Y_n(\Omega)]\,. \tag{6.42}$$

The toroidal parts of the decompositions introduce the seventh and eighth elements to the solution vector $\mathbf{y}_n^M(r)$: $W_n^i(r)$ and $T_{r\varphi,n}^{M,i}(r)$, where the latter is the radial coefficient of the toroidal component of the stress tensor $\boldsymbol{\tau}_{r\varphi}^M$. Second, with the toroidal counterparts of eqs (6.8) and (6.15) we obtain the counterpart of eq. (6.22) for the toroidal components:

$$\frac{d}{dr}\mathbf{z}_n^{M,i+1}(r) = \boldsymbol{B}_n^E(r)\mathbf{z}_n^{M,i+1}(r) + \mathbf{r}_n^{M,i}(r)\,. \tag{6.43}$$

The homogeneous boundary conditions, corresponding to a vertical load, imply a trivial solution $\mathbf{z}_n^{M,i} = \mathbf{0}$ for each i, but a load with a non-zero tangential component or a coupling of the spheroidal to the toroidal system can cause a non-trivial solution $\mathbf{z}_n^{M,i} \neq \mathbf{0}$.

With the toroidal expressions for $\mathbf{r}_n^{M,i}(r)$ and $\boldsymbol{B}_n^E(r)$, the last step is the fully 3-D expression of the spherical decomposition of $\nabla\cdot\boldsymbol{\tau}^V$, given by eq. (6.5), with $M^i = M^i(r,\Omega)$:

$$-\nabla\cdot\boldsymbol{\tau}^{V,i} = \sum_n [\gamma_n^i(r)Y_n(\Omega)\boldsymbol{e}_r + \delta_n^i(r)\nabla_\Omega Y_n(\Omega) + \eta_n^i(r)\boldsymbol{e}_r \times \nabla_\Omega Y_n(\Omega)]\,. \tag{6.44}$$

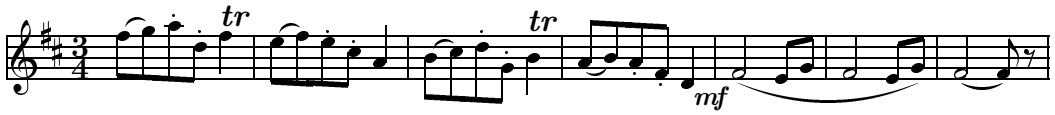

ANTONÍN DVOŘÁK, *Slavonic Dances, Op. 46. No. 6 in D major. Allegretto scherzando* (1878)

Chapter 7

Initial-Value Approach for Viscoelastic Responses of the Earth's Mantle[1]

We have developed a theory based on the direct numerical integration in time for studying the temporal viscoelastic responses of earth models to surface loads. Modelling in the time domain is motivated by the fact that realistic elastically compressible models generate an infinite number of modes and the width of such "continuous spectrum" may cover several orders of magnitude in the Laplacian spectral domain for complicated viscosity stratification, which causes numerical difficulties for the normal-mode method. From our numerical solutions, we have directed our attention on the influences of elastic compressibility, thickness of the lithosphere, the nature of the internal mantle boundaries with density jumps and the viscosity structure near the interface between the lower and the upper mantle. There is a great difference between the responses of compressible and incompressible models mainly for shorter wavelengths and thus incompressible models seem to be inadequate for short-wavelength responses. The sensitivity of the viscoelastic responses to the lithospheric thickness in the presence of a low viscosity asthenosphere is substantial. This points to the need for constructing models with a 3-D viscosity variations, which would yield more realistic lithospheric-asthenospheric structure globally than models with a constant lithospheric thickness. The sensitivity of the Earth's viscoelastic behaviour to the other parameters is weaker but still is noteworthy.

7.1 Introduction

The Earth's mantle behaves as a viscoelastic solid for timescales ranging from one year to possibly millions of years. Viscoelastic models have been used to study the attenuation of the seismic normal modes (Peltier et al. 1981; Yuen & Peltier 1982), earth tides (Lambeck & Nakiboglu 1983; Sabadini et al. 1985), postseismic rebound (Nur & Mavko 1974; Rundle 1982; Boschi et al. 1985;

[1]Original reference: Hanyk, L., Matyska, C. & Yuen, D.A., 1998. Initial-value approach for viscoelastic responses of the Earth's mantle, in *Dynamics of the Ice Age Earth: A Modern Perspective*, ed. by P. Wu, pp. 135–154, Trans Tech Publ., Switzerland. (Received July 6, 1997.)

Piersanti et al. 1995), postglacial rebound (e.g., Peltier 1974, Cathles 1975; Wu & Peltier 1982), rotational dynamics (Sabadini & Peltier 1981; Yuen et al. 1982; Sabadini et al. 1984; Ricard et al. 1992; Moser et al. 1993; Ivins et al. 1993; Steinberger 1996; Mitrovica & Forte 1997) and tectonics (Vermeersen et al. 1994). Various types of methods have been employed in solving the viscoelastic problems, ranging from normal modes (Peltier 1974), integral transform (Rundle 1982), finite elements (Melosh & Raefsky 1983; Sabadini et al. 1986; Wu 1992) and initial-value techniques with spectral expansion in the spatial domain (Cathles 1975; Ivins et al. 1993; Hanyk et al. 1995; Hanyk et al. 1996). There are distinct advantages for each of these methods, depending on the nature and spatial scale of the phenomenon being studied.

In the last several years there has been a resurgence of interest in the usage of initial-value techniques on integrating the set of ordinary differential equations obtained by spectral expansion of the partial differential equations of a pre-stressed, self-gravitating viscoelastic spherical model. The need for considering such an approach in contrast to the more traditional normal mode expansion using the Laplace transform (Peltier 1974) arises from the continuous spectrum found in stratified elastically compressible models (Han & Wahr 1995) and continuous viscosity profiles (Fang & Hager 1994; Fang & Hager 1995; Hanyk et al. 1995; Hanyk et al. 1996). In this work we will elaborate further on the differences between the initial-value and normal-mode approach, since there have been some issues raised recently (Vermeersen et al. 1996a; Vermeersen et al. 1996b; Vermeersen & Sabadini 1997).

We begin by discussing the mathematical formalism of this initial-value approach. We then follow by a discussion of the influences of the complex viscosity profiles on the temporal responses due to surface loads. The issues of compressibility versus incompressibility in the elastic regime and the influence of the thickness of the lithosphere will be discussed next. Next we delve into the role played by the nature of the boundary condition suggested by the transition zone's phase changes on viscoelastic responses. Our final topic will deal with the effects of viscosity stratification under the transition zone on the viscoelastic responses.

7.2 Theory

7.2.1 Fundamental Equations

The linear Maxwell viscoelastic rheology can be expressed as

$$\boldsymbol{\tau}^M(t) \quad = \quad \boldsymbol{\tau}^E(t) - \int_0^t \frac{\mu}{\eta}(\boldsymbol{\tau}^M(t') - K\nabla\cdot\mathbf{u}(t')\boldsymbol{I})\,dt'\,, \tag{7.1}$$

where

$$\boldsymbol{\tau}^E = (K - \frac{2}{3}\mu)\nabla\cdot\mathbf{u}\boldsymbol{I} + \mu(\nabla\mathbf{u} + (\nabla\mathbf{u})^T) \tag{7.2}$$

is the elastic part of the "Maxwellian" stress tensor $\boldsymbol{\tau}^M$; $\boldsymbol{I}$ denotes the identity tensor, $\mathbf{u}$ is the displacement vector and t is the time. Elastic properties of the Earth are described by the bulk modulus K and the shear-stress modulus μ, the viscous part of the rheology is represented by the dynamic viscosity η. The scalar product is denoted by $\cdot$ and the superscript ^{T} means the transposition.

The momentum equation of the pre-stressed self-gravitating continuum in a non-rotating reference system with inertial forces neglected is

$$\nabla \cdot \boldsymbol{\tau}^M - \varrho_0 \nabla \varphi_1 + \nabla \cdot (\varrho_0 \mathbf{u}) \nabla \varphi_0 - \nabla(\varrho_0 \mathbf{u} \cdot \nabla \varphi_0) = \mathbf{0}\,, \tag{7.3}$$

where φ_0 is the gravitational potential generated by the unperturbed density distribution ϱ_0. Finally, the perturbation of the gravitational potential φ_1 satisfies the Poisson equation

$$\nabla^2 \varphi_1 + 4\pi G \nabla \cdot (\varrho_0 \mathbf{u}) = 0\,, \tag{7.4}$$

where G is the gravitational constant.

7.2.2 Spherical Harmonic Decomposition

For density distribution and rheology parameters, which are spherically symmetric, i.e., $\varrho_0 = \varrho_0(r)$, $K = K(r)$, $\mu = \mu(r)$ and $\eta = \eta(r)$ with r being the radial distance from the Earth's centre, the system (7.1)–(7.4) can be decomposed by means of the spherical harmonic functions $Y_n(\Omega)$ representing any linear combination of the spherical harmonics $Y_{nm}(\vartheta, \varphi) = P_{nm}(\cos\vartheta)\exp(im\varphi)$; here P_{nm} are the associated Legendre functions (Jones 1985) and $\Omega \equiv (\vartheta, \varphi)$ denotes the pair of angular coordinates formed by the colatitude ϑ and the longitude φ. Using $\boldsymbol{e}_r$, $\boldsymbol{e}_\vartheta$ and $\boldsymbol{e}_\varphi$ as the unit basis vectors of the spherical coordinates, we can introduce the basis functions $\{Y_n(\Omega)\boldsymbol{e}_r$, $\nabla_\Omega Y_n(\Omega)$, $\boldsymbol{e}_r \times \nabla_\Omega Y_n(\Omega)\}$ in the space of vector functions defined on a unit sphere, where

$$\nabla_\Omega Y_n(\Omega) \equiv \frac{\partial Y_n}{\partial \vartheta}\boldsymbol{e}_\vartheta + \frac{1}{\sin\vartheta}\frac{\partial Y_n}{\partial \varphi}\boldsymbol{e}_\varphi\,, \quad \boldsymbol{e}_r \times \nabla_\Omega Y_n(\Omega) \equiv -\frac{1}{\sin\vartheta}\frac{\partial Y_n}{\partial \varphi}\boldsymbol{e}_\vartheta + \frac{\partial Y_n}{\partial \vartheta}\boldsymbol{e}_\varphi\,. \tag{7.5}$$

The first and second component of this spherical harmonic vector function represent the basis function in the space of spheroidal vector functions whereas the last component is the basis function in the space of toroidal functions. We will use this basis in the following expansions

$$\mathbf{u} = \textstyle\sum_n [U_n(r)Y_n(\Omega)\boldsymbol{e}_r + V_n(r)\nabla_\Omega Y_n(\Omega) + W_n(r)\boldsymbol{e}_r \times \nabla_\Omega Y_n(\Omega)]\,, \tag{7.6}$$

$$\boldsymbol{e}_r \cdot \boldsymbol{\tau}^{E|M} = \textstyle\sum_n [R_n^{E|M}(r)Y_n(\Omega)\boldsymbol{e}_r + S_n^{E|M}(r)\nabla_\Omega Y_n(\Omega) + T_n^{E|M}(r)\boldsymbol{e}_r \times \nabla_\Omega Y_n(\Omega)]\,, \tag{7.7}$$

$$\boldsymbol{e}_r \cdot \int_0^t \frac{\mu}{\eta}(\boldsymbol{\tau}^{E|M} - K\nabla \cdot \mathbf{u}\boldsymbol{I})\,dt' = \textstyle\sum_n [\alpha_n^{E|M}(r)Y_n(\Omega)\boldsymbol{e}_r + \beta_n^{E|M}(r)\nabla_\Omega Y_n(\Omega) + \chi_n^{E|M}(r)\boldsymbol{e}_r \times \nabla_\Omega Y_n(\Omega)]\,, \tag{7.8}$$

$$\nabla \cdot \int_0^t \frac{\mu}{\eta}(\boldsymbol{\tau}^{E|M} - K\nabla \cdot \mathbf{u}\boldsymbol{I})\,dt' = \textstyle\sum_n [\gamma_n^{E|M}(r)Y_n(\Omega)\boldsymbol{e}_r + \delta_n^{E|M}(r)\nabla_\Omega Y_n(\Omega) + \psi_n^{E|M}(r)\boldsymbol{e}_r \times \nabla_\Omega Y_n(\Omega)]\,, \tag{7.9}$$

where the symbol $E|M$ means "either E or M". Moreover, we will employ the expansion of φ_1 and $\nabla \cdot \mathbf{u}$ as follows,

$$\varphi_1 = \textstyle\sum_n F_n(r)Y_n(\Omega)\,, \tag{7.10}$$

$$\nabla \cdot \mathbf{u} = \textstyle\sum_n X_n(r)Y_n(\Omega)\,, \quad X_n = \dfrac{d}{dr}U_n + \dfrac{2}{r}U_n - \dfrac{n(n+1)}{r}V_n\,. \tag{7.11}$$

7.2.3 Spheroidal Part of the Equations

We follow here the well-known fact from the theory of elasticity that the system of fundamental equations can be decoupled into its spheroidal and toroidal parts (e.g., Farrell 1972). After introducing the vectors $\mathbf{y}_n^E$, $\mathbf{h}_n$,

$$\mathbf{y}_n^E(t) = (U_n, V_n, R_n^E, S_n^E, F_n, Q_n)^T\,, \tag{7.12}$$
$$\mathbf{h}_n(t) = (0, 0, \gamma_n^M, \delta_n^M, 0, 0)^T\,, \tag{7.13}$$

where $Q_n = \dfrac{d}{dr}F_n + \dfrac{n+1}{r}F_n + 4\pi G\varrho_0 U_n$, and the matrix $\boldsymbol{A}_n$ (see also Peltier 1974)

$$\boldsymbol{A}_n = \begin{pmatrix} -\dfrac{2\lambda}{r\beta} & \dfrac{N\lambda}{r\beta} & \dfrac{1}{\beta} & 0 & 0 & 0 \\ -\dfrac{1}{r} & \dfrac{1}{r} & 0 & \dfrac{1}{\mu} & 0 & 0 \\ \dfrac{4\,(\gamma - r\varrho_0 g_0)}{r^2} & \dfrac{N\,(-2\gamma + r\varrho_0 g_0)}{r^2} & -\dfrac{4\mu}{r\beta} & \dfrac{N}{r} & -\dfrac{\varrho_0(n+1)}{r} & \varrho_0 \\ \dfrac{-2\gamma + r\varrho_0 g_0}{r^2} & \dfrac{-2\mu + N(\gamma+\mu)}{r^2} & -\dfrac{\lambda}{r\beta} & -\dfrac{3}{r} & \dfrac{\varrho_0}{r} & 0 \\ -4\pi G\varrho_0 & 0 & 0 & 0 & -\dfrac{n+1}{r} & 1 \\ -\dfrac{4\pi G\varrho_0(n+1)}{r} & \dfrac{4\pi G\varrho_0 N}{r} & 0 & 0 & 0 & \dfrac{n-1}{r} \end{pmatrix} \tag{7.14}$$

where we have used the abbreviations $\beta = K + \dfrac{4}{3}\mu$, $\gamma = \dfrac{3\mu K}{\beta}$, $\lambda = K - \dfrac{2}{3}\mu$, $N = n(n+1)$ and $g_0 = \nabla\varphi_0$, the spheroidal part of the system of fundamental equations (7.1)–(7.4) can be written as

$$\frac{d}{dr}\mathbf{y}_n^E(t) = \boldsymbol{A}_n\mathbf{y}_n^E(t) + \mathbf{h}_n(t)\,. \tag{7.15}$$

Introducing the vector $\mathbf{y}_n^M$,

$$\begin{aligned} \mathbf{y}_n^M(t) &= (U_n, V_n, R_n^M, S_n^M, F_n, Q_n)^T \\ &= \mathbf{y}_n^E(t) - (0, 0, \alpha_n^M, \beta_n^M, 0, 0)^T\,, \end{aligned} \tag{7.16}$$

we can write an analogous relation

$$\frac{d}{dr}\mathbf{y}_n^M(t) = \boldsymbol{A}_n\mathbf{y}_n^M(t) + \mathbf{q}_n^M(t)\,. \tag{7.17}$$

For $\mathbf{q}_n^M = \mathbf{h}_n + \dfrac{d}{dr}(\mathbf{y}_n^M - \mathbf{y}_n^E) - \boldsymbol{A}_n(\mathbf{y}_n^M - \mathbf{y}_n^E)$, it follows from (7.13), (7.14), (7.16) that

$$\mathbf{q}_n^M = \begin{pmatrix} \dfrac{\alpha_n^M}{\beta} \\ \dfrac{\beta_n^M}{\mu} \\ \gamma_n^M - \dfrac{d}{dr}\alpha_n^M - \dfrac{4\mu}{r\beta}\alpha_n^M + \dfrac{N}{r}\beta_n^M \\ \delta_n^M - \dfrac{d}{dr}\beta_n^M - \dfrac{\lambda}{r\beta}\alpha_n^M - \dfrac{3}{r}\beta_n^M \\ 0 \\ 0 \end{pmatrix}. \tag{7.18}$$

These manipulations show that we must apply the same differential operator to $\mathbf{y}_n^M$ as in the elastic problems. However, the system (7.17) of ordinary differential equations becomes now non-homogeneous. The vector $\mathbf{q}_n^M$ represents the memory of the system. For performing the time-stepping of such a system, one needs to express $\mathbf{q}_n^M$ by means of $\mathbf{y}_n^M$ and to employ an appropriate integration scheme. These topics are discussed in Appendices 7.A and 7.B, respectively.

7.2.4 Toroidal Part of the Equations

Following the derivation of the spheroidal part, we may introduce the vectors $\mathbf{z}_n^{E|M}(t)$,

$$\mathbf{z}_n^{E|M}(t) = (W_n, T_n^{E|M})^T \,, \tag{7.19}$$

and the matrix $\boldsymbol{B}_n$,

$$\boldsymbol{B}_n = \begin{pmatrix} \dfrac{1}{r} & \dfrac{1}{\mu} \\ \dfrac{\mu(n-1)(n+2)}{r^2} & -\dfrac{3}{r} \end{pmatrix} . \tag{7.20}$$

The toroidal part of the fundamental equations (7.1)–(7.3) is then given by the system

$$\frac{d}{dr}\mathbf{z}_n^M(t) = \boldsymbol{B}_n \mathbf{z}_n^M(t) + \mathbf{p}_n^M(t) \,, \tag{7.21}$$

where

$$\mathbf{p}_n^M = \begin{pmatrix} \dfrac{\chi_n^M}{\mu} \\ \psi_n^M - \dfrac{d}{dr}\chi_n^M - \dfrac{3}{r}\chi_n^M \end{pmatrix} . \tag{7.22}$$

Detailed derivations of (7.22) as well as integration schemes are left again to Appendices 7.A and 7.B.

7.2.5 Boundary Conditions

In elastic problems, it is generally assumed that each interior boundary inside the mantle can be characterized by the continuity of $\mathbf{u}$ and $\boldsymbol{e}_r \cdot \boldsymbol{\tau}^E$. The core boundaries are described by the continuity of $\boldsymbol{e}_r \cdot \mathbf{u}$ as well as $\boldsymbol{e}_r \cdot \boldsymbol{\tau}^E \cdot \boldsymbol{e}_r$ and by the free-slip, i.e., $\boldsymbol{e}_r \cdot \boldsymbol{\tau}^E - (\boldsymbol{e}_r \cdot \boldsymbol{\tau}^E \cdot \boldsymbol{e}_r)\boldsymbol{e}_r = \mathbf{0}$. The boundary conditions inside the mantle mean that each inner boundary deforms together with boundary particles, i.e., there is no mass flux through the boundary.

In viscoelastic applications it is common to consider the same conditions as in elastic problems. However, if a boundary is caused by a phase transition, its position with respect to mantle particles can change. To satisfy conservation of mass, the continuity of $\boldsymbol{e}_r \cdot \mathbf{u}$ then must be replaced by the continuity of $\varrho_0 \boldsymbol{e}_r \cdot \left(\dfrac{\partial \mathbf{u}}{\partial t} - \mathbf{v} \right)$, where $\mathbf{v}$ is the velocity of the boundary motion. The conditions for horizontal components of displacement and for the traction $\boldsymbol{e}_r \cdot \boldsymbol{\tau}^M$ remain unchanged in the linearized case because the conservation of momentum requires $\varrho_0 \boldsymbol{e}_r \cdot \left[\dfrac{\partial \mathbf{u}}{\partial t} \left(\dfrac{\partial \mathbf{u}}{\partial t} - \mathbf{v} \right) - \boldsymbol{\tau}^M \right]$ to be

continuous. In the general case, **v** is a function of time. Therefore we can readily incorporate these boundary conditions only by direct time-integration of the viscoelastic responses.

At the surface we include the spectral representation of the Heaviside boundary condition for the point-mass load (Farrell 1972):

$$R_n^M = -g_0\Gamma_n\,, \quad S_n^M = T_n^M = 0\,, \quad Q_n = -4\pi G\Gamma_n\,, \tag{7.23}$$

where $\Gamma_n = (2n+1)/4\pi a^2$ are the spectral coefficients of the Legendre series for the Dirac δ-function.

7.3 Models and Numerical Results

The initial-value method has been proposed to be a direct numerical solver for computations of the temporal responses of viscoelastic Earth models with complicated viscosity profiles and realistic compressible elastic properties to all kinds of loading. Unless stated otherwise, we will employ the PREM model (Dziewonski & Anderson 1981) for the density $\varrho_0(r)$, the bulk modulus $K(r)$ and the shear-stress modulus $\mu(r)$. To demonstrate complex viscoelastic response of the Earth, we start with the viscosity profile C (called C3 in Hanyk et al. 1996) that contains purely elastic lithosphere, low viscosity in the asthenosphere and a high "viscosity hill" in the lower mantle, consistent with the geodynamical modelling (Ricard & Wuming 1991; van Keken et al. 1994) (Fig. 7.1).

The time dependences of the Love numbers h_n and l_n for the Heaviside load obtained from explicit-like time integration scheme (see the case $\omega = 1$ in Appendix 7.B) are drawn in Fig. 7.2. For comparing these results with the normal-mode technique employing the correspondence principle in the Laplace transform domain (e.g., Wu & Peltier 1982; Han & Wahr 1995), we have attempted to compute normal modes corresponding to the chosen model. The principal obstacle to be overcome lies in the fact that the number of modes tends to infinity and one needs a sophisticated numerical solver to be able to catch such weak modes that cannot be neglected a priori, as their sum may represent an observable part of the total response. We were able to find hundreds of modes for each angular order. However, when even a relatively large number of modes have been taken into account, we would still have difficulties in matching the curves obtained by direct time integration, as clearly seen in Fig. 7.2 for $n = 6$ and 60.

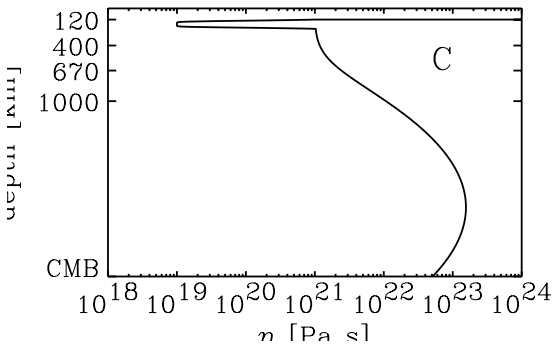

Fig. 7.1. The viscosity profile C with values spreading continuously over four orders in magnitude between the asthenosphere and the lower mantle. The elastic lithosphere is taken to be 120 km thick.

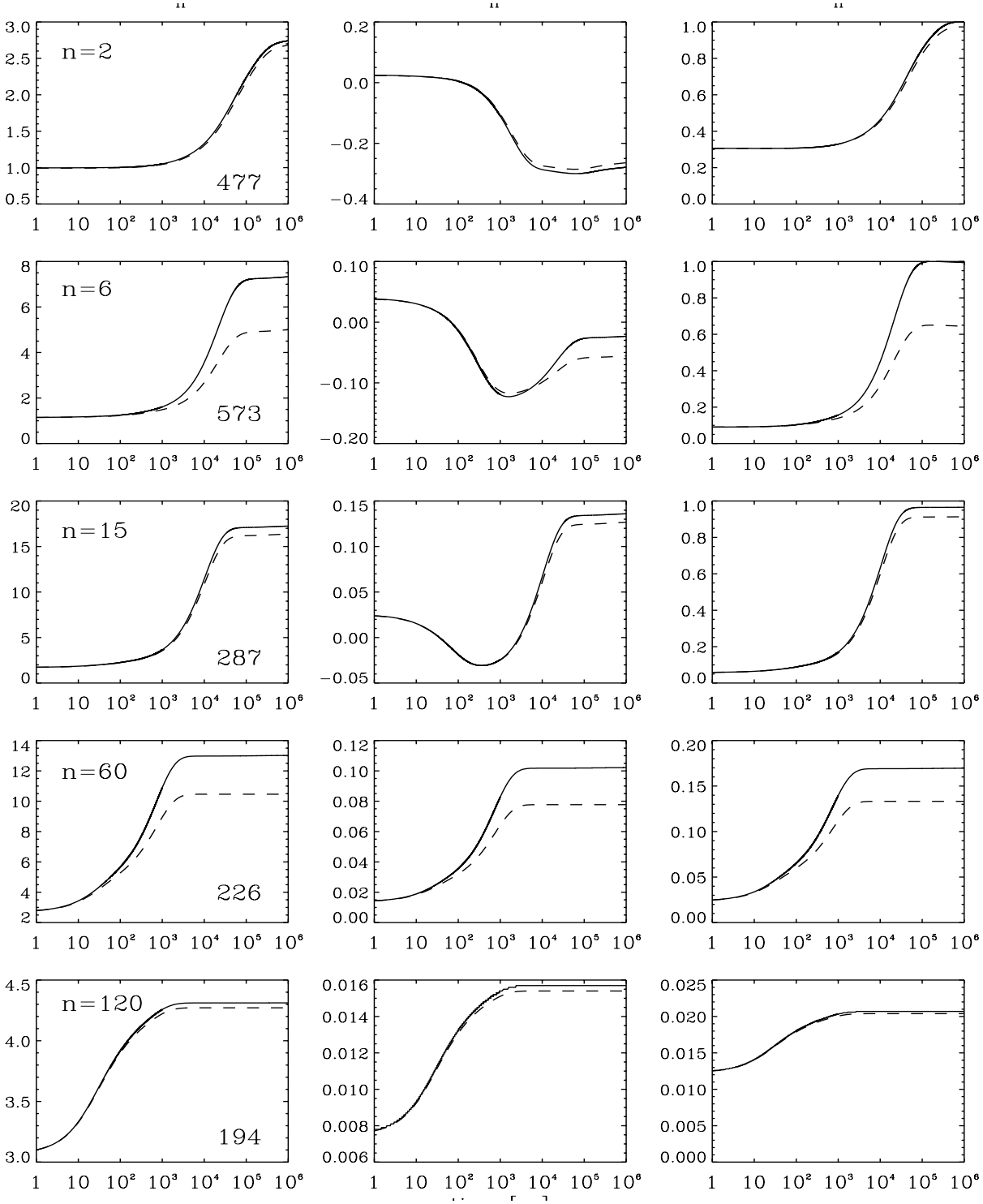

Fig. 7.2. Time evolution of the surface values of the load Love numbers h_n, l_n and k_n ($n = 2$, 6, 15, 60, 120) for the PREM model and the viscosity profile C (1 yr $< t <$ 1 Myr). Results for both the initial-value (solid curves) and the modal (dashed curves) approaches are plotted. Numbers of modes found by the modal solver for each n are given at the right lower corners of the h_n-panels.

The existence of this "continuous spectrum" stems from these two facts. First, due to the continuity of the viscosity and/or the shear modulus variations the Laplacian shear modulus becomes singular at least at one depth for a singular bound of values of the Laplacian variable s (Fang & Hager 1995). Because of the complexity of the viscosity profile, the singular bound of our model corresponds to the interval of relaxation times spanning from years to tens of kyr. To avoid the numerical difficulties with the propagator matrix in the Laplacian domain, we have made the continuous profiles of the shear modulus and viscosity discrete with a step corresponding to several kilometers. The singular bound of the discretized model is then a discrete set of values and we have scanned only the values of s lying outside this discrete singular bound in a mode searching procedure. Second, the compressibility results in a generation of infinite number of weak modes (Han & Wahr 1995), see also (Vermeersen et al. 1996b) and the question again arises whether they may be neglected. This sharp difference, occurring mainly in the horizontal displacement, was discussed by Mitrovica & Davis (1995).

Fig. 7.3 shows the comparison between values of the Love numbers for elastically compressible and incompressible models at the time instants $t = 0$ (elastic response), 1 kyr, 10 kyr and infinity (the isostatic limit). The elastically compressible model has the bulk modulus $K(r)$ the same as the PREM, whereas the incompressible model uses the value of K reaching infinity. The PREM values of the shear modulus and the viscosity profile drawn in Fig. 7.1 were considered in both cases. There is a fundamental difference between the elastically incompressible and compressible models at high angular orders because the incompressible models yield much higher attenuation of the Love numbers. We can clearly recognize that the relative difference in the Love number h_n may exceed 100% for high angular orders. This fact would dictate against employing incompressible models, which are used mainly in regional studies.

However, even more important parameter is the thickness of the lithosphere, which can be much lower than 120 km (which is traditionally adopted in postglacial rebound modelling) in oceanic regions (e.g., Wolf 1993; Nakada 1996). The values of the Love numbers of the compressible model C for t =1 kyr, 10 kyr and infinity and several lithosphere thicknesses (120, 100, 80 km) are shown in Fig. 7.4. One can clearly recognize that the response is faster with decreasing lithosphere thickness. Moreover, the amplitude of the whole spectrum of the Love number h_n increases for thinner lithosphere. We can explain this in physical terms: a thinner lithosphere increases a role played by a low viscosity asthenosphere (the bottom of the asthenosphere was fixed at the depth of 220 km in each of the models). The thickness of the lithosphere can thus be a key parameter in viscoelastic modelling. Since the lithosphere properties are strongly laterally dependent mainly due to the difference between the continents and the oceans, our results point to an importance of developing more reliable methods capable of handling viscosities that could change several orders in the horizontal direction. Finite-element modelling, though effective for regional studies, may be hard-pressed in global modelling of 3-D viscosity structure for spherical geometries.

A fundamental problem of mantle dynamics is the nature of boundaries with large density jumps and their relevant mathematical description. If a boundary is caused by a phase transition, it can potentially move with respect to surrounding particles during a dynamic process associated with changes of physical conditions. In elastic problems, such a mass flow through the boundary is prohibited because the time scale of elastic problems is very short in comparison with the time scale of phase transition kinetics, which ranges on the order between 10^3 and 10^4 years (Daessler & Yuen 1996). However, the time scale of phase transition kinetics is comparable with the time scale

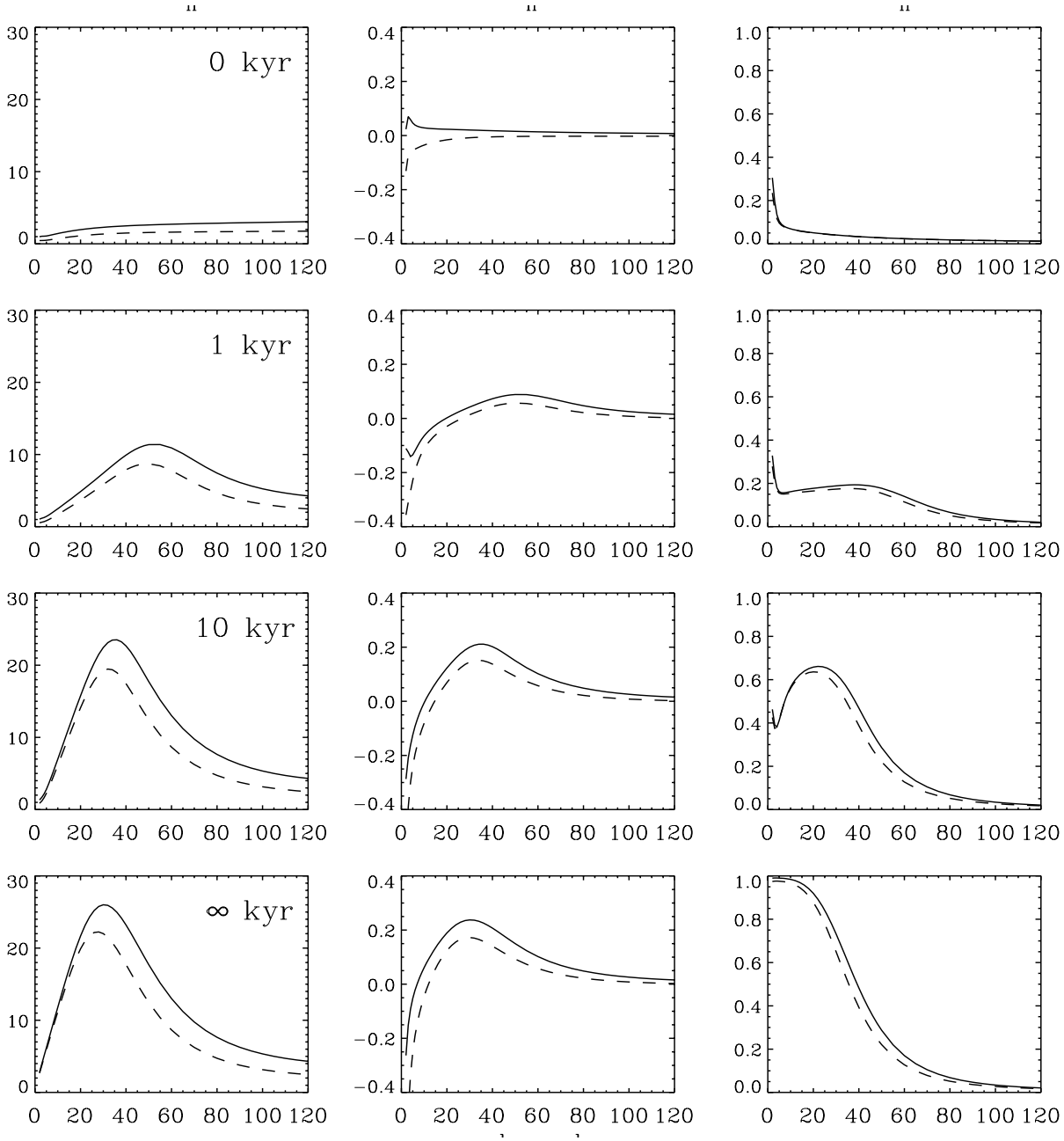

Fig. 7.3. Surface values of the load Love numbers h_n, l_n and k_n ($2 \leq n \leq 120$) for the PREM model and the viscosity profile C (t = 0, 1, 10, ∞ kyr). Solid and dashed curves represent the compressible and incompressible responses, respectively.

of viscoelastic responses, which should be taken into account in description of boundary conditions. To distinguish between the two end-member cases, we will denote a boundary without a mass flux as "chemical" and the one with a mass flux as the "phase" boundary. In the case of the phase boundary, the radial component of velocity $\dot{U}_n$, where the dot denotes time derivative, cannot be continuous because of the conservation of mass.

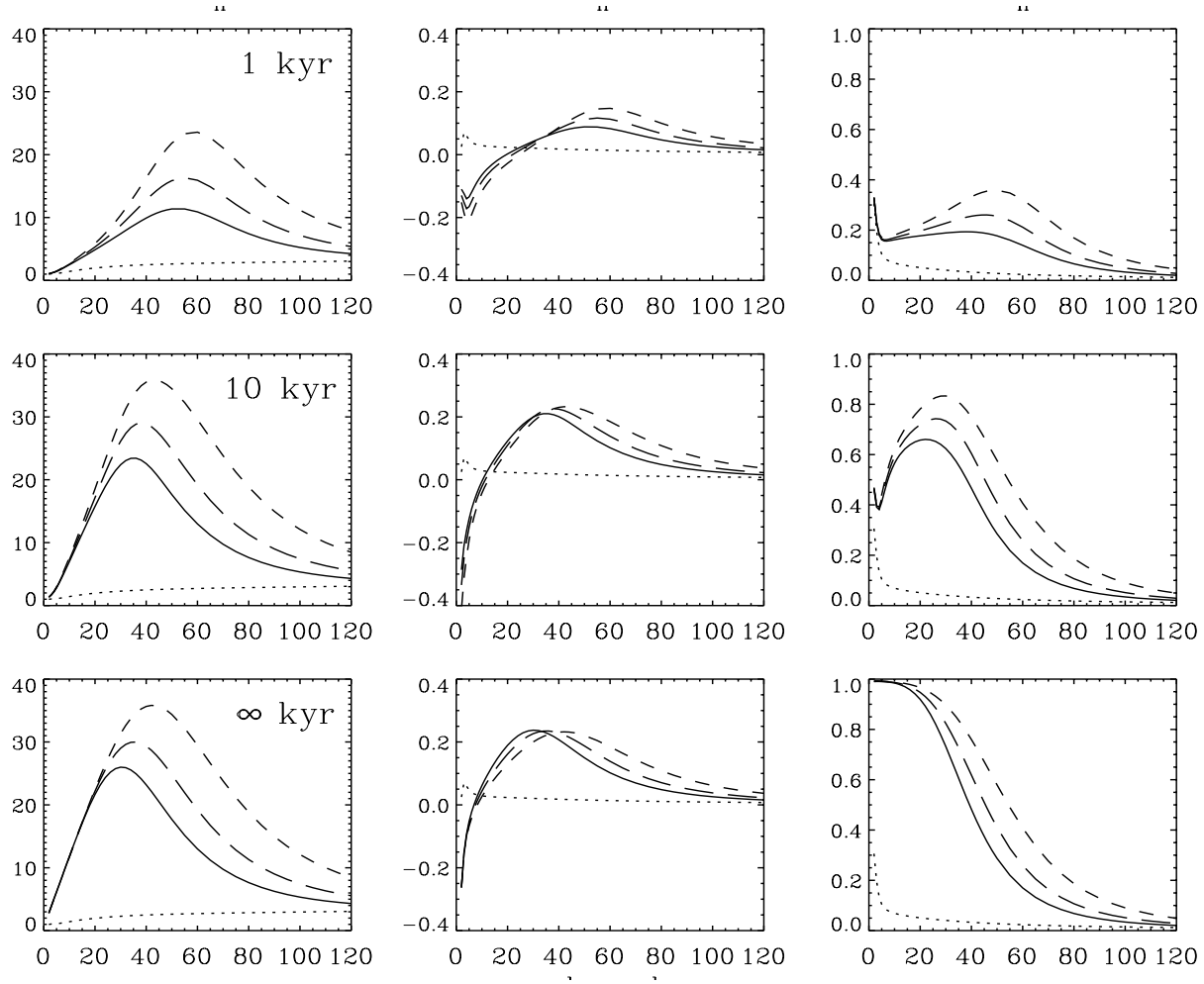

Fig. 7.4. Surface values of the load Love numbers h_n, l_n and k_n ($2 \leq n \leq 120$) for the PREM model at the time levels $t = 1$, 10 and ∞ kyr. The thickness of the lithosphere is 120, 100 or 80 km (solid, long-dashed or dashed curves, respectively). The asthenosphere with the bottom kept at the depth of 220 km is stretched upwards correspondingly, the viscosity profile C is matched otherwise. The dotted curves stand for the elastic Love numbers ($t = 0$).

In order to study the sensitivity of viscoelastic responses to the nature of the internal boundaries, we will here restrict ourselves only to the two limiting cases: i) the chemical boundaries with no mass flux and/or ii) the phase boundaries with $\mathbf{v} = 0$, which correspond to boundaries with ultrafast kinetics immediately reaching their isostatic equilibrium position (see also Johnston et al. 1997). The set of models taken into account can be described by a 4-index vector (i_1, i_2, i_3, i_4), where the indices i_1, i_2 and i_3 correspond to the nature of the boundaries at the depths 400, 520 and 670 km respectively and may be equal to either the symbol c meaning the chemical boundary or the symbol p denoting the phase boundary. The density jumps in the depths 400 and 670 km are given by the PREM, densities around the depth 520 km were constructed by a slight modification of the PREM profile to get the same jump as that in the 400 km. Finally, the last index denotes one of the three viscosity profiles (see Wu & Peltier 1982): $L1$ is the model with constant viscosity $\eta = 10^{21}$ Pa s, $L2$ has a viscosity jump by a factor of 10 across the 670 km discontinuity and the same value of upper-mantle viscosity as the L1 model, and the third model $L3$ has a low viscosity

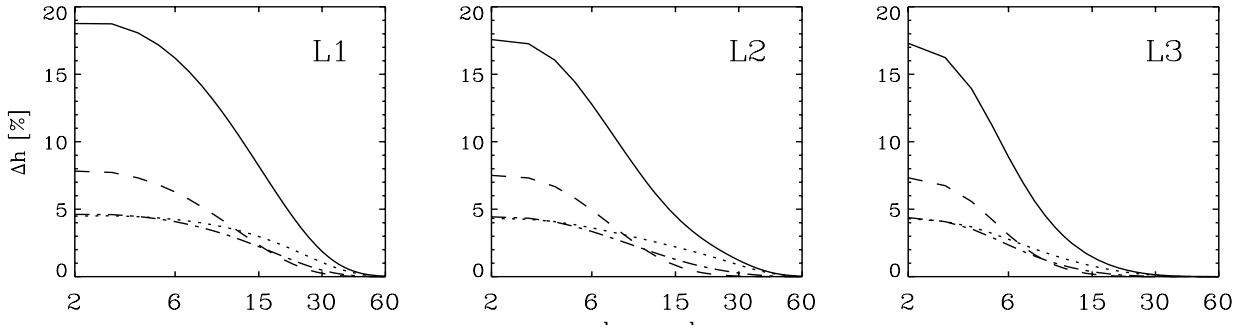

Fig. 7.5. Percentual difference in the load Love numbers h_n at the surface. The difference is taken between the predictions from models with all chemical boundaries (baseline case) and those with phase transitions as decribed in the text. Time is taken at $t = 20$ kyr and three viscosity profiles, L1, L2 and L3, have been employed.

channel of 10^{19} Pa s lying between 120 and 220 km depth, otherwise the same viscosity structure as for $L2$. Note that all models have purely elastic lithosphere of the thickness 120 km. For example, the model $(p, p, c, L1)$ is that with the constant viscosity and the phase boundaries at the depths 400 and 520 km, the 670 km discontinuity is chemical in nature.

Fig. 7.5 shows the relative changes in the surface values of the Love number h_n at the time $t = 20$ kyr after the application of a Heaviside load if the models $(c, c, c, \{L1, L2, L3\})$ play the role of the reference models represented by the base level. The solid, dashed, dash-dotted and dotted curves represent respectively the responses from the models $(p, p, p, \{L1, L2, L3\})$, $(c, c, p, \{L1, L2, L3\})$, $(c, p, c, \{L1, L2, L3\})$, $(p, c, c, \{L1, L2, L3\})$. We can clearly recognize that the sensitivity of the Love number h_n to the changes of the nature of the mantle internal boundaries may exceed 15% for this particular time. These relative changes are not very sensitive to a choice of the viscosity profile; only the presence of the low viscosity zone acts as a filter for suppressing the role of the boundaries for the higher angular orders. The influence of the boundary at 400 km depth is dominant for angular orders greater than 15, while the deepest boundary at 670 km depth is more influential for longer wavelengths. Inclusion of the phase boundary at 520 km (Shearer 1993) yields an additional contribution comparable to that at 400 km.

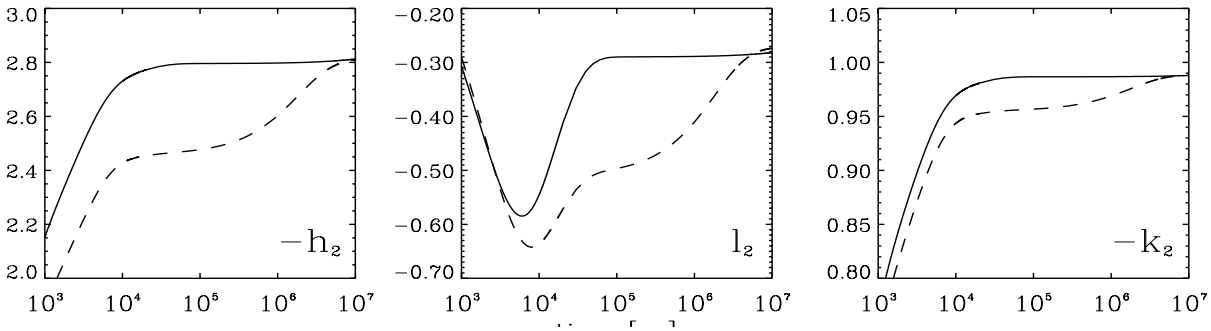

Fig. 7.6. Surface values of the load Love numbers h_2, l_2 and k_2 as a function of time. Solid and dashed curves denote respectively the phase transition and chemical boundary cases with three discontinuities at 400, 520 and 670 km depth. The viscosity profile L1 has been used.

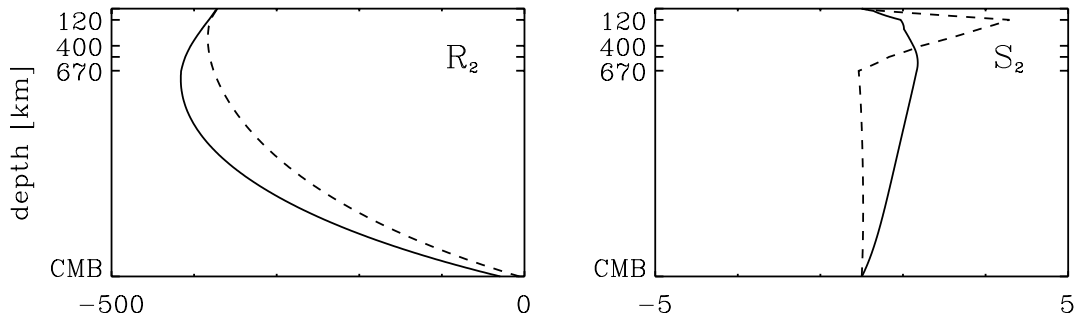

Fig. 7.7. Depth variations of the radial (R_2) and tangential (S_2) spherical harmonic components of the stress tensor at the time $t = 20$ kyr. Solid and dashed curves denote the same models as in Fig. 7.6. The stress quantities have been non-dimensionalized.

The time evolution of the Love numbers h_2, l_2 and k_2 for the models $(p, p, p, L1)$ (solid line) and $(c, c, c, L1)$ (dashed line) is compared in Fig. 7.6. A time necessary to reach hydrostatic equilibrium, when the two responses reach the same value, is very long (10 Myr). This value is comparable with characteristic times of mantle convection. This result points to the fact that a general viscoelastic response of the Earth's mantle may be influenced not only by a time-evolution of a load but also by a time-evolution of model parameters, e.g., by an increase of viscosity in time, caused by tectonic evolution. We would like to emphasize that potential time-dependences of the model parameters would not require any change of our integration schemes.

Fig. 7.7 portrays the depth variations of the stress components R_2^M and S_2^M for the same models as in Fig. 7.6 and the time $t = 20$ kyr. The vertical traction is by two orders of magnitude higher than the horizontal one but the horizontal traction is very sensitive to the nature of the interior boundaries. While the model with the chemical boundaries yields maximal horizontal traction at the interface between the lower and upper mantle, the phase boundaries generate maximal horizontal traction at the base of the lithosphere.

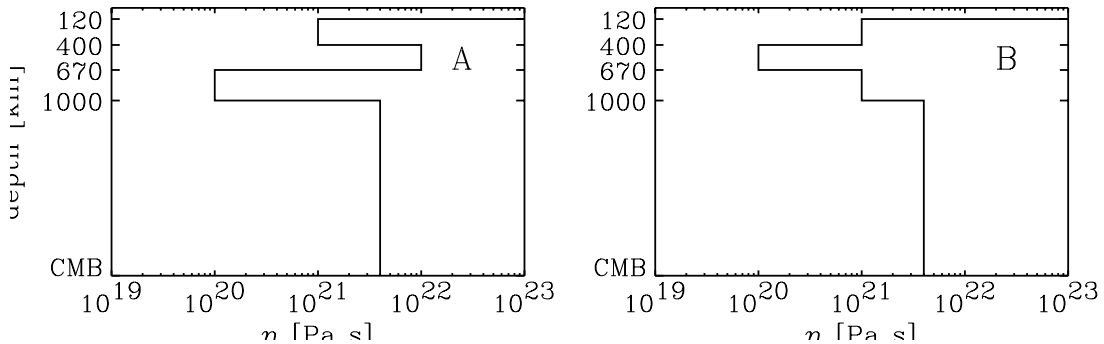

Fig. 7.8. The viscosity profiles A, B are used in discussing effects of viscosity stratification near the transition zone on viscoelastic responses.

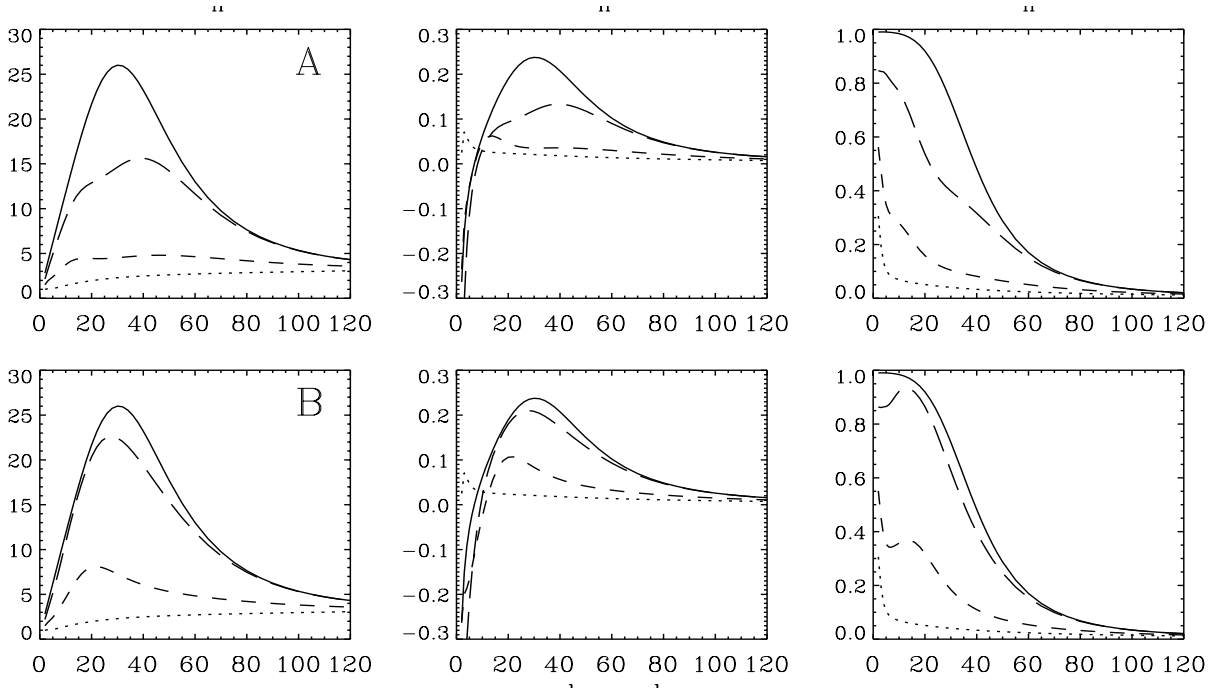

Fig. 7.9. The surface values of the load Love numbers h_n, l_n and k_n ($2 < n < 120$) for the PREM model and the viscosity profiles A (top), B (bottom). Dotted, dashed, long-dashed and solid curves show the time evolution ($t = 0$, 1, 10, ∞ kyr.)

Recently increased attention has been paid to the viscosity structure near the 670-km interface in geodynamical modelling (e.g., Kido & Čadek 1997; Wen & Anderson 1997), which relates to the nature of the interfaces in the 670 and 1000 km depths. To study the sensitivity of the viscoelastic responses to potential viscosity changes at the top of the lower mantle, we will compare the results for the two models from Fig. 7.8. The model A is characterized by relatively high viscosity in the transition zone between the depths of 400 and 670 km and by a low viscosity layer in the upper part of the lower mantle. On the contrary, there is only a zone of lower viscosity just in the transition zone in the model B. The values of the Love numbers at the time instants $t = 0$, 1 kyr, 10 kyr and infinity are then shown in Fig. 7.9. We can see that the response of the model B is substantially faster. There is another interesting difference between the two models in the Love numbers h_n and l_n for times of about several kyr: the peaks of the Love numbers for the model A are obtained for higher angular numbers than 30, which corresponds to the peak in the isostatic equilibrium, and, on the other side, the peaks of the model B are for lower angular numbers than 30. These results suggest that an effort to employ postglacial rebound data for constraining strongly depth-dependent viscosity models, used in geodynamical modelling might be profitable, provided we assume that the viscosities employed in the Maxwellian rheological models of the Earth's viscoelastic response correspond to the viscosities employed in the geodynamical modelling.

7.4 Conclusions

There are five fundamental reasons for further development and the future increasing use of the initial-value technique in the modelling of viscoelastic responses:

1. The existence of the shear modulus singular bound in the Laplacian domain for models with a continuously changing profile (Fang & Hager 1995).
2. An infinite number of modes for elastically compressible models (Han & Wahr 1995).
3. The possibility to incorporate a time-dependent feedback (e.g., phase-change kinetics) into the formulation of internal boundary conditions and structural time-dependences into the response modelling without a change of the integration scheme.
4. A possibility to incorporate general 3-D models of viscosity without any changes of the propagator matrix in the radial distance.
5. The increase in speed of raw computer power has made the time-marching scheme quite affordable. This scheme also allows for the code to be readily parallelized, thus further increasing the computational possibilities, especially for 3-D viscosity structure.

We have demonstrated that the viscoelastic responses of the mantle to surface loads are strongly sensitive to the lithospheric thickness, and thus models with realistic lithospheric and asthenospheric structures are highly desirable. The initial-value technique presented here can, in principle, be extended to models with an arbitrary 3-D viscosity. The differences between the compressible and incompressible models are especially acute for the higher angular degrees. Hence, employing elastically incompressible models for regional studies seems to be not of great value, in view of more accurate local geodetic measurements. The sensitivity of the viscoelastic response to the nature of the internal boundaries with density jumps and/or an order of magnitude viscosity jumps near the 670 km boundary are weaker but they can still exceed 10% for low angular orders.

Acknowledgements. We thank Z. Martinec for stimulating discussions. This research has been supported by the Grant Agency of the Czech Republic under the Project Nos. 205/96/0212 and 205/97/1015, by the grant of the Charles University 1/97/B-GEO/MFF, and the Geosciences Program of the Department of Energy (USA).

References

Boschi, E.V., Sabadini, R. & Yuen, D.A., 1985. The transient polar motions and the nature of the asthenosphere for short time scales, *J. Geophys. Res.*, **90**, 3559–3568.

Cathles, L.M., 1975. *The Viscosity of the Earth's Mantle*, Princeton University Press, Princeton, New Jersey.

D'Agostino, G., Spada, G. & Sabadini, R., 1997. Postglacial rebound and lateral viscosity variations: a semi-analytical approach based on a spherical model with Maxwell rheology, *Geophys. J. Int.*, **129**, F9–F13.

Daessler, R. & Yuen, D.A., 1996. The metastable wedge in fast subducting slabs: constraints from thermokinetic coupling, *Earth Planet. Sci. Lett.*, **137**, 109–118.

Dziewonski, A.M. & Anderson, D.L., 1981. Preliminary reference Earth model, *Phys. Earth planet. Inter.*, **25**, 297–356.

Fang, M. & Hager, B.H., 1994. A singularity free approach to post glacial rebound calculations, *Geophys. Res. Lett.*, **21**, 2131–2134.

Fang, M. & Hager, B.H., 1995. The singularity mystery associated with a radially continuous Maxwell viscoelastic structure, *Geophys. J. Int.*, **123**, 849–865.

Farrell, W.E., 1972. Deformation of the earth by surface loads, *Rev. Geophys. Space Phys.*, **10**, 761–797.

Han, D. & Wahr, J., 1995. The viscoelastic relaxation of a realistically stratified earth, and a further analysis of postglacial rebound, *Geophys. J. Int.*, **120**, 287–311.

Hanyk, L., Moser, J., Yuen, D.A. & Matyska, C., 1995. Time-domain approach for the transient responses in stratified viscoelastic Earth models, *Geophys. Res. Lett.*, **22**, 1285–1288.

Hanyk, L., Yuen, D.A. & Matyska, C., 1996. Initial-value and modal approaches for transient viscoelastic responses with complex viscosity profiles, *Geophys. J. Int.*, **127**, 348–362.

Ivins, E.R., Sammis, C.G. & Yoder, C.F., 1993. Deep mantle viscous structure with prior estimate and satellite constraint, *J. Geophys. Res.*, **98**, 4579–4609.

Jones, M.N., 1985. *Spherical Harmonics and Tensors for Classical Field Theory*, Research Studies Press Ltd, Letchworth.

Johnston, P., Lambeck, K. & Wolf, D., 1997. Material versus isobaric internal boundaries in the Earth and their influence on postglacial rebound, *Geophys. J. Int.*, **129**, 252–268.

Kido, M. & Čadek, O., 1997. Inferences of viscosity from the oceanic geoid: Indication of a low viscosity zone below the 660-km discontinuity, *Earth Planet. Sci. Lett.*, **151**, 125–137.

Lambeck, L. & Nakiboglu, S.M., 1983. Long-period Love numbers and their frequency dependence due to dispersion effects, *Geophys. Res. Lett.*, **10**, 857–860.

Martinec, Z., 1999. Spectral, initial value approach for viscoelastic relaxation of a spherical earth with a three-dimensional viscosity–I. Theory, *Geophys. J. Int.*, **137**, 469–488.

Melosh, H.J. & Raefsky, A., 1983. Anelastic responses of the Earth to a dip slip earthquake, *J. Geophys. Res.*, **88**, 515–526.

Mitrovica, J.X. & Davis, J.L., 1995. Some comments on the 3-D impulse response of a Maxwell viscoelastic earth, *Geophys. J. Int.*, **120**, 227–234.

Mitrovica, J.X. & Forte, A.M., 1997. Radial profile of mantle viscosity: Results from the joint inversion of convection and postglacial rebound, *J. Geophys. Res.*, **102**, 2751–2770.

Moser, J., Matyska, C., Yuen, D.A., Malevsky, A.V. & Harder, H., 1993. Mantle rheology, convection and rotational dynamics, *Phys. Earth Planet. Inter.*, **79**, 367–381.

Nakada, M., 1996. Viscosity structure of the oceanic lithosphere inferred from the differential late Quaternary sea-level variations for the southern Cook Islands, *Geophys. J. Int.*, **126**, 829–844.

Nur, A. & Mavko, G., 1974. Postseismic viscoelastic rebound, *Science*, **183**, 204–206.

Peltier, W.R., 1974. The impulse response of a Maxwell earth, *Rev. Geophys. Space Phys.*, **12**, 649–669.

Peltier, W.R., Wu, P. & Yuen, D.A., 1981. The viscosities of the Earth's mantle, in *Anelasticity of the Earth, A.G.U. Geodynamics Series*, ed. by F.D. Stacey, M.S. Peterson and A. Nicolas, pp. 59–71.

Piersanti, A., Spada, G., Sabadini, R. & Bonafede, M., 1995. Global post-seismic deformation, *Geophys. J. Int.*, **120**, 544–566.

Ricard, Y. & Wuming, B., 1991. Inferring the viscosity and the 3-D density structure of the mantle from geoid, topography and plate velocities, *Geophys. J. Int.*, **105**, 561–571.

Ricard, Y., Sabadini, R. & Spada, G., 1992. Isostatic deformations and polar wander induced by redistribution of mass within the Earth, *J. Geophys. Res.*, **97**, 14223–14236.

Rundle, J.B., 1982. Viscoelastic-gravitational deformation by a rectangular thrust fault in a layered Earth, *J. Geophys. Res.*, **87**, 10729–10744.

Sabadini, R. & Peltier, W.R., 1981. Pleistocene deglaciation and the earth's rotation: Implications for mantle rheology, *Geophys. J. R. astr. Soc.*, **66**, 553–578.

Sabadini, R., Yuen, D.A. & Boschi, E., 1984. A comparison of the complete and truncated versions of the polar wander equations, *J. Geophys. Res.*, **89**, 7609–7620.

Sabadini, R., Yuen, D.A. & Widmer, R., 1985. Constraints on short-term mantle rheology from the J2 observation and the dispersion of the 18.6 yr. Love number, *Phys. Earth Planet. Inter.*, **38**, 235–249.

Sabadini, R., Yuen, D.A. & Portney, M., 1986. The effects of upper-mantle lateral heterogeneities on postglacial rebound, *Geophys. Res. Lett.*, **13**, 337–340.

Shearer, P.M., 1993. Global mapping of upper mantle reflectors from long-period SS precursors, *Geophys. J. Int.*, **115**, 878–904.

Steinberger, B.M., 1996. Motion of hotspots and changes of the Earth's rotation axis caused by a convecting mantle, *PhD thesis*, Harvard University, Cambridge, Massachusetts.

van Keken, P., Yuen, D.A. & van den Berg, A., 1994. Implications for mantle dynamics from the high melting temperature of perovskite, *Science*, **264**, 1437–1439.

Vermeersen, L.L.A., Sabadini, R., Spada, G. & Vlaar, N.J., 1994. Mountain building and earth rotation, *Geophys. J. Int.*, **117**, 610–624.

Vermeersen, L.L.A., Sabadini, R. & Spada, G., 1996a. Analytical visco-elastic relaxation models, *Geophys. Res. Lett.*, **23**, 697–700.

Vermeersen, L.L.A., Sabadini, R. & Spada, G., 1996b. Compressible rotational deformation, *Geophys. J. Int.*, **126**, 735–761.

Vermeersen, L.L.A. & Sabadini, R., 1997. A new class of stratified viscoelastic models by analytical techniques, *Geophys. J. Int.*, **129**, 531–570.

Wen, L. & Anderson, D.L., 1997. Layered mantle convection: A model for geoid and topography, *Earth Planet. Sci. Lett.*, **146**, 367–377.

Wolf, D., 1993. The changing role of the lithosphere in models of glacial isostasy: a historical review, *Global and Planet. Change*, **8**, 95–106.

Wu, P., 1992. Deformation of an incompressible viscoelastic flat Earth with power-law creep: A finite element approach, *Geophys. J. Int.*, **108**, 35–51.

Wu, P. & Peltier, W.R., 1982. Viscous gravitational relaxation, *Geophys. J. R. astr. Soc.*, **70**, 435–485.

Yuen, D.A. & Peltier, W.R., 1982. Normal modes of the viscoelastic earth, *Geophys. J. R. astr. Soc.*, **69**, 495–526.

Yuen, D.A., Sabadini, R. & Boschi, E., 1982. Viscosity of the lower mantle as inferred from rotational data, *J. Geophys. Res.*, **87**, 10745–10762.

Appendix 7.A: Derivation of the Memory Part of the Equations

First, (7.17) yields the expression of $\frac{d}{dr}U_n$ that may be put into (7.11). We obtain

$$X_n = \frac{2\mu}{r\beta}(2U_n - NV_n) + \frac{1}{\beta}R_n^M + q_{n,1}^M \,. \tag{7.24}$$

Now, it is clear from eqs (7.18) and (7.22) that $q^M_{n,1}$, $q^M_{n,2}$ and $p^M_{n,1}$ may be written as

$$\begin{aligned} q^M_{n,1} &= \frac{1}{\beta}\int_0^t \frac{\mu}{\eta}(R^M_n - KX_n)\,dt' \\ &= \frac{1}{\beta}\int_0^t \frac{\mu}{\eta}\left[-\frac{2\gamma}{3r}(2U_n - NV_n) + \frac{4\mu}{3\beta}R^M_n - Kq^M_{n,1}\right]dt', \end{aligned} \tag{7.25}$$

$$q^M_{n,2} = \frac{1}{\mu}\int_0^t \frac{\mu}{\eta}S^M_n\,dt', \tag{7.26}$$

$$p^M_{n,1} = \frac{1}{\mu}\int_0^t \frac{\mu}{\eta}T^M_n\,dt'. \tag{7.27}$$

Derivation of the remaining terms is more complicated. If we use the relation (7.1) defining the kind of rheology, we may write analogous relations for the coefficients of the expansions (7.8) and (7.9):

$$\begin{aligned} \int_0^t \frac{\mu}{\eta}(\boldsymbol{\tau}^M - K\nabla\cdot\mathbf{u}\boldsymbol{I})\cdot\boldsymbol{e}_r\,dt' &= \int_0^t \frac{\mu}{\eta}(\boldsymbol{\tau}^E - K\nabla\cdot\mathbf{u}\boldsymbol{I})\cdot\boldsymbol{e}_r\,dt' - \\ &- \int_0^t \frac{\mu}{\eta}\left[\int_0^{t'}\frac{\mu}{\eta}(\boldsymbol{\tau}^M - K\nabla\cdot\mathbf{u}\boldsymbol{I})\cdot\boldsymbol{e}_r\,dt''\right]dt' \end{aligned} \tag{7.28}$$

and

$$\begin{aligned} \int_0^t \nabla\cdot\left[\frac{\mu}{\eta}(\boldsymbol{\tau}^M - K\nabla\cdot\mathbf{u}\boldsymbol{I})\right]dt' &= \int_0^t \nabla\cdot\left[\frac{\mu}{\eta}(\boldsymbol{\tau}^E - K\nabla\cdot\mathbf{u}\boldsymbol{I})\right]dt' - \\ -\int_0^t \frac{d}{dr}\left(\frac{\mu}{\eta}\right)\left[\int_0^{t'}\frac{\mu}{\eta}(\boldsymbol{\tau}^M - K\nabla\cdot\mathbf{u}\boldsymbol{I})\cdot\boldsymbol{e}_r\,dt''\right]dt' &- \int_0^t \frac{\mu}{\eta}\left[\int_0^{t'}\nabla\cdot\left[\frac{\mu}{\eta}(\boldsymbol{\tau}^M - K\nabla\cdot\mathbf{u}\boldsymbol{I})\right]dt''\right]dt'. \end{aligned} \tag{7.29}$$

In other words,

$$\mathbf{q}^M_n = \mathbf{q}^E_n - \int_0^t \frac{\mu}{\eta}\mathbf{q}^M_n\,dt'. \tag{7.30}$$

Now we may use the expression of $\nabla\cdot\boldsymbol{\tau}^E$ by means of the displacement vector in spherical coordinates to obtain

$$\begin{aligned} q^M_{n,3} &= \int_0^t \frac{\mu}{\eta}\frac{3}{r}(R^E_n - KX_n)\,dt' - \frac{4\mu}{r\beta}\int_0^t \frac{\mu}{\eta}(R^E_n - KX_n)\,dt' - \int_0^t \frac{\mu}{\eta}q^M_{n,3}\,dt' \\ &= \frac{\gamma}{\mu r}\int_0^t \frac{\mu}{\eta}\left(-\frac{2\mu}{3}X_n + 2\mu\frac{d}{dr}U_n\right)dt' - \int_0^t \frac{\mu}{\eta}q^M_{n,3}\,dt' \\ &= \int_0^t \frac{\mu}{\eta}\left[\frac{2\gamma}{r^2}\left(\frac{2r}{3}X_n - 2U_n + NV_n\right) - q^M_{n,3}\right]dt' \\ &= \int_0^t \frac{\mu}{\eta}\left[-\frac{2\gamma K}{r^2\beta}(2U_n - NV_n) + \frac{4\gamma}{3r\beta}R^M_n + \frac{4\gamma}{3r}q^M_{n,1} - q^M_{n,3}\right]dt'. \end{aligned} \tag{7.31}$$

Analogously,

$$\begin{aligned} q^M_{n,4} &= \int_0^t \frac{\mu}{\eta}\frac{2\mu}{r}\left(\frac{\partial Y_n}{\partial\vartheta}\right)^{-1}\left[\frac{\partial}{\partial\vartheta}\left(-\frac{1}{3}X_nY_n + \frac{1}{r}U_nY_n + \frac{1}{r}V_n\frac{\partial^2 Y_n}{\partial\vartheta^2}\right) + \right. \\ &+ \left.\frac{V_n}{r\sin^2\vartheta}\left(\frac{\partial^3 Y_n}{\partial\vartheta\partial\varphi^2} - \cot\vartheta\frac{\partial^2 Y_n}{\partial\varphi^2}\right) + \frac{V_n\cot\vartheta}{r}\left(\frac{\partial^2 Y_n}{\partial\vartheta^2} - \frac{\partial Y_n}{\partial\vartheta}\cot\vartheta - \frac{1}{\sin^2\vartheta}\frac{\partial^2 Y_n}{\partial\varphi^2}\right)\right]dt' - \\ &- \frac{2\lambda\mu}{r\beta}\int_0^t \frac{\mu}{\eta}(\frac{2}{3}X_n - \frac{2}{r}U_n + \frac{N}{r}V_n)\,dt' - \int_0^t \frac{\mu}{\eta}q^M_{n,4}\,dt'. \end{aligned} \tag{7.32}$$

Since (Jones 1985)

$$\begin{aligned} -N\frac{\partial}{\partial\vartheta}Y_n &= \frac{\partial}{\partial\vartheta}\left(\frac{\partial^2 Y_n}{\partial\vartheta^2}+\cot\vartheta\frac{\partial Y_n}{\partial\vartheta}+\frac{1}{\sin^2\vartheta}\frac{\partial^2 Y_n}{\partial\varphi^2}\right) \\ &= \frac{\partial^3 Y_n}{\partial\vartheta^3}+\cot\vartheta\frac{\partial^2 Y_n}{\partial\vartheta^2}+\frac{1}{\sin^2\vartheta}\frac{\partial^3 Y_n}{\partial\vartheta\partial\varphi^2}-2\frac{\cot\vartheta}{\sin^2\vartheta}\frac{\partial^2 Y_n}{\partial\varphi^2}-(\cot^2\vartheta+1)\frac{\partial Y_n}{\partial\vartheta}\,, \end{aligned} \tag{7.33}$$

we finally arrive at

$$\begin{aligned} q_{n,4}^M &= \int_0^t \frac{\mu}{\eta}\left[\frac{2\gamma}{r^2}\left(-\frac{r}{3}X_n+U_n\right)+\frac{2\mu-N(\gamma+\mu)}{r^2}V_n-q_{n,4}^M\right]dt' \\ &= \int_0^t \frac{\mu}{\eta}\left[\frac{2\gamma K}{r^2\beta}U_n+\frac{2\mu-N\left(\frac{\gamma K}{\beta}+\mu\right)}{r^2}V_n-\frac{2\gamma}{3r\beta}R_n^M-\frac{2\gamma}{3r}q_{n,1}^M-q_{n,4}^M\right]dt'\,. \end{aligned} \tag{7.34}$$

The expressions (7.25), (7.26), (7.31) and (7.34) can be summarized as

$$\mathbf{q}_n^M(t)=\int_0^t\frac{\mu}{\eta}\left[\tilde{\boldsymbol{Q}}_n\mathbf{y}_n^M(t')+\tilde{\tilde{\boldsymbol{Q}}}_n\mathbf{q}_n^M(t')\right]dt'\,, \tag{7.35}$$

where

$$\tilde{\boldsymbol{Q}}_n=\begin{pmatrix} -\frac{4\gamma}{3r\beta} & \frac{2N\gamma}{3r\beta} & \frac{4\mu}{3\beta^2} & 0 & 0 & 0\\ 0 & 0 & 0 & \frac{1}{\mu} & 0 & 0\\ -\frac{4\gamma K}{r^2\beta} & \frac{2N\gamma K}{r^2\beta} & \frac{4\gamma}{3r\beta} & 0 & 0 & 0\\ \frac{2\gamma K}{r^2\beta} & \frac{2\mu-N(\frac{\gamma K}{\beta}+\mu)}{r^2} & -\frac{2\gamma}{3r\beta} & 0 & 0 & 0\\ 0 & 0 & 0 & 0 & 0 & 0\\ 0 & 0 & 0 & 0 & 0 & 0 \end{pmatrix},\quad \tilde{\tilde{\boldsymbol{Q}}}_n=\begin{pmatrix} -\frac{K}{\beta} & 0 & 0 & 0 & 0 & 0\\ 0 & 0 & 0 & 0 & 0 & 0\\ \frac{4\gamma}{3r} & 0 & -1 & 0 & 0 & 0\\ -\frac{2\gamma}{3r} & 0 & 0 & -1 & 0 & 0\\ 0 & 0 & 0 & 0 & 0 & 0\\ 0 & 0 & 0 & 0 & 0 & 0 \end{pmatrix}. \tag{7.36}$$

The same procedure applied to $p_{n,2}^M$ yields

$$\begin{aligned} p_{n,2}^M &= \int_0^t \frac{\mu}{\eta}\frac{\mu}{r^2}\left(\frac{\partial Y_n}{\partial\vartheta}\right)^{-1}W_n\left[\frac{\partial}{\partial\vartheta}\left(\frac{\partial^2 Y_n}{\partial\vartheta^2}-\frac{1}{\sin^2\vartheta}\frac{\partial^2 Y_n}{\partial\varphi^2}-\frac{\partial Y_n}{\partial\vartheta}\cot\vartheta\right)+\right. \\ &+ \left.\frac{2}{\sin^2\vartheta}\left(\frac{\partial^3 Y_n}{\partial\vartheta\partial\varphi^2}-\cot\vartheta\frac{\partial^2 Y_n}{\partial\varphi^2}\right)+2\cot\vartheta\left(\frac{\partial^2 Y_n}{\partial\vartheta^2}-\frac{\partial Y_n}{\partial\vartheta}\cot\vartheta-\frac{1}{\sin^2\vartheta}\frac{\partial^2 Y_n}{\partial\varphi^2}\right)\right]dt'-\int_0^t\frac{\mu}{\eta}p_{n,2}^M\,dt' \\ &= -\int_0^t\frac{\mu}{\eta}\frac{\mu(N+1)}{r^2}W_n\,dt'-\int_0^t\frac{\mu}{\eta}p_{n,2}^M\,dt'\,, \end{aligned} \tag{7.37}$$

and thus the analogy of (7.35) and (7.36) is

$$\mathbf{p}_n^M(t)=\int_0^t\frac{\mu}{\eta}\left[\tilde{\boldsymbol{P}}_n\mathbf{z}_n^M(t')+\tilde{\tilde{\boldsymbol{P}}}_n\mathbf{p}_n^M(t')\right]dt'\,, \tag{7.38}$$

where[2]

$$\tilde{\boldsymbol{P}}_n=\begin{pmatrix} 0 & \frac{1}{\mu}\\ -\frac{\mu(N+1)}{r^2} & 0 \end{pmatrix},\quad \tilde{\tilde{\boldsymbol{P}}}_n=\begin{pmatrix} 0 & 0\\ -1 & 0 \end{pmatrix}. \tag{7.39}$$

[2]Incorrect; see (3.64).

Appendix 7.B: Time and Spatial Integration Schemes

Let $t^0 = 0 < t^1 < \ldots < t^{i+1}$ be a series of successive time levels, let us denote $M^i = \frac{\mu}{\eta}(t^{i+1} - t^i)$, and let us consider the integration scheme for a function $f(t)$ in the form

$$\int_0^{t^{i+1}} \frac{\mu}{\eta} f(t)\, dt = \int_0^{t^i} \frac{\mu}{\eta} f(t)\, dt + M^i \left[(\omega f^i + (1-\omega) f^{i+1}\right] , \tag{7.40}$$

with $0 \le \omega \le 1$, $f^i = f(t^i)$ and $f^{i+1} = f(t^{i+1})$. The discretized eqs (7.17), (7.21) for $t = t^{i+1}$ read

$$\frac{d}{dr}\mathbf{y}_n^{M,i+1} = \boldsymbol{A}_n \mathbf{y}_n^{M,i+1} + \mathbf{q}_n^{M,i+1} , \tag{7.41}$$

$$\frac{d}{dr}\mathbf{z}_n^{M,i+1} = \boldsymbol{B}_n \mathbf{z}_n^{M,i+1} + \mathbf{p}_n^{M,i+1} . \tag{7.42}$$

Applying (7.40) in (7.35), we get for $\mathbf{q}_n^{M,i+1}$

$$\mathbf{q}_n^{M,i+1} = \mathbf{q}_n^{M,i} + M^i \left[\omega(\tilde{\boldsymbol{Q}}_n \mathbf{y}_n^{M,i} + \tilde{\tilde{\boldsymbol{Q}}}_n \mathbf{q}_n^{M,i}) + (1-\omega)(\tilde{\boldsymbol{Q}}_n \mathbf{y}_n^{M,i+1} + \tilde{\tilde{\boldsymbol{Q}}}_n \mathbf{q}_n^{M,i+1})\right] . \tag{7.43}$$

It yields

$$\left[\boldsymbol{I} - M^i(1-\omega)\tilde{\tilde{\boldsymbol{Q}}}_n\right] \mathbf{q}_n^{M,i+1} = \left[\boldsymbol{I} + M^i\omega\tilde{\tilde{\boldsymbol{Q}}}_n\right] \mathbf{q}_n^{M,i} + M^i(1-\omega)\tilde{\boldsymbol{Q}}_n \mathbf{y}_n^{M,i+1} + M^i\omega\tilde{\boldsymbol{Q}}_n \mathbf{y}_n^{M,i} , \tag{7.44}$$

which—after substitution into (7.41)—gives the final expression,

$$\frac{d}{dr}\mathbf{y}_n^{M,i+1} = \left[\boldsymbol{A}_n + M^i(1-\omega)\tilde{\boldsymbol{A}}_n^{\,i}\right] \mathbf{y}_n^{M,i+1} + M^i\omega\tilde{\boldsymbol{A}}_n^{\,i}\mathbf{y}_n^{M,i} + \tilde{\tilde{\boldsymbol{A}}}_n^{\,i}\mathbf{q}_n^{M,i} . \tag{7.45}$$

We introduced

$$\tilde{\boldsymbol{A}}_n^{\,i} = \left[\boldsymbol{I} - M^i(1-\omega)\tilde{\tilde{\boldsymbol{Q}}}_n\right]^{-1} \tilde{\boldsymbol{Q}}_n , \tag{7.46}$$

$$\tilde{\tilde{\boldsymbol{A}}}_n^{\,i} = \left[\boldsymbol{I} - M^i(1-\omega)\tilde{\tilde{\boldsymbol{Q}}}_n\right]^{-1} \left(\boldsymbol{I} + M^i\omega\tilde{\tilde{\boldsymbol{Q}}}_n\right) , \tag{7.47}$$

where

$$\left[\boldsymbol{I} - M^i(1-\omega)\tilde{\tilde{\boldsymbol{Q}}}_n\right]^{-1} = \begin{pmatrix} c_3 & 0 & 0 & 0 & 0 & 0 \\ 0 & 1 & 0 & 0 & 0 & 0 \\ 2c_1c_2c_3 & 0 & c_2 & 0 & 0 & 0 \\ -c_1c_2c_3 & 0 & 0 & c_2 & 0 & 0 \\ 0 & 0 & 0 & 0 & 1 & 0 \\ 0 & 0 & 0 & 0 & 0 & 1 \end{pmatrix} \tag{7.48}$$

with $c_1 = \dfrac{2\gamma}{3r} M^i(1-\omega)$, $c_2 = \dfrac{1}{1 + M^i(1-\omega)}$ and $c_3 = \dfrac{1}{1 + M^i(1-\omega)\frac{K}{\beta}}$. Note that the matrices $\tilde{\boldsymbol{A}}_n^{\,i}$, $\tilde{\tilde{\boldsymbol{A}}}_n^{\,i}$ are time-dependent only when the factors M^i are time-dependent. The eq. (7.45) with the special choice of $\omega = 1$,

$$\frac{d}{dr}\mathbf{y}_n^{M,i+1} = \boldsymbol{A}_n \mathbf{y}_n^{M,i+1} + M^i\tilde{\boldsymbol{Q}}_n \mathbf{y}_n^{M,i} + (\boldsymbol{I} + M^i\tilde{\tilde{\boldsymbol{Q}}}_n)\mathbf{q}_n^{M,i} , \tag{7.49}$$

was recently published by Hanyk et al. (1996) in a slightly modified form.

The scheme for the toroidal part is

$$\frac{d}{dr}\mathbf{z}_n^{M,i+1} = \left[\boldsymbol{B}_n + M^i(1-\omega)\tilde{\boldsymbol{B}}_n^i\right]\mathbf{z}_n^{M,i+1} + M^i\omega\tilde{\boldsymbol{B}}_n^i\mathbf{z}_n^{M,i} + \tilde{\tilde{\boldsymbol{B}}}_n^i\mathbf{p}_n^{M,i}\,, \tag{7.50}$$

where

$$\tilde{\boldsymbol{B}}_n^i = \begin{pmatrix} 0 & \dfrac{1}{\mu} \\ -\dfrac{\mu(N+1)}{r^2[1+M^i(1-\omega)]} & 0 \end{pmatrix}, \quad \tilde{\tilde{\boldsymbol{B}}}_n^i = \begin{pmatrix} 1 & 0 \\ 0 & 1-M^i\omega \end{pmatrix}. \tag{7.51}$$

Appendix 7.C: Extension of the Theory to Problems with 3-D Viscosity

In a case with three-dimensional viscosity, it is necessary to work with the basis formed by the spherical harmonics Y_{nm} instead of harmonic functions Y_n, i.e., the basis in the space of vector functions on a sphere is $\{Y_{nm}\boldsymbol{e}_r,\ \nabla_\Omega Y_{nm}, \boldsymbol{e}_r \times \nabla_\Omega Y_{nm}\}$. From the formal point of view, it is sufficient to replace the subscript n by nm in all formulas in Section 7.2. Note, however, that the propagator matrix A_{nm} is not dependent on m and is still defined by the relation (7.14). Let us take into account the following expansion

$$\begin{aligned}\int_0^t \left[\frac{1}{r}\nabla_\Omega\left(\frac{\mu}{\eta}\right) + \frac{\mu}{\eta}\left(\nabla - \frac{\partial}{\partial r}\boldsymbol{e}_r\right)\right]\cdot(\boldsymbol{\tau}^M - K\nabla\cdot\mathbf{u}\boldsymbol{I})\,dt' \quad &= \\ = \quad \textstyle\sum_{nm}[\bar{\gamma}_{nm}Y_{nm}\boldsymbol{e}_r + \bar{\delta}_{nm}\nabla_\Omega Y_{nm} + \bar{\psi}_{nm}\boldsymbol{e}_r\times\nabla_\Omega Y_{nm}]\,.\end{aligned} \tag{7.52}$$

The expression on the right-hand side of (7.18) can thus be replaced by

$$\mathbf{q}_{nm}^M = \begin{pmatrix} \dfrac{\alpha_{nm}^M}{\beta} \\ \dfrac{\beta_{nm}^M}{\mu} \\ \bar{\gamma}_{nm} - \dfrac{4\mu}{r\beta}\alpha_{nm}^M + \dfrac{N}{r}\beta_{nm}^M \\ \bar{\delta}_{nm} - \dfrac{\lambda}{r\beta}\alpha_{nm}^M - \dfrac{3}{r}\beta_{nm}^M \\ 0 \\ 0 \end{pmatrix} \tag{7.53}$$

and (7.22) by

$$\mathbf{p}_{nm}^M = \begin{pmatrix} \dfrac{\chi_{nm}^M}{\mu} \\ \bar{\psi}_{nm} - \dfrac{3}{r}\chi_{nm}^M \end{pmatrix}. \tag{7.54}$$

The explicit scheme of integration of the expansions can now be written as follows,

$$\sum_{nm}[\alpha_{nm}^{M,i+1}Y_{nm}\boldsymbol{e}_r + \beta_{nm}^{M,i+1}\nabla_\Omega Y_{nm} + \chi_{nm}^{M,i+1}\boldsymbol{e}_r \times \nabla_\Omega Y_{nm}] \quad = \tag{7.55}$$
$$= \sum_{nm}[\alpha_{nm}^{M,i}Y_{nm}\boldsymbol{e}_r + \beta_{nm}^{M,i}\nabla_\Omega Y_{nm} + \chi_{nm}^{M,i}\boldsymbol{e}_r \times \nabla_\Omega Y_{nm}] + M^i(\boldsymbol{\tau}^{M,i} - K\nabla\cdot\mathbf{u}^i\boldsymbol{I})\cdot\boldsymbol{e}_r\,,$$
$$\sum_{nm}[\bar{\gamma}_{nm}^{i+1}Y_{nm}\boldsymbol{e}_r + \bar{\delta}_{nm}^{i+1}\nabla_\Omega Y_{nm} + \bar{\psi}_{nm}^{i+1}\boldsymbol{e}_r \times \nabla_\Omega Y_{nm}] \quad = \tag{7.56}$$
$$= \sum_{nm}[\bar{\gamma}_{nm}^{i}Y_{nm}\boldsymbol{e}_r + \bar{\delta}_{nm}^{i}\nabla_\Omega Y_{nm} + \bar{\psi}_{nm}^{i}\boldsymbol{e}_r \times \nabla_\Omega Y_{nm}] \;+$$
$$+ \quad \Delta t\left[\frac{1}{r}\nabla_\Omega\left(\frac{\mu}{\eta}\right) + \frac{\mu}{\eta}\left(\nabla - \frac{\partial}{\partial r}\boldsymbol{e}_r\right)\right]\cdot(\boldsymbol{\tau}^{M,i} - K\nabla\cdot\mathbf{u}^i\boldsymbol{I})\,,$$

To be able to perform the time-stepping (7.55) and (7.56), we need to know the time evolution of the whole tensor $\boldsymbol{\tau}^M$. Let us denote $\boldsymbol{\tau}^V = -\int_0^t(\boldsymbol{\tau}^M - K\nabla\cdot\mathbf{u}\boldsymbol{I})\,dt'$. The integration scheme is

$$\boldsymbol{\tau}^{M,i} = \boldsymbol{\tau}^{E,i} + \boldsymbol{\tau}^{V,i-1} - \omega M^{i-1}(\boldsymbol{\tau}^{M,i-1} - K\nabla\cdot\mathbf{u}^{i-1}\boldsymbol{I}) - (1-\omega)M^{i-1}(\boldsymbol{\tau}^{M,i} - K\nabla\cdot\mathbf{u}^i\boldsymbol{I}) \tag{7.57}$$

and thus

$$\boldsymbol{\tau}^{M,i} = \frac{1}{1+(1-\omega)M^i}\left[\boldsymbol{\tau}^{E,i} + (1-\omega)M^{i-1}K\nabla\cdot\mathbf{u}^i\boldsymbol{I} + \boldsymbol{\tau}^{V,i-1} - \omega M^{i-1}(\boldsymbol{\tau}^{M,i-1} - K\nabla\cdot\mathbf{u}^{i-1}\boldsymbol{I})\right]. \tag{7.58}$$

Tensors $\boldsymbol{\tau}^{E,i}$ and $\nabla\cdot\mathbf{u}^i$ are linear combinations of U_{nm}^i, V_{nm}^i, W_{nm}^i, $\frac{d}{dr}U_{nm}^i$, $\frac{d}{dr}V_{nm}^i$, $\frac{d}{dr}W_{nm}^i$ and due to (7.17) these quantities can be written as a linear combination of $\mathbf{y}_{nm}^{M,i}$, $\mathbf{z}_{nm}^{M,i}$, $\mathbf{q}_{nm}^{M,i}$ and $\mathbf{p}_{nm}^{M,i}$. Hence, the time-stepping is, in principle, computable (see also Martinec 1999). Note here that the Laplace transform technique applied to problems with 3-D viscosity requires one to solve a coupled set of equations for each value of the Laplacian variable s. D'Agostino et al. (1997) employed an iterative technique to solve these coupled equations for a model containing an axisymmetric craton with a modest increase in the lateral variations of the viscosity. The question arises as to the convergence of these iterations for a more general class of models, namely for more difficult models with sharp lateral variations in the viscosity involving several orders in magnitude.

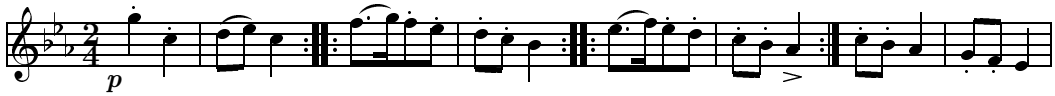

ANTONÍN DVOŘÁK, *Slavonic Dances, Op. 46. No. 7 in C minor. Allegro assai* (1878)

Chapter 8

Secular Gravitational Instability of a Compressible Viscoelastic Sphere[1]

For a self-gravitating viscoelastic compressible sphere we have shown that unstable modes can exist by means of the linear viscoelastic theory by both initial-value and normal-mode approaches. For a uniform sphere we have derived analytical expressions for the roots of the secular determinant based on the asymptotic expansion of the spherical Bessel functions. From the two expressions, both the destabilizing nature of gravitational forces and the stabilizing influences of increasing elastic strength are revealed. Fastest growth times on the order of ten thousand years are developed for the longest wavelength. In contrast, a self-gravitating incompressible viscoelastic model is found to be stable. This result of linear approximation suggests that a more general approach, e.g., non-Maxwellian rheology or a non-linear finite-amplitude theory, should be considered in global geodynamics.

8.1 Introduction

It is commonly assumed that the Maxwellian viscoelastic responses of the Earth models to surface loads with the Heaviside time-dependence reach a static equilibrium after sufficiently long times (e.g., Wu & Peltier 1982). There has been a long debate as to the conditions required for static stability of this fluid (see Fang 1998). It was shown (Longman 1963) that the compressible fluid can be stable, if the density distribution satisfies the Adams-Williamson equation.

The density distribution of realistic Earth models, e.g. PREM (Dziewonski & Anderson 1981), does not satisfy the Adams-Williamson equation, neither do simplified compressible models consisting of a finite number of homogeneous layers. The question arises as to the long-time asymptotic behaviour of such models. Plag & Jüttner (1995) investigated the instabilities of the PREM model. They found unstable modes with the characteristic times comparable to those of the stable modes. On the other hand, Wolf (1985) considered a uniform compressible half-space model and did not find any instabilities in the analytical solution, based on field equations with neglected internal buoyancy.

[1]Original reference: Hanyk, L., Matyska, C. & Yuen, D.A., 1999. Secular gravitational instability of a compressible viscoelastic sphere, *Geophys. Res. Lett.*, **26**, 557–560. (Received September 23, 1998; revised November 25, 1998; accepted January 7, 1999.)

Here we will present results for one-, two- and three-layered self-gravitating spherical compressible models. In particular, we will demonstrate the secular instability of a homogeneous compressible sphere analytically. Although the considered models are rather simple to represent a sufficient approximation of the real Earth, we can gain valuable insights into the fundamental physics and be in a better position to learn more when a more complicated model will be investigated.

8.2 Analysis of the Gravitational Instability

Responses of the self-gravitating viscoelastic compressible spherical models have already been studied by means of normal-mode expansion (e.g., Yuen & Peltier 1982; Wu & Peltier 1982). We have employed our initial-value technique (Hanyk et al. 1996, 1998) for examining the behaviour of the response for the homogeneous model, both elastically compressible and elastically incompressible, with parameters listed in Table 8.1 (i.e., density ρ, shear modulus μ, bulk modulus K and viscosity η). Much to our surprise, we have found that a secular instability with a growing trend appears in the compressible model. Both the vertical displacement and the gravitional perturbation load Love numbers, $h_n(t)$ and $k_n(t)$, are shown for angular order $n = 2$ in Fig. 8.1, where a growing unstable timescale of around 20 kyr is obtained. On the contrary, an equilibrium state is attained for the incompressible model. We will now employ the normal-mode theory for verifying this result.

The analytical solutions for the homogeneous compressible sphere in the Laplace domain were given by Wu & Peltier (1982) and recently by Vermeersen et al. (1996). Our purpose is to search for roots of the secular determinant $\det M(s)$ of this model for the positive values of the Laplace variable, $s > 0$. In the upper panel of Fig. 8.2 we show a set of roots which appear in the region of

Table 8.1. Physical Parameters of the Models

model 1:	homogeneous sphere	
	radius	6371 km
	density	5517 $\mathrm{kg\,m^{-3}}$
	shear modulus	1.4519×10^{11} Pa
	bulk modulus	4.4967×10^{11} Pa
	viscosity	10^{21} Pa s
model 2:	core-mantle sphere	
	core radius	3480 km
	core density	10926 $\mathrm{kg\,m^{-3}}$
	mantle density	4314 $\mathrm{kg\,m^{-3}}$
	core bulk modulus	3.5288×10^{11} Pa
	core shear modulus	0 Pa
	core viscosity	0 Pa s
	otherwise see model 1	
model 3:	core-mantle sphere with a lithosphere	
	lithospheric thickness	120 km
	lithospheric viscosity	$\to \infty$ Pa s
	otherwise see model 2	

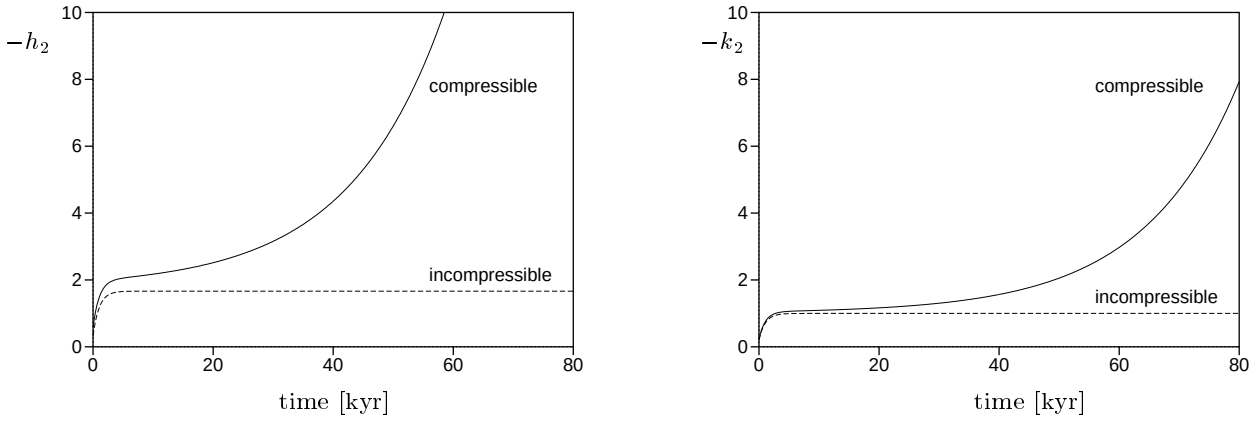

Fig. 8.1. Temporal responses of the vertical displacement and the gravitational perturbation load Love numbers $h_2(t)$ and $k_2(t)$ for both compressible (solid curves) and incompressible (dashed curves) homogeneous spheres (model 1). A Heaviside function in time has been used. Angular order $n = 2$ has been considered.

$s \to 0_+$. Following the notation by Plag & Jüttner (1995), we will refer to the RT (Rayleigh-Taylor) modes for the unstable responses corresponding to these positive roots of the secular determinant.

A simple calculation clarifies the presence of these roots: the secular determinant is expressed in terms of spherical Bessel functions of the argument $k(s)r$, where r denotes the radius and for $k(s)$ see Wu & Peltier (1982). In the limit of $s \to 0_+$, the value of $k(s)$ goes[2] to $+\infty$, hence the number of roots of spherical Bessel functions goes to $+\infty$ and the infinite number of roots of the secular determinant can be anticipated.

We have substantiated this preliminary calculation by derivation of the asymptotic expansion

[2]See also (3.28) with $\mu(s) \to 0$ for $s \to 0_+$.

Table 8.2. Responses of the Model 1, $n = 2$

mode i	s_2^i [10^{-11} s^{-1}]	$1/s_2^i$ [kyr]	h_2^i/s_2^i	k_2^i/s_2^i
M0	−2.891240	−1.096	−1.40088	−0.83084
D0	−14.158778	−0.224	−0.00585	−0.00033
D1	−8.935232	−0.355	0.00000	0.00000
D2	−9.948630	−0.319	−0.00012	+0.00005
RT1	+0.200408	+15.81	+0.20535	+0.04479
RT2	+0.025711	+123.25	+0.04034	+0.00431
RT3	+0.007258	+436.57	+0.01852	+0.00113
h_2^e, k_2^e			−0.58151	−0.22005
$\sum_{e,\mathrm{M0,D0-D10}}$			−1.98840	−1.05116
$\sum_{e,\mathrm{M0,D0-D10,RT1-RT100}}$			−1.66921	−1.00000

The analytical values of the isostatic load Love numbers are $h_n^{\mathrm{is}} = -(2n+1)/3\,, \quad k_n^{\mathrm{is}} = -1\,.$

of the secular equation $\det M(s) = 0$, using the asymptotic forms of the spherical Bessel functions involving large arguments. In the $s \to 0_+$ limit, the secular equation becomes $\sin(k(s)r - n\pi/2) = 0$, from which the analytical formula for the roots of the RT modes follows,

$$s_n^{\mathrm{RT}m} = \frac{n(n+1)}{K\eta} \frac{\left(r^2\rho\xi\right)^2}{\left[(2m+n)\frac{\pi}{2}\right]^4} \,. \tag{8.1}$$

In (8.1), n is the angular order, m the overtone number and $\xi = \frac{4}{3}\pi G\rho$. The asymptotic validity of this formula is demonstrated in Fig. 8.2, where the roots according to (8.1) are denoted by diamonds lying on the zero line.

It follows from (8.1) that the $s_n^{\mathrm{RT}m}$ are positive (and the RT modes unstable) for all finite and positive values of the physical parameters. On the other hand, the values $s_n^{\mathrm{RT}m}$ go to the stable limit with a value of 0 in both incompressible ($K \to \infty$) and elastic limits ($\eta \to \infty$). The lowest growth time $1/s_n^{\mathrm{RT}1}$, which dominates the response, must be found numerically by root-finding procedures, as the asymptotic formula (8.1) is not accurate for low m. However, formula (8.1) can be considered as the analytical proof of existence of the unstable modes and of the initial-value results shown in Fig. 8.1.

For the sake of completeness, we also discuss the previous analysis of the stable branch of the secular determinant, $s < 0$, by Vermeersen et al. (1996). In that paper, both the mistakingly used

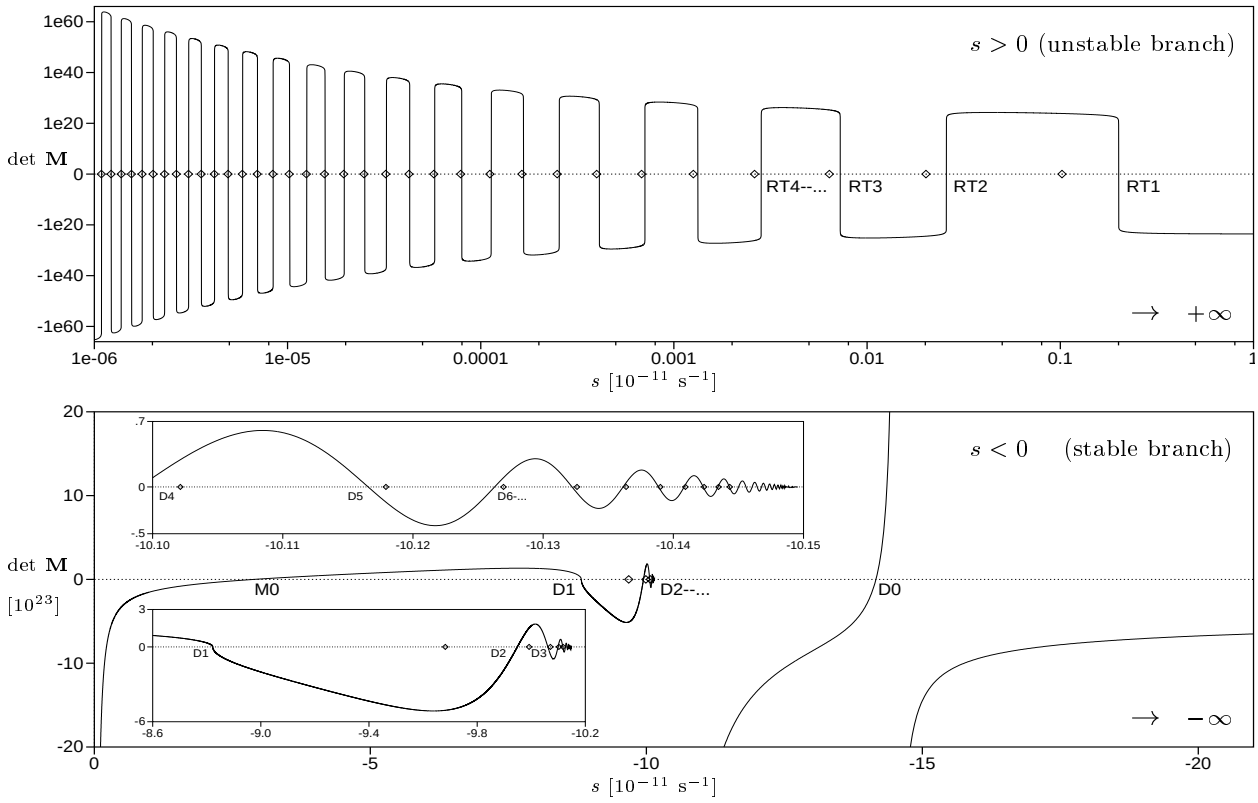

Fig. 8.2. Secular determinant as a function of s (solid lines), inverse relaxation times (diamonds) according to eqs (8.1) and (8.2) for both unstable (upper panel) and stable (lower panel) modes. Model 1 for angular order $n = 2$ is considered. Zoom-in views are shown for the so-called dilatation modes (Dm).

expression (33) and sign confusions in the solution vector (27)–(32) caused the incorrect evaluation of the secular determinant, most noticeable in locations of the roots of the dilatation modes (D modes) with low overtone numbers. The plot of the corrected analytical secular determinant for negative values of the Laplace variable s and the angular order $n = 2$ is shown in the lower panel of Fig. 8.2.

From the asymptotic expansion of spherical Bessel functions in the region of $s \to \left[-\frac{K}{K+4\mu/3}\frac{\mu}{\eta}\right]_+$, where the argument $k(s)$ goes to $+\infty$ again, we obtained the secular equation in the asymptotical form $\cos(k(s)r - n\pi/2) = 0$, in contrast to eq. (44) by Vermeersen et al. (1996). Our analytical formula for the roots of the dilatation modes reads

$$s_n^{\mathrm{D}m} = -\frac{\mu}{\eta}\frac{\left[(2m+n-1)\frac{\pi}{2}\right]^2 K - 4r^2\rho\xi}{\left[(2m+n-1)\frac{\pi}{2}\right]^2 (K+\frac{4}{3}\mu) - 4r^2\rho\xi}\,, \tag{8.2}$$

with n being the angular order and m the overtone number. The dilatation modes can become also unstable, as was already shown by Vermeersen & Mitrovica (1998). There is a transition from the stable to the unstable modes with decreasing bulk modulus K from the numerator in (8.2), while μ is fixed. From the denominator one sees that with a further decrease in K the modes can become stable again.

We give the numerical roots s_n^i of the M0 mode and the first D and RT modes, corresponding growth times $1/s_n^i$, the elastic parts h_n^e, k_n^e of the load Love numbers and their modal amplitudes h_n^i, k_n^i for angular order $n = 2$ in Table 8.2. An interesting observation can be made from the last two columns of Table 8.2: the so-called isostatic limits, h_n^{is} and k_n^{is}, calculated independently as the response of a fluid incompressible sphere, cannot be reached by the values h_n^∞ and k_n^∞ from the criterion of the completeness of the modal decomposition,

$$h_n^\infty = h_n^e + \sum_i^\infty h_n^i/s_n^i\,, \quad k_n^\infty = k_n^e + \sum_i^\infty k_n^i/s_n^i\,, \tag{8.3}$$

when the M0 mode and the D modes only are included in summation. However, the expressions (8.3) do fit the isostatic limits accurately when the RT modes are taken into account.

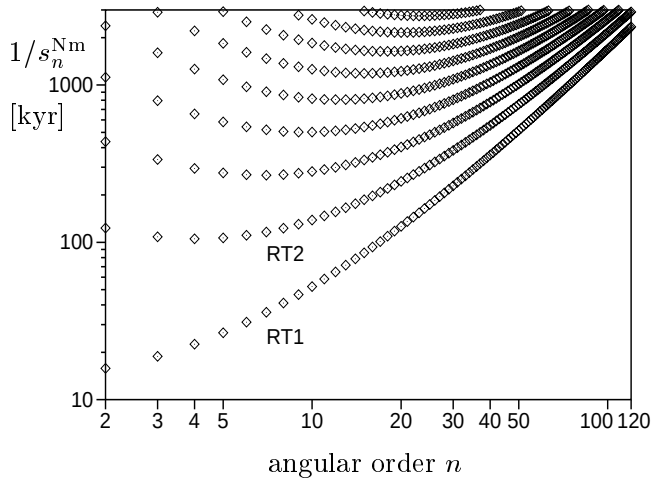

Fig. 8.3. Growth times $1/s_n^{\mathrm{RT}m}$ of the unstable RT modes as a function of angular order n of the model 1. The fundamental (RT1) and the overtone branches (RT2–...) are shown.

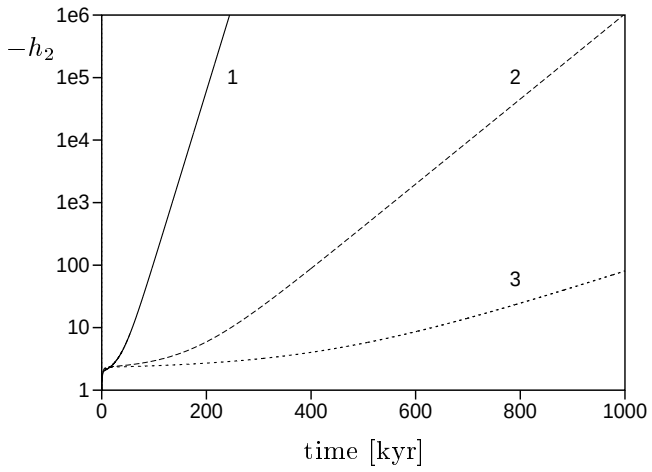

Fig. 8.4. Temporal history of the vertical displacement load Love number $h_n(t)$ for angular order $n = 2$. Results for three different models with increasing number of layers (see Table 8.1 for their physical parameters) are shown.

In Fig. 8.3 we show a collection of growth times for unstable modes of the homogeneous compressible sphere (model 1) for several angular orders n. We note that the fastest growth times are obtained for the lowest n and that for $n < 16$ the growth times are less than 100 kyr.

In Fig. 8.4 we show the influences of increasing complexity in the model. Table 8.1 gives the physical parameters for the additional models 2 and 3 to the homogeneous model 1, discussed up to now. The responses in the vertical displacement or the load Love number $h_n(t)$ for angular order $n = 2$ are shown. The increase in the layering serves to increase the growth time. This means that more complicated Earth models would also have longer growth times than the simpler models.

8.3 Concluding Remarks

In this study we have uncovered a set of unstable modes for a homogeneous Maxwellian viscoelastic sphere. From analytical expressions for the secular determinant, these modes can be shown to have origins arising from the gravitational Rayleigh-Taylor instability of a compressible viscoelastic layer. Gravitation in combination with compresibility is a crucial destabilizing factor; higher viscosity plays a stabilizing role. The fact of existence of gravitational instabilities in linear viscoelastic models raises the tantalizing question of the influences played by finite-amplitude viscoelasticity in geodynamics, as has already been discussed by several authors (Harder 1991; Bercovici et al. 1992; Moser et al. 1993; Plag & Jüttner 1995). In the linear theory, the growth times of the unstable modes are the shortest for the lowest angular orders, which suggests that also in the finite-amplitude viscoelastic regime they may play a decisive role in secular rotational instabilities (Moser et al. 1993). A recent citation of a large-amplitude rotational instability with a deep geobiological consequence (Kirschvink et al. 1997) has been invoked on the basis of paleomagnetic data.

Acknowledgements. We thank D. Wolf and P. Johnston for thorough and constructive reviews and Z. Martinec, J. Matas and Y. Ricard for discussions. This research has been supported by the Grant Agency of the Czech Republic under Nos. 205/96/0212 and 205/97/1015, the Charles University grants 1/97/B-GEO/MFF and 170/98/B-GEO/MFF and the Geosciences Program of the Department of Energy.

References

Bercovici, D.B., Dick, H.B. & Wagner, T., 1992. Non-linear viscoelasticity and the formation of transverse ridges, *J. Geophys. Res.*, **97**, 14495–14506.

Dziewonski, A.M. & Anderson, D.L., 1981. Preliminary reference Earth model, *Phys. Earth Planet. Inter.*, **25**, 297–356.

Fang, M., 1998. Static deformation of the outer core, in *Dynamics of the Ice Age Earth: A Modern Perspective*, ed. by P. Wu, pp. 155–190, Trans Tech Publ., Switzerland.

Hanyk, L., Yuen, D.A. & Matyska, C., 1996. Initial-value and modal approaches for transient viscoelastic responses with complex viscosity profiles, *Geophys. J. Int.*, **127**, 348–362.

Hanyk, L., Matyska, C. & Yuen, D.A., 1998. Initial-value approach for viscoelastic responses of the Earth's mantle, in *Dynamics of the Ice Age Earth: A Modern Perspective*, ed. by P. Wu, pp. 135–154, Trans Tech Publ., Switzerland.

Harder, H., 1991. Numerical simulation of thermal convection with Maxwellian viscoelasticity, *J. Non-Newton. Fluid Mech.*, **39**, 67–88.

Kirschvink, J.L., Ripperdan, R.L. & Evans, D.A., 1997. Evidence for a large-scale reorganization of early Cambrian continental masses by inertial interchange true polar wander, *Science*, **277**, 541–545.

Longman, I.M., 1963. A Green's function for determining the deformation of the earth under surface mass loads, 2. Computations and numerical results, *J. Geophys. Res.*, **68**, 485–496.

Moser, J., Matyska, C., Yuen, D.A., Malevsky, A.V. & Harder, H., 1993. Mantle rheology, convection and rotational dynamics, *Phys. Earth Planet. Inter.*, **79**, 367–381.

Plag, H.-P. & Jüttner, H.-U., 1995. Rayleigh-Taylor instabilities of a self-gravitating Earth, *J. Geodynamics*, **20**, 267–288.

Vermeersen, L.L.A., Sabadini, R. & Spada, G., 1996. Compressible rotational deformation, *Geophys. J. Int.*, **126**, 735–761.

Vermeersen, L.L.A. & Mitrovica, J.X., 1998. Gravitational stability of viscoelastic relaxation models (abstract), *Annales Geophys. Suppl.*, **16/I**, C 55.

Wolf, D., 1985. The normal modes of a uniform, compressible Maxwell half-space, *J. Geophys.*, **56**, 100–105.

Wu, P. & Peltier, W.R., 1982. Viscous gravitational relaxation, *Geophys. J. R. astr. Soc.*, **70**, 435–485.

Yuen, D.A. & Peltier, W.R., 1982. Normal modes of the viscoelastic earth, *Geophys. J. R. astr. Soc.*, **69**, 495–526.

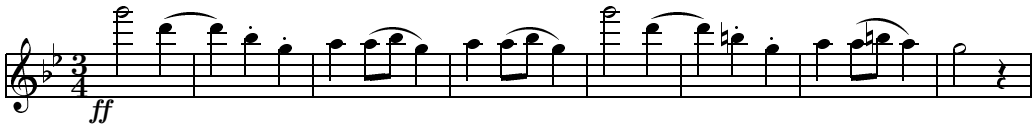

ANTONÍN DVOŘÁK, *Slavonic Dances, Op. 46. No. 8 in G minor. Presto* (1878)

Appendices

Appendix A

Scalar Spherical Harmonics

Fundamental features of scalar spherical harmonics are introduced. The relation between spherical harmonics and the associated Legendre functions and several other relations involving spherical harmonics are collected. The transform method for the evaluation of coefficients of spherical harmonic expansions by means of the fast Fourier transform and the Gauss-Legendre quadrature is discussed and presented on the particular case of a product of two scalar fields. Finally the transform method is applied to the evaluation of coefficients of a product of two zonal scalar fields expressed in terms of spherical harmonics or the derivatives of spherical harmonics.

A.1 Fundamental Features

The scalar spherical harmonics $Y_{nm}(\vartheta,\varphi)$ are unique, continuous and bounded complex functions of two real variables, colatitude ϑ and longitude φ, defined on the unit sphere, i.e., within the bounds of $0 \le \vartheta \le \pi$, $0 \le \varphi < 2\pi$; they are also referred to as the surface spherical harmonics. The two indices, degree n and order m (also angular order and azimuthal order, respectively), can take values of $n = 0, 1, 2, \ldots$ and $m = -n, -n+1, \ldots, n$. The following survey of features and expressions involving spherical harmonics is based on Jones (1985) and Varshalovich et al. (1988). Throughout this section, i denotes the imaginary unit and the asterisk stands for the complex conjugation.

The spherical harmonics $Y_{nm}(\vartheta,\varphi)$ are constructed to satisfy the two differential equations,

$$\left[\frac{1}{\sin\vartheta}\frac{\partial}{\partial\vartheta}\left(\sin\vartheta\frac{\partial}{\partial\vartheta}\right) + \frac{1}{\sin^2\vartheta}\frac{\partial^2}{\partial\varphi^2} + n(n+1)\right] Y_{nm}(\vartheta,\varphi) = 0\,, \tag{A.1}$$

$$\left[i\frac{\partial}{\partial\varphi} + m\right] Y_{nm}(\vartheta,\varphi) = 0\,, \tag{A.2}$$

with the boundary conditions

$$Y_{nm}(\vartheta,0) = Y_{nm}(\vartheta,2\pi)\,, \tag{A.3}$$

$$\left.\frac{\partial}{\partial\varphi}Y_{nm}(\vartheta,\varphi)\right|_{\vartheta=0} = \left.\frac{\partial}{\partial\varphi}Y_{nm}(\vartheta,\varphi)\right|_{\vartheta=\pi} = 0\,. \tag{A.4}$$

The spherical harmonics are orthogonal for different n and m, and they are normalized so that

$$\int_0^{2\pi}\int_0^{\pi} Y_{nm}Y^*_{n'm'}\sin\vartheta\,d\vartheta\,d\varphi = \delta_{nn'}\delta_{mm'}\,, \tag{A.5}$$

while the phase is chosen to fulfil the condition

$$Y_{n0}(0,0) = \sqrt{\frac{2n+1}{4\pi}}\,. \tag{A.6}$$

As a consequence, several symmetries emerge, e.g.,

$$\begin{aligned} Y_{nm}(\vartheta,\varphi) &= (-1)^m Y^*_{n-m}(\vartheta,\varphi) &&= (-1)^m Y_{nm}(-\vartheta,\varphi) \\ &= (-1)^m Y_{n-m}(\vartheta,-\varphi) &&= Y_{n-m}(-\vartheta,-\varphi)\,, \end{aligned} \tag{A.7}$$

and the zonal spherical harmonics $Y_n(\vartheta)$,

$$Y_n(\vartheta) \equiv Y_{n0}(\vartheta)\,, \tag{A.8}$$

are both real for arbitrary values of ϑ and independent of φ. In Section 3.2, here and in Appendix B we adhere to the notation for the partial derivatives of $Y_{nm}(\vartheta,\varphi)$ and $Y_n(\vartheta)$ as follows:

$$\begin{aligned} Z_{nm}(\vartheta,\varphi) &= \frac{\partial Y_{nm}(\vartheta,\varphi)}{\partial\vartheta}\,, & \widetilde{Y}_{nm}(\vartheta,\varphi) &= \frac{1}{\sin\vartheta}\frac{\partial Y_{nm}(\vartheta,\varphi)}{\partial\varphi} = \frac{im\,Y_{nm}(\vartheta,\varphi)}{\sin\vartheta}\,, \\ Z_n(\vartheta) &= \frac{\partial Y_n(\vartheta)}{\partial\vartheta}\,, & \widetilde{Y}_n(\vartheta) &= \frac{1}{\sin\vartheta}\frac{\partial Y_n(\vartheta)}{\partial\varphi} = 0\,, \end{aligned} \tag{A.9}$$

where (A.2) has been substituted. All the partial derivatives of $Y_{nm}(\vartheta,\varphi)$ are also unique, continuous and bounded functions on the unit sphere. With r the radial distance from the center of the coordinate system r, ϑ, φ, it can be shown that functions $r^n Y_{nm}(\vartheta,\varphi)$ and $r^{-n-1}Y_{nm}(\vartheta,\varphi)$, referred to as the solid spherical harmonics, satisfy the Laplace equation,

$$\nabla^2 f(r,\vartheta,\varphi) = 0\,. \tag{A.10}$$

With $z_n(kr) = \sqrt{\frac{\pi}{2kr}}Z_{n+\frac{1}{2}}(kr)$ and $Z_n(kr)$ the spherical and the ordinary Bessel (or Neumann, or Hankel) functions of order n, respectively, it can be shown that functions $z_n(kr)Y_{nm}(\vartheta,\varphi)$ satisfy the homogeneous scalar Helmholtz equation with the constant eigenvalue k,

$$\left(\nabla^2 + k^2\right) f(r,\vartheta,\varphi) = 0\,. \tag{A.11}$$

Indeed, eq. (A.1) emerges during solution to these differential equations.

A.2 Connection with Associated Legendre Functions

The spherical harmonics $Y_{nm}(\vartheta,\varphi)$ are related to the associated Legendre functions $P_n^m(\cos\vartheta)$ by the equation applicable for $m \geq 0$, otherwise see (A.7),

$$Y_{nm}(\vartheta,\varphi) = (-1)^m N_{nm} P_n^m(\cos\vartheta)e^{im\varphi}\,, \qquad N_{nm} = \sqrt{\frac{2n+1}{4\pi}\frac{(n-m)!}{(n+m)!}}\,. \tag{A.12}$$

The associated Legendre functions $P_n^m(x)$, $x = \cos\vartheta$, can be defined in terms of the ordinary Legendre polynomials $P_n(x)$, which in turn can be introduced by the Rodrigues formula, respectively,

$$P_n^m(x) = (1-x^2)^{\frac{m}{2}}\frac{d^m}{dx^m}P^n(x)\,, \tag{A.13}$$

$$P_n(x) = \frac{1}{2^n n!}\frac{d^n}{dx^n}(x^2-1)^n\,. \tag{A.14}$$

Functions $P_n^m(x)$ satisfy numerous recursion relations, among them the following recurrence on n, supplemented by the closed-form expressions for the two starting values, is numerically stable,

$$(n-m)P_n^m(x) = (2n-1)xP_{n-1}^m(x) - (n+m-1)P_{n-2}^m(x)\,, \tag{A.15}$$

$$P_n^n(x) = (-1)^n \frac{(2n-1)!}{2^n n!}(1-x^2)^{\frac{n}{2}}\,, \tag{A.16}$$

$$P_{n+1}^n(x) = (2n+1)xP_n^n(x)\,. \tag{A.17}$$

For the zonal spherical harmonics, eq. (A.12) takes the simplified form

$$Y_n(\vartheta) = \sqrt{\frac{2n+1}{4\pi}} P_n(\cos\vartheta)\,. \tag{A.18}$$

The evaluation of the associated Legendre functions and the corresponding spherical harmonics of degrees $n \le 2$ leads to the following explicit expressions:

$$\begin{array}{llll}
P_0^0(x) = 1 & Y_{00} = \sqrt{\frac{1}{4\pi}} & Z_{00} = 0 \\
P_1^0(x) = x & Y_{10} = \sqrt{\frac{3}{4\pi}}\cos\vartheta & Z_{10} = -\sqrt{\frac{3}{4\pi}}\sin\vartheta \\
P_1^1(x) = -\left(1-x^2\right)^{\frac{1}{2}} & Y_{1\pm1} = \mp\sqrt{\frac{3}{8\pi}}\sin\vartheta e^{\pm i\varphi} & Z_{1\pm1} = \mp\sqrt{\frac{3}{8\pi}}\cos\vartheta e^{\pm i\varphi} \\
P_2^0(x) = \frac{3}{2}x^2 - \frac{1}{2} & Y_{20} = \sqrt{\frac{5}{16\pi}}\left(3\cos^2\vartheta - 1\right) & Z_{20} = -\sqrt{\frac{45}{4\pi}}\sin\vartheta\cos\vartheta \\
P_2^1(x) = -3x\left(1-x^2\right)^{\frac{1}{2}} & Y_{2\pm1} = \mp\sqrt{\frac{15}{8\pi}}\sin\vartheta\cos\vartheta e^{\pm i\varphi} & Z_{2\pm1} = \pm\sqrt{\frac{15}{8\pi}}\left(1-2\cos^2\vartheta\right)e^{\pm i\varphi} \\
P_2^2(x) = 3\left(1-x^2\right) & Y_{2\pm2} = \sqrt{\frac{15}{32\pi}}\sin^2\vartheta e^{\pm 2i\varphi} & Z_{2\pm2} = \sqrt{\frac{15}{8\pi}}\sin\vartheta\cos\vartheta e^{\pm 2i\varphi} \\
\text{and} & \cos\vartheta = \sqrt{\frac{4\pi}{3}}Y_{10} & \sin^2\vartheta = \frac{4}{3}\sqrt{\pi}\left(Y_{00} - \sqrt{\frac{1}{5}}Y_{20}\right)\,.
\end{array} \tag{A.19}$$

Numerous algebraic relations involving the spherical harmonics $Y_{nm}(\vartheta,\varphi)$ and $Y_n(\vartheta)$ and the derivatives $Z_{nm}(\vartheta,\varphi)$ and $Z_n(\vartheta)$ are available:

$$Z_{nm}\sin\vartheta = n\sqrt{\frac{(n+1)^2-m^2}{(2n+1)(2n+3)}}Y_{n+1,m} - (n+1)\sqrt{\frac{n^2-m^2}{(2n+1)(2n-1)}}Y_{n-1,m} \tag{A.20}$$

$$Z_n\sin\vartheta = \frac{n(n+1)}{\sqrt{(2n+1)(2n+3)}}Y_{n+1} - \frac{n(n+1)}{\sqrt{(2n+1)(2n-1)}}Y_{n-1} \tag{A.21}$$

$$Y_{nm}\cos\vartheta = \sqrt{\frac{(n-m+1)(n+m+1)}{(2n+1)(2n+3)}}Y_{n+1,m} + \sqrt{\frac{(n-m)(n+m)}{(2n-1)(2n+1)}}Y_{n-1,m} \tag{A.22}$$

$$Y_n\cos\vartheta = \frac{n+1}{\sqrt{(2n+1)(2n+3)}}Y_{n+1} + \frac{n}{\sqrt{(2n+1)(2n-1)}}Y_{n-1} \tag{A.23}$$

$$Z_n\cos\vartheta = \frac{n}{\sqrt{(2n+1)(2n+3)}}Z_{n+1} + \frac{n+1}{\sqrt{(2n+1)(2n-1)}}Z_{n-1} \tag{A.24}$$

$$Y_n\sin^2\vartheta = -\frac{(n+1)(n+2)Y_{n+2}}{(2n+3)\sqrt{(2n+1)(2n+5)}} + \frac{2(n^2+n-1)Y_n}{(2n-1)(2n+3)} - \frac{n(n-1)Y_{n-2}}{(2n-1)\sqrt{(2n-3)(2n+1)}} \tag{A.25}$$

$$Z_n\sin^2\vartheta = -\frac{n(n+1)Z_{n+2}}{(2n+3)\sqrt{(2n+1)(2n+5)}} + \frac{2n(n+1)Z_n}{(2n-1)(2n+3)} - \frac{n(n+1)Z_{n-2}}{(2n-1)\sqrt{(2n-3)(2n+1)}} \tag{A.26}$$

$$Z_n\sin\vartheta\cos\vartheta = \frac{n(n+1)(n+2)Y_{n+2}}{(2n+3)\sqrt{(2n+1)(2n+5)}} - \frac{n(n+1)Y_n}{(2n-1)(2n+3)} - \frac{(n-1)n(n+1)Y_{n-2}}{(2n-1)\sqrt{(2n-3)(2n+1)}}\,. \tag{A.27}$$

A.3 Spherical Harmonic Expansion of a Scalar Field

The spherical harmonics $Y_{nm}(\vartheta,\varphi)$ of integral degree and order, $n \geq 0$ and $|m| \leq n$, form a complete orthonormal basis of square-integrable functions of two real variables ϑ, φ on the unit sphere, $0 \leq \vartheta \leq \pi$, $0 \leq \varphi < 2\pi$. This means that for any function $f(\vartheta,\varphi)$ defined on the unit sphere and satisfying the condition

$$\int_0^{2\pi} \int_0^{\pi} |f(\vartheta,\varphi)|^2 \sin\vartheta \, d\vartheta \, d\varphi < \infty \,, \tag{A.28}$$

it is possible to find the spherical harmonic expansion of $f(\vartheta,\varphi)$,

$$f(\vartheta,\varphi) = \sum_{n=0}^{\infty} \sum_{m=-n}^{n} f_{nm} Y_{nm}(\vartheta,\varphi) \,, \tag{A.29}$$

where the coefficients f_{nm} can be expressed from (A.5),

$$f_{nm} = \int_0^{2\pi} \int_0^{\pi} f(\vartheta,\varphi) Y^*_{nm}(\vartheta,\varphi) \sin\vartheta \, d\vartheta \, d\varphi \,. \tag{A.30}$$

Condition (A.28) guarantees that

$$\sum_{n=0}^{\infty} \sum_{m=-n}^{n} |f_{nm}|^2 < \infty \qquad \text{and} \qquad \lim_{n\to\infty} |f_{nm}| = 0 \,. \tag{A.31}$$

Formula (A.30) can be rewritten into the form of the Legendre-Fourier transform,

$$f_{nm} \;=\; \int_{-1}^{1} \left[\int_0^{2\pi} f(x,\varphi) e^{-im\varphi} \, d\varphi \right] (-1)^m N_{nm} P_n^m(x) \, dx \,, \tag{A.32}$$

with $x = \cos\vartheta$, which allows for the efficient evaluation using the fast Fourier transform and the Gauss-Legendre quadrature. The transform, or spectral, method based on the evaluation of (A.32) was first employed in the context of atmospheric modelling and, at present, it appears to be the regular textbook material (e.g., Dahlen & Tromp 1998, p. 943ff.). We apply it in the next two sections for the evaluation of coefficients of products of two scalar fields.

A.4 Spherical Harmonic Expansion of a Product of Two Scalar Fields

It is a common task to solve for coefficients of the spherical harmonic expansion of the product of two scalar fields, $h(\vartheta,\varphi) = f(\vartheta,\varphi) g(\vartheta,\varphi)$, given by the finite spherical harmonic expansions,

$$f(\vartheta,\varphi) \;=\; \sum_{n_1=0}^{N_1} \sum_{m_1=-n_1}^{n_1} f_{n_1 m_1} Y_{n_1 m_1}(\vartheta,\varphi) \,, \tag{A.33}$$

$$g(\vartheta,\varphi) \;=\; \sum_{n_2=0}^{N_2} \sum_{m_2=-n_2}^{n_2} g_{n_2 m_2} Y_{n_2 m_2}(\vartheta,\varphi) \,, \tag{A.34}$$

$$h(\vartheta,\varphi) \;=\; \sum_{n=0}^{N} \sum_{m=-n}^{n} h_{nm} Y_{nm}(\vartheta,\varphi) \,, \tag{A.35}$$

with the truncation degree of the expansion of $h(\vartheta,\varphi)$ bounded by $N \le N_1 + N_2$. Taking into account the Clebsch-Gordan expansion of the product of two spherical harmonics,

$$Y_{n_1m_1}(\vartheta,\varphi)Y_{n_2m_2}(\vartheta,\varphi) = \textstyle\sum_{nm} Q^{nm}_{n_1m_1n_2m_2} Y_{nm}(\vartheta,\varphi)\,, \tag{A.36}$$

$$Q^{nm}_{n_1m_1n_2m_2} = \sqrt{\frac{(2n_1+1)(2n_2+1)}{4\pi(2n+1)}}\, C^{n0}_{n_10n_20} C^{nm}_{n_1m_1n_2m_2}\,, \tag{A.37}$$

where $C^{nm}_{n_1m_1n_2m_2}$ are called the Clebsch-Gordan coefficients, the coefficients h_{nm} can be expressed by the sum

$$h_{nm} = \sum_{n_1m_1}\sum_{n_2m_2} f_{n_1m_1} g_{n_2m_2} Q^{nm}_{n_1m_1n_2m_2}\,. \tag{A.38}$$

However, it is more efficient, in terms of both computer time and memory, to evaluate the coefficients h_{nm} using the transform method based on (A.32). Here it takes the form of

$$h_{nm} = \int_0^{2\pi}\int_0^{\pi} h(\vartheta,\varphi) Y^*_{nm}(\vartheta,\varphi)\sin\vartheta\, d\vartheta\, d\varphi \tag{A.39}$$

$$= \int_{-1}^{1}\left[\int_0^{2\pi}\left(\sum_{n_1m_1} f_{n_1m_1} Y_{n_1m_1}(\vartheta,\varphi)\right)\left(\sum_{n_2m_2} g_{n_2m_2} Y_{n_2m_2}(\vartheta,\varphi)\right) e^{-im\varphi}\, d\varphi\right] \bar{Y}_{nm}(x)\, dx\,, \tag{A.40}$$

with $\bar{Y}_{nm}(x) \equiv (-1)^m N_{nm} P^m_n(\cos\vartheta)$ and $x = \cos\vartheta$. The expression in the brackets should be evaluated using the fast Fourier transform on the grid $\varphi_l = 2\pi l/L$, $l = 0,\ldots,L-1$. The rest can be accomplished by the Gauss-Legendre quadrature on the grid x_k, $k = 1,\ldots,K$. The grid points x_k should be equal to the roots of the Legendre polynomial $P_K(x)$, i.e., $P_K(x_k) = 0$. The sums in the parentheses should be evaluated for all the grid points $x_k = \cos\vartheta_k$ and φ_l. Hence, the following expressions are to be evaluated,

$$h(x_k,\varphi_l) = \left(\sum_{n_1=0}^{N_1}\sum_{m_1=-n_1}^{n_1} f_{n_1m_1} Y_{n_1m_1}(\vartheta_k,\varphi_l)\right)\left(\sum_{n_2=0}^{N_2}\sum_{m_2=-n_2}^{n_2} g_{n_2m_2} Y_{n_2m_2}(\vartheta_k,\varphi_l)\right) \tag{A.41}$$

$$\text{for } k = 1,\ldots,K, \quad l = 0,\ldots,L-1,$$

$$\bar{h}_m(x_k) = \frac{2\pi}{L}\sum_{l=0}^{L-1} h(x_k,\varphi_l) e^{-2\pi i m l/L} \qquad \text{for } |m| \le N, \quad k = 1,\ldots,K, \tag{A.42}$$

$$h_{nm} = \sum_{k=1}^{K} w^{(K)}_k \bar{h}_m(x_k)\bar{Y}_{nm}(x_k) \qquad \text{for } n = 0,\ldots,N, \quad |m| \le N\,, \tag{A.43}$$

where $w^{(K)}_k$ are the Gauss-Legendre weights. The choice of the values K, L is based on the chosen value of N. Generally, the coefficients h_{nm} are non-zero for any $n \le N = N_1 + N_2$, while the computed h_{nm}'s are often limited to $n \le N = N_1 = N_2$. In the former case, the choice of $L > N_1 + N_2 + N = 2(N_1 + N_2)$ is needed for the alias-free evaluation and L taken as a power of 2 is suitable for standard implementations of the fast Fourier transform; $K > (N_1 + N_2 + N)/2 = N_1 + N_2$ is required as the K-point Gauss-Legendre quadrature scheme ensures exact integration of degree $2K - 1$ polynomials. In the latter case, the choice of $L > N_1 + N_2 + N = 3N$ (L is a power of 2) and $K > (N_1 + N_2 + N)/2 = \frac{3}{2}N$ is desirable. Note that the roots x_k of the Legendre polynomial $P_K(x)$ and the Gauss-Legendre weights $w^{(K)}_k$ are thought to be provided by any eligible routine, e.g., `gauleg` by Press et al. (1996).

For the zonal functions $f(\vartheta)$, $g(\vartheta)$ and $h(\vartheta) = f(\vartheta)g(\vartheta)$, with $Y_n(\vartheta) = \bar{Y}_n(x) = N_{n0}P_n(\cos\vartheta)$,

$$f(\vartheta) = \sum_{n_1=0}^{N_1} f_{n_1} Y_{n_1}(\vartheta)\,, \quad g(\vartheta) = \sum_{n_2=0}^{N_2} g_{n_2} Y_{n_2}(\vartheta)\,, \quad h(\vartheta) = \sum_{n=0}^{N} h_n Y_n(\vartheta)\,, \tag{A.44}$$

the transform method can be simplified to the evaluation of

$$h_n \;=\; 2\pi \int_{-1}^{1} h(x)\bar{Y}_n(x)\,dx \;=\; 2\pi \sum_{k=1}^{K} w_k^{(K)} \left(\sum_{n_1=0}^{N_1} f_{n_1} \bar{Y}_{n_1}(x_k) \right) \left(\sum_{n_2=0}^{N_2} g_{n_2} \bar{Y}_{n_2}(x_k) \right) \bar{Y}_n(x_k) \tag{A.45}$$

for $n = 0, \ldots, N$. Martinec (1989) implemented (A.40) as the routine `vcsum`, written in Fortran 77. For the zonal functions, we show the "one-statement" implementation of (A.45) using Fortran 90 in Appendix C.3.

A.5 Expansions in Terms of Derivatives of Spherical Harmonics

In Section 3.2 the coefficients of the spherical harmonic expansions of the products of two scalar axisymmetric (zonal) fields are presumed to be evaluated by the above outlined transform method. Specifically, products of the field $a(r,\vartheta)$, constant in time and prescribed a priori (viscosity, in particular), and of various fields $b(r,\vartheta)$, variable in time (e.g., displacement components), are to be evaluated. Fields $b(r,\vartheta)$ are given by the coefficients $b_n(r)$ of the two kinds of expansions, either $b(r,\vartheta) = \sum_{n=0}^{N} B_n(r) Y_n(\vartheta)$ or $b(r,\vartheta) = \sum_{n=1}^{N} B_n(r) Z_n(\vartheta)\sin\vartheta$, where $Z_n(\vartheta) = \partial Y_n(\vartheta)/\partial\vartheta$. Functions $Z_n(\vartheta)$ appear in the expansions accompanied with $\sin\vartheta$ since these products can be expressed as linear combinations of spherical harmonics $Y_{n-1}(\vartheta)$ and $Y_{n+1}(\vartheta)$, cf. (A.21). We remark that $Z_0(\vartheta)$ is zero identically.

The coefficients of the spherical harmonic expansions of the products $a(r,\vartheta)b(r,\vartheta)$, being also expressed as the linear combinations of either $Y_n(\vartheta)$ or $Z_n(\vartheta)\sin\vartheta$, will be denoted $\langle a; B_{n'}\rangle_{YY,n}$, $\langle a; B_{n'}\rangle_{ZY,n}$, $\langle a; B_{n'}\rangle_{YZ,n}$ and $\langle a; B_{n'}\rangle_{ZZ,n}$, in accordance with the following definitions,

$$\begin{aligned}
a(r,\vartheta) \textstyle\sum_{n=0}^{N} B_n(r)\, Y_n(\vartheta) \quad &= \quad \textstyle\sum_{n=0}^{\bar{N}} \langle a; B_{n'}\rangle_{YY,n}(r) Y_n(\vartheta)\,, \\
a(r,\vartheta) \textstyle\sum_{n=1}^{N} B_n(r)\, Z_n(\vartheta)\sin\vartheta \quad &= \quad \textstyle\sum_{n=0}^{\bar{N}} \langle a; B_{n'}\rangle_{ZY,n}(r) Y_n(\vartheta)\,, \\
a(r,\vartheta) \textstyle\sum_{n=0}^{N} B_n(r)\, Y_n(\vartheta) \quad &= \quad \textstyle\sum_{n=1}^{\bar{N}} \langle a; B_{n'}\rangle_{YZ,n}(r) Z_n(\vartheta)\sin\vartheta\,, \\
a(r,\vartheta) \textstyle\sum_{n=1}^{N} B_n(r)\, Z_n(\vartheta)\sin\vartheta \quad &= \quad \textstyle\sum_{n=1}^{\bar{N}} \langle a; B_{n'}\rangle_{ZZ,n}(r) Z_n(\vartheta)\sin\vartheta\,.
\end{aligned} \tag{A.46}$$

In general, the maximal truncation degree $\bar{N}$ of the first r.h.s. expansion equals to the sum of N and the truncation degree of the spherical harmonic expansion of $a(r,\vartheta)$. The truncation degree of the second r.h.s. expansion is one greater, as follows from (A.21). The truncation degrees of the third and the fourth r.h.s. expansions into $Y_n(\vartheta)$ would be identical with those of the first and the second r.h.s. expansions, respectively, but the expansions into $Z_n(\vartheta)\sin\vartheta$ can generally be infinite. However, we will presume that the spectral power of the constituents with $n > N$ is negligible, and $\bar{N} = N$ will be considered in the all cases.

We express the coefficients $\langle a; B_{n'}\rangle_{YY,n}$ and $\langle a; B_{n'}\rangle_{ZY,n}$ via the Gauss-Legendre quadrature, analogically to (A.45),

$$\begin{aligned}
\langle a; B_{n'}\rangle_{YY,n} &= 2\pi \int_{-1}^{1} a(r,x)b(r,x)\bar{Y}_n(x)\,dx \\
&= 2\pi \sum_{k=1}^{K} w_k^{(K)} a(r,x_k) \left[\sum_{n'=0}^{N} B_{n'}(r)\bar{Y}_{n'}(x_k)\right] \bar{Y}_n(x_k)\,, \qquad \text{(A.47)} \\
\langle a; B_{n'}\rangle_{ZY,n} &= 2\pi \int_{-1}^{1} a(r,x)b(r,x)\bar{Y}_n(x)\,dx \\
&= 2\pi \sum_{k=1}^{K} w_k^{(K)} a(r,x_k) \left[\sum_{n'=0}^{N+1} \left[\omega_{n'-1}^{+} B_{n'-1}(r) + \omega_{n'+1}^{-} B_{n'+1}(r)\right] \bar{Y}_{n'}(x_k)\right] \bar{Y}_n(x_k)\,, \qquad \text{(A.48)}
\end{aligned}$$

where relation (A.21), arranged according to

$$\sum_{n=1}^{N} B_n Z_n \sin\vartheta = \sum_{n=1}^{N} B_n \left(\omega_n^{+} Y_{n+1} + \omega_n^{-} Y_{n-1}\right) = \sum_{n=0}^{N+1} \left(\omega_{n-1}^{+} B_{n-1} + \omega_{n+1}^{-} B_{n+1}\right) Y_n\,, \qquad \text{(A.49)}$$

has been involved; for coefficients ω_n^{+} and ω_n^{-} see also (A.21). Applying similar reordering to the second pair of the r.h.s. expansions from (A.46), we arrive at the following tridiagonal systems of linear algebraic equations for $\langle a; B_{n'}\rangle_{YZ,n}$ and $\langle a; B_{n'}\rangle_{ZZ,n}$,

$$\begin{aligned}
\omega_{n-1}^{+}\langle a; B_{n'}\rangle_{YZ,n-1} + \omega_{n+1}^{-}\langle a; B_{n'}\rangle_{YZ,n+1} &= 2\pi \int_{-1}^{1} a(r,x)b(r,x)\bar{Y}_n(x)\,dx \\
&= 2\pi \sum_{k=1}^{K} w_k^{(K)} a(r,x_k) \left[\sum_{n'=0}^{N} B_{n'}(r)\bar{Y}_{n'}(x_k)\right] \bar{Y}_n(x_k)\,, \qquad \text{(A.50)} \\
\omega_{n-1}^{+}\langle a; B_{n'}\rangle_{ZZ,n-1} + \omega_{n+1}^{-}\langle a; B_{n'}\rangle_{ZZ,n+1} &= 2\pi \int_{-1}^{1} a(r,x)b(r,x)\bar{Y}_n(x)\,dx \\
&= 2\pi \sum_{k=1}^{K} w_k^{(K)} a(r,x_k) \left[\sum_{n'=0}^{N+1} \left[\omega_{n'-1}^{+} B_{n'-1}(r) + \omega_{n'+1}^{-} B_{n'+1}(r)\right] \bar{Y}_{n'}(x_k)\right] \bar{Y}_n(x_k)\,. \qquad \text{(A.51)}
\end{aligned}$$

We recall that $\langle a; B_{n'}\rangle_{YZ,0} = \langle a; B_{n'}\rangle_{ZZ,0} = 0$ and that N is the maximal truncation degree. By formal setting $\langle a; B_{n'}\rangle_{YZ,-1} = \langle a; B_{n'}\rangle_{ZZ,-1} = 0$, these two tridiagonal systems can be viewed as the recursion relations for $\langle a; B_{n'}\rangle_{YZ,n+1}$ and $\langle a; B_{n'}\rangle_{ZZ,n+1}$, with $n = 0, 1, \ldots, N-1$. Hence, we have derived the formulas (A.47)–(A.48) and (A.50)–(A.51) for the efficient evaluation of the coefficients introduced by (3.78) and (A.46).

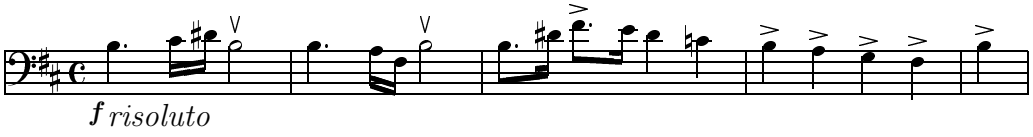

ANTONÍN DVOŘÁK, *Concerto for Cello and Orchestra No. 2 in B minor, Op. 104. I. Allegro* (1895)

Appendix B

Scalar Representation of Vector and Tensor Fields

A subset of scalar representations of differential operators acting on scalar, vector and second-order tensor fields is derived. Concepts not necessarily needed for the purpose of this thesis are not involved; in particular, quantities are expressed in terms of physical rather than covariant and contravariant components. However, collected expressions form the apparatus which allows for the conversion of the field PDEs into the systems of ODEs and PDEs in Chapters 2 and 3. We begin from the formulas for the differential operators in orthogonal curvilinear coordinates (e.g., Morse & Feshbach 1953) and finish, essentially, with the expressions given by Backus (1967).

B.1 Differential Operators in Orthogonal Curvilinear Coordinates

Let ξ_1, ξ_2 and ξ_3 be the orthogonal curvilinear coordinates, $\boldsymbol{e}_1$, $\boldsymbol{e}_2$ and $\boldsymbol{e}_3$ the corresponding unit basis vectors and h_1, h_2 and h_3 the Lamé coefficients defined by the relations to the Cartesian coordinates x, y and z,

$$h_i^2 = \left(\frac{\partial x}{\partial \xi_i}\right)^2 + \left(\frac{\partial y}{\partial \xi_i}\right)^2 + \left(\frac{\partial z}{\partial \xi_i}\right)^2 , \quad H = h_1 h_2 h_3 , \quad i = 1, 2, 3 . \tag{B.1}$$

The differential operators grad, div and rot acting on the scalar and vector functions

$$f = f(\xi_1, \xi_2, \xi_3) , \tag{B.2}$$

$$\mathbf{u} = \mathbf{u}(\xi_1, \xi_2, \xi_3) = u_1(\xi_1, \xi_2, \xi_3)\boldsymbol{e}_1 + u_2(\xi_1, \xi_2, \xi_3)\boldsymbol{e}_2 + u_3(\xi_1, \xi_2, \xi_3)\boldsymbol{e}_3 , \tag{B.3}$$

can be introduced as follows (Morse & Feshbach 1953[1]):

[1] Initial expressions of Section B.1 can be derived from definitions of differential operators given in terms of covariant derivatives. Expressions (B.1), (B.4)–(B.7) and (B.9) are retyped from Chapter 1 of the Russian translation of Morse & Feshbach (1953); however, we inverted the sign of the second r.h.s. term of (B.7). This correction is justifiable by derivation of (B.7) from the general definition of the ∇ operator (not presented here), and also can be validated by comparing consequent expressions (B.8) and (B.26) with, e.g., Martinec (1989, p. 204) and Dahlen & Tromp (1998, p. 836), respectively.

$$\text{grad } f \equiv \nabla f = \sum_{i=1}^{3} \frac{\boldsymbol{e}_i}{h_i}\frac{\partial f}{\partial \xi_i} = \frac{1}{h_1}\frac{\partial f}{\partial \xi_1}\boldsymbol{e}_1 + \frac{1}{h_2}\frac{\partial f}{\partial \xi_2}\boldsymbol{e}_2 + \frac{1}{h_3}\frac{\partial f}{\partial \xi_3}\boldsymbol{e}_3\,, \tag{B.4}$$

$$\text{div } \mathbf{u} \equiv \nabla\cdot\mathbf{u} = \frac{1}{H}\sum_{i=1}^{3}\frac{\partial}{\partial \xi_i}\left(\frac{Hu_i}{h_i}\right) = \frac{1}{h_1h_2h_3}\left[\frac{\partial(h_2h_3u_1)}{\partial\xi_1} + \frac{\partial(h_1h_3u_2)}{\partial\xi_2} + \frac{\partial(h_1h_2u_3)}{\partial\xi_3}\right], \tag{B.5}$$

$$\text{rot } \mathbf{u} \equiv \nabla\times\mathbf{u} = \frac{1}{H}\sum_{ijk}\varepsilon_{ijk}h_i\boldsymbol{e}_i\frac{\partial(h_ku_k)}{\partial\xi_j} \tag{B.6}$$

$$= \frac{1}{h_2h_3}\left[\frac{\partial(h_3u_3)}{\partial\xi_2} - \frac{\partial(h_2u_2)}{\partial\xi_3}\right]\boldsymbol{e}_1 + \frac{1}{h_1h_3}\left[\frac{\partial(h_1u_1)}{\partial\xi_3} - \frac{\partial(h_3u_3)}{\partial\xi_1}\right]\boldsymbol{e}_2 + \frac{1}{h_1h_2}\left[\frac{\partial(h_2u_2)}{\partial\xi_1} - \frac{\partial(h_1u_1)}{\partial\xi_2}\right]\boldsymbol{e}_3\,,$$

$$\text{grad } \mathbf{u} \equiv \nabla\mathbf{u} = \frac{1}{2}\left[\nabla\mathbf{u} + (\nabla\mathbf{u})^T\right] + \frac{1}{2}\left[\boldsymbol{I}\times(\nabla\times\mathbf{u})\right] \tag{B.7}$$

$$= \sum_{k=1}^{3}\sum_{l=1}^{3}\left[\left(\frac{1}{H_k}\frac{\partial u_l}{\partial\xi_k} - \frac{u_k}{H_kH_l}\frac{\partial H_k}{\partial\xi_l} + \frac{\delta_{kl}}{H_k}\sum_{m=1}^{3}\frac{u_m}{H_m}\frac{\partial H_l}{\partial\xi_m}\right)\boldsymbol{e}_k\boldsymbol{e}_l\right], \tag{B.8}$$

$$\frac{1}{2}\left[\nabla\mathbf{u} + (\nabla\mathbf{u})^T\right] = \left[\sum_{ij}\left[\frac{\partial}{\partial\xi_i}\left(\frac{u_i}{h_i}\right) + \mathbf{u}\cdot\nabla\left(\ln h_i\right)\right]\delta_{ij} + \frac{1}{2}\sum_{ij,i\neq j}\left[\frac{h_i}{h_j}\frac{\partial}{\partial\xi_j}\left(\frac{u_i}{h_i}\right) + \frac{h_j}{h_i}\frac{\partial}{\partial\xi_i}\left(\frac{u_j}{h_j}\right)\right]\right]\boldsymbol{e}_i\boldsymbol{e}_j\,, \tag{B.9}$$

with δ_{kl} denoting the Kronecker symbol ($\delta_{kl} = 1$ for $k = l$, otherwise 0) and ε_{ijk} the Levi-Civita symbol ($\varepsilon_{123} = \varepsilon_{231} = \varepsilon_{312} = -\varepsilon_{132} = -\varepsilon_{312} = -\varepsilon_{213} = 1$, otherwise 0). Expressions for the second-order differential operators follow from (B.4)–(B.7); e.g., expression for the Laplace operator $\Delta \equiv \text{div grad} \equiv \nabla^2 \equiv \nabla\cdot\nabla$ can be obtained by substitution of (B.4) into (B.5),

$$\nabla^2 f = \frac{1}{H}\sum_{i=1}^{3}\frac{\partial}{\partial\xi_i}\left(\frac{H}{h_i^2}\frac{\partial f}{\partial\xi_i}\right) = \frac{1}{h_1h_2h_3}\left[\frac{\partial}{\partial\xi_1}\left(\frac{h_2h_3}{h_1}\frac{\partial f}{\partial\xi_1}\right) + \frac{\partial}{\partial\xi_2}\left(\frac{h_1h_3}{h_2}\frac{\partial f}{\partial\xi_2}\right) + \frac{\partial}{\partial\xi_3}\left(\frac{h_1h_2}{h_3}\frac{\partial f}{\partial\xi_3}\right)\right]. \tag{B.10}$$

Similarly, expressions for the second-order operators

$$\text{grad div } \mathbf{u} \equiv \nabla\nabla\cdot\mathbf{u}\,, \tag{B.11}$$

$$\text{rot rot } \mathbf{u} \equiv \nabla\times\nabla\times\mathbf{u}\,, \tag{B.12}$$

follow from (B.4)–(B.5) and (B.7), respectively. Expressions involving tensor grad $\mathbf{u}$,

$$\text{div grad } \mathbf{u} \equiv \nabla^2\mathbf{u}\,, \tag{B.13}$$

$$\text{div}(\text{grad } \mathbf{u})^T \equiv \nabla\cdot(\nabla\mathbf{u})^T\,, \tag{B.14}$$

can be derived from (B.11), (B.12) and the relations

$$\text{div grad } \mathbf{u} = \text{grad div } \mathbf{u} - \text{rot rot } \mathbf{u}\,, \qquad \nabla^2\mathbf{u} = \nabla\nabla\cdot\mathbf{u} - \nabla\times\nabla\times\mathbf{u}\,, \tag{B.15}$$

$$\text{div } (\text{grad } \mathbf{u})^T = \text{grad div } \mathbf{u}\,, \qquad \nabla\cdot(\nabla\mathbf{u})^T = \nabla\nabla\cdot\mathbf{u}\,. \tag{B.16}$$

The last two admissible second-order differential operators, rot grad and div rot, are zero identically,

$$\text{rot grad } f \equiv \nabla\times\nabla f = \mathbf{0}\,, \tag{B.17}$$

$$\text{div rot } \mathbf{u} \equiv \nabla\cdot\nabla\times\mathbf{u} = \mathbf{0}\,. \tag{B.18}$$

We do not express the second-order differential operators in the orthogonal curvilinear coordinates explicitly. However, the spherical harmonic expansions of both the first-order (B.4)–(B.7) and the second-order (B.10)–(B.13) differential operators are given in Appendix B.3.

B.2 Differential Operators in Spherical Coordinates

Let $\xi_1 = r$, $\xi_2 = \vartheta$ and $\xi_3 = \varphi$ be the spherical coordinates defined by the relations to the Cartesian coordinates x, y and z,

$$x = r\sin\vartheta\cos\varphi\,, \quad y = r\sin\vartheta\sin\varphi\,, \quad z = r\cos\vartheta\,, \tag{B.19}$$

with $\boldsymbol{e}_r$, $\boldsymbol{e}_\vartheta$ and $\boldsymbol{e}_\varphi$ the unit basis vectors. The Lamé coefficients of the spherical coordinates are equal to

$$h_r = 1\,, \quad h_\vartheta = r\,, \quad h_\varphi = r\sin\vartheta\,. \tag{B.20}$$

For the scalar and vector functions

$$f = f(r,\vartheta,\varphi)\,, \tag{B.21}$$

$$\mathbf{u} = \mathbf{u}(r,\vartheta,\varphi) = u_r(r,\vartheta,\varphi)\boldsymbol{e}_r + u_\vartheta(r,\vartheta,\varphi)\boldsymbol{e}_\vartheta + u_\varphi(r,\vartheta,\varphi)\boldsymbol{e}_\varphi\,, \tag{B.22}$$

expressions (B.4)–(B.7) take the specific form:

$$\nabla f = \frac{\partial f}{\partial r}\boldsymbol{e}_r + \frac{1}{r}\nabla_\Omega f = \frac{\partial f}{\partial r}\boldsymbol{e}_r + \frac{1}{r}\frac{\partial f}{\partial\vartheta}\boldsymbol{e}_\vartheta + \frac{1}{r\sin\vartheta}\frac{\partial f}{\partial\varphi}\boldsymbol{e}_\varphi\,, \tag{B.23}$$

$$\nabla\cdot\mathbf{u} = \frac{1}{r^2}\frac{\partial(r^2u_r)}{\partial r} + \frac{1}{r\sin\vartheta}\frac{\partial(u_\vartheta\sin\vartheta)}{\partial\vartheta} + \frac{1}{r\sin\vartheta}\frac{\partial u_\varphi}{\partial\varphi}\,, \tag{B.24}$$

$$\nabla\times\mathbf{u} = \frac{1}{r\sin\vartheta}\left[\frac{\partial(u_\varphi\sin\vartheta)}{\partial\vartheta} - \frac{\partial u_\vartheta}{\partial\varphi}\right]\boldsymbol{e}_r + \frac{1}{r}\left[\frac{1}{\sin\vartheta}\frac{\partial u_r}{\partial\varphi} - \frac{\partial(ru_\varphi)}{\partial r}\right]\boldsymbol{e}_\vartheta + \frac{1}{r}\left[\frac{\partial(ru_\vartheta)}{\partial r} - \frac{\partial u_r}{\partial\vartheta}\right]\boldsymbol{e}_\varphi\,, \tag{B.25}$$

$$\nabla\mathbf{u} = \sum_{k=1}^{3}\sum_{l=1}^{3}\left[(\nabla\mathbf{u})_{kl}\boldsymbol{e}_k\boldsymbol{e}_l\right]\,, \tag{B.26}$$

$$\begin{aligned}
(\nabla\mathbf{u})_{rr} &= \frac{\partial u_r}{\partial r}\,, \quad (\nabla\mathbf{u})_{\vartheta r} = \frac{1}{r}\frac{\partial u_r}{\partial\vartheta} - \frac{u_\vartheta}{r}\,, \quad (\nabla\mathbf{u})_{\varphi r} = \frac{1}{r\sin\vartheta}\frac{\partial u_r}{\partial\varphi} - \frac{u_\varphi}{r}\,,\\
(\nabla\mathbf{u})_{r\vartheta} &= \frac{\partial u_\vartheta}{\partial r}\,, \quad (\nabla\mathbf{u})_{\vartheta\vartheta} = \frac{1}{r}\frac{\partial u_\vartheta}{\partial\vartheta} + \frac{u_r}{r}\,, \quad (\nabla\mathbf{u})_{\varphi\vartheta} = \frac{1}{r\sin\vartheta}\frac{\partial u_\vartheta}{\partial\varphi} - \frac{u_\varphi}{r}\frac{\cos\vartheta}{\sin\vartheta}\,,\\
(\nabla\mathbf{u})_{r\varphi} &= \frac{\partial u_\varphi}{\partial r}\,, \quad (\nabla\mathbf{u})_{\vartheta\varphi} = \frac{1}{r}\frac{\partial u_\varphi}{\partial\vartheta}\,, \qquad (\nabla\mathbf{u})_{\varphi\varphi} = \frac{1}{r\sin\vartheta}\frac{\partial u_\varphi}{\partial\varphi} + \frac{u_r}{r} + \frac{u_\vartheta}{r}\frac{\cos\vartheta}{\sin\vartheta}\,.
\end{aligned}$$

By $\nabla_\Omega \equiv \boldsymbol{e}_\vartheta\dfrac{\partial}{\partial\vartheta} + \boldsymbol{e}_\varphi\dfrac{1}{\sin\vartheta}\dfrac{\partial}{\partial\varphi}$ we denote the angular part of the ∇ operator, the surface gradient. From the second-order differential operators, expression for the Laplace operator (B.10) is only rewritten here:

$$\nabla^2 f = \frac{1}{r^2}\frac{\partial}{\partial r}\left(r^2\frac{\partial f}{\partial r}\right) + \frac{1}{r^2\sin\vartheta}\frac{\partial}{\partial\vartheta}\left(\sin\vartheta\frac{\partial f}{\partial\vartheta}\right) + \frac{1}{r^2\sin^2\vartheta}\frac{\partial^2 f}{\partial\varphi^2}\,. \tag{B.27}$$

B.3 Differential Operators Acting on Spherical Harmonic Expansions

Let r, ϑ and φ be the spherical coordinates related to the Cartesian coordinates x, y and z by (B.19), $\boldsymbol{e}_r$, $\boldsymbol{e}_\vartheta$ and $\boldsymbol{e}_\varphi$ the corresponding unit basis vectors, $Y_{nm}(\vartheta,\varphi)$ the scalar spherical harmonics (A.12) and $Z_{nm}(\vartheta,\varphi)$ and $\widetilde{Y}_{nm}(\vartheta,\varphi)$ the partial derivatives of $Y_{nm}(\vartheta,\varphi)$ defined by (A.9). Let $\boldsymbol{S}^{(-1)}_{nm}$, $\boldsymbol{S}^{(1)}_{nm}$ and $\boldsymbol{S}^{(0)}_{nm}$ be the vector spherical harmonics,

$$\boldsymbol{S}^{(-1)}_{nm}(\vartheta,\varphi) = Y_{nm}(\vartheta,\varphi)\boldsymbol{e}_r\,, \tag{B.28}$$

$$\nabla_\Omega Y_{nm}(\vartheta,\varphi) \equiv \boldsymbol{S}^{(1)}_{nm}(\vartheta,\varphi) = Z_{nm}(\vartheta,\varphi)\boldsymbol{e}_\vartheta + \widetilde{Y}_{nm}(\vartheta,\varphi)\boldsymbol{e}_\varphi\,, \tag{B.29}$$

$$\boldsymbol{e}_r \times \nabla_\Omega Y_{nm}(\vartheta,\varphi) \equiv \boldsymbol{S}^{(0)}_{nm}(\vartheta,\varphi) = -\widetilde{Y}_{nm}(\vartheta,\varphi)\boldsymbol{e}_\vartheta + Z_{nm}(\vartheta,\varphi)\boldsymbol{e}_\varphi\,. \tag{B.30}$$

forming the orthogonal basis for square-integrable vector functions defined on the unit sphere. (See also p. 11.) The spherical harmonic expansions of scalar and vector functions can be expressed as

$$f(r,\vartheta,\varphi) = \sum_{nm} F_{nm}(r)Y_{nm}(\vartheta,\varphi)\,, \tag{B.31}$$

$$\mathbf{u}(r,\vartheta,\varphi) = \sum_{nm}\left[U_{nm}(r)\boldsymbol{S}^{(-1)}_{nm}(\vartheta,\varphi) + V_{nm}(r)\boldsymbol{S}^{(1)}_{nm}(\vartheta,\varphi) + W_{nm}(r)\boldsymbol{S}^{(0)}_{nm}(\vartheta,\varphi)\right]. \tag{B.32}$$

Expressions for the scalar components of $\mathbf{u}(r,\vartheta,\varphi)$ in the directions of $\boldsymbol{e}_r$, $\boldsymbol{e}_\vartheta$ and $\boldsymbol{e}_\varphi$ follow from substitution of the vector spherical harmonics (B.28)–(B.30) into (B.32),

$$u_r(r,\vartheta,\varphi) = \sum_{nm}\left[U_{nm}(r)Y_{nm}(\vartheta,\varphi)\right], \tag{B.33}$$

$$u_\vartheta(r,\vartheta,\varphi) = \sum_{nm}\left[V_{nm}(r)Z_{nm}(\vartheta,\varphi) - W_{nm}\widetilde{Y}_{nm}(\vartheta,\varphi)\right], \tag{B.34}$$

$$u_\varphi(r,\vartheta,\varphi) = \sum_{nm}\left[V_{nm}(r)\widetilde{Y}_{nm}(\vartheta,\varphi) + W_{nm}Z_{nm}(\vartheta,\varphi)\right]. \tag{B.35}$$

Expressions (B.23)–(B.26) for the first-order differential operators acting on the spherical harmonic expansions (B.31)–(B.32) can be rewritten using (B.33)–(B.35) into the form

$$\nabla f = \sum_{nm}\left(F'_{nm}\boldsymbol{S}^{(-1)}_{nm} + \frac{F_{nm}}{r}\boldsymbol{S}^{(1)}_{nm}\right), \tag{B.36}$$

$$\nabla\cdot\mathbf{u} = \sum_{nm}\left(U'_{nm} + \frac{2U_{nm} - NV_{nm}}{r}\right)Y_{nm}\,, \tag{B.37}$$

$$\nabla\times\mathbf{u} = \sum_{nm}\left[-\frac{NW_{nm}}{r}\boldsymbol{S}^{(-1)}_{nm} - \left(W'_{nm} + \frac{W_{nm}}{r}\right)\boldsymbol{S}^{(1)}_{nm} + \left(V'_{nm} + \frac{V_{nm}-U_{nm}}{r}\right)\boldsymbol{S}^{(0)}_{nm}\right], \tag{B.38}$$

where $N = n(n+1)$ and the prime $'$ stands for the derivative with respect to r. From now on we suppress the degree and order subscripts of the coefficients F_{nm}, U_{nm}, V_{nm} and W_{nm}. The second-order differential operators take the form as follows:

$$\text{div grad } f = \sum_{nm}\left(F'' + \frac{2F'}{r} - \frac{NF}{r^2}\right)Y_{nm}\,, \tag{B.39}$$

$$\text{grad div } \mathbf{u} = \sum_{nm}\left[\left(U' + \frac{2U-NV}{r}\right)'\boldsymbol{S}^{(-1)}_{nm} + \frac{1}{r}\left(U' + \frac{2U-NV}{r}\right)\boldsymbol{S}^{(1)}_{nm}\right], \tag{B.40}$$

$$\begin{aligned}\text{rot rot } \mathbf{u} &= \sum_{nm}\left\{\left[-\frac{N}{r}\left(V' + \frac{V-U}{r}\right)\right]\boldsymbol{S}^{(-1)}_{nm} - \left[\left(V' + \frac{V-U}{r}\right)' + \frac{1}{r}\left(V' + \frac{V-U}{r}\right)\right]\boldsymbol{S}^{(1)}_{nm}\right.\\ &\qquad\left. - \left[\left(W' + \frac{W}{r}\right)' + \frac{1}{r}\left(W' + \frac{W}{r}\right) - \frac{NW}{r^2}\right]\boldsymbol{S}^{(0)}_{nm}\right\}\end{aligned} \tag{B.41}$$

$$= \sum_{nm}\left[-\frac{N}{r}\left(V' + \frac{V-U}{r}\right)\boldsymbol{S}^{(-1)}_{nm} - \left(V'' + \frac{2V'-U'}{r}\right)\boldsymbol{S}^{(1)}_{nm} - \left(W'' + \frac{2W'}{r} - \frac{NW}{r^2}\right)\boldsymbol{S}^{(0)}_{nm}\right],$$

$$\text{div grad } \mathbf{u} = \sum_{nm}\left\{\left[\left(U' + \frac{2U-NV}{r}\right)' + \frac{N}{r}\left(V' + \frac{V-U}{r}\right)\right]\boldsymbol{S}^{(-1)}_{nm}\right. \tag{B.42}$$

$$
\begin{aligned}
&+\left[\frac{1}{r}\left(U'+\frac{2U-NV}{r}\right)+\left(V'+\frac{V-U}{r}\right)'+\frac{1}{r}\left(V'+\frac{V-U}{r}\right)\right]\boldsymbol{S}^{(1)}_{nm}\\
&+\left[\left(W'+\frac{W}{r}\right)'+\frac{1}{r}\left(W'+\frac{W}{r}\right)-\frac{NW}{r^2}\right]\boldsymbol{S}^{(0)}_{nm}\Bigg\}\\
=\;&\sum_{nm}\left[\left(U''+\frac{2U'}{r}-\frac{(N+2)U}{r^2}+\frac{2NV}{r^2}\right)\boldsymbol{S}^{(-1)}_{nm}+\left(V''+\frac{2V'}{r}+\frac{2U-NV}{r^2}\right)\boldsymbol{S}^{(1)}_{nm}\right.\\
&\left.+\left(W''+\frac{2W'}{r}-\frac{NW}{r^2}\right)\boldsymbol{S}^{(0)}_{nm}\right].
\end{aligned}
$$

Expressions (B.39) and (B.40) follow from (B.36)–(B.37), expression (B.41) is obtained from (B.38) and expression (B.42) from (B.15). Two relations involving the scalar spherical harmonics have also been used,

$$
\begin{aligned}
\frac{\partial Z_{nm}}{\partial\vartheta}+\frac{\cos\vartheta}{\sin\vartheta}Z_{nm}+\frac{1}{\sin\vartheta}\frac{\partial\widetilde{Y}_{nm}}{\partial\varphi} &= -NY_{nm}\,, &\text{(B.43)}\\
\frac{\partial\widetilde{Y}_{nm}}{\partial\vartheta}+\frac{\cos\vartheta}{\sin\vartheta}\widetilde{Y}_{nm}-\frac{1}{\sin\vartheta}\frac{\partial Z_{nm}}{\partial\varphi} &= 0\,, &\text{(B.44)}
\end{aligned}
$$

the former being (A.1) rewritten in terms of Z_{nm} and $\widetilde{Y}_{nm}$ and the latter following from the definition of $\widetilde{Y}_{nm}$ in (A.9) by differentiation with respect to ϑ. Finally, we supply the selected expressions for the differential operators acting on components of $\mathbf{u}$ in the basis $\boldsymbol{S}^{(-1)}_{nm}$, $\boldsymbol{S}^{(1)}_{nm}$ and $\boldsymbol{S}^{(0)}_{nm}$. Specifically, the div operator,

$$
\begin{aligned}
\nabla\cdot U\boldsymbol{S}^{(-1)}_{nm} &= (U'+2U/r)\,Y_{nm}\,,\\
\nabla\cdot V\boldsymbol{S}^{(1)}_{nm} &= -(NV/r)Y_{nm}\,, &\text{(B.45)}\\
\nabla\cdot W\boldsymbol{S}^{(0)}_{nm} &= 0\,,
\end{aligned}
$$

the rot operator,

$$
\begin{aligned}
\nabla\times U\boldsymbol{S}^{(-1)}_{nm} &= -(U/r)\boldsymbol{S}^{(0)}_{nm}\,,\\
\nabla\times V\boldsymbol{S}^{(1)}_{nm} &= (V'+V/r)\,\boldsymbol{S}^{(0)}_{nm}\,, &\text{(B.46)}\\
\nabla\times W\boldsymbol{S}^{(0)}_{nm} &= -(NW/r)\boldsymbol{S}^{(-1)}_{nm}-(W'+W/r)\,\boldsymbol{S}^{(1)}_{nm}\,,
\end{aligned}
$$

the grad div operator,

$$
\begin{aligned}
\nabla\nabla\cdot U\boldsymbol{S}^{(-1)}_{nm} &= (U'+2U/r)'\,\boldsymbol{S}^{(-1)}_{nm}+\left(U'/r+2U/r^2\right)\boldsymbol{S}^{(1)}_{nm}\,,\\
\nabla\nabla\cdot V\boldsymbol{S}^{(1)}_{nm} &= -\left(NV/r\right)'\boldsymbol{S}^{(-1)}_{nm}-\left(NV/r^2\right)\boldsymbol{S}^{(1)}_{nm}\,, &\text{(B.47)}\\
\nabla\nabla\cdot W\boldsymbol{S}^{(0)}_{nm} &= 0\,,
\end{aligned}
$$

and the rot rot operator are provided,

$$
\begin{aligned}
\nabla\times\nabla\times U\boldsymbol{S}^{(-1)}_{nm} &= (NU/r^2)\boldsymbol{S}^{(-1)}_{nm}+(U'/r)\boldsymbol{S}^{(1)}_{nm}\,,\\
\nabla\times\nabla\times V\boldsymbol{S}^{(1)}_{nm} &= -\left(NV'/r+NV/r^2\right)\boldsymbol{S}^{(-1)}_{nm}-(V''+2V'/r)\,\boldsymbol{S}^{(1)}_{nm}\,, &\text{(B.48)}\\
\nabla\times\nabla\times W\boldsymbol{S}^{(0)}_{nm} &= -\left(W''+2W'/r-NW/r^2\right)\boldsymbol{S}^{(0)}_{nm}\,.
\end{aligned}
$$

B.4 Strain Tensor

The scalar components of the symmetric strain tensor $\boldsymbol{e}$, defined by

$$\boldsymbol{e} \;=\; \frac{1}{2}\left[\nabla\mathbf{u} + (\nabla\mathbf{u})^T\right], \tag{B.49}$$

can be expressed in the spherical coordinates using the components of $\nabla\mathbf{u}$ by (B.26), and the spherical harmonic expansions of these components can be obtained by the subsequent substitution from (B.33)–(B.35) as follows,

$$\begin{pmatrix} e_{rr} & 2e_{r\vartheta} & 2e_{r\varphi} \\ \text{"} & e_{\vartheta\vartheta} & 2e_{\vartheta\varphi} \\ \text{"} & \text{"} & e_{\varphi\varphi} \end{pmatrix} = \begin{pmatrix} \dfrac{\partial u_r}{\partial r} & \dfrac{1}{r}\dfrac{\partial u_r}{\partial\vartheta} + \dfrac{\partial u_\vartheta}{\partial r} - \dfrac{u_\vartheta}{r} & \dfrac{1}{r\sin\vartheta}\dfrac{\partial u_r}{\partial\varphi} + \dfrac{\partial u_\varphi}{\partial r} - \dfrac{u_\varphi}{r} \\ \text{"} & \dfrac{1}{r}\dfrac{\partial u_\vartheta}{\partial\vartheta} + \dfrac{u_r}{r} & \dfrac{1}{r\sin\vartheta}\dfrac{\partial u_\vartheta}{\partial\varphi} + \dfrac{1}{r}\dfrac{\partial u_\varphi}{\partial\vartheta} - \dfrac{u_\varphi}{r}\dfrac{\cos\vartheta}{\sin\vartheta} \\ \text{"} & \text{"} & \dfrac{1}{r\sin\vartheta}\dfrac{\partial u_\varphi}{\partial\varphi} + \dfrac{u_r}{r} + \dfrac{u_\vartheta}{r}\dfrac{\cos\vartheta}{\sin\vartheta} \end{pmatrix} \tag{B.50}$$

$$= \sum_{nm} \begin{pmatrix} U'Y_{nm} & \left(V'+\dfrac{U-V}{r}\right)Z_{nm} - \left(W'-\dfrac{W}{r}\right)\widetilde{Y}_{nm} & \left(V'+\dfrac{U-V}{r}\right)\widetilde{Y}_{nm} + \left(W'-\dfrac{W}{r}\right)Z_{nm} \\ \text{"} & \dfrac{U}{r}Y_{nm} + \dfrac{V}{r}\dfrac{\partial Z_{nm}}{\partial\vartheta} - \dfrac{W}{r}\dfrac{\partial\widetilde{Y}_{nm}}{\partial\vartheta} & \dfrac{2V}{r}\dfrac{\partial\widetilde{Y}_{nm}}{\partial\vartheta} + \dfrac{W}{r}\left(2\dfrac{\partial Z_{nm}}{\partial\vartheta} + NY_{nm}\right) \\ \text{"} & \text{"} & \dfrac{U}{r}Y_{nm} - \dfrac{V}{r}\left(\dfrac{\partial Z_{nm}}{\partial\vartheta} + NY_{nm}\right) + \dfrac{W}{r}\dfrac{\partial\widetilde{Y}_{nm}}{\partial\vartheta} \end{pmatrix} \tag{B.51}$$

Symmetry of the tensors is indicated by the double quotes. From (B.51), the first invariant of $\boldsymbol{e}$ can be found,

$$\bar{\boldsymbol{e}} \;\equiv\; e_{rr} + e_{\vartheta\vartheta} + e_{\varphi\varphi} \;=\; \textstyle\sum_{nm}\left(U' + \dfrac{2U - NV}{r}\right)Y_{nm} \;=\; \nabla\cdot\mathbf{u}\,. \tag{B.52}$$

We express the spherical harmonic expansions of the vectors $\boldsymbol{e}_r\cdot\boldsymbol{e}$, $\boldsymbol{e}_\vartheta\cdot\boldsymbol{e}$ and $\boldsymbol{e}_\varphi\cdot\boldsymbol{e}$,

$$\begin{aligned} \boldsymbol{e}_r\cdot\boldsymbol{e} &= e_{rr}\boldsymbol{e}_r + e_{r\vartheta}\boldsymbol{e}_\vartheta + e_{r\varphi}\boldsymbol{e}_\varphi \\ &= \textstyle\sum_{nm}\left[U'\boldsymbol{S}^{(-1)}_{nm} + \dfrac{1}{2}\left(V' + \dfrac{U-V}{r}\right)\boldsymbol{S}^{(1)}_{nm} + \dfrac{1}{2}\left(W' - \dfrac{W}{r}\right)\boldsymbol{S}^{(0)}_{nm}\right], \end{aligned} \tag{B.53}$$

$$\begin{aligned} \boldsymbol{e}_\vartheta\cdot\boldsymbol{e} &= e_{r\vartheta}\boldsymbol{e}_r + e_{\vartheta\vartheta}\boldsymbol{e}_\vartheta + e_{\vartheta\varphi}\boldsymbol{e}_\varphi \\ &= \textstyle\sum_{nm}\left\{\left[\dfrac{1}{2}\left(V' + \dfrac{U-V}{r}\right)Z_{nm} - \dfrac{1}{2}\left(W' - \dfrac{W}{r}\right)\widetilde{Y}_{nm}\right]\boldsymbol{e}_r\right. \\ &\qquad \left. + \dfrac{U}{r}Y_{nm}\boldsymbol{e}_\vartheta + \dfrac{V}{r}\dfrac{\partial\boldsymbol{S}^{(1)}_{nm}}{\partial\vartheta} + \dfrac{W}{r}\left(\dfrac{\partial\boldsymbol{S}^{(0)}_{nm}}{\partial\vartheta} + \dfrac{N}{2}Y_{nm}\boldsymbol{e}_\varphi\right)\right\}, \end{aligned} \tag{B.54}$$

$$\begin{aligned} \boldsymbol{e}_\varphi\cdot\boldsymbol{e} &= e_{r\varphi}\boldsymbol{e}_r + e_{\vartheta\varphi}\boldsymbol{e}_\vartheta + e_{\varphi\varphi}\boldsymbol{e}_\varphi \\ &= \textstyle\sum_{nm}\left\{\left[\dfrac{1}{2}\left(V' + \dfrac{U-V}{r}\right)\widetilde{Y}_{nm} + \dfrac{1}{2}\left(W' - \dfrac{W}{r}\right)Z_{nm}\right]\boldsymbol{e}_r\right. \\ &\qquad \left. + \dfrac{U}{r}Y_{nm}\boldsymbol{e}_\varphi - \dfrac{V}{r}\left(\dfrac{\partial\boldsymbol{S}^{(0)}_{nm}}{\partial\vartheta} + NY_{nm}\boldsymbol{e}_\varphi\right) + \dfrac{W}{r}\left(\dfrac{\partial\boldsymbol{S}^{(1)}_{nm}}{\partial\vartheta} + \dfrac{N}{2}Y_{nm}\boldsymbol{e}_\vartheta\right)\right\}, \end{aligned} \tag{B.55}$$

and the spherical harmonic expansion of $\nabla\cdot\boldsymbol{e}$, invoking relations (B.16), (B.40) and (B.42),

$$\begin{aligned} \nabla\cdot\boldsymbol{e} \;=\; \frac{1}{2}\left[\nabla\cdot\nabla\mathbf{u} + \nabla\nabla\cdot\mathbf{u}\right] \;&=\; \frac{1}{2}\left(2U'' + \frac{4U' - NV'}{r} - \frac{(N+4)U - 3NV}{r^2}\right)\boldsymbol{S}^{(-1)}_{nm} \\ &+ \frac{1}{2}\left(V'' + \frac{U' + 2V'}{r} + \frac{4U - 2NV}{r^2}\right)\boldsymbol{S}^{(1)}_{nm} + \frac{1}{2}\left(W'' + \frac{2W'}{r} - \frac{NW}{r^2}\right)\boldsymbol{S}^{(0)}_{nm}\,. \end{aligned} \tag{B.56}$$

B.5 Elastic Stress Tensor and Elastic Stress Vectors

The elastic stress tensor $\boldsymbol{\tau}^E$ is defined by the elastic constitutive relation, cf. (2.10),

$$\boldsymbol{\tau}^E \;=\; \lambda\nabla\cdot\mathbf{u}\boldsymbol{I} + 2\mu\,\boldsymbol{e} \;=\; \lambda\nabla\cdot\mathbf{u}\boldsymbol{I} + \mu\left[\nabla\mathbf{u} + (\nabla\mathbf{u})^T\right]. \tag{B.57}$$

Tensor $\boldsymbol{\tau}^E$ is symmetric. To obtain the components of $\boldsymbol{\tau}^E$, both in the spherical coordinates and in the spherical harmonic expansions, expressions (B.50)–(B.51) for the strain tensor $\boldsymbol{e}$ can be used,

$$\begin{pmatrix} \tau^E_{rr} & \tau^E_{r\vartheta} & \tau^E_{r\varphi} \\ " & \tau^E_{\vartheta\vartheta} & \tau^E_{\vartheta\varphi} \\ " & " & \tau^E_{\varphi\varphi} \end{pmatrix} = \begin{pmatrix} \lambda\nabla\cdot\mathbf{u} + 2\mu\dfrac{\partial u_r}{\partial r} & \mu\left(\dfrac{1}{r}\dfrac{\partial u_r}{\partial\vartheta} + \dfrac{\partial u_\vartheta}{\partial r} - \dfrac{u_\vartheta}{r}\right) & \mu\left(\dfrac{1}{r\sin\vartheta}\dfrac{\partial u_r}{\partial\varphi} + \dfrac{\partial u_\varphi}{\partial r} - \dfrac{u_\varphi}{r}\right) \\ " & \lambda\nabla\cdot\mathbf{u} + \dfrac{2\mu}{r}\left(\dfrac{\partial u_\vartheta}{\partial\vartheta} + u_r\right) & \dfrac{\mu}{r}\left(\dfrac{1}{\sin\vartheta}\dfrac{\partial u_\vartheta}{\partial\varphi} + \dfrac{\partial u_\varphi}{\partial\vartheta} - u_\varphi\dfrac{\cos\vartheta}{\sin\vartheta}\right) \\ " & " & \lambda\nabla\cdot\mathbf{u} + \dfrac{2\mu}{r}\left(\dfrac{1}{\sin\vartheta}\dfrac{\partial u_\varphi}{\partial\varphi} + u_r + u_\vartheta\dfrac{\cos\vartheta}{\sin\vartheta}\right) \end{pmatrix} \tag{B.58}$$

$$= \sum_{nm} \begin{pmatrix} \left(\lambda X + 2\mu U'\right) Y_{nm} & \mu\left[\left(V' + \dfrac{U-V}{r}\right) Z_{nm} - \left(W' - \dfrac{W}{r}\right)\widetilde{Y}_{nm}\right] & \cdots \\ " & \left(\lambda X + \dfrac{2\mu U}{r}\right) Y_{nm} + \dfrac{2\mu}{r}\left[V\dfrac{\partial Z_{nm}}{\partial\vartheta} - W\dfrac{\partial\widetilde{Y}_{nm}}{\partial\vartheta}\right] & \cdots \\ " & " & \cdots \end{pmatrix} \tag{B.59}$$

$$\begin{pmatrix} \cdots & \mu\left[\left(V' + \dfrac{U-V}{r}\right)\widetilde{Y}_{nm} + \left(W' - \dfrac{W}{r}\right) Z_{nm}\right] \\ \cdots & \dfrac{2\mu}{r}\left[V\dfrac{\partial\widetilde{Y}_{nm}}{\partial\vartheta} + W\left(\dfrac{\partial Z_{nm}}{\partial\vartheta} + \dfrac{N}{2}Y_{nm}\right)\right] \\ \cdots & \left(\lambda X + \dfrac{2\mu U}{r}\right) Y_{nm} + \dfrac{2\mu}{r}\left[-V\left(\dfrac{\partial Z_{nm}}{\partial\vartheta} + NY_{nm}\right) + W\dfrac{\partial\widetilde{Y}_{nm}}{\partial\vartheta}\right] \end{pmatrix},$$

where symbols X denote the coefficients of the spherical harmonic expansion (B.37) of div $\mathbf{u}$,

$$X_{nm} \;=\; U'_{nm} + \frac{2U_{nm} - NV_{nm}}{r}. \tag{B.60}$$

The first invariant of $\boldsymbol{\tau}^E$ equals to

$$\bar{\boldsymbol{\tau}} \;\equiv\; \tau^E_{rr} + \tau^E_{\vartheta\vartheta} + \tau^E_{\varphi\varphi} \;=\; \textstyle\sum_{nm}(3\lambda + 2\mu)X_{nm}Y_{nm} \;=\; (3\lambda + 2\mu)\nabla\cdot\mathbf{u} \;=\; 3K\nabla\cdot\mathbf{u}. \tag{B.61}$$

The stress vectors along the directions of $\boldsymbol{e}_r$, $\boldsymbol{e}_\vartheta$ and $\boldsymbol{e}_\varphi$ (with the degree and order subscripts of the stress vector coefficients $T^E_{rr,nm}$, …, $T^E_{\varphi\varphi,nm}$ suppressed):

$$\begin{aligned} \boldsymbol{T}^E_r \;&\equiv\; \boldsymbol{e}_r\cdot\tau^E \;=\; \tau^E_{rr}\boldsymbol{e}_r + \tau^E_{r\vartheta}\boldsymbol{e}_\vartheta + \tau^E_{r\varphi}\boldsymbol{e}_\varphi \;=\; \textstyle\sum_{nm}\left[T^E_{rr}\boldsymbol{S}^{(-1)}_{nm} + T^E_{r\vartheta}\boldsymbol{S}^{(1)}_{nm} + T^E_{r\varphi}\boldsymbol{S}^{(0)}_{nm}\right] \qquad \text{(B.62)} \\ &=\; \textstyle\sum_{nm}\left[\left(\lambda X + 2\mu U'\right)\boldsymbol{S}^{(-1)}_{nm} + \mu\left(V' + \dfrac{U-V}{r}\right)\boldsymbol{S}^{(1)}_{nm} + \mu\left(W' - \dfrac{W}{r}\right)\boldsymbol{S}^{(0)}_{nm}\right], \\ \boldsymbol{T}^E_\vartheta \;&\equiv\; \boldsymbol{e}_\vartheta\cdot\tau^E \;=\; \tau^E_{\vartheta r}\boldsymbol{e}_r + \tau^E_{\vartheta\vartheta}\boldsymbol{e}_\vartheta + \tau^E_{\vartheta\varphi}\boldsymbol{e}_\varphi \;=\; \textstyle\sum_{nm}\left[T^E_{\vartheta r}\boldsymbol{S}^{(-1)}_{nm} + T^E_{\vartheta\vartheta}\boldsymbol{S}^{(1)}_{nm} + T^E_{\vartheta\varphi}\boldsymbol{S}^{(0)}_{nm}\right] \qquad \text{(B.63)} \\ &=\; \textstyle\sum_{nm}\left\{\left[\mu\left(V' + \dfrac{U-V}{r}\right)Z_{nm} - \mu\left(W' - \dfrac{W}{r}\right)\widetilde{Y}_{nm}\right]\boldsymbol{e}_r \right. \end{aligned}$$

$$+\left(\lambda X+\frac{2\mu U}{r}\right)Y_{nm}\boldsymbol{e}_{\vartheta}+\frac{2\mu V}{r}\frac{\partial \boldsymbol{S}^{(1)}_{nm}}{\partial\vartheta}+\frac{2\mu W}{r}\left(\frac{\partial \boldsymbol{S}^{(0)}_{nm}}{\partial\vartheta}+\frac{N}{2}Y_{nm}\boldsymbol{e}_{\varphi}\right)\Bigg\}\,,$$

$$\boldsymbol{T}^{E}_{\varphi} \equiv \boldsymbol{e}_{\varphi}\cdot\tau^{E} = \tau^{E}_{\varphi r}\boldsymbol{e}_{r}+\tau^{E}_{\varphi\vartheta}\boldsymbol{e}_{\vartheta}+\tau^{E}_{\varphi\varphi}\boldsymbol{e}_{\varphi} = \sum_{nm}\left[T^{E}_{\varphi r}\boldsymbol{S}^{(-1)}_{nm}+T^{E}_{\varphi\vartheta}\boldsymbol{S}^{(1)}_{nm}+T^{E}_{\varphi\varphi}\boldsymbol{S}^{(0)}_{nm}\right] \tag{B.64}$$

$$= \sum_{nm}\Bigg\{\left[\mu\left(V'+\frac{U-V}{r}\right)\widetilde{Y}_{nm}+\mu\left(W'-\frac{W}{r}\right)Z_{nm}\right]\boldsymbol{e}_{r}$$

$$+\left(\lambda X+\frac{2\mu U}{r}\right)Y_{nm}\boldsymbol{e}_{\varphi}-\frac{2\mu V}{r}\left(\frac{\partial \boldsymbol{S}^{(0)}_{nm}}{\partial\vartheta}+NY_{nm}\boldsymbol{e}_{\varphi}\right)+\frac{2\mu W}{r}\left(\frac{\partial \boldsymbol{S}^{(1)}_{nm}}{\partial\vartheta}+\frac{N}{2}Y_{nm}\boldsymbol{e}_{\vartheta}\right)\Bigg\}\,.$$

It is possible to relate the coefficients T^{E}_{rr}, $T^{E}_{r\vartheta}$ and $T^{E}_{r\varphi}$ to the coefficients U, V and W of the same degree and order,

$$T^{E}_{rr,nm} = \lambda X_{nm}+2\mu U'_{nm} = (\lambda+2\mu)U'_{nm}+\lambda\frac{2U_{nm}-NV_{nm}}{r}\,, \tag{B.65}$$

$$T^{E}_{r\vartheta,nm} = \mu\left(V'_{nm}+\frac{U_{nm}-V_{nm}}{r}\right)\,, \tag{B.66}$$

$$T^{E}_{r\varphi,nm} = \mu\left(W'_{nm}-\frac{W_{nm}}{r}\right)\,. \tag{B.67}$$

However, no such simple relations are available for the coefficients of the spherical harmonic expansions of $\boldsymbol{T}^{E}_{\vartheta}$ and $\boldsymbol{T}^{E}_{\varphi}$. The expression for $\nabla\cdot\boldsymbol{\tau}^{E}$ with the radial distribution of the elastic Lamé parameters, $\lambda=\lambda(r)$, $\mu=\mu(r)$, can be found as follows:

$$\nabla\cdot\boldsymbol{\tau}^{E} = \lambda\nabla\nabla\cdot\mathbf{u}+2\mu\nabla\cdot\boldsymbol{e}+\lambda'\nabla\cdot\mathbf{u}\boldsymbol{e}_{r}+2\mu'\boldsymbol{e}_{r}\cdot\boldsymbol{e}$$

$$= \sum_{nm}\Bigg[\left(T^{E\,\prime}_{rr}+\frac{4\mu}{r}U'-\frac{N\mu}{r}V'-\frac{(N+4)\mu}{r^{2}}U+\frac{3N\mu}{r^{2}}V\right)\boldsymbol{S}^{(-1)}_{nm} \tag{B.68}$$

$$+\left(T^{E\,\prime}_{r\vartheta}+\frac{\lambda}{r}U'+\frac{3\mu}{r}V'+\frac{2\lambda+5\mu}{r^{2}}U-\frac{N\lambda+(2N+1)\mu}{r^{2}}V\right)\boldsymbol{S}^{(1)}_{nm}$$

$$+\left(T^{E\,\prime}_{r\varphi}+\frac{3\mu}{r}W'-\frac{(N+1)\mu}{r^{2}}W\right)\boldsymbol{S}^{(0)}_{nm}\Bigg]$$

$$= \sum_{nm}\Bigg[\left(T^{E\,\prime}_{rr}-\frac{4\mu(3\lambda+2\mu)}{r^{2}\beta}U+\frac{2N\mu(3\lambda+2\mu)}{r^{2}\beta}V+\frac{4\mu}{r\beta}T^{E}_{rr}-\frac{N}{r}T^{E}_{r\vartheta}\right)\boldsymbol{S}^{(-1)}_{nm} \tag{B.69}$$

$$+\left(T^{E\,\prime}_{r\vartheta}+\frac{2\mu(3\lambda+2\mu)}{r^{2}\beta}U-\frac{N\mu(3\lambda+2\mu)+(N-2)\mu\beta}{r^{2}\beta}V+\frac{\lambda}{r\beta}T^{E}_{rr}+\frac{3}{r}T^{E}_{r\vartheta}\right)\boldsymbol{S}^{(1)}_{nm}$$

$$+\left(T^{E\,\prime}_{r\varphi}-\frac{(N-2)\mu}{r^{2}}W+\frac{3}{r}T^{E}_{r\varphi}\right)\boldsymbol{S}^{(0)}_{nm}\Bigg]\,,$$

with $\beta=\lambda+2\mu$. In (B.69), relations which follows from (B.65)–(B.67),

$$U' = -\frac{2\lambda}{r\beta}U+\frac{N\lambda}{r\beta}V+\frac{1}{\beta}T^{E}_{rr}\,, \tag{B.70}$$

$$V' = -\frac{1}{r}U+\frac{1}{r}V+\frac{1}{\mu}T^{E}_{r\vartheta}\,, \tag{B.71}$$

$$W' = \frac{1}{r}W+\frac{1}{\mu}T^{E}_{r\varphi}\,, \tag{B.72}$$

$$X = \frac{2\mu}{r}(2U-NV)+\frac{1}{\beta}T^{E}_{rr}\,, \tag{B.73}$$

have been used.

We rewrite the stress vectors for the zonal functions $\mathbf{u}(r,\vartheta)$, $\varphi_1(r,\vartheta)$ and $\boldsymbol{\tau}(r,\vartheta)$, cf. (3.67). The zonal scalar and vector spherical harmonics, respectively, are involved,

$$\begin{aligned} Y_n(\vartheta) &= Y_{n0}(\vartheta)\,, \qquad Z_n(\vartheta) = \frac{\partial Y_n}{\partial\vartheta}\,, \qquad \widetilde{Y}(\vartheta) = \frac{1}{\sin\vartheta}\frac{\partial Y_n}{\partial\varphi} = 0\,, \\ \boldsymbol{S}_n^{(-1)}(\vartheta) &= Y_n\boldsymbol{e}_r\,, \qquad \boldsymbol{S}_n^{(1)}(\vartheta) = Z_n\boldsymbol{e}_\vartheta\,, \qquad \boldsymbol{S}_n^{(0)}(\vartheta) = Z_n\boldsymbol{e}_\varphi\,. \end{aligned} \tag{B.74}$$

cf. (B.28)–(B.30). With relation (B.43) in the reduced form for the zonal spherical harmonics,

$$\frac{\partial Z_n}{\partial\vartheta} + \frac{\cos\vartheta}{\sin\vartheta}Z_n + NY_n = 0\,, \tag{B.75}$$

the zonal stress vectors can be obtained from (B.62)–(B.64) as follows:

$$\begin{aligned} \boldsymbol{T}_r^E &= \textstyle\sum_n \left[T_{rr,n}^E\boldsymbol{S}_n^{(-1)} + T_{r\vartheta,n}^E\boldsymbol{S}_n^{(1)} + T_{r\varphi,n}^E\boldsymbol{S}_n^{(0)}\right] \qquad (B.76)\\ &= \textstyle\sum_n \left[\left(\lambda X_n + 2\mu U_n'\right)Y_n\boldsymbol{e}_r + \mu\left(V_n' + \frac{U_n - V_n}{r}\right)Z_n\boldsymbol{e}_\vartheta + \mu\left(W_n' - \frac{W_n}{r}\right)Z_n\boldsymbol{e}_\varphi\right], \\ \boldsymbol{T}_\vartheta^E &= \textstyle\sum_n \left[T_{\vartheta r,n}^E\boldsymbol{S}_n^{(-1)} + T_{\vartheta\vartheta,n}^E\boldsymbol{S}_n^{(1)} + T_{\vartheta\varphi,n}^E\boldsymbol{S}_n^{(0)}\right] \qquad (B.77)\\ &= \textstyle\sum_n \left\{\left[\mu\left(V_n' + \frac{U_n - V_n}{r}\right)Z_n\right]\boldsymbol{e}_r + \left[\left(\lambda X_n + 2\mu\frac{U_n - NV_n}{r}\right)Y_n - 2\mu\frac{V_n}{r}\frac{\cos\vartheta}{\sin\vartheta}Z_n\right]\boldsymbol{e}_\vartheta\right. \\ &\quad \textstyle\left. - \left[N\mu\frac{W_n}{r}Y_n + 2\mu\frac{W_n}{r}\frac{\cos\vartheta}{\sin\vartheta}Z_n\right]\boldsymbol{e}_\varphi\right\}, \\ \boldsymbol{T}_\varphi^E &= \textstyle\sum_n \left[T_{\varphi r,n}^E\boldsymbol{S}_n^{(-1)} + T_{\varphi\vartheta,n}^E\boldsymbol{S}_n^{(1)} + T_{\varphi\varphi,n}^E\boldsymbol{S}_n^{(0)}\right] \qquad (B.78)\\ &= \textstyle\sum_n \left\{\left[\mu\left(W_n' - \frac{W_n}{r}\right)Z_n\right]\boldsymbol{e}_r - \left[N\mu\frac{W_n}{r}Y_n + 2\mu\frac{W_n}{r}\frac{\cos\vartheta}{\sin\vartheta}Z_n\right]\boldsymbol{e}_\vartheta\right. \\ &\quad \textstyle\left. + \left[\left(\lambda X_n + 2\mu\frac{U_n}{r}\right)Y_n + 2\mu\frac{V_n}{r}\frac{\cos\vartheta}{\sin\vartheta}Z_n\right]\boldsymbol{e}_\varphi\right\}. \end{aligned}$$

B.6 Other Spherical Harmonic Expansions

In Section 2.2 the spherical harmonic expansions of the forcing term $\boldsymbol{f}$ in (2.13) and of the l.h.s. of the Poisson equation (2.14) for the incremental field φ_1 are needed. Introducing the spherical harmonic expansion of φ_1,

$$\varphi_1 = \textstyle\sum_{nm} F_{nm}Y_{nm}\,, \tag{B.79}$$

cf. (2.21), and the auxiliary coefficient $Q_{nm}(r)$,

$$Q_{nm} = F_{nm}' + \frac{n+1}{r}F_{nm} + 4\pi G\varrho_0 U_{nm}\,, \tag{B.80}$$

cf. (2.32), the spherical harmonic expansion of $\boldsymbol{f}$ can be found (the degree and order subscripts of F_{nm} and Q_{nm} are suppressed):

$$\begin{aligned} \boldsymbol{f} &= -\varrho_0\nabla\varphi_1 + \nabla\cdot(\varrho_0\mathbf{u})g_0\boldsymbol{e}_r - \nabla(\varrho_0 g_0\boldsymbol{e}_r\cdot\mathbf{u}) = -\varrho_0\nabla\varphi_1 + \varrho_0\nabla\cdot\mathbf{u}g_0\boldsymbol{e}_r - \varrho_0\nabla(g_0\boldsymbol{e}_r\cdot\mathbf{u}) \\ &= \textstyle\sum_{nm}\left[-\varrho_0\left(F'\boldsymbol{S}_{nm}^{(-1)} + \frac{F}{r}\boldsymbol{S}_{nm}^{(1)}\right) + \varrho_0 g_0\left(U' + \frac{2U - NV}{r}\right)\boldsymbol{S}_{nm}^{(-1)} - \varrho_0\left((g_0U)'\boldsymbol{S}_{nm}^{(-1)} + \frac{g_0U}{r}\boldsymbol{S}_{nm}^{(1)}\right)\right] \\ &= \textstyle\sum_{nm}\left[\left(\frac{4\varrho_0 g_0}{r}U_{nm} - \frac{N\varrho_0 g_0}{r}V_{nm} + \frac{(n+1)\varrho_0}{r}F_{nm} - \varrho_0 Q_{nm}\right)\boldsymbol{S}_{nm}^{(-1)}\right. \qquad (B.81)\\ &\quad \textstyle\left. - \left(\frac{\varrho_0 g_0}{r}U_{nm} + \frac{\varrho_0}{r}F_{nm}\right)\boldsymbol{S}_{nm}^{(1)}\right], \end{aligned}$$

where the Poisson equation (2.4) for the initial field φ_0 in the case of $\varrho_0 = \varrho_0(r)$ has been used,

$$g_0' + \frac{2}{r} g_0 - 4\pi G \varrho_0 = 0\,. \tag{B.82}$$

The spherical harmonic expansion of the l.h.s. of the Poisson equation (2.14) can be derived in the two steps:

$$\begin{aligned}
\nabla\varphi_1 + 4\pi G\varrho_0 \mathbf{u} &= \sum_{nm} \left[\left(F' + 4\pi G\varrho_0 U \right) \boldsymbol{S}_{nm}^{(-1)} + \left(\frac{F}{r} + 4\pi G\varrho_0 V \right) \boldsymbol{S}_{nm}^{(1)} + 4\pi G\varrho_0 W \boldsymbol{S}_{nm}^{(0)} \right] \\
&= \sum_{nm} \left[\left(-\frac{n+1}{r} F + Q \right) \boldsymbol{S}_{nm}^{(-1)} + \left(\frac{F}{r} + 4\pi G\varrho_0 V \right) \boldsymbol{S}_{nm}^{(1)} + 4\pi G\varrho_0 W \boldsymbol{S}_{nm}^{(0)} \right] , \\
\nabla \cdot (\nabla\varphi_1 + 4\pi G\varrho_0 \mathbf{u}) &= \sum_{nm} \left[\left(-\frac{n+1}{r} F + Q \right)' + \frac{2}{r} \left(-\frac{n+1}{r} F + Q \right) - \frac{N}{r} \left(\frac{F}{r} + 4\pi G\varrho_0 V \right) \right] Y_{nm} \\
&= \sum_{nm} \left[Q' + 4\pi G \frac{(n+1)\varrho_0}{r} U - 4\pi G \frac{N\varrho_0}{r} V - \frac{n-1}{r} Q \right] Y_{nm}\,.
\end{aligned} \tag{B.83}$$

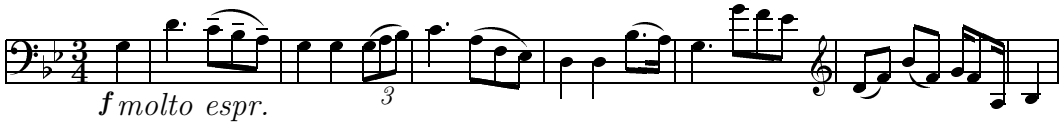

ANTONÍN DVOŘÁK, *Concerto for Cello and Orchestra No. 2 in B minor, Op. 104. II. Adagio, ma non troppo* (1895)

Appendix C

Excerpts of Fortran Codes

We deliver some routines which might be of interest to a programmer of the IV/MOL approach. The routines are coded in Fortran 90 (Metcalf & Reid 1997). This standardized, high-level language is designed for writing codes which can be effectively optimized on multiprocessor computers. Fortran 90 provides the means for so-called data parallelization to avoid language constructs which force a compiler to generate a code executing serially even when it is not necessary (e.g., matrix multiplication). However, not all syntactic elements are appropriate on both the single-processor and the multiprocessor computers, and not all new features have been optimally handled by recent Fortran 90 compilers. It is a kind of art to exploit the parallelizing features of Fortran 90 and not to harm simultaneously the efficiency of a code on single-processor machines. From this point of view, the excerpts in Appendix C.1 lost the game; on the other hand, they and the other excerpts, too, demonstrate the high conciseness of the language. The excerpts appear in order of being referred to in the preceding text.

C.1 Weights of Finite-Difference Formulas

In Section 4.2.2 the algorithm by Fornberg (1996) for evaluation of weights of FD formulas for derivatives of functions on arbitrarily spaced grids has been introduced. Fornberg provides two routines, `weights(xi,x,n,m,c)` and `weights1(xi,x,n,m,c)`. On input of the both routines, `xi` represents a point at which the FD formulas should be applied, `x(0:n)` is the array containing coordinates of `n`+1 grid points, and `m` is the highest order of a derivative to be approximated. The only output parameter of the former routine is the array `c(0:n,0:n,0:m)` whose elements `c(i,j,k)` contain the weights to be applied at `x(j)` when the `k`th derivative is approximated by the grid extending over `x(0)`, `x(1)`, ..., `x(i)`. The latter routine returns the array `c(0:n,0:m)` with elements `c(j,k)` which contain the weights to be applied at `x(j)` when the `k`th derivative is approximated by the grid extending over the whole set `x(0)`, `x(1)`, ..., `x(n)`. In Fornberg (1996) the routines are offered in both a symbolic language (p. 18) and Fortran 77 (p. 167ff.). We present the routines in the syntax of Fortran 90, preserving the meaning of all the arguments. The routines present a valuable example of the advanced features of Fortran 90 in both the positive and negative meaning. The number of cycles is reduced from three, which appear in the original Fortran 77 code, to only one in the Fortran 90 code; the other two cycles are handled by operations applied

to array sections and may be subjected to internal parallelization. The usability of our routines on single-processor machines is limited, however: compiled by the optimizing Microsoft Fortran PowerStation compiler, the running time is one order of magnitude worse than that of the original Fortran 77 routines; Fortran 90 compiler for HP-UX produces a code slower by a factor of four. A reason of this deterioration can be traced to the calls to the replicating function `spread` and invoked memory management. However, `spread` appears to be indispensable for parallelization of a vast body of expressions. It is an exemplary case of the "single- versus multiprocessor" dilemma of Fortran 90.

```
SUBROUTINE weights90(xi,x,n,m,c)
IMPLICIT NONE
INTENT(in) :: xi,x,n,m
INTENT(out):: c
INTEGER    :: n,m,i,mn,ii,jj
INTEGER,PARAMETER :: DP=8,NMAX=8,MMAX=4,k(NMAX,MMAX) = reshape &
  ((/((jj,ii=1,NMAX),jj=1,MMAX)/),(/NMAX,MMAX/))
LOGICAL,PARAMETER :: tmask(NMAX,NMAX) = reshape &
  ((/((.FALSE.,ii=1,jj),(.TRUE.,ii=jj+1,NMAX),jj=0,NMAX-1)/),(/NMAX,NMAX/))
REAL(DP)   :: xi,x(0:n),c(0:n,0:n,0:m), xxi(0:n),xx(1:n,0:n-1,1:n),ab(0:n)
c(0,0,0) = 1._DP
xxi(0:n) = x(0:n)-xi
xx(1:n,0:n-1,1:n) = spread(spread(x(1:n),2,n)-spread(x(0:n-1),1,n),3,n)
ab(0)    = 1._DP
ab(1:n)  = product(xx(1:n,0:n-1,1),2,tmask)
ab(1:n)  = ab(0:n-1)/ab(1:n)
do i = 1,n
  mn     = min(i,m)
  c(0:i-1,i,0) = xxi(i)*c(0:i-1,i-1,0)/xx(i,0:i-1,1)
  c(i,i,0)     = -ab(i)*xxi(i-1)*c(i-1,i-1,0)
  c(0:i-1,i,1:mn) = (xxi(i)*c(0:i-1,i-1,1:mn)-k(1:i,1:mn)*c(0:i-1,i-1,0:mn-1)) &
                 /xx(i,0:i-1,1:mn)
  c(i,i,1:mn)  = ab(i)*(k(1,1:mn)*c(i-1,i-1,0:mn-1)-xxi(i-1)*c(i-1,i-1,1:mn))
enddo
END

SUBROUTINE weights91(xi,x,n,m,c)
IMPLICIT NONE
INTENT(in) :: xi,x,n,m
INTENT(out):: c
INTEGER    :: n,m,i,mn,ii,jj
INTEGER,PARAMETER :: DP=8,NMAX=8,MMAX=4,k(NMAX,MMAX) = reshape &
  ((/((jj,ii=1,NMAX),jj=1,MMAX)/),(/NMAX,MMAX/))
LOGICAL,PARAMETER :: tmask(NMAX,NMAX) = reshape &
  ((/((.FALSE.,ii=1,jj),(.TRUE.,ii=jj+1,NMAX),jj=0,NMAX-1)/),(/NMAX,NMAX/))
REAL(DP)   :: xi,x(0:n),c(0:n,0:m), xxi(0:n),xx(1:n,0:n-1,1:n),ab(0:n)
c        = 0._DP
c(0,0)   = 1._DP
xxi(0:n) = x(0:n)-xi
xx(1:n,0:n-1,1:n) = spread(spread(x(1:n),2,n)-spread(x(0:n-1),1,n),3,n)
ab(0)    = 1._DP
ab(1:n)  = product(xx(1:n,0:n-1,1),2,tmask)
ab(1:n)  = ab(0:n-1)/ab(1:n)
do i = 1,n
  mn     = min(i,m)
  c(i,1:mn)  = ab(i)*(k(1,1:mn)*c(i-1,0:mn-1)-xxi(i-1)*c(i-1,1:mn))
```

```
  c(i,0)     = -ab(i)*xxi(i-1)*c(i-1,0)
  c(0:i-1,1:mn) = (xxi(i)*c(0:i-1,1:mn)-k(1:i,1:mn)*c(0:i-1,0:mn-1)) &
                /xx(i,0:i-1,1:mn)
  c(0:i-1,0) = xxi(i)*c(0:i-1,0)/xx(i,0:i-1,1)
enddo
END
```

C.2 Rosenbrock Stiff Integrator

In Sections 4.3.2 and 4.3.3 we have described two methods appropriate for numerical solution to IV problems for stiff sets of ODEs. The Rosenbrock and the semi-implicit extrapolation method, implemented by Press et al. (1996), have been adapted for the system of ODEs (4.14) with the Jacobian matrix in the form $\boldsymbol{P}^{-1}\boldsymbol{Q}$, with $\boldsymbol{P}$ and $\boldsymbol{Q}$ the band-diagonal matrices. For the Rosenbrock method, the band-diagonal algebraic system (4.31) has been found as the advisable replacement of the general system (4.28).

We present here the excerpt of the routine `stiff` by Press et al. (1996), rewritten for (4.31). Being anxious not to violate © of Numerical Recipes Software, we do not bring the complete subroutine; we only disclose the newly rewritten parts. In particular, we do not present the adaptive stepsize control which can be taken from the original `stiff` without a change, and we do not present specification statements which are mostly the same again. The main alteration made in the excerpt is the replacement of the calls to the solver to general systems of linear algebraic equations, `ludcmp` & `lubksb`, by the calls to the analogical pair for band-diagonal systems, `bandec` and `banbks`, all by Press et al. (1996). The band-diagonal solver ought to be accompanied with a subroutine for efficient evaluation of the band-diagonal r.h.s. of (4.31) what can be done similarly as in the routine `banmul`. Thus, the presented excerpt is rather the exposition of how to modify the routine `stiff` and only makes sense when the original `stiff` and `bandec` & `banbks` are available.

```
! Based on stiff by Press et al. (1996a), p. 732ff.
! Matrices P and Q and vector q are stored in arrays
! pban(NMAX,MPMAX), qban(NMAX,MQMAX) and qvec(NMAX), respectively.
! xban(NMAX,MXMAX), also band-diagonal matrix, keeps (P/(gamma*h)-Q).
! Matrices are in the compact storage form by Press et al. (1996a), p. 44.
! n denotes the actual size size of P and Q,
! mp1 and mq1 denote the widths of the subdiagonal (left) part of P and Q,
! mp2 and mq2 denote the widths of the superdiagonal (right) part of P and Q,
! the total widths are mp1+1+mp2 and mq1+1+mq2 for P and Q, respectively.
h        = htry
xsav     = x
ysav(:n) = y(:)
call derivsban(qban,n,mq1,mq2,NMAX,MQMAX,y,qvec,dysav)
do jtry=1,MAXTRY
  xban(:n,:) = pban(:n,:)/(GAM*h)-qban(:n,:)
  call bandec(xban,n,mx1,mx2,NMAX,MXMAX,xbanl,MXMAXL,indx,det)
  g1(:n)=dysav(:n)
  call banbks(xban,n,mx1,mx2,NMAX,MXMAX,xbanl,MXMAXL,indx,g1)
  y(:)=ysav(:n)+A21*g1(:n)
  call derivsban(qban,n,mq1,mq2,NMAX,MQMAX,y,qvec,dydx)
  call derivsban(pban,n,mp1,mp2,NMAX,MPMAX,C21*g1(:n)/h,dydx,g2)
```

```
  call banbks(xban,n,mx1,mx2,NMAX,MXMAX,xbanl,MXMAXL,indx,g2)
  y(:n)=ysav(:n)+A31*g1(:n)+A32*g2(:n)
  call derivsban(qban,n,mq1,mq2,NMAX,MQMAX,y,qvec,dydx)
  call derivsban(pban,n,mp1,mp2,NMAX,MPMAX,(C31*g1(:n)+C32*g2(:n))/h,dydx,g3)
  call banbks(xban,n,mx1,mx2,NMAX,MXMAX,xbanl,MXMAXL,indx,g3)
  call derivsban(pban,n,mp1,mp2,NMAX,MPMAX,(C41*g1(:n)+C42*g2(:n)+C43*g3(:n))/h,dydx,g4)
  call banbks(xban,n,mx1,mx2,NMAX,MXMAX,xbanl,MXMAXL,indx,g4)
  y(:n)=ysav(:n)+B1*g1(:n)+B2*g2(:n)+B3*g3(:n)+B4*g4(:n)
  err(:n)=E1*g1(:n)+E2*g2(:n)+E3*g3(:n)+E4*g4(:n)
  x=xsav+h
  if(x.eq.xsav) pause 'stepsize not significant in stiff'
! ... Adaptive stepsize control as in the original stiff,
! ... beginning from the statement commented as "Evaluate accuracy.".
enddo
pause 'exceeded MAXTRY in stiff'
END

! Based on banmul by Press et al. (1996a), p. 44.
SUBROUTINE derivsban(a,n,m1,m2,np,mp,y,qvec,dydx)
IMPLICIT NONE
INTEGER,PARAMETER  :: DP=8
INTEGER  :: n,m1,m2,np,mp,i,j,k
REAL(DP) :: a(np,mp),y(n),qvec(n),dydx(n)
do i=1,n
  dydx(i)=qvec(i)
  k=i-m1-1
  do j=max(1,1-k),min(m1+m2+1,n-k)
    dydx(i)=dydx(i)+a(i,j)*y(j+k)
  enddo
enddo
END
```

C.3 Spherical Harmonic Expansion of a Product of Two Scalar Fields

In Appendix A.4 the transform method for the evaluation of the coefficients of the spherical harmonic expansion of a product of two scalar fields has been outlined. The method is implemented by Martinec (1989) as the subroutine `vcsum`. In `vcsum`, for the two input arrays, `AJM` and `BJM`, representing the two scalar fields $a(\vartheta,\varphi)$ and $b(\vartheta,\varphi)$ with the cut-off degree `NP`, and for the desired cut-off degree `NR` of the product $c(\vartheta,\varphi)=a(\vartheta,\varphi)b(\vartheta,\varphi)$, the array `CJM` representing $c(\vartheta,\varphi)$ is returned. For the detailed description of `vcsum(NP,AJM,BJM,NR,CJM)` see the original reference.

The presented Fortran 90 excerpt implements the transform method for two zonal fields, i.e., for the evaluation of the coefficients h_n in accord with (A.45). Let us itemize the variables employed in the excerpt and the corresponding quantities used in Appendix A.4: `na` $=N_1$, `aj(0:na)` $=f_{n_1}$, `nb` $=N_2$, `bj(0:nb)` $=g_{n_2}$, `nc` $=N$, `cj(0:nc)` $=h_n$, `nk` $=K$, `xk(1:nk)` $=x_k$, `wk(1:nk)` $=w_k^{(K)}$ and `yleg(1:nk,0:ny)` $=\bar{Y}_n(x_k)$, where `ny` $\geq N$. It is advantageous to separate the task into two subroutines, `initvcsum2` and `vcsum2`. The aim of the initializing subroutine `initvcsum2` is, for given `nk`, to evaluate (i) the roots `xk(1:nk)` of the normalized Legendre polynomial $P_K(x)$, (ii) the weights `wk(1:nk)` of the K-point Gauss-Legendre quadrature scheme and (iii) the values of

$\bar{Y}_n(x) = N_{n0}P_n(x)$, $n = 0, \ldots,$ `ny`, on the grid `xk(1:nk)`. After just one call to `initvcsum2` (provided that `nk` and `ny` remain fixed), the operative subroutine `vcsum2` may be called repeatedly to return the coefficients `cj(0:nc)` of the product of two arbitrary zonal fields with the coefficients stored in the arrays `aj(0:na)` and `bj(0:nb)`. In `initvcsum2`, the routine `gauleg` by Press et al. (1996a) is called, and a variant of the routine `plgndr` from the same reference has been used for the evaluation of $\bar{Y}_n(x)$. Data sharing between `initvcsum2` and `vscum2` is accomplished via the modul `mvcsum2`, what is the preferable mechanism of Fortran 90, although the same effect could also be achieved by either `COMMON` blocks or `ENTRY` & `SAVE`, available in both Fortran 77 and Fortran 90, or simply by passing the arrays `wk` and `yleg` to `vcsum2` as the additional arguments.

Exploiting the array-handling features of Fortran 90, namely the array-section syntax, the array multiplication capability and the function `matmul` for matrix multiplication, we have reduced the executive part of the subroutine `vcsum2` to just one statement. Since the performance of the intrinsic function `matmul` is superior to other ways of coding matrix multiplication on both single-processor and multiprocessor machines, the presented Fortran 90 subroutines should be equally efficient as a properly structured Fortran 77 code on the single-processor machines and could be of interest for coding the multiprocessor machines as well.

```
MODULE mvcsum2
INTEGER,PARAMETER :: DP=8
INTEGER  :: nk,ny
REAL(DP),ALLOCATABLE :: wk(:),yleg(:,:)
END MODULE mvcsum2

SUBROUTINE initvcsum2(nk,xk,wk,ny,yleg)
IMPLICIT NONE
INTEGER,PARAMETER  :: DP=8
REAL(DP),PARAMETER :: PI=3.141592653589793_DP,PI4=PI*4
INTEGER  :: nk,ny,j
REAL(DP) :: xk(nk),wk(nk),yleg(nk,0:ny)
REAL(DP),DIMENSION(nk) :: pmm,pmmp1,pll
call gauleg(-1._DP,1._DP,xk,wk,nk)
pmm   = 1.
yleg(:,0) = pmm*sqrt(1./PI4)
if (ny.ge.1) then
  pmmp1 = xk
  yleg(:,1) = pmmp1*sqrt(3./PI4)
endif
do j=2,ny
  pll=(xk*(2*j-1)*pmmp1-(j-1)*pmm)/j
  yleg(:,j)=pll*sqrt((2*j+1)/PI4)
  pmm=pmmp1
  pmmp1=pll
enddo
END

SUBROUTINE vcsum2(na,aj,nb,bj,nc,cj)
USE mvcsum2
IMPLICIT NONE
REAL(DP),PARAMETER :: PI=3.141592653589793_DP,PI2=PI*2
INTEGER  :: na,nb,nc
REAL(DP) :: aj(0:na),bj(0:nb),cj(0:nc)
cj(0:nc)=PI2*matmul(matmul(yleg(1:nk,0:na),aj)*matmul(yleg(1:nk,0:nb),bj)*wk(1:nk),yleg(1:nk,0:nc))
```

```
END

PROGRAM testvcsum2
USE mvcsum2
IMPLICIT NONE
INTEGER  :: na,nb,nc
REAL(DP),ALLOCATABLE :: xk(:),aj(:),bj(:),cj(:)
na = 2
nb = 2
nc = na+nb
nk = (na+nb+nc)/2+1
ny = nc+1
allocate (xk(nk),wk(nk),yleg(nk,0:ny))
call initvcsum2(nk,xk,wk,ny,yleg)
allocate (aj(0:na),bj(0:nb),cj(0:nc))
aj = 0.
bj = 0.
cj = 0.
aj(1) = 1.
bj(1) = 1.
call vcsum2(na,aj,nb,bj,nc,cj)
print '(f12.7)',cj(0:nc)
END
```

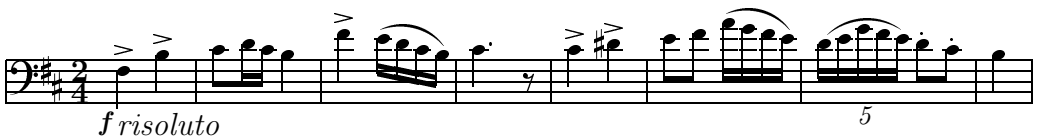

ANTONÍN DVOŘÁK, *Concerto for Cello and Orchestra No. 2 in B minor, Op. 104. III. Finale. Allegro moderato* (1895)